Technical Report Documentation Page

1. Report No.	2. Government Accession No.	3. Recipient's Catalog No.
FHWA/RD-86/075		PB86 180080/AS

4. Title and Subtitle	5. Report Date
Improved Methods to Eliminate Reflection Cracking	September, 1985
	6. Performing Organization Code
	8. Performing Organization Report No.
7. Author(s) Kamran Majidzadeh, George J. Ilves and V.R. Kumar	
9. Performing Organization Name and Address	10. Work Unit No. (TRAIS)
Resource International, Inc. 281 Enterprise Drive Westerville, Ohio 43081	11. Contract or Grant No. DOT-FH-61-C-0120
	13. Type of Report and Period Covered September 1980-September 1985
12. Sponsoring Agency Name and Address Federal Highway Administration U.S. Department of Transportation Washington, D.C. 20590	14. Sponsoring Agency Code

15. Supplementary Notes

FHWA Contract Managers: Richard W. May and Peter A. Kopac

16. Abstract

Existing elastic and viscoelastic fracture mechanics theories have been reviewed and modified to develop a theory capable of predicting the formation of reflective cracking in flexible overlays over rigid pavements due to thermal forces. The developed cracking model is based on fundamental material properties (creep compliance, indirect tensile strength, fracture toughness) and does not use a empirical distress function. Models have also been developed to predict the formation of reflective cracking due to load-associated fatigue. To this extent a FEM analysis model was developed to compute the critical tensile strain in the asphalt overlay over the existing joint or crack and this strain has been related to the allowable strain through laboratory fatigue tests. The developed models have been validated with limited field data, but a complete verification was not possible due to the lack of field projects that also have the required input data.

17. Key Words	18. Distribution Statement
Reflection Cracking, viscoelastic Fracture Mechanics, Rigid, Flexible, Overlay, Crack Propagation	No restrictions. This document is available to the public through the National Technical Information Service, Springfield, Virginia, 22161

19. Security Classif. (of this report)	20. Security Classif. (of this page)	21. No. of Pages	22. Price
Unclassified	Unclassified	199	

Form DOT F 1700.7 (8-72) Reproduction of completed page authorized

TABLE OF CONTENTS

NOTICE

This document is disseminated under the sponsorship of the Department of Transportation in the interest of information exchange. The United States Government assumes no liability for its contents or use thereof.

The contents of this report reflect the views of the contractor, who is responsible for the accuracy of the data presented herein. The contents do not necessarily reflect the official policy of the Department of Transportation.

This report does not constitute a standard, specification, or regulation.

The United States Government does not endorse products or manufacturers. Trade or manufacturers' names appear herein only because they are considered essential to the object of this document.

LIST OF FIGURES

LIST OF TABLES

CHAPTER I. INTRODUCTION

1.1 Background

Reflective cracking refers to the cracking of a flexible surfacing or overlay above underlying cracks or joints. This problem occurs in both rigid and flexible pavements, but is most serious in asphalt surfacings over jointed concrete pavements. The importance of this type of distress became apparent in the mid-fifties when many resurfacing projects experienced premature cracking failures in zones of underlying joints or cracks. In the old rigid pavements this new problem presented unique maintenance difficulties as once a crack develops, the deterioration of surface characteristics and the pavement support conditions in the areas immediate to the reflected cracks are accelerated.

The investigations of causes of reflective cracking have pointed out the influence of pavement horizontal movements, vertical displacements, curling, and warping as the contributing factors. It should be noted, however, that the cause of reflective cracking is still under debate among present technologists.

In order to obtain an optimal solution for elimination of reflective cracking, two approaches are possible: (1) a trial and error solution, which obviously would be cost prohibitive and time consuming, and (2) a rational analysis and development of a rational procedure to evaluate effectiveness of various alternatives.

The purpose of this investigation is to develop a rational procedure for looking at relative effectiveness of preventive methods and conditions which are most effective, and to conduct a theoretical modeling and evaluation of the various preventive methods.

1.2 Objectives

This study involves the development of a rational analysis and testing method that simulates the behavior of reflective cracking of flexible overlays of both flexible and rigid pavements. The procedure is based on mathematical models that are capable of evaluating the effectiveness of various alternatives.

The review of literature has indicated that a number of treatments have been used in the field in an attempt to control reflection cracking. However, very little information is available relating performance to critical factors. The examination of this relationship is therefore a primary objective of the laboratory investigation conducted in this study.

In order to achieve this objective, a small scale model was developed to test the relative effectiveness of various promising treatments that have been reported to reduce or prevent the formation of reflective cracking. The techniques evaluated in the laboratory are:

Rigid Overlays

- High modulus fabric strips placed over joints and cracks prior to overlay.
- Fiber asphalt (SAMI) placed on the slab prior to overlay.
- Open-graded asphalt crack relief cushion placed on the slab prior to overlay (similar to the method suggested by the Asphalt Institute).

Flexible Overlays

- One high and one low modulus fabric placed full width over the existing pavement prior to overlay.
- Fiber asphalt (SAMI) placed on the pavement prior to overlay.

Control samples with conventional overlays were used in both cases to evaluate the effectiveness of the treatments.

Fabrics and asphalt fiber SAMI were selected for use in this study based on their widespread past use, easy installation, and economics. As noted in a Virginia study and in Arizona studies, both methods are promising techniques.[1,2] The relationship between effectiveness, overlay thickness, and load transfer needs to be established for these two techniques.

Cushions have been successful in preventing cracking. However, thick aggregate cushions are expensive and often impractical to construct because of grade restrictions or clearance requirements on overhead structures. Few aggregate cushions have been built in recent years. The thinner asphalt stabilized cushions are often more practical to build and might be effective in delaying reflection cracking where load transfer between slabs is low.

Both fiber asphalt and rubber asphalt SAMI mixtures have shown laboratory properties which should enhance their cracking resistance. Their ability to resist reflection cracking warrants further investigation.

Although there is some disagreement among researchers, it is generally assumed that reflection cracking is the result of temperature induced stresses and those resulting from moving traffic. Since thermal stresses act over extended time periods,

a visco-elastic analysis is used; however, stresses resulting from moving loads are analyzed through a two-dimensional elastic finite element model. These models will be discussed in detail in chapter III of this report.

1.3 Outline of Report

This report documents the research activities of this study and is divided into the following major sections:

Chapter I: Introduction
Chapter II: Review of Current Methods
Chapter III: Development of the Analysis Model
Chapter IV: Laboratory Testing
Chapter V: Analysis of Test Data
Chapter VI: Analysis of Field Data
Chapter VII: Conclusions and Guidelines

A critical review of various reflection cracking analysis models is presented in chapter II along with their advantages and shortcomings. Chapter III deals with the development of the analysis models, and chapter IV discusses the design of laboratory experiments and the testing results. The laboratory test data are analyzed using the developed models in chapter V, and field data are analyzed in chapter VI. Finally, chapter VII contains the conclusions as well as guidelines for using the various reflection cracking arrest techniques.

CHAPTER II. REVIEW OF CURRENT METHODS

Reflection cracking is the cracking of a resurfacing or overlay above underlying cracks or joints. This cracking occurs in overlays of both flexible and rigid pavements and is a major cause of future pavement distress including spalling, surface water infiltration to underlying base and subgrade layers, and a general reduction in the stiffness of the pavement structure. Reflective cracks require continued future maintenance for crack sealing and patching, thus becoming a significant maintenance expense item.

The problem of reflection cracking is not a new one to the pavement engineer. Since the early 1950's many different materials, methods, and techniques have been tried to prevent or at least delay reflection cracking. Most of these efforts have been in the asphalt concrete overlay over existing Portland cement concrete (PCC) slab application, where existing cracks or joints are usually reflected through the asphalt overlay within a 1-year period.[3] Early research recognized that the probable cause of reflection cracking was movement of some form in the underlying pavement at existing cracks and joints. This movement can result from both traffic and environmentally induced forces. The movement includes differential vertical movement; and thermal- or moisture-induced expansion, contraction, or distortion (curling), at underlying joints and cracks. Because the overlay is bonded to the existing pavement, movement at underlying joints or cracks induces stresses in the overlay. If sufficiently high, these stresses cause fracture or cracking of the overlay. If the induced stresses do not exceed the yield strength of the overlay material, cracking could still develop as the result of cyclic load applications which produce fatigue fracture of the asphalt concrete.

2.1 Field Trials

Techniques or measures which have been used to arrest reflection cracking in field installations are summarized below:

(a) Several States have utilized bond breakers at the overlay/existing pavement interface which permit horizontal slippage between the overlay and underlying layer. Aluminum foil and wax paper placed over PCC slab joints prior to overlaying reduced reflective cracking by 50 percent in a California study.[4] However, a stone-dust bond breaker did not retard reflection cracking in a similar study in New York.[3] It was suspected that the emulsion tack coat utilized to hold the stone dust in place prior to overlay placement may have actually coated the dust causing it to adhere to both the pavement and the overlay, thus negating its bond-breaking effect. A sand bond breaker was utilized on three projects in Virginia.[1] Of the three projects,

only one showed any indication of fewer reflection cracks on joints with the sand bond breaker. An emulsion tack coat was also used on the Virginia projects, similar to the New York study. Thus, the degree of actual bond breaking accomplished with the sand layer is questionable.

(b) Cushions

Several State and airport agencies have tried utilizing aggregate cushions placed between the overlay and existing pavement to minimize reflection cracking. It is thought that the movement of the underlying layer will induce stresses only into the cushion layer. Michigan reported varying success with this technique, concluding that aggregate cushions do reduce reflection cracking but 8-inch (203-mm) thicknesses did not completely eliminate the problem.[5] A 3/4-inch (19-mm) thick layer of uniform coarse aggregate placed over the PCC slab prior to overlay has been effective in minimizing reflection cracking at a general aviation airport in Jacksonville, Florida.[6] However, similar interlayers have not reduced reflection cracking at airports in Wilmington, N.C. and Macon, Georgia.[6]

The Asphalt Institute has published a method describing construction of asphalt crack-relief layers. The layer is an open-graded asphalt mixture with low binder content (1.5 to 3.0 percent) and large size (2 to 3 in (51 to 76 mm) maximum aggregate) with a recommended thickness of 3.5 inches (88.9 mm).[7] These mixtures have low resistance to horizontal movement of the underlying layer. Any reflection cracks which develop in the crack relief layer may have their upward propagation retarded due to the presence of large voids within the mixture, similar to the reduction in crack propagation in metals when a hole or notch is placed at the crack tip.

(c) Asphalt - Rubber Interlayer (SAMI)

Arizona has reported the successful use of asphalt-rubber stress-absorbing membrane interlayer (SAMI) to reduce reflection cracking.[2,8] The typical asphalt rubber SAMI is a mixture by weight of about 75 to 80 percent paving grade asphalt cement, 20 to 25 percent ground rubber, and 2 to 5 percent rubber-extender oil. This mixture is blended together in a conventional distributor truck and spray applied to the surface to a thickness of 1/4 to 1/2 inch (6.3 to 12.7 mm). The rubber fraction reduces the stiffness and enhances the ductility of the membrane. At an Arizona study conducted in conjuction with the Federal Highway Administration's (FHWA) NEEP program on reducing reflection cracking in bituminous overlays, the asphalt-rubber SAMI has been the most successful method

in reducing reflection cracking of a 1 3/4-inch (44.5-mm) overlay over a badly cracked flexible pavement.[2] Seven years after construction of the overlay the percentage of reflective cracking is 2.1 for the rubber-asphalt SAMI test sections. Arizona researchers state that the SAMI acts as a crack tip retarder because it has such a low modulus of elasticity (estimated at 5000 psi (3.4 MPa)). Since 1975, Arizona DOT has built 33 overlay projects with asphalt-rubber membrane.

(d) Fabrics

Currently, the technique subjected to the most extensive field testing to determine its effectiveness in delaying reflection cracking is the placement of engineering fabrics over cracks or joints prior to overlay. There are numerous experimental projects of this type throughout the country. Reference 5 contains a tabulation of experimental projects using "Petromat" fabric including location, test features, evaluation procedures, and observations to date. "Petromat" is a non woven polypropylene fabric produced by Phillips Petroleum and has been the most widely used fabric to date. There are at least six other major U.S. corporations manufacturing fabrics from such materials as nylon, polyester, polypropylene, or polyvinylidene chloride. FHWA has recently published guidelines for the use of fabrics, and properties of fabrics as determined by the manufacturer.[9,10]

Fabrics are available in rolls and are placed as sheets tack coated to the existing pavement prior to overlay. Recently manufacturers have started producing 2- to 3-foot- (.6- to .9-m) wide rolls so that the fabric can be placed as strips over joints or cracks. These narrow rolls sometimes have an adhesive (usually rubberized asphalt) on one side so they can be placed without tack coating the existing surface. The strip type fabrics are usually used on rigid pavements while sheet fabrics which cover the entire area are used on flexible pavements. In a Virginia project 3-foot- (.9-m) wide strips of nonwoven polypropylene fabric were placed over a composite pavement at existing transverse reflection cracks.[3] Joint spacing of the PCC base was 30 feet (.9 m). Emulsion tack coat was applied before fabric placement, with the overlay thickness at 1.25 in (31.75 mm). After 3 months under traffic, many of the joints were reflected through the second overlay, although there was somewhat more cracking in an adjacent section where no fabric had been used. Virginia constructed other projects with fabric placed directly on PCC slabs at joints and cracks prior to overlay and attempted to correlate the fabrics' crack prevention performance with differential vertical movement or load transfer under an 18-kip (80-kN) axle

load at the joints. The Virginia study found a significant correlation between fabric performance and joint load transfer. The researchers stated that, "...it is likely that many of the 20 fabric-treated joints that were uncracked and had a differential deflection of 0 (100 load transfer) were working joints where the fabric served its intended purpose of reducing overlay stresses to the point that no cracking occurred. Conversely, it is likely that, for those joints that had higher differential deflections, the fabric, a thin sheet, could not sufficiently distribute the shear stresses and was thus unable to reduce reflection cracking significantly." The study also concluded that at differential deflections greater than .002 inches (.05 mm), reflection cracks form very early. The formation of cracks is delayed at lower differential deflections; but, cracks will occur as the magnitude and frequency of wheel loads increase.

The Virginia study appears to validate the fatigue fracture mechanism for reflection cracking under traffic load first presented by Luther and Majidzadeh.[11] The Virginia results are very important and may explain why other States have had difficulty in assessing fabric reflection crack prevention performance. A recent state-of-the-art review, conducted by the Federal Aviation Administration (FAA) summarizing highway experience with fabrics, stated that no definite conclusions could be drawn from the collective results.[5] In some instances, the fabric (Petromat or others) appeared to be effective, but in similar situations, at other locations, results would contradict previous conclusions. Based upon Army Corps of Engineers experience, there is some evidence that fabrics are more effective on asphalt over asphalt than on asphalt over jointed concrete in retarding reflection cracking.[12] However, fabric placed beneath the 1 3/4-inch (44.5-mm) overlay over the existing flexible pavement, in the previously noted Arizona study, did not perform favorably. This technique was not among the five most successful methods for reducing reflection cracking at the Arizona site.

In a 1978 FHWA memorandum, it was concluded that, because of contradictory results and insufficient quantitative data, criteria for the use of fabrics to reduce reflection cracking cannot be developed, and their use on pavements must remain on an experimental basis.[10] It may well be that fabrics are beneficial in reducing reflection cracking induced by horizontal movement of the underlying pavement, but this benefit has been negated by the lack of load transfer data in the field installations which were studied.

(e) Modify Existing Pavement

Breaking and seating PCC slabs prior to overlay has been successful in some States as a means of reducing reflection cracks.[13,14] Both Louisiana and Minnesota reported that breaking up slabs reduced reflection cracking significantly. This technique is believed effective since seating improves slab support, and the reduction in slab size reduces thermal movement at slab joints and cracks. In a New York study, an existing 8-inch (203-mm) PCC slab was broken into either 1 ft by 1 ft or 3 ft by 4 ft (.3 by .3 m or .9 by 1.2 m) sizes, a 50-ton (222-kN) roller traversed the broken pieces, then a 7-inch (178-mm) overlay was placed.[1] The study concluded that the pavement breaking did retard reflection cracking as compared to control sections; neither breaking pattern appeared to have any significant advantage. However, researchers did not feel that the 50-ton (222-kN) roller was effective in seating the broken pieces.

For existing flexible pavements, surface heater scarification to a depth of .75 inches (19.1 mm) and its rejuvenation to 200/300 penetration prior to overlay was successful in preventing reflection cracking in Airzona.[2] After 8 years the percentage of reflection cracking in the 1 3/4-inch (44.5-mm) overlay was only 7.4 percent with this technique. It is believed that this process remolds the top 3/4 to 1 inch (19.1 to 25.4 mm) of old AC into a material similar to new AC and thus reduces the existing crack length by 3/4 to 1 inch (19.1 to 25.4 mm). More loading cycles are required to propagate the shorter crack, thus delaying reflection cracking.

(f) Stronger Overlays

Several States have used steel wire mesh reinforcement to enhance the tensile strength of the overlay and thus resist cracking caused by horizontal movement of the existing pavement. Michigan experiments concluded that reinforcement offered no advantage in control of reflection cracking.[5] A similar California study reported inconclusive evidence of reinforcement benefits.[15] The wire mesh was placed directly on the existing rigid slab on both the Michigan and California studies.[5,4] Reinforcement placed at mid depth of the overlay was partially successful in reducing cracks in Florida.[16]

The introduction of sulfur or rubber into conventional asphaltic concrete mixtures to improve overlay crack resistance has also been tried. Sulfur increases mixture stiffness, stability, fatigue life, and is reported to be

resistant to low temperature cracking.[17,18] Although some sulfur overlays have been built, a 1-mile (1.6-km) test section in Winfield, Alberta is reported to be the only project monitored with respect to reflection cracking.[6] Constructed in 1974, this project is said to be performing well. Rubber affects asphalt mixtures in a different manner. Rubber decreases mixture stability, but increases ductility, resilience, and toughness over conventional mixes.[18]

Increased overlay thickness has generally not been effective in eliminating reflection cracking, although some States have reported some delay in cracking by using thicker overlays.[19,20] Research in Ohio found that cracked or broken PCC slabs resurfaced with as much as 5 inches (127 mm) of asphalt still developed reflection cracks, often in less than a year.[21,18] Austin Research Engineers state that results of several reflection cracking studies, where the overlay varied from 1 1/2 to 10 inches (38.1 to 254 mm), all showed some degree of reflection cracking.[22]

In summary, the reflection cracking studies and field experimental projects to date have generally been of an empirical nature with little control or even identification of the parameters known to affect cracking. Characterization of the existing pavement in terms of joint width, load transfer, crack spacing, crack and joint opening under known temperature conditions, and deflection under load has usually not been part of these studies. Obviously, certain crack prevention treatments are sensitive to some of these factors, as was shown in the Virginia study where fabric performance was related to load transfer. Unfortunately, past research has not established the quantitative relationship between these factors and success or failure of the preventative techniques shown in figures 1 and 2.

2.2 Evaluation of Existing Reflection Cracking Models

Within the last 10 years, several theoretical (mathematical) models have been developed to analyze and predict the occurrence of reflection cracking. All of the models consider the same mechanisms as previously noted (e.g., reflection cracking is caused by differential horizontal or vertical movements in the underlying layer). The models differ in the methods for predicting the magnitude of underlying layer movements, on the magnitude of stresses induced into the overlay by the movements, and in the response of the overlay to stress state (sudden fracture vs. fatigue fracture). The following discussions summarize the reflection cracking models which currently exist and present an evaluation of the limitation of each model.

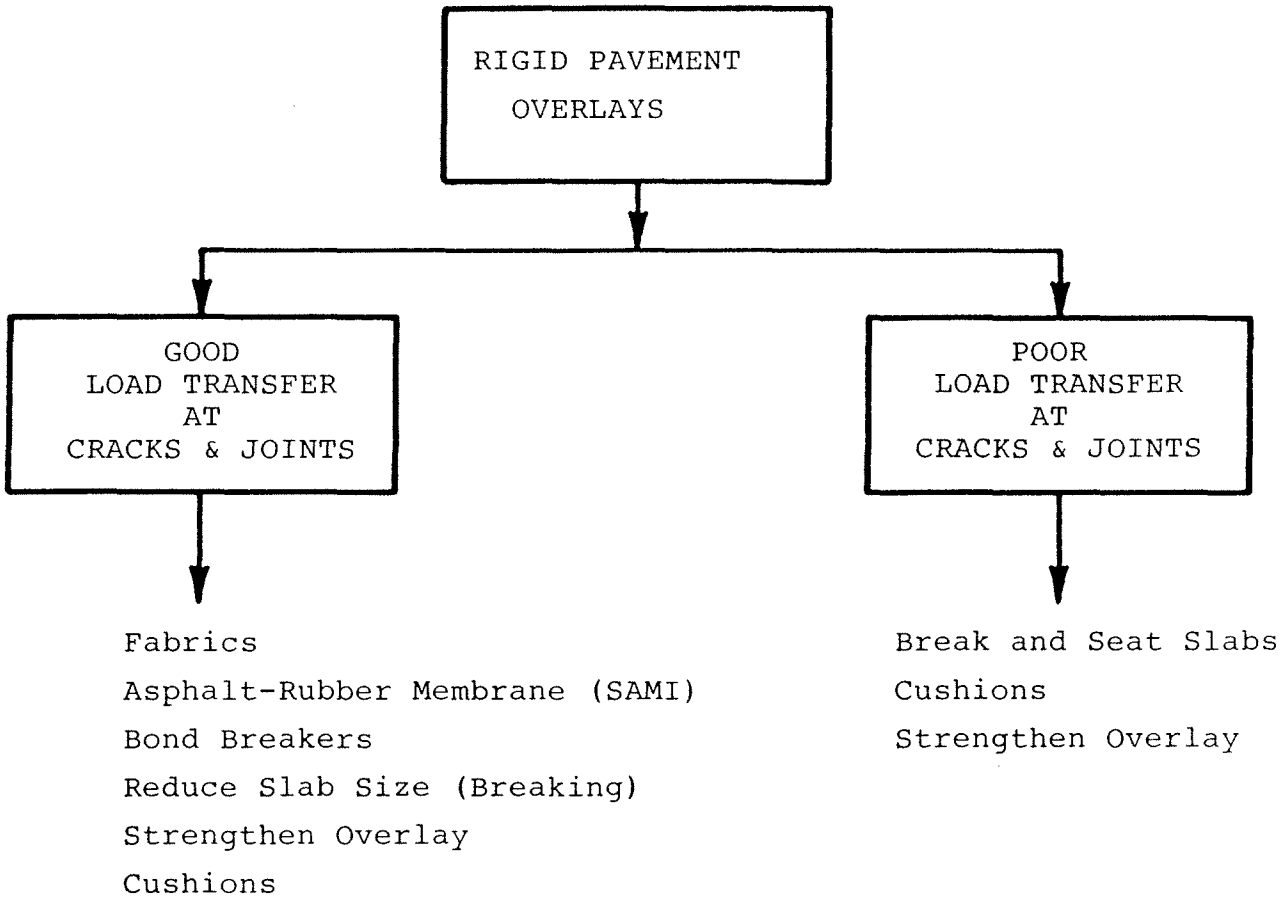

Figure 1. Reflection crack prevention techniques for flexible overlays of rigid pavements.

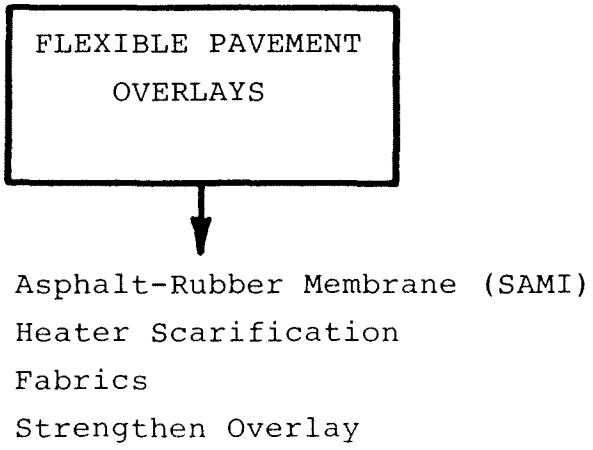

Figure 2. Reflection crack prevention techniques for flexible overlays of flexible pavements.

2.2.1 OSU - Ultimate Strength Model

This model developed by researchers at Ohio State University [21], is a nomograph procedure for predicting Asphalt Concrete overlay stresses over joints or cracks resulting from thermally induced movements in underlying PCC slabs. Separate stress analyses are performed for horizontal slab movements, due to seasonal changes in average slab temperature, and vertical slab movements which occur due to curling of slabs. Curling is the temperature state where the top of the PCC slab is colder than the bottom of the slab.

Horizontal movement of the PCC slab, d, for a change in slab temperature, T, (F), is given as

$$d = d_2 - d_1 \qquad (1)$$

where:

d = slab movement at joint or crack, in inches

d_2 = theoretical movement of an unrestrained slab = $\alpha TL/2$

α = thermal coefficient of concrete

L = slab length or crack spacing

d_1 = movement restrained by friction between slab and subgrade = $\frac{F_t L}{2AE_c}$

$F_t = f(\gamma_c h_c + \gamma_a h_a)L/2$

f = coefficient of friction between slab and subgrade

γ_c = unit weight of concrete

γ_a = unit weight of asphalt overlay

h_a, h_c = thickness of slab and asphalt layers

A = unit cross section of slab, in /ft

E_c = modulus of elasticity of concrete, psi

Equation 1 uses an average value, f, for the friction coefficient, similar to the calculation for determining temperature reinforcement in jointed reinforced concrete pavements. Most importantly, this model neglects the resistance to joint movement provided by the uncracked overlay which is

bonded by a tack coat to the underlying slab. The OSU model assumes that this resistance is small and that thin overlays do not affect the movement of the joint due to temperature change.

To study the effect of the joint movement on the overlay, a two-dimensional finite element technique is used. Figure 3 shows a sample of the mesh used in this analysis. The model consists of an overlay layer on top of two slabs, with a thin asphalt cement tack coat between the overlay and the slabs. A horizontal movement of the slabs is induced at the joint location while the center line of each slab is held fixed. The stresses in the overlay along with the shearing stresses in the tack coat were computed by the finite element program; and, nomographs for determining overlay stresses shown in figures 4 and 5 were developed from this model.

To study the maximum shearing stresses that the asphalt tack coat can bear (which is bonding the overlay to the pavement), experiments were run on laboratory specimens using the test setup shown in figure 6. It was concluded that the maximum bonding stress of the tack coat varies from = 6 to 10 psi (41.4 to 68.9 kPa). Therefore, it was assumed that if the stresses in the bonding layer exceed 10 psi, (68.9 kPa), the horizontal joint movement will transfer no more stresses to the overlay because of the slipping that occurs between the pavement and the overlay. This limiting condition was included in the formulation of figures 4 and 5. The bonding stress between asphalt and concrete ought to be temperature dependent. The OSU study did not state the temperature range for the experiments shown in figure 6, nor was the surface texture of the PCC layers, thickness and type of tack coat described.

Similar to the horizontal joint movement, the effect of vertical movements on the overlay due to slab curling is also based upon the premise that the thin overlays do not affect the curling of slabs significantly. Thus, the restraint against curling of the slabs provided by the uncracked overlay is again neglected. This important assumption permits the curved shapes of slabs to be predicted utilizing a computer simulation (program called "PLATES") of the Westergaard solution for temperature differentials between top and bottom of the slab. Curling-induced overlay stresses are estimated on the assumption that the induced overlay takes the slope illustrated in figure 7. For a joint width j and edge slopes (in radians), calculated from the "PLATES" program, the radius of curvature in the overlay can be estimated from:

$$R = \frac{j}{2\theta} \qquad (2)$$

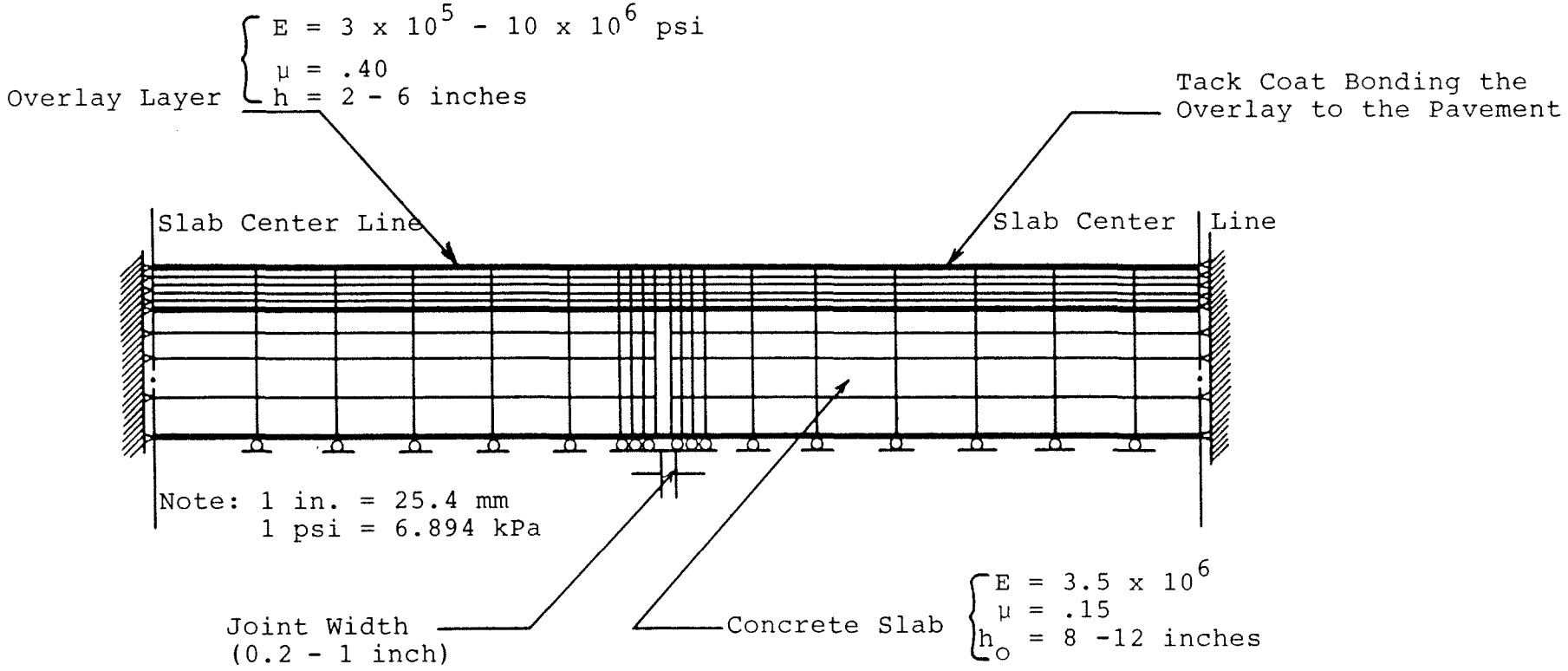

Figure 3. Finite element mesh to study the stress in the overlay due to joint opening.

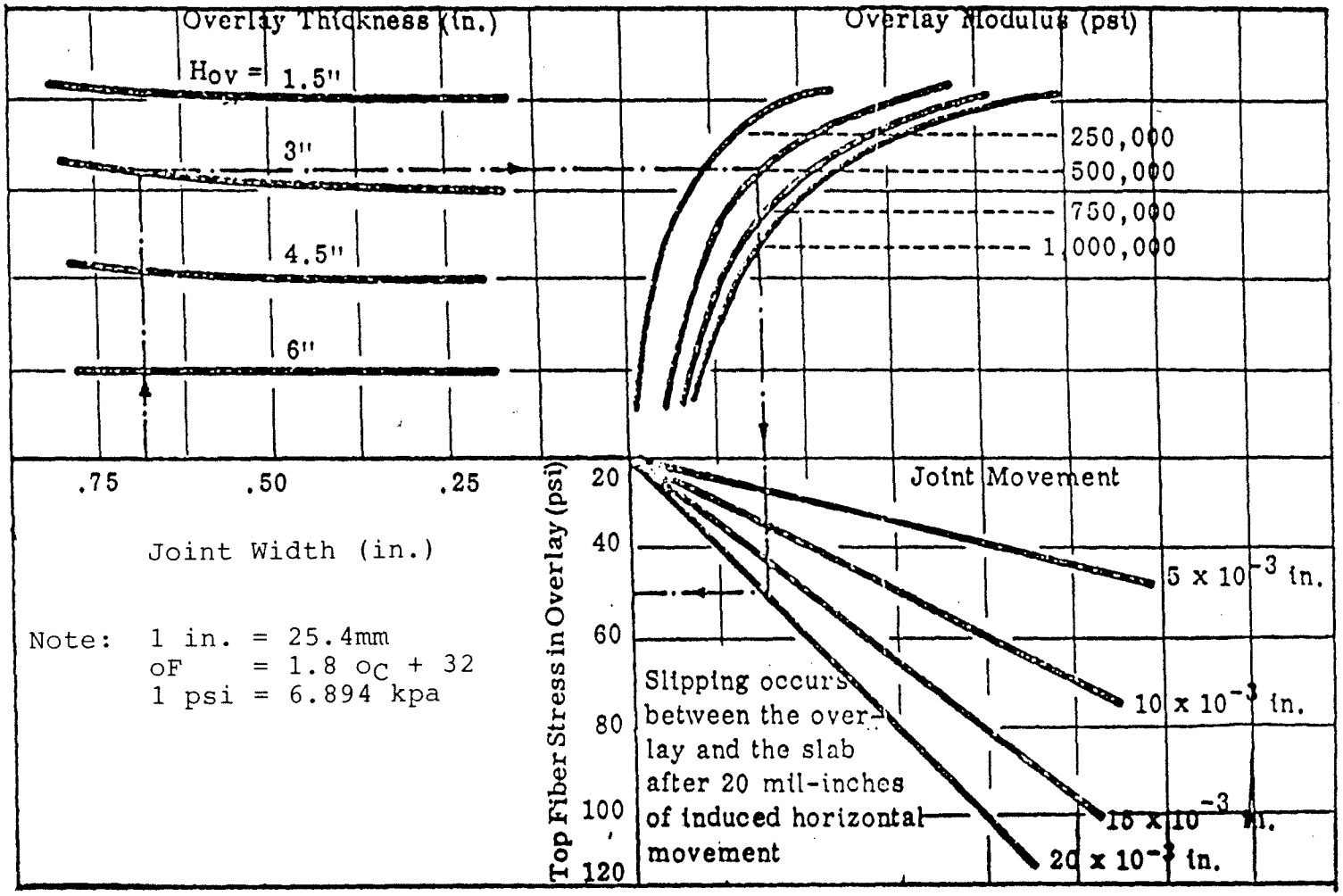

Figure 4. Top fiber stress in overlay due to JRCP joint movement.

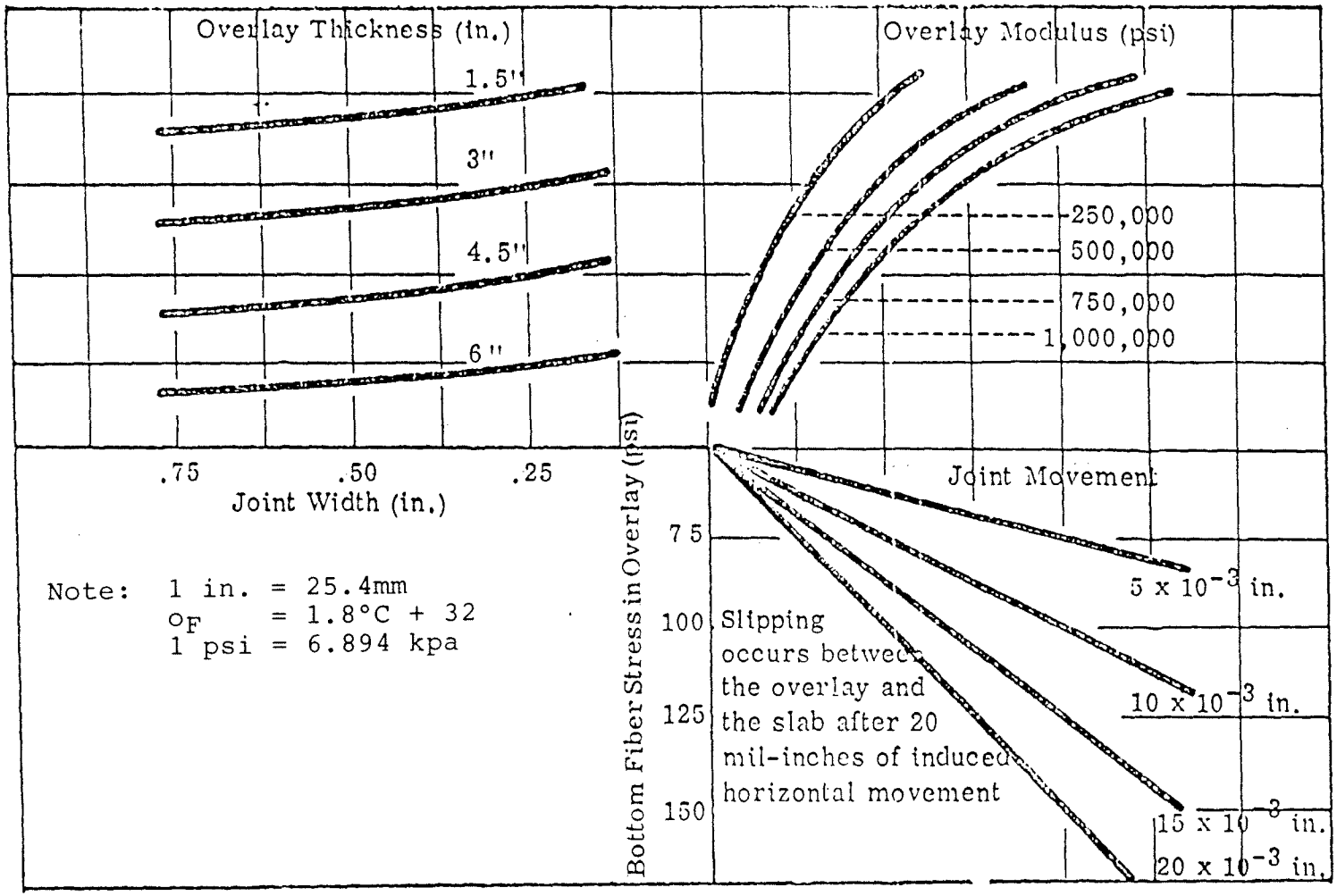

Figure 5. Bottom fiber stress in overlay due to JRCP joint movement.

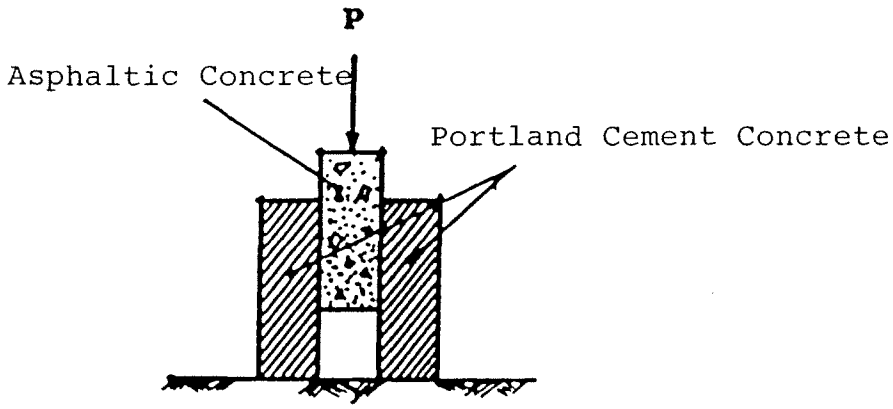

Figure 6. Laboratory specimen for bond testing.

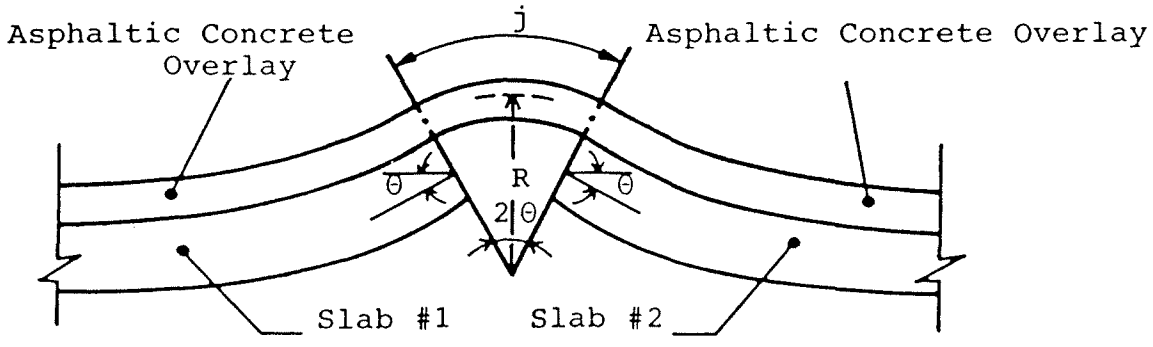

Figure 7. Bending of overlay by joint vertical movement.

In turn, overlay stresses can be calculated from the expression:

$$\sigma_{ov} = \theta \frac{E_{ov} h_{ov}}{j} \quad (3)$$

where:

= overlay stiffness

= overlay thickness

Equation 3 is derived from the basic strength of materials for pure bending

$$\varepsilon(u) = u/R \quad (4)$$

where:

$\varepsilon(u)$ = axial strain at distance from the neutral axis

R = radius of curvature

Since equation 3 is derived from pure bending, symmetric bending of the overlay with tension at the top and compression at the bottom is implied. The nomograph in figure 8 was derived using the above theory. This nomograph could be used for the computation of the maximum stress in the overlay resulting from 1 F (.56 C) temperature differential in the slab. For a different temperature differential (T), the results obtained from the nomograph should be multiplied by T to obtain the stress in the overlay due to slab curling. Note that the stress given in figure 8 is for "pure" curling only. "Pure" curling means that the average slab temperature has not changed from the reference temperature, but the top of slab is cooler than the bottom of the slab.

The OSU-Ultimate Strength Model presents an easy nomographic procedure for determining overlay stresses from thermal movements of underlying PCC slabs. However, the accuracy of the stress computation is suspect for the following reasons:

- Restraint imposed by the uncracked overlay against slab movements (both horizontal and curling) is not considered. Thus, the calculated force in the overlay at the time of cracking is probably incorrect.

- The overlay stresses due to horizontal joint movement appear low, and should be validate by additional finite element investigation.

- The tack coat bonding stress values also seem low and should be established by a laboratory investigation which

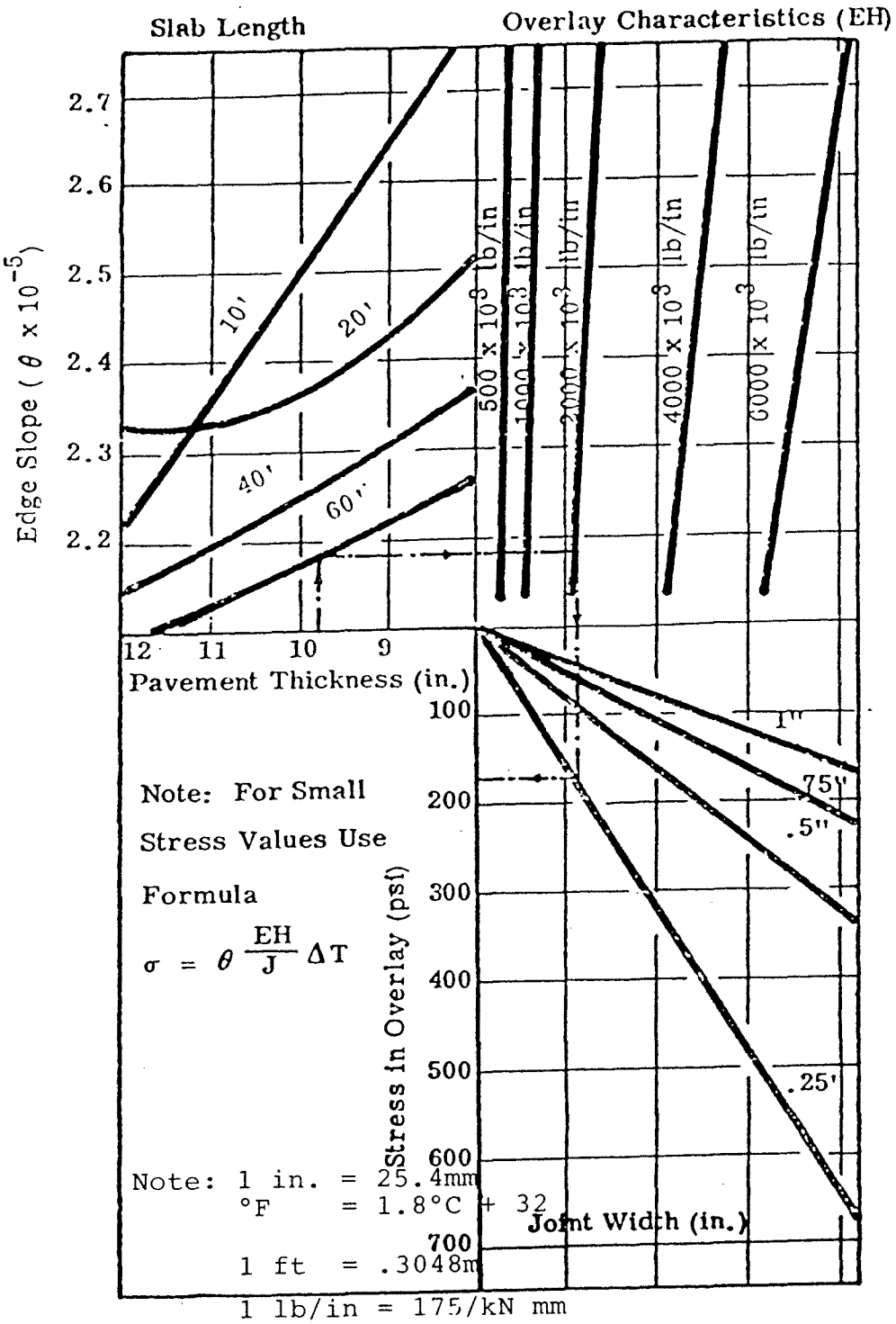

Figure 8. Maximum stress in overlay due to 1°F temperature differential in a rigid pavement - curling.

considers temperatures, tack coat type and amount and roughness of the PCC slab.

- The Westergaard analysis used to predict slab curling neglects the weight of slab and overlay which would tend to reduce the curl.

- The simplistic analysis of overlay stresses due to curling should be verified by finite element analysis. The fact that curling introduces a horizontal joint opening is neglected by the analyses. This horizontal movement could be significant, and thus change the stress state considerably.

- The model is not capable of assessing the effects of crack prevention measures upon stresses in the overlay.

- The model does not present recommendations for selecting design parameters such as temperature change T or curling T, asphalt concrete modulus, and asphalt concrete strength.

2.2.2 ARE - Ultimate Strength Model

Austin Research Engineers have developed a procedure for reflection crack stress or strain analysis.[22] Two different modes are considered. The first is an opening mode (figure 9) due to horizontal movements of the underlying PCC slab, resulting from a seasonal temperature reduction. Both joints or cracks without steel reinforcement or cracks with steel reinforcement (such as CRCP) can be analyzed for horizontal movement. The second is a shearing mode (figure 9) resulting from a differential deflection across the joint or crack as the traffic load moves across the discontinuity.

In developing the model, a number of assumptions have been made, including: the materials are elastic in response; temperature variations are uniformly distributed in the existing concrete slab (no curling); concrete movement is continuous with slab length; and movement is uniform with depth in a particular layer.

Horizontal movements are determined by characterizing the existing concrete pavement through field measurements to define a representative joint spacing and crack or joint movement associated with a specific temperature change. From this data a measure of the frictional force between slab and base on subgrade layer is determined. Provision is included to modify the force displacement relationship due to increased overburden pressure from the overlay. The model also contains a method for calculating overlay stresses when a bond breaker is placed over the joint.

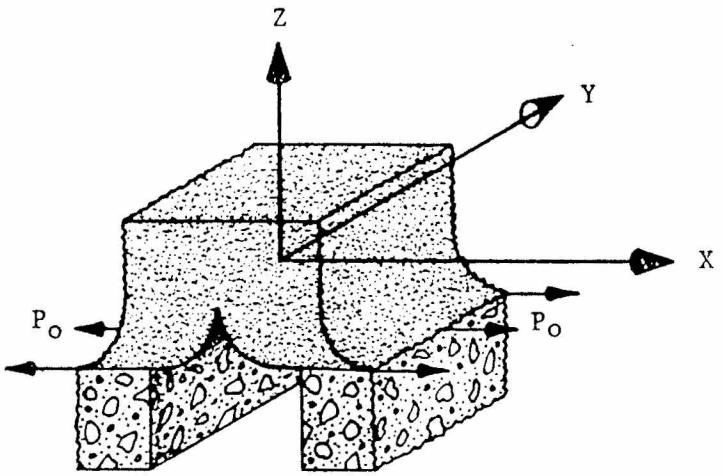

(a.) Opening Mode - Horizontal Movement of Underlying Layer

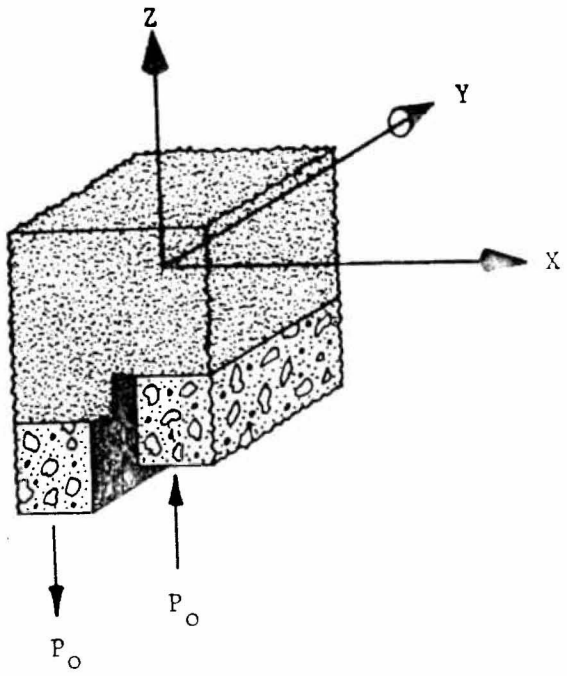

(b.) Shearing Mode - Differential Vertical Deflections Across a Joint or Crack

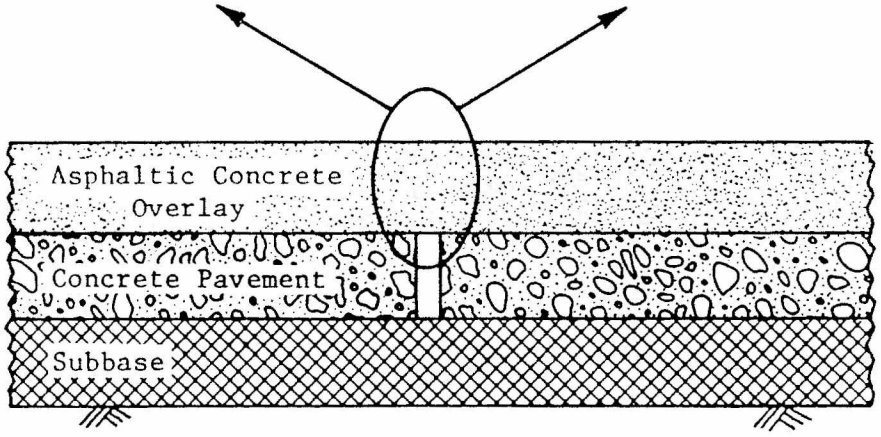

(c.) General Pavement Cross-section.

Figure 9 . Different failure modes considered for the reflection cracking model.

Movement of the existing pavement for the bonded overlay condition is expressed as:

$$Y_{cB}(x) = \alpha_c \Delta T \left[x - \beta_B x^{\beta_B} \right]_o^{X_B} \quad (5)$$

and

$$Y_{cu}(x) = Y_{cB}(X_B) + \alpha_c \Delta T \left[x - \beta_u x^{\beta_u} \right]_o^{X_{BB}} \quad (6)$$

where:

$Y_{cB}(x)$ = Concrete movement where the overlay and existing pavement are bonded (figure 10a) at a distance x from the slab's center

$Y_{cu}(x)$ = Concrete movement where the overlay and existing pavement are unbounded (figure 10b) at a distance $X_B + x$ from slab's center

x_B = Distance from slab's center to the edge of the bond breaker

x_{BB} = Width of bond breaker on one side of the joint

The concrete force at midslab is computed by:

$$F_{cB} = E_c A_c \left[\alpha_c \Delta T - \frac{Y_c(X_B)}{X_B} \right] \quad (7)$$

where:

$Y_c(X_B)$ = Concrete movement at the edge of the bond break where the two layers are unbonded,

E_c = concrete modulus of elasticity

A_c = area of concrete pavement per unit width

α_c = thermal coefficient of concrete

ΔT = slab temperature change

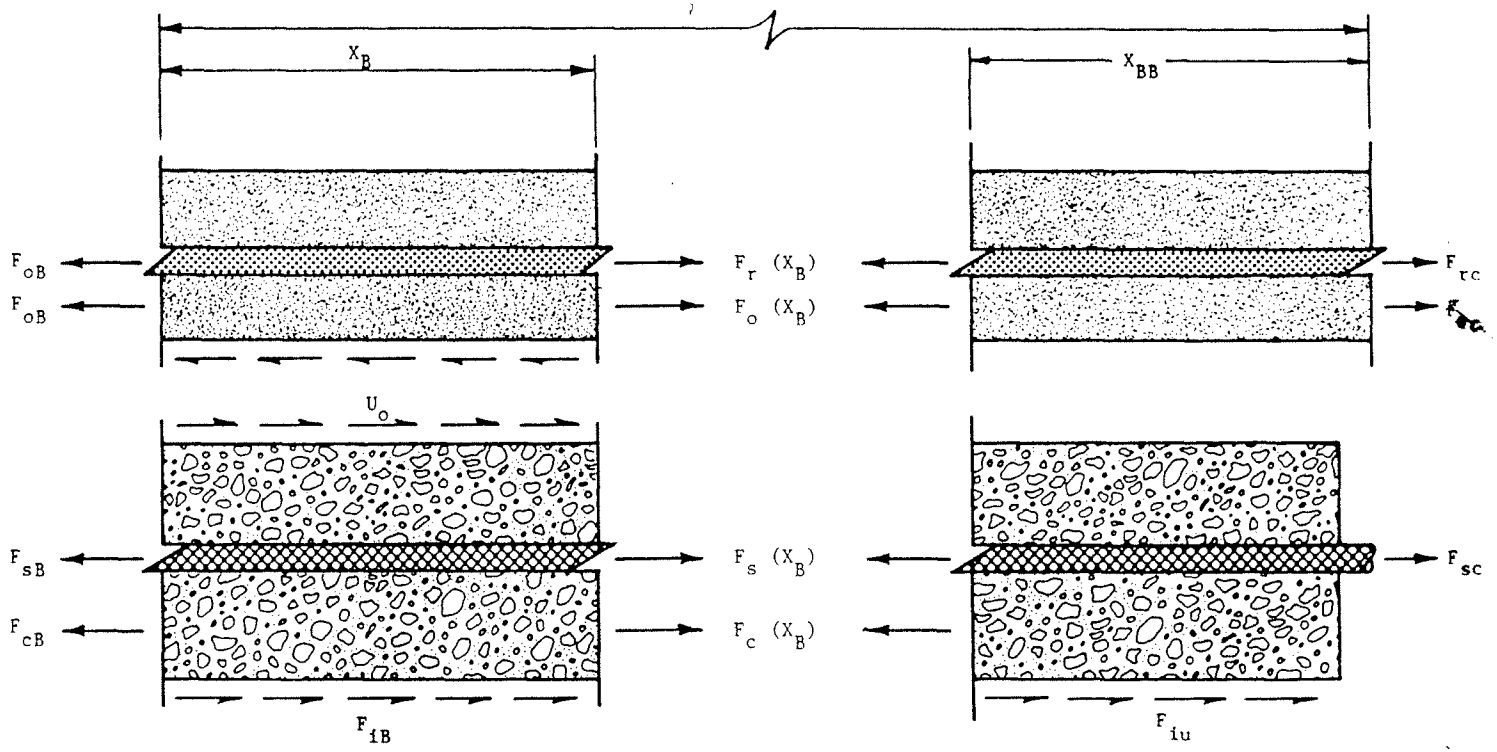

(a.) Bonded portion of the overlay which is related to the restraint coefficient β_B.

(b.) Unbonded portion of the overlay which is related to the restraint coefficient β_u.

Figure 10. Free body diagram illustrating the forces used in evaluating a bonded overlay for reflection cracking potential.

The frictional force generated by slab movement is:

$$F_i = \int_o^{X_B} m_o Y_{cB}(x)\,dx + \int_{X_B}^{\lambda} m_o Y_{cu}(x)\,dx \qquad (8)$$

where:

λ = one half the slab length or crack spacing

m_o = slope of force displacement curve adjusted for overburden weight

The following relationship is used to relate forces in the concrete and overlay layers where movement of both layers are equal.

$$F_{oB} = F_{cB}\frac{E_o A_o}{E_c A_c} + E_o A_o \Delta T_o(\alpha_o - \alpha_c) \qquad (9)$$

where:

F_{oB} = Force in the overlay material between two adjacent joints or cracks in the existing pavement, lb/ft (1.35 N/m) width

A_o = The cross-sectional area of overlay material per foot width of pavement, sq in/ft width (196.6 sq mm/m)

E_o = asphalt overlay creep modulus

ΔT_o = overlay temperature change

α_o = thermal coefficient of asphalt concrete

The creep modulus is used due to the long-term loading condition and should be determined for various temperatures and each mix design considered. If this data is not available, the Shell nomographs are presented in the ARE report which enable the modulus to be determined knowing the penetration index, Ring and Ball temperature, and design overlay temperature.[23,22] A loading time of 20,000 seconds has normally been used, although the designer may select a 12-hour loading time due to daily temperature cycles.

The force in the overlay at a joint or crack is determined by:

$$F_{oc} = E_o A_o \left[\alpha_o \Delta T_o + \frac{Y_c(X_B)}{X_o + X_{BB}} \right] \quad (10)$$

For various materials and different asphaltic concrete mix designs, the force transferred from the existing pavement to the overlay is related to concrete movement in the form of a force-displacement curve, as between the concrete slab and subbase, or is in the form of bonding forces caused by slippage as between the concrete and steel. No data are available to adequately define a relationship to explain the force transfer between the two materials. Therefore, two purely theoretical conditions were used to estimate this relationship. The first assumes, in the section where concrete and overlay are bonded, that overlay movement equals movement of the slab, and is constant with pavement thickness. Asphaltic concrete is a visco-elastic material that approaches an elastic state at low temperatures. The critical conditions occur at these low temperatures; hence, the above assumption was believed to be reasonable. The second uses an average bonding stress between overlay and existing surface, in the section where existing pavement and overlay are bonded, to compute the force transferred between the two layers.

$$U_o = 12 \, \mu_o X_o \quad (11)$$

where:

U_o = Force transferred between overlay and existing pavement layers, lb/ft width (1.35 N/m width)

μ_o = Average bonding stress between the overlay and existing pavement; theoretical values for asphaltic concrete overlays are given in table 1

X_o = Distance over which slippage occurs between overlay and existing surface in the bonded overlay

Table 1 lists values of bonding stress which were estimated using engineering judgment and physical characteristics of existing concrete pavements. Note that these values differ significantly from that used by the OSU model. By equating equation 11 with the portion of equation 10 which represents the force transfer due to slab movement, X_o can be found in terms of $Y_c(X_B)$:

$$X_o = \left[\frac{E_o A_o Y_c (X_B)}{12\ \mu_o}\right]^{\frac{1}{2}} \qquad (12)$$

Table 1

Theoretical average bonding stress between the existing concrete pavement and asphaltic concrete overlay.

	Condition of Existing Surface	Average Bonding Stress, psi*
1.	Smooth: polished surface; no exposed coarse aggregate.	50
2.	Rough: Same as for a smooth surface but some of as-constructed texture remains; small amount of coarse aggregate exposed.	500
3.	Very Rough: Worn surface with exposed coarse aggregate; contains aggregate popout; contains surface texture.	1200
4.	Jagged: Grooves present; numerous aggregate popouts; coarse aggregate highly exposed.	Very large, Assumed infinite

*Bonding stresses are theoretical values, which should be verified from future field studies.
Note: 1 psi = 6.894 kPa

Various values of the restraint coefficient, β_B, are chosen until the frictional, concrete, and overlay forces balance (figure 10):

$$F_{cB} + F_{oB} = F_i + F_{oc} \qquad (13)$$

(for the case without steel reinforcement).

The horizontal tensile strain in the overlay is given by:

$$\varepsilon_{oc} = \frac{F_{oc}}{A_o E_o} \qquad (14)$$

This strain is compared to an allowable tensile strain to determine if temperature reflection cracks will occur. The allowable tensile strain is given as 1.7 x 10 in/in (mm/mm). Apparently this was calculated from the ARE fatigue equation at an Nf of 1.9:

$$N_f = 9.73\ (10^{-15})(1/\varepsilon)^{5.16} \tag{15}$$

The model for shearing mode failure due to differential vertical deflection between slabs under traffic load is based upon the load transfer prior to overlay. Deflections are measured on each side of the joint or crack for a load applied to one side, and the load transfer, L , is estimated from the expression:

$$L_t = 1 - \frac{W_\lambda - W_u}{W_\lambda} = \frac{W_u}{W\lambda} \tag{16}$$

where:

W_λ = deflection measured at the joint on the loaded slab

W_u = deflection measured at the joint on the unloaded slab

The shear force in the overlay at the joint is then determined:

$$P_o = L_D(1 - L_T) \tag{17}$$

where:

P_o = shear load

L_D = design load

Shear stress in the overlay, τ_o , is estimated by assuming a constant shear force over the width of the applied load:

$$\tau_o = \frac{P_o}{D_o' W} \tag{18}$$

where:

D'_o = effective overlay thickness

W = width of the applied load

D is the thickness of the overlay itself. When reinforcement exists in the overlay or when a leveling or intermediate layer exists, the total effective overlay thickness D is determined using:

$$D'_o = D_o + \sum_{i=1}^{n} D_i \frac{E'_i}{E'_o} \qquad (19)$$

where:

E'_o = Dynamic modulus of the overlay material, psi

E'_i = Dynamic modulus of layer i, psi

D_i = Thickness of layer i, (when reinforcement is used ares should be used) inches

n = Number of layers

The shear strain, γ_o, is calculated from the expression:

$$\gamma_o = \frac{2\tau_o(1 + D_o)}{E_o} \qquad (20)$$

with E_o and ν_o being the dynamic modulus and Poisson's ratio (measured at a short time of loading) for the asphalt concrete overlay. The value is then compared to a limiting value for shear strain which presumably is developed from experience.

The ARE-Ultimate Strength Model has been computerized (program called RFLCR1) which minimizes difficulties in using the model. The model is the most versatile procedure currently available in that it can consider slab or overlay reinforcement, bond breakers, and granular cushions (shear failure analysis only). However, the simplifications in the model which permit strain calculation without the use of analytical computations for stress distribution have not been validated. This appears to be the primary question of the ARE model. Although force magnitudes may be reasonable, the assumed simplistic distribution of

stresses within the overlay for both opening and shear failure modes is very suspect since no concentration of stresses at the joint/crack tip are considered. Other less significant questions regarding the ARE model include:

- Characterization of the existing pavement by joint opening measurements over a certain temperature range cannot necessarily be extrapolated to a different design temperature range. For example, restraint exhibited between 70 to 50 ^{o}F (21 to 10 ^{o}C) may not identify the restraint between 70 and 20 ^{o}F (21 and -9 ^{o}C).

- The assumed value for bonding stress between overlay and slab is very important in the analysis, since it establishes the gage length over which the overlay force at the joint is distributed. The suggested values in table 1 need to be validated experimentally. If bonding stress can approach an infinite value (as table 1 states for a jagged slab surface) how is overlay strain calculated? It is unclear, but apparently a gage length equaling one-half the original joint opening would be used.

- The concept that a bond breaker reduces overlay strain by merely increasing the gage length for force transfer, should be validated by analytical investigation of stress distribution.

- Load transfer is determined from pre-overlay measurements without any adjustment for the effect of the overlay. This effect may not be negligible. Also load transfer is probably load and temperature dependent.

- The temperature for determination of dynamic modulus in the shear model is not specified. By the model a high temperature would be critical since larger strains would result. However, the allowable strain is likely to be temperature dependent.

2.2.3 OSU - Fracture Mechanics Model

Fracture mechanics has been utilized to develop a reflection crack propagation model for asphalt overlays over PCC slabs. [11,24] The model considers only traffic-induced fatigue cracking resulting from differential deflection at slab joints or cracks.

The first step in applying fracture mechanics principles was to identify the fracture mode or modes associated with crack initiation and extension (figure 11). A finite element stress analysis of full-scale pavements predicted that the asphaltic overlay would be in compression, thus leading to the conclusion

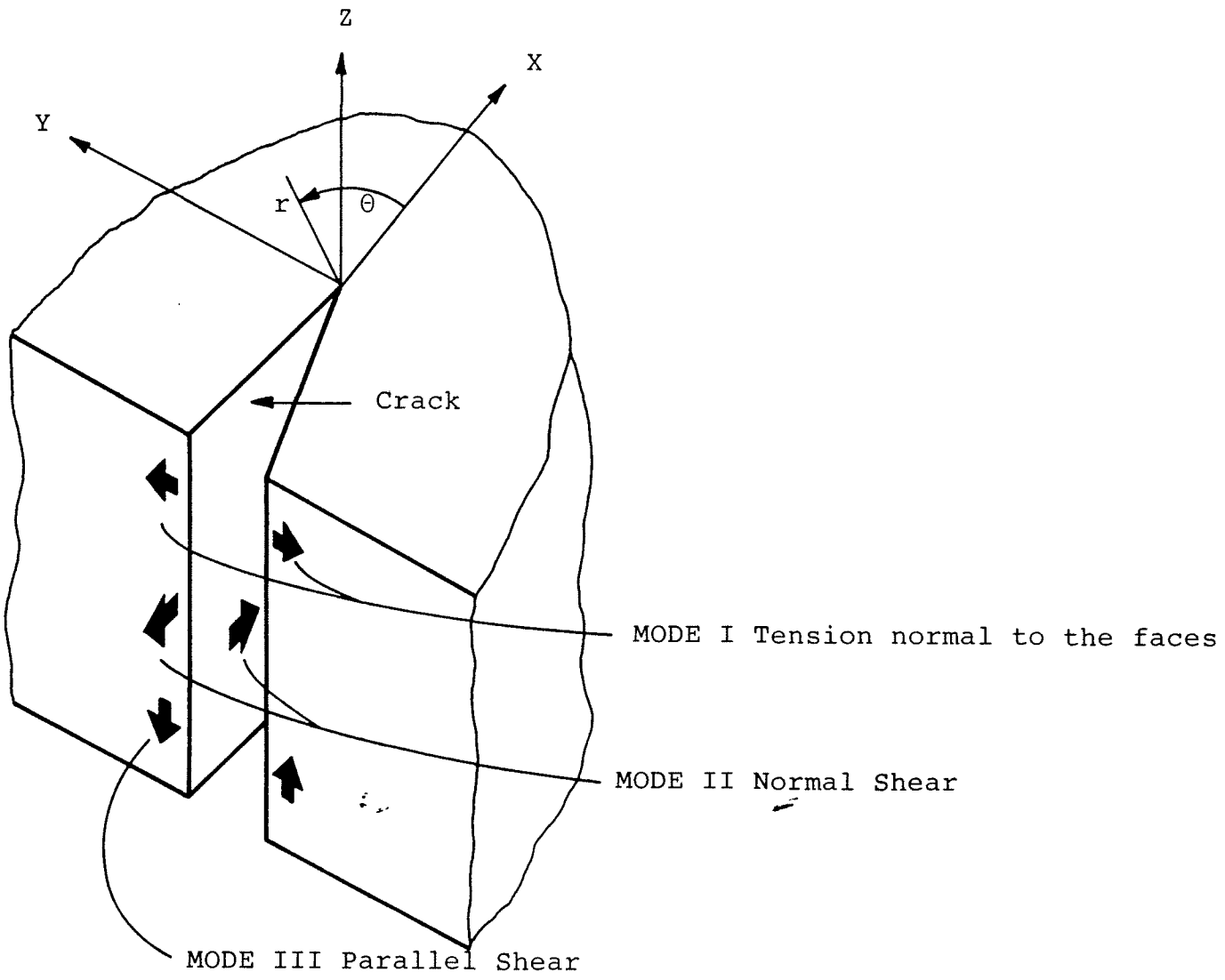

Figure 11. Modes of deformation of a crack.

that opening mode (Mode I) type fracture does not occur. Additionally, the computer analysis predicted there would be significant relative vertical displacement (Mode II) between the two concrete slabs when loaded with the edge of the load over the center of the crack position. These conclusions led to the hypothesis that load-induced reflection cracking is a result of general or mixed mode fracture of the bituminous material occurring under the simultaneous interaction of -K1 (negative σx), K2, and K3. Laboratory testing of 2- and 3-dimensional model overlay pavements supported this hypothesis.

Sih's theory of fracture, based on the field strength of the local strain-energy-density, was utilized to analyze mixed mode crack propagation.[24] The amplitude or intensity of the strain-energy-density field is given by:

$$S = a_{11} k_1^2 + 2a_{12} k_1 k_2 + a_{22} k_2^2 + a_{33} k_3^2 \qquad (21)$$

The coefficients a_{ij} (i, j=1, 2, 3) are:

$$\begin{aligned} a_{11} &= 1/16\mu[(3-4\nu-\cos\theta)(1+\cos\theta)] \\ a_{12} &= 1/16\mu\ 2\sin\theta[(\cos\theta-(1-2\nu)] \\ a_{22} &= 1/16\mu[4(1-\nu)(1-\cos\theta)+(1+\cos\theta)(3\cos\theta-1)] \\ a_{33} &= 1/4\mu \end{aligned} \qquad (22)$$

where the polar angle is shown by figure 12 and μ is the Poisson's ratio. The k_i terms in equation 21 are related to the classical stress-intensity factors defined by Irwin.[26,27]

$$k_i = \frac{k_i}{\sqrt{\pi}} \qquad (23)$$

The two fundamental hypothesis of crack extension in Sih's theory are: [25]

- The crack will spread in the direction of maximum potential energy density, or minimum strain energy density.
- The critical intensity S_{cr} of this potential field governs the onset of rapid or brittle crack propagation.

In two-dimensional problems, the direction of crack

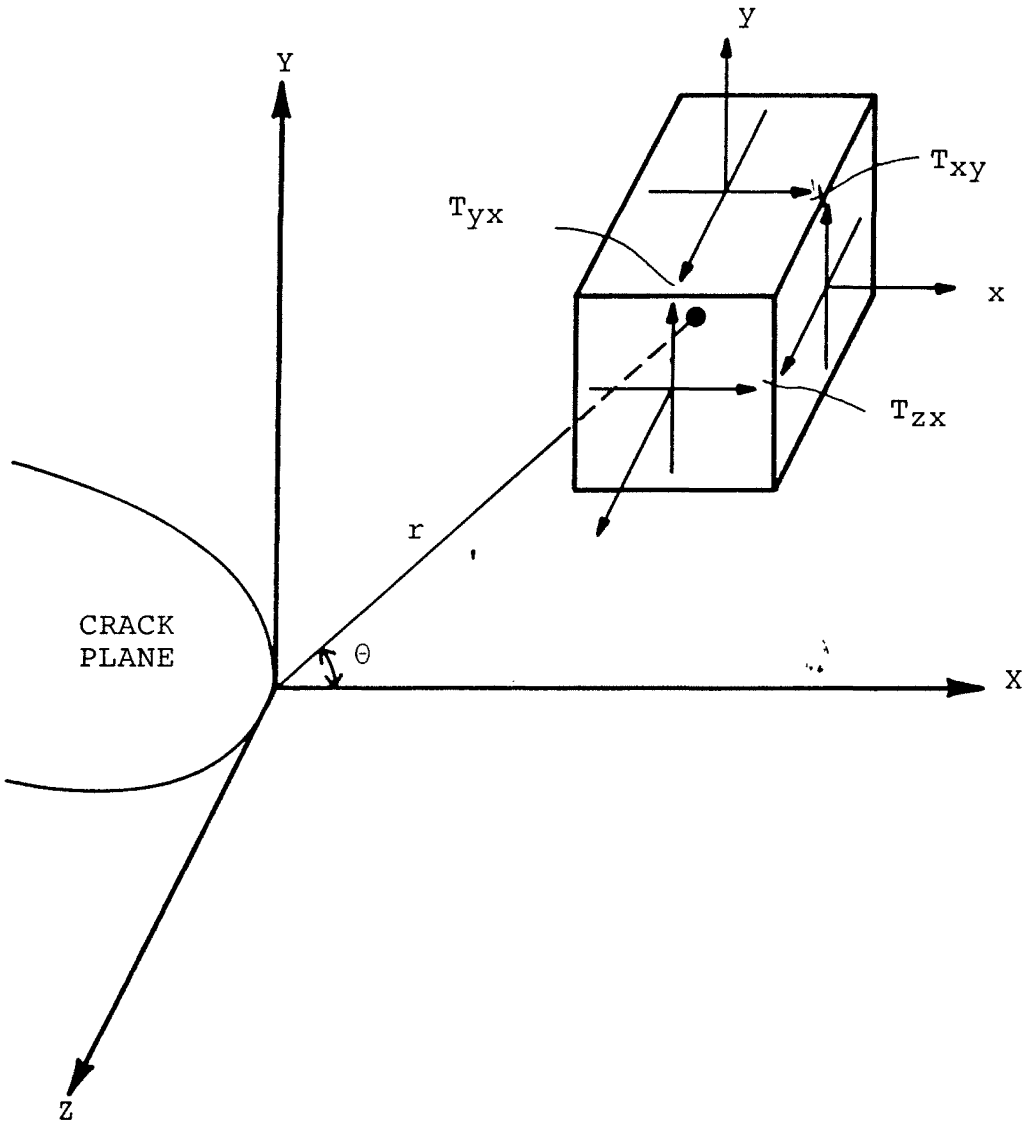

Figure 12. Stress components near crack border.

propagation θ_o is determined by writing the crack extension conditions in terms of the strain-energy-density function as:

$$\delta S/\delta\theta = 0 \qquad \delta^2 S/\delta\theta^2 > 0 \quad \text{at} \quad \theta = \theta_o \tag{24}$$

and solving equation (21) by calculus for θ_o and S_{min}.

In those cases where a fracture is not a rapid, unstable process, (i.e., the stress intensity factor under the applied load condition does not exceed the critical stress intensity factor, or the strain-energy-density factor S is less than the critical value S_{cr}) slow stable fatigue crack growth is presumed. Typically, crack growth laws relate the rate of change of crack length to the stress level or stress intensity factor such as:

$$\frac{dc}{dn} = A(\Delta K)^n \tag{25}$$

For mixed mode fracture the OSU model utilizes the crack growth law in terms of the strain-energy-density factor along the direction of fracture (S_{min}):

$$\frac{dc}{dn} = B(\Delta S\ min)^n \tag{26}$$

The fatigue life, or number of load applications to produce a crack through the overlay is given by:

$$N_f = \int_{c_o}^{c_f} \frac{1}{B(\Delta S\ min)^n} dc \tag{27}$$

where:

c = initial starter flaw
c = crack length at which the overlay is considered failed (either its thickness or the length at which the critical $S_{min}=S_{cr}$, is reached, whichever is less)

S_{cr}, B, and n are material constants derived from fatigue tests on asphaltic concrete beams.

The OSU-fracture mechanics model is not a complete method for predicting the occurrence of reflection cracking. An analytical method for computation of stress intensity factors and Smin (such as finite element model) must be coupled to a program

which calculates fatigue life in an incremental fashion using the growth law shown in equation 26. It is likely that a nomographic procedure could be developed from this model similar to that of Majidzadeh et al. for fracture mechanics prediction of load-associated fatigue cracking in flexible pavements.[27] Thus, further development of the OSU fracture mechanics model would be necessary before it could be implemented by pavement engineers.

2.2.4 TTI - Fracture Mechanics Model

The TTI model also uses fracture mechanics crack propagation theory to predict cracking.[29] Only Mode I fracture, and therefore the K_I stress-intensity factor, induced by horizontal thermal movements of the underlying layer, is considered. However, rather than the simple crack growth law given in equation 25, the TTI model utilizes Schapery's theory on crack growth in viscoelastic materials to develop the following growth law: [30]

$$\frac{dc}{dn} = B_t (\Delta K)^{2(1+1/m)} \tag{28}$$

where:

$$B_t = \frac{\pi}{6\sigma_m^2 I_1^2} \left[\frac{(1-\nu^2)D_2}{2r}\right]^{1/m} \left[\int_o^{\Delta t} W(t)^{2(1+1/m)} dt\right] \tag{29}$$

and

ν = Poisson's ratio

σ_m = maximum tension stress the asphalt concrete mixture can sustain

I_1 = a dimensionless integral between 0 and 2

Δt = the period of the load cycle

$W(t)$ = wave shape of the stress-intensity factor

m = slope of the straight line portion of the tension creep compliance curve for the asphalt cement binder

D_2 = intercept of straight line with log t = 0 on creep compliance curve

Γ = fracture energy density (force times displacement) to produce a unit area of crack surface

The TTI model is also not a complete procedure for predicting the occurrence of reflection cracking. It is merely a technique for obtaining crack growth laws without having to perform fatigue tests. Fatigue life is then obtained by integrating equation 28 from the limits of C to C , similar to that of equation 27 in the OSU fracture mechanics model. The limitations discussed for the OSU fracture mechanics model also apply to the TTI model.

2.2.5 RII - Phenomenological Model

Resource International engineers have developed a phenomenological model for crack prediction in overlaid flexible pavement structures which are reinforced by placement of engineering fabrics on the existing surface prior to overlay, as indicated in figure 13. The model considers only traffic load stresses in predicting the fatigue life of the overlaid pavement and has been utilized for the design computer program called HWYPAV-1.

The model was established after extensive laboratory testing was conducted which established the relationship between the fatigue life of reinforced and normal or unreinforced asphalt concrete beams. All fatigue tests were with beams placed on an elastic foundation tested at a constant load and temperature of 70 ^{o}F (21 ^{o}C). Figure 14 shows the general relationship between fatigue lives of the two beam types (reinforced and plain) as a function of load (strain). The performance factor of the fabric in enhancing fatigue and/or delaying reflective cracking, is called fabric effectiveness factor (FEF):

$$FEF = \frac{N_{f\ reinforced}}{N_{f\ reinforced}} \qquad (30)$$

where FEF is simply the ratio of fatigue lives as obtained from the beam tests. FEF generally ranges from 4 to 8 depending upon strain level, placement depth within the beam, and fabric type.

The FEF function is expressed as:

$$FEF = a_1 (\varepsilon_h)^{a_2} . GEO \qquad (31)$$

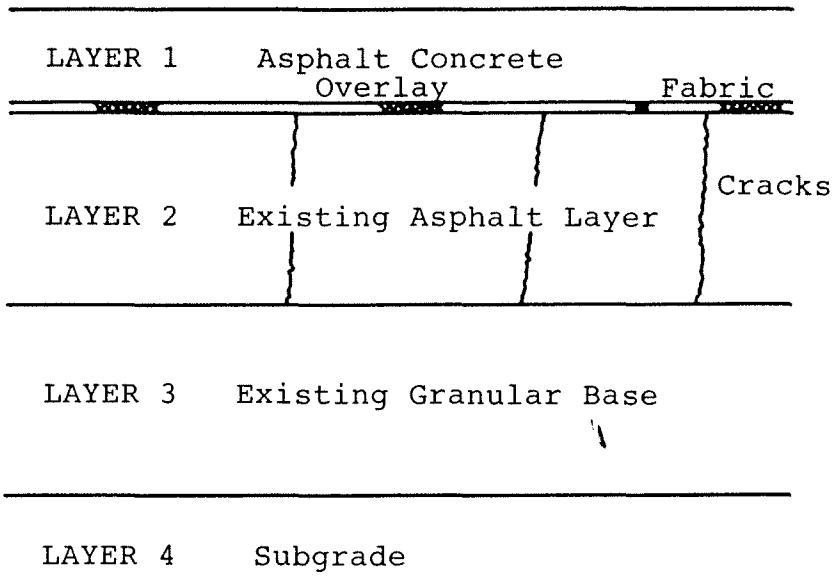

Figure 13. Fabric - reinforced asphalt overlay.

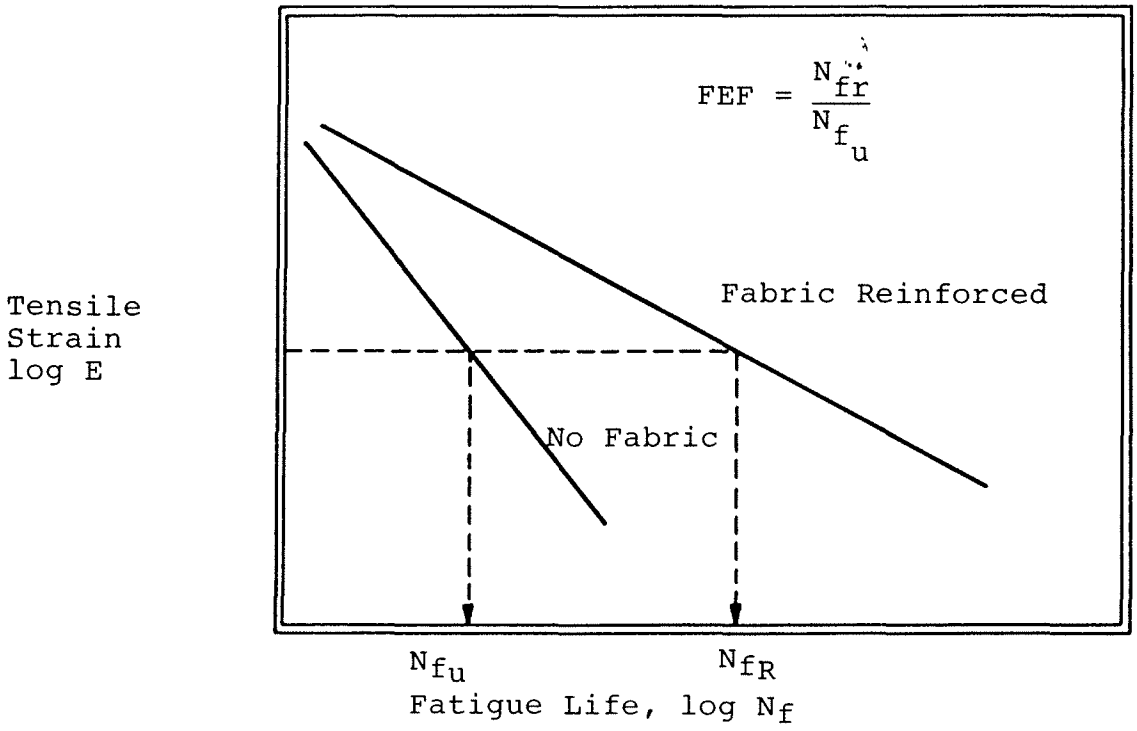

Figure 14. Fabric effectiveness in fatigue.

where:

a_1 and a_2 = constants depending upon fabric type

ε_h = horizontal strain at the bottom of the existing asphalt bound layer, in/in

GEO = geometry factor which considers depth of fabric placement relative to neutral axis, as shown in figure 15.

The fatigue life of the pavement in the HWYPAV-1 program is:

$$N_f = N'_{f_u} \cdot FEF \qquad (32)$$

where:

N_{fu}' is a strain dependent distress function for asphalt concrete developed from AASHO Road Test data.

Cracking of the existing pavement is accounted for by reducing the elastic modulus of this layer. The HWYPAV-1 program uses the elastic modulus of multilayer program ELSYM-5 [31] to calculate pavement strains.

The RII model has the following limitations:

- Since the model is phenomenological, the mechanics of crack propagation and crack arrest are not identified.
- FEF values need to be investigated to determine if they are temperature or scale dependent. FEF values were established from small beam test, and may differ from those under full-scale conditions.

2.2.6 Arkansas Model

Recently McCullough et al. modified and revised the ARE procedure (described in section 2.2.2) to make it applicable to the Arkansas open-graded relief layer, which is similar to that recommended by the Asphalt Institute and used in this study as one of the treatments in overlays of rigid pavements.[32] The improvements include a new restraint relationship (slab measurement vs. subbase friction), inclusion of the effect of an intermediate layer, improved shear strain model, and the development of a fatigue damage model. The most significant improvement is the consideration of fatigue based on differential slab movement for load-associated shear, and horizontal thermal

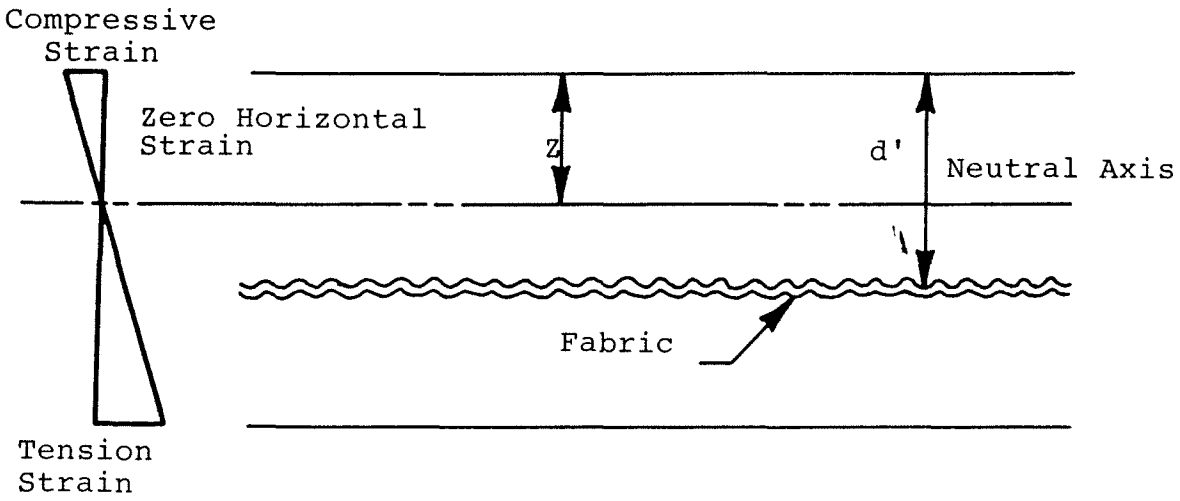

Geometry Adjustment for Depth of
Fabric Placement in Asphalt Layer

Note: For overlay design d' equals the overlay thickness.

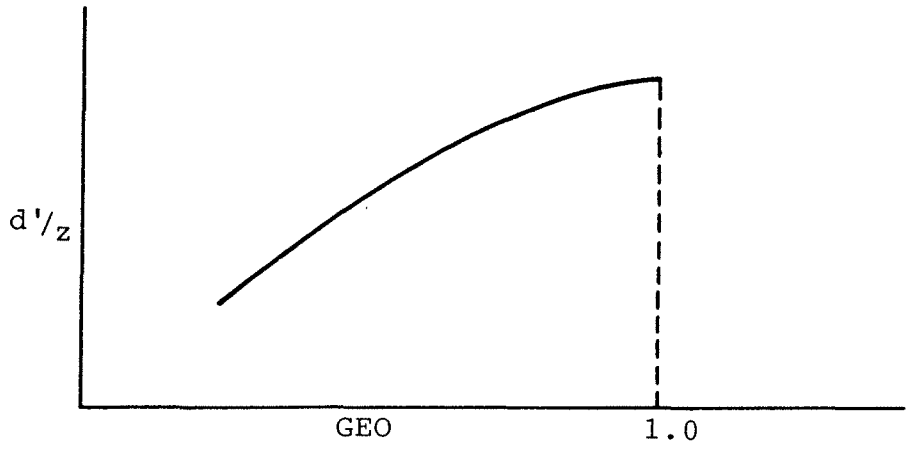

Figure 15. Effect of location on the geometric factor, GEO.

movements for thermal fatigue. A new fatigue distress function has been developed for this purpose; but, it is not clear on what basis this function was derived. The authors emphasize that the model is calibrated to field conditions; however, only a few projects were used, so the validity is open to debate.

Other improvements in the model include decreasing the amount of detailed field measurements required for pavement characterization. The model now requires only measurements of the load transfer ratio across joints and/or cracks, and slab horizontal movement with temperature, in addition to average crack/joint spacing; and the slab movement measurements can be avoided if the recommendations of the OAR procedure are followed, i.e., if a friction factor between slab and its support is assumed, the slab movement can be calculated from temperature changes.[33]

This version of the reflection cracking model is an improvement over the older ARE model; but, most of the limitations of that model apply here also, since the same rather simplistic theory has been used in stress analysis.[22]

2.2.7 Schapery Viscoelastic Model for Metals

Schapery and others investigated the problem of modeling crack initiation, propagation, and unstable failure in a viscoelastic medium.[34] In their work, the above reseachers developed a theoretical model for predicting the time to fracture initiation and crack tip velocity using assumptions that the second derivative of the logarithm of creep compliance with respect to logarithm of time is small. This work is an extension to Dugdale cohesive zone fracture model.[35]

Considering figure 16 for normal stress along the crack plane defined by y = o, the crack front is parallel to the z-axis with its tip located at x = a(t) relative to the fixed coordinate system x-y-z. Following Dugdale cohesive zone fracture model, the material exhibits non proportional behavior in the zone 0 < r < where is the length of this cohesive zone. Outside this zone, Dugdale assumed that the material exhibits elastic properties, while Schapery and others assumed that the material exhibits linear, isotrogic viscoelastic behavior. The stress σ_f is called the "failure stress" and represents the reaction of the failing material near the tip on the surrounding linearly viscoelastic medium. In Schapery's work, the three most important equations relavent to this work are written below as equations 33 through 36. The requirement of finite stress at the crack tip yields an equation of the form:

$$\alpha = \frac{\pi}{2}(Ki/\sigma_m I_1)^2 \qquad (33)$$

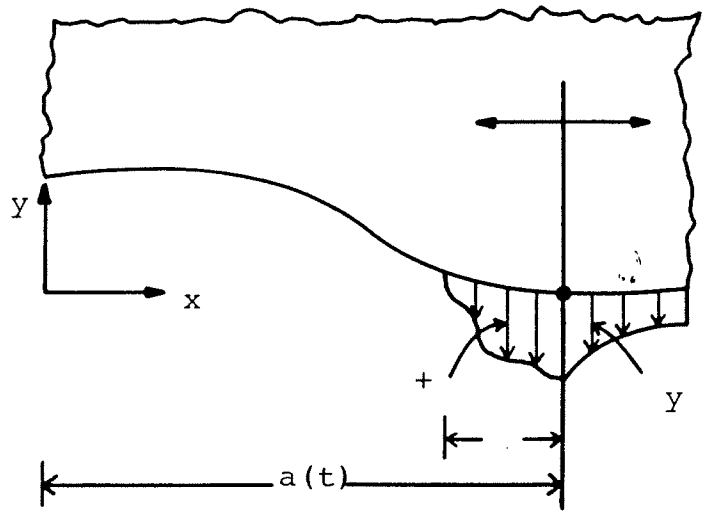

Figure 16. Normal stress along crack plane.

and

$$I_1 = \int_0^1 f\, \eta^{\frac{1}{2}} d\eta \qquad (34)$$

where:

α = length of the cohesive zone

K_1 = mode I stress intensity factor

σ_m = the maximum value of

ξ = dummy variable

The opening displacement, v, in the neighborhood of the tip is:

$$v = \frac{1}{2\pi} \int_{t_1}^{t} C_v(t-\tau) \frac{2}{2\tau} \left\{ \int_0^{\alpha} \sigma_f(\xi\xi') \; 2(\xi/\xi')^{\frac{1}{2}} - \right. \qquad (35)$$

$$\left. \ell\eta \left[\frac{(\xi)^{\frac{1}{2}} + (\xi)^{\frac{1}{2}}}{(\xi)^{\frac{1}{2}} - (\xi)^{\frac{1}{2}}} \right] d\xi' \right\} d\tau$$

where: $t > t_1$ and $\xi' = \xi(x, \xi) = a(\xi) - x$.

$C(t-\xi)$ = creep compliance

ξ, ξ' = dummy variables

The crack growth rate $\dot{a}$ has also been found to be:

$$\frac{da}{dt} = \frac{\pi}{2} \left[\frac{C_2}{8\Gamma[1-(K_1/K_g)^2]} \right]^{1/m} \lambda_m^{1/m} \; \frac{K_1^2(1+1/m)}{\sigma_m^2 \, I_1^2} \qquad (36)$$

where:

λ, m, C_2 = creep compliance parameter

Γ = function that depends on the creep compliance stress intensity factor

K_1, K_g = short and long decades stress intensity factor

Although the TTI model is based upon Schapery's work, the lack of prediction of the occurrence of reflection cracking procedure and the use of time independent mode I stress intensity factor lead this model to be of limited laboratory and field implementation.[28] The model developed in this work, on the other hand, was geared towards addressing the above two limitations, as well as establishing easy-to-find model parameters. If time dependency is excluded from consideration, then a simple model will result; however, it is doubtful that this model will predict thermal-induced cracking and failure time in a satisfactory manner. More details about the development of the mechanistic model, fitting to small scale and large scale test data, effect of fabric treatment, and implementation procedures are discussed in a later section of this report.

CHAPTER III. DEVELOPMENT OF THE ANALYSIS MODEL

3.1 Overlays of Rigid Pavements

Simulation of reflective cracking of rigid pavement overlays requires modeling of both thermal and traffic loading conditions. As previously noted in the literature review, thermal stresses result from both seasonal and daily changes in slab temperature.

The thermal loading can be represented by the superposition of two different thermal conditions:

- Uniform change (ΔT) in slab temperature. This condition represents seasonal changes in average slab temperature which occur over long time periods.

- "Pure" curling. This condition represents the daily or short-time-period temperature variation within the slab. For "pure" curling, the average slab temperature has not been changed; however, the top of the slab is colder than the bottom of the slab with the temperature assumed linearly related to slab depth. The curling gradient (CG) is given in degrees per unit thickness of the slab.

Figure 17 shows the representation of thermal loading using these two definitions. Reference temperature (To) is the "zero-stress" temperature for the overlay. Slab temperatures below T will transfer tensile stresses to the overlay. Figure 18 shows the expected monthly average slab temperature and curling gradient for overlaid concrete slabs in Ohio. This figure is based upon computer prediction of pavement temperature developed from field temperature measurements at several pavements in the central Ohio area.[21] Slab thickness varied from 8 to 10 inches (203 to 254 mm) and asphalt overlay thickness varied from 2.5 to 5.0 inches (63.5 to 127 mm) for the pavements used in the Ohio study. Figure 18 provides an estimate of the thermal load magnitudes. Expected curling gradients (CG) vary from .5 ^{o}F/in. (.01 ^{o}C/mm) in the spring and fall to about 1 ^{o}F/in. (.02 ^{o}C/mm) in the winter months. Mean slab temperature changes by about 40 ^{o}F (22.2 ^{o}C) from summer to winter, dropping at a rate of about 8 ^{o}F (4.4 ^{o}C) per month during the fall. This is the range of thermal loading parameters which should be simulated in the laboratory testing.

The manufacture of full-scale pavement models and subjecting them to actual thermal loads as experienced in the field, is neither economically feasible nor possible in the laboratory. Therefore, model pavements, with external forces applied to produce joint movements equal to those of full

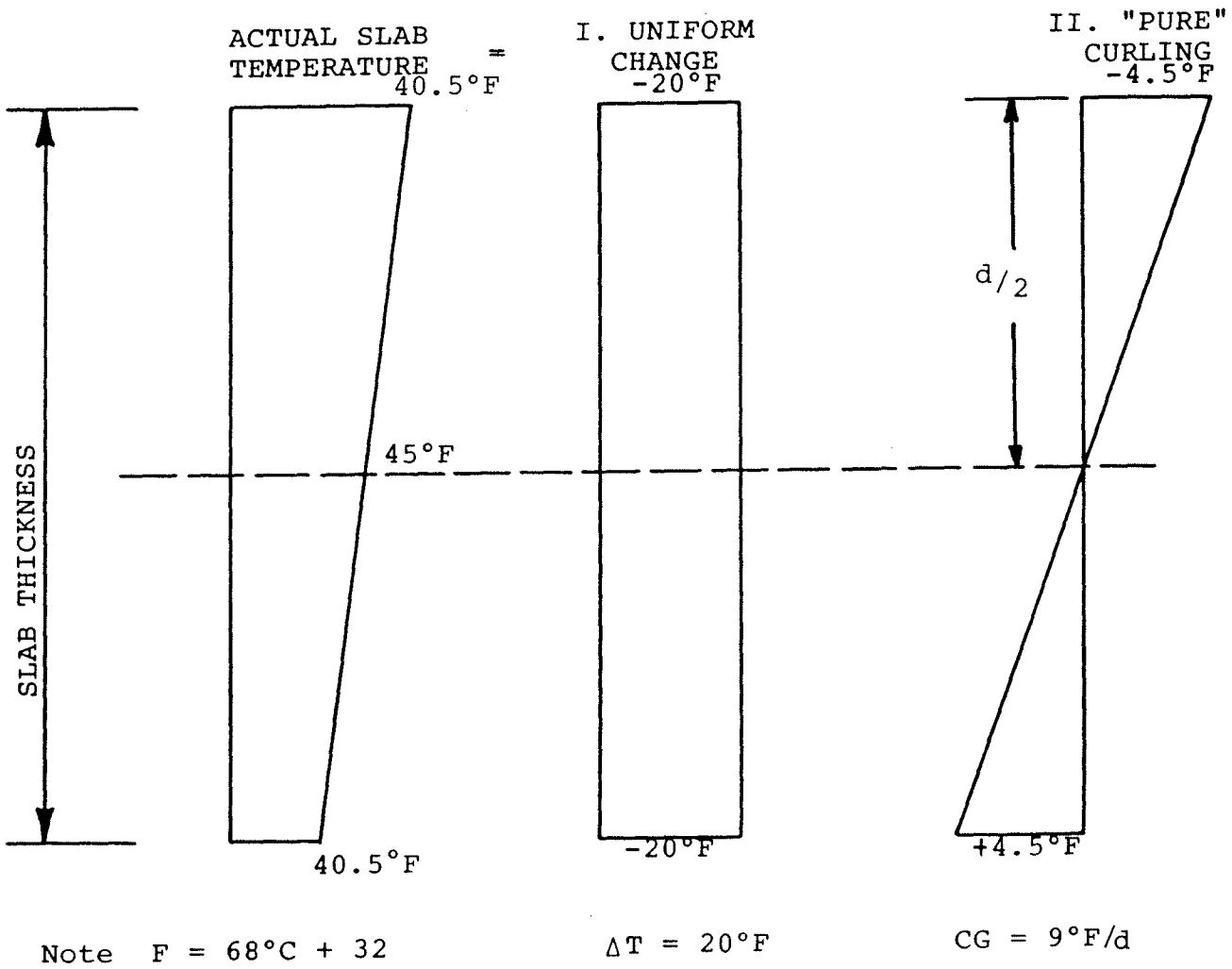

Figure 17. An example of PCC slab thermal loading.

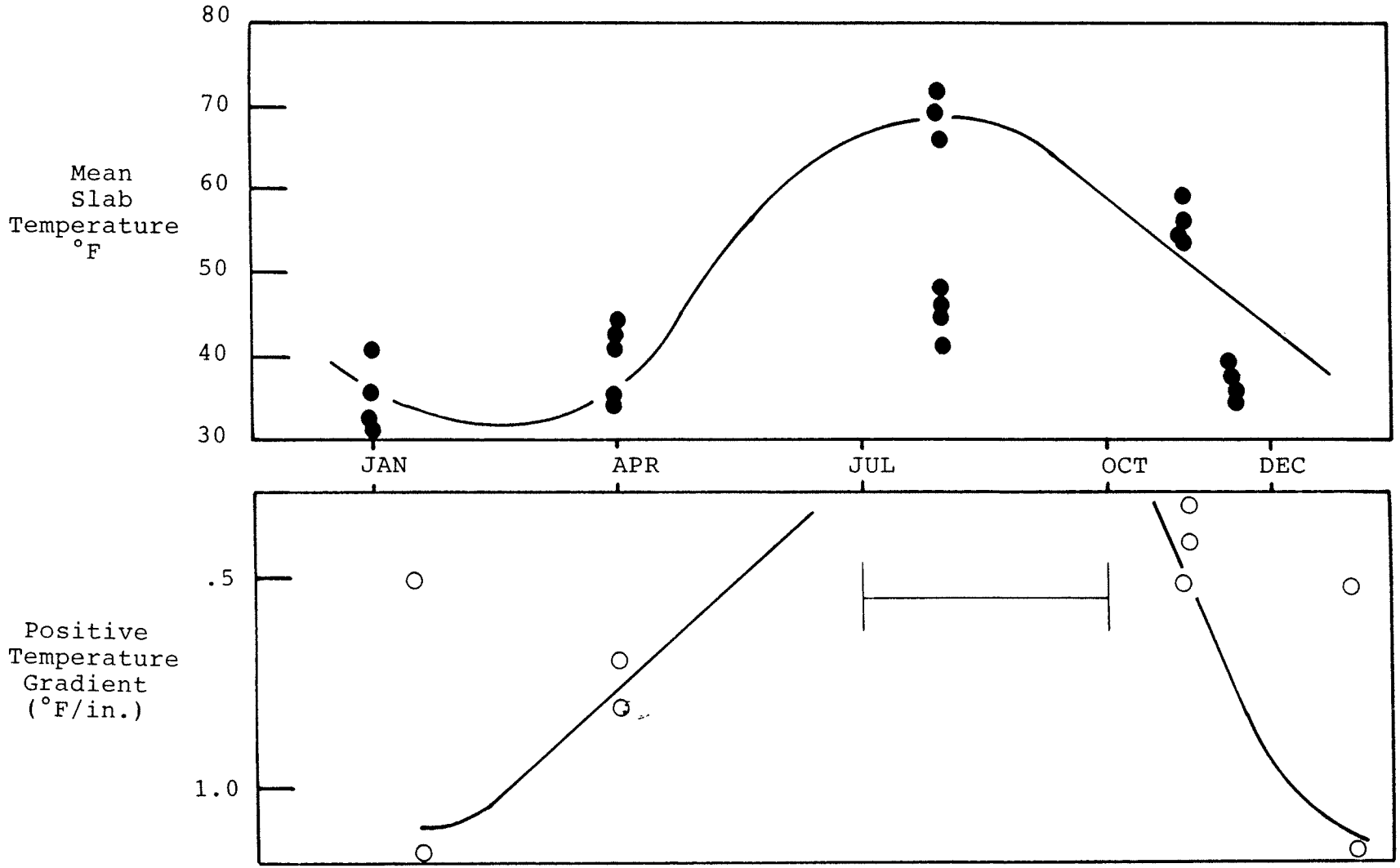

Figure 18. Expected pavement temperature and curling temperature gradient.

scale pavements under field thermal loadings, are utilized. Uniform or seasonal reductions in slab temperature can be simulated by applying horizontal tensile forces to the PCC slabs which produce joint openings similar to those of full scale pavements. Traffic forces are simulated by applying dynamic vertical loads to the model pavements, with the model supported on an elastic foundation similar to previous work at OSU.[25,28] The most difficult simulation is the curling of the PCC slab. Recent studies at the University of California and PCA were not successful in inducing temperature curling of model PCC slabs.[36,37] Thermal gradients are difficult to establish in the laboratory. In addition, the gradients necessary to curl model slabs of short length have to be very large to produce the same curled shape as full-scale slabs. This is because the curling deformation is directly proportional to slab length, L, squared.

3.1.1 Initial Investigation

Based upon the difficulties in modeling curling, and the shortcomings of the OSU Ultimate Strength Model (previously discussed) in predicting the significance of overlay stresses resulting from slab curling, a theoretical investigation of curling in full-scale slabs was conducted. The purpose of this investigation was to determine the stresses in the overlays by curling, and to determine if curling could be equated to uniform temperature change. Specifically, does curling produce horizontal joint opening; and if so, could these stresses be equated to joint opening resulting from uniform temperature change (ΔT)?

A 2-D finite element analysis using the SAP IV program of the full-scale pavement, shown in figure 19, was completed.[38] As shown in figure 19, only asphalt overlay modulus and overlay thickness were varied in these analyses. Slab length was 20 feet (6.1 m) in all cases. Two separate thermal loading conditions were analyzed: 1) a uniform reduction (ΔT) of 30 ^{o}F (16.7 ^{o}C) in slab temperature, and 2) "pure" curling with gradient (CG) of .5 ^{o}F/in. (.01 ^{o}C/mm). For constant overlay thickness and modulus, overlay stresses and joint opening were found to be linearly related to T and CG. Both full friction (no slip) and no friction (slip), between the PCC slab and aggregate base, were investigated. Full friction reduced overlay maximum stress by less than 6 percent for uniform temperature change and 4 percent for curling, as compared to the no friction condition. Full bond between asphalt overlay and PCC slabs was assumed in all cases.

Figures 20 through 23 show computed stresses in the overlay at the center of the joint as a function of depth (z). In all cases, for both curling load and uniform temperature change, maximum stress occurs at the bottom of

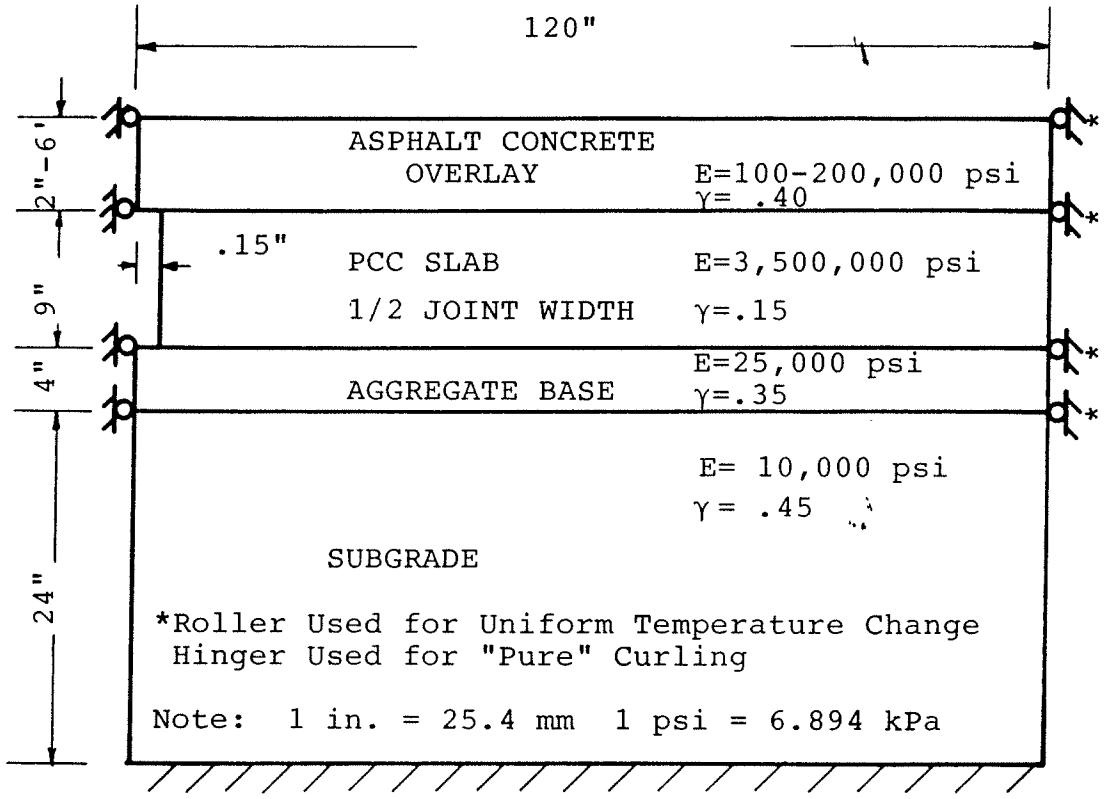

Figure 19. Schematic 2-D finite element model.

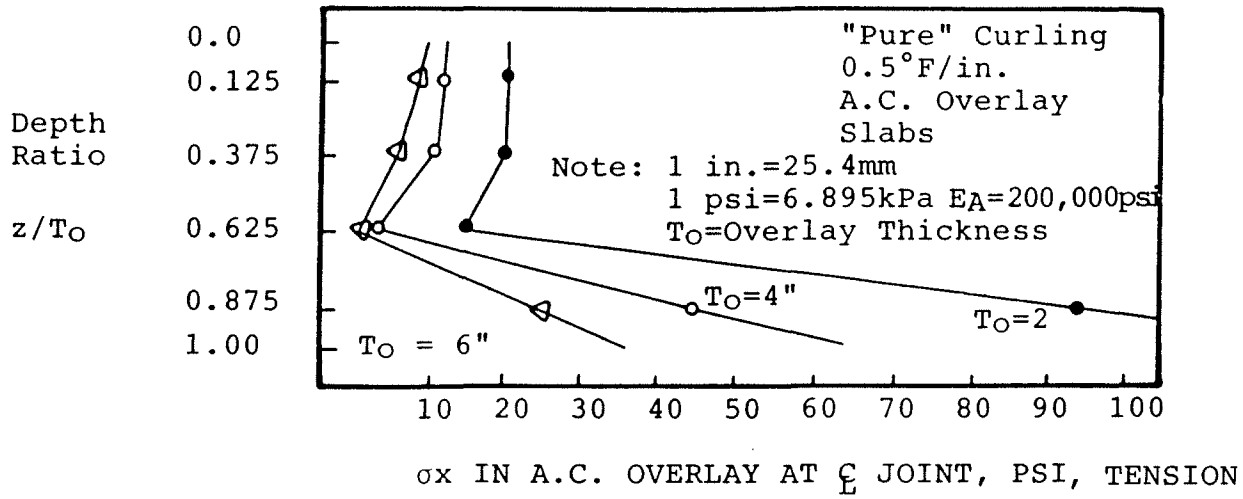

Figure 20. Stress distribution in overlay due to "pure" curling.

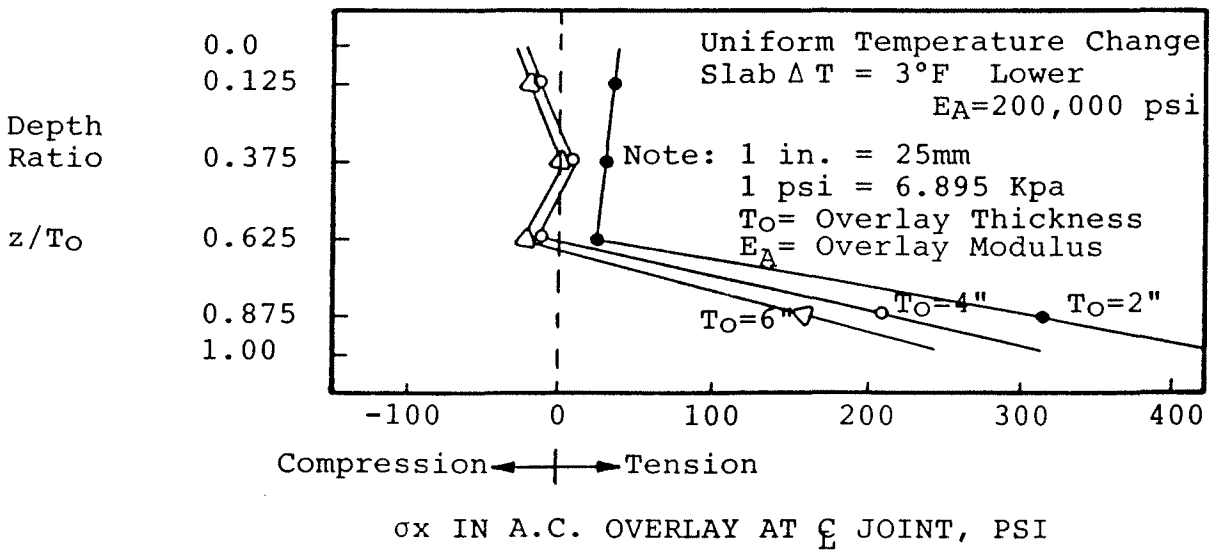

Figure 21. Stress distribution in overlay due to uniform temperature change.

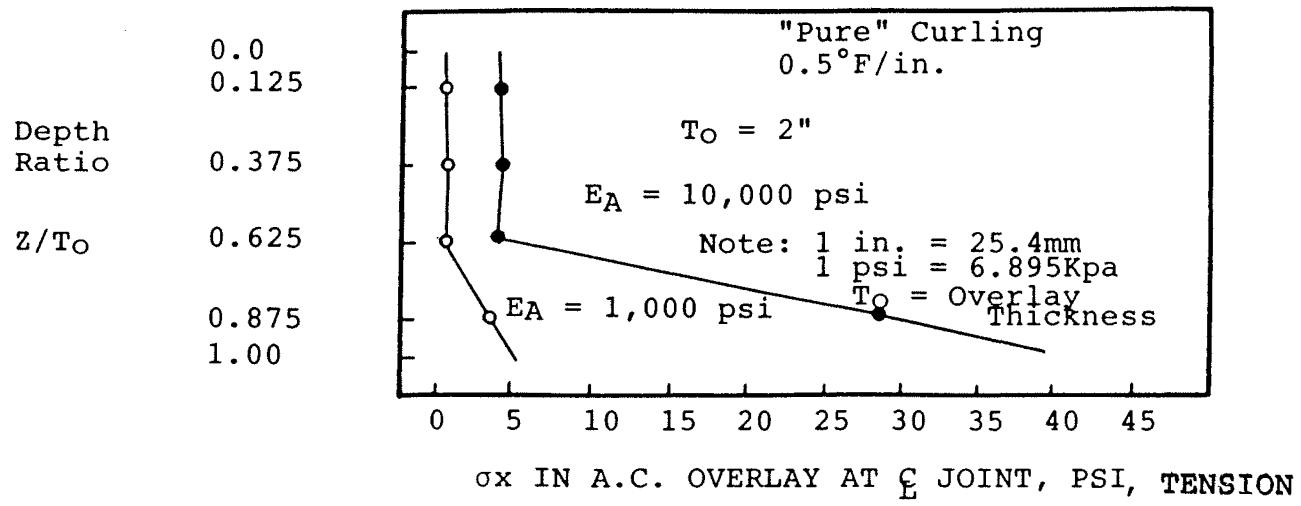

Figure 22. Stress distribution in overlay due to "pure" curling.

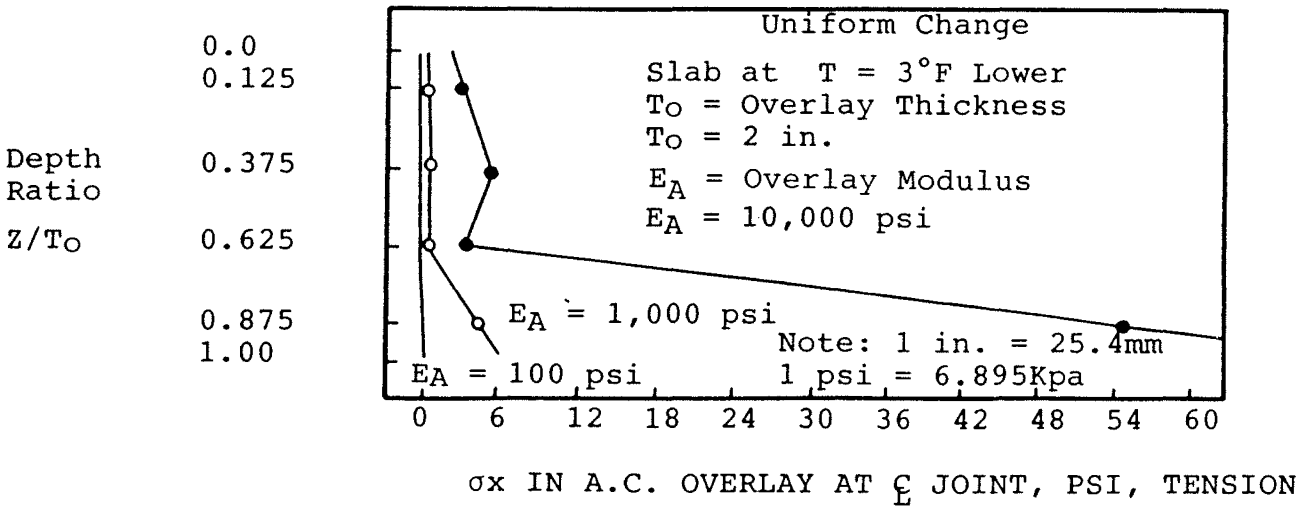

Figure 23. Stress distribution in overlay due to uniform temperature change.

the overlay. The stress distributions are very similar for the uniform temperature change and curling loading conditions. The similarities occur throughout the range of overlay thickness (To) and overlay moduli (Ea) investigated in the study. (Note that a T of 3 ^{O}F (1.67 ^{O}C) was used to plot figures 21 and 23 simply to provide stresses of closer magnitude to those of the curling load. (It should be noted that stress is linearly related to ΔT). Figures 20 and 22 show that for curling load, the overlay stress at the joint in the horizontal (X) direction is tensile throughout overlay depth, rapidly increasing in magnitude below .6 times the overlay thickness.

Figures 24 and 25 show the computed shear stress at the overlay/slab interface. Again, the stress distributions are similar for the two loading conditions. These shear stresses would have to exceed the tack coat bonding stress to cause slippage between the two layers. The maximum shear stresses are well above the 6 to 10 psi (41 to 69 kPa) bonding stresses, suggested in reference [21], but are generally below the bonding stresses given by ARE in table 1.[22] Figure 26 shows the effect of breaking the bond, either by slippage or introduction of a bond breaker, upon maximum overlay stress. A dramatic reduction in stress is predicted for bond breaker lengths as short as 1 in (25 mm). Figure 26 indicates that the ARE model, which simply uses bond breaker length to increase gage length for the overlay stress calculation, probably underestimates the stress reduction by a significant amount.[22] Thus, the bond condition between overlay and slab will be an important parameter in laboratory testing. Figure 26 indicates that improper bonding near the joint could affect test results greatly.

The high sensitivity of overlay stress to overlay stiffness is clearly demonstrated in figures 27 and 28. As noted earlier, ARE suggests that creep modulus, Ec, be utilized for stress calculations. However, Ec is both temperature and time-of-loading dependent. Figure 29 presents this dependency for a typical dense-graded asphalt concrete, with Ec calculated by the Heukelom and Klomp (or Shell) procedure.[23] This procedure determines the compressive creep modulus. The tension creep modulus is actually needed for reflection cracking analysis; however, no procedure for predicting tension creep modulus has been published. If tension creep modulus curves are similar to those of figure 29, then the implications to thermal reflection cracking analysis and modeling are very significant. An incremental analysis which utilizes the loading time and temperature-dependent creep modulus would be necessary to calculate overlay stresses and joint opening. Seasonal changes occur over long periods of time (time required to drop from T by T amount), while curling can occur over relatively short time periods (less than 1/2 day) and at all temperatures. The fact that curling occurs over

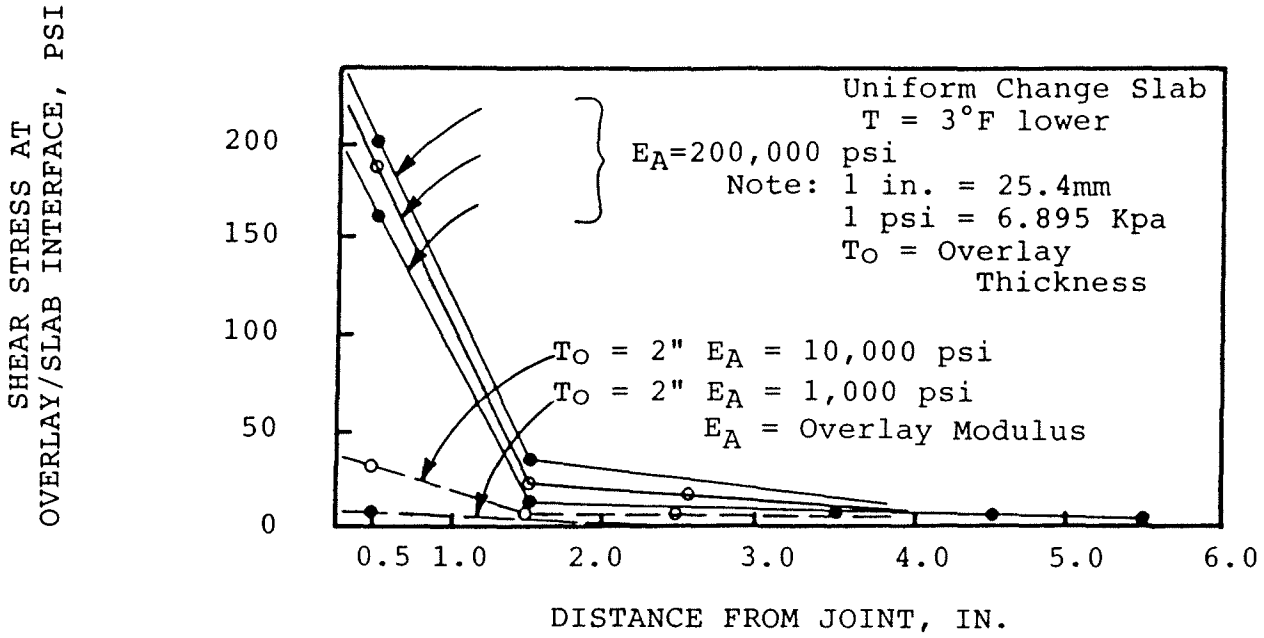

Figure 24. Shear stress distribution in overlay due to uniform change in slab temperature.

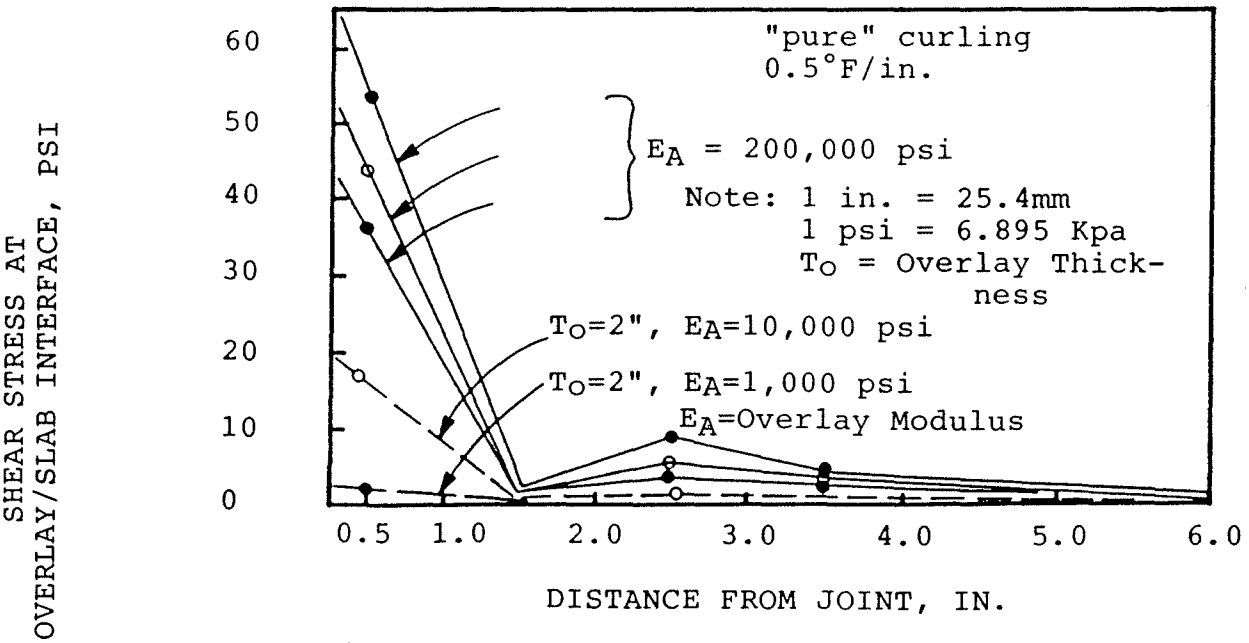

Figure 25. Shear stress distributions in overlay due to "pure" curling.

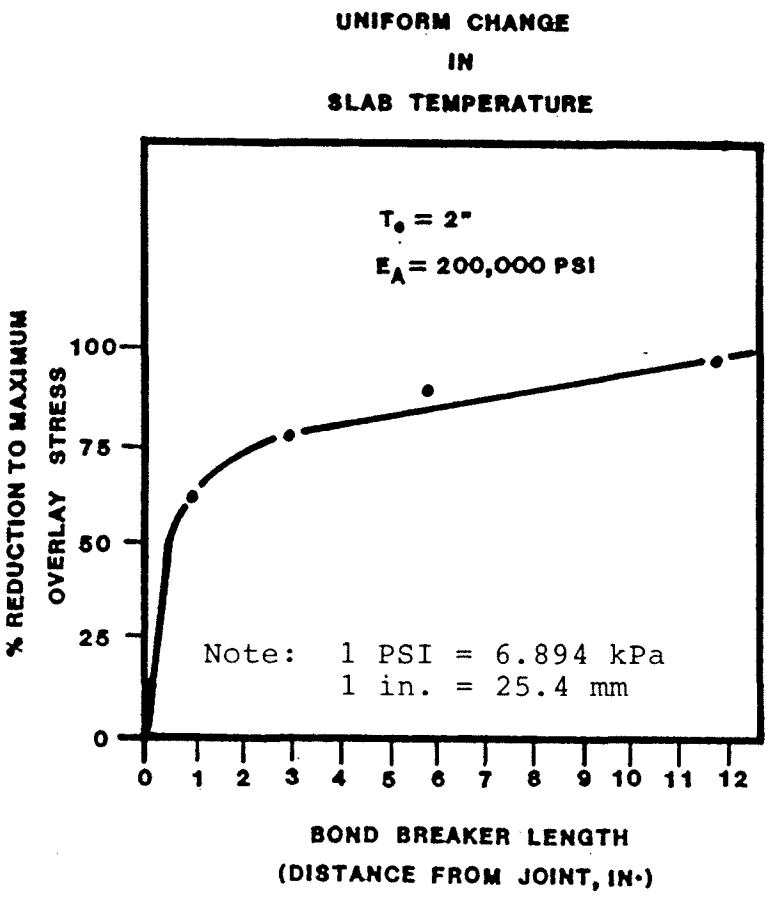

Figure 26. Stress reduction with bond breaker length.

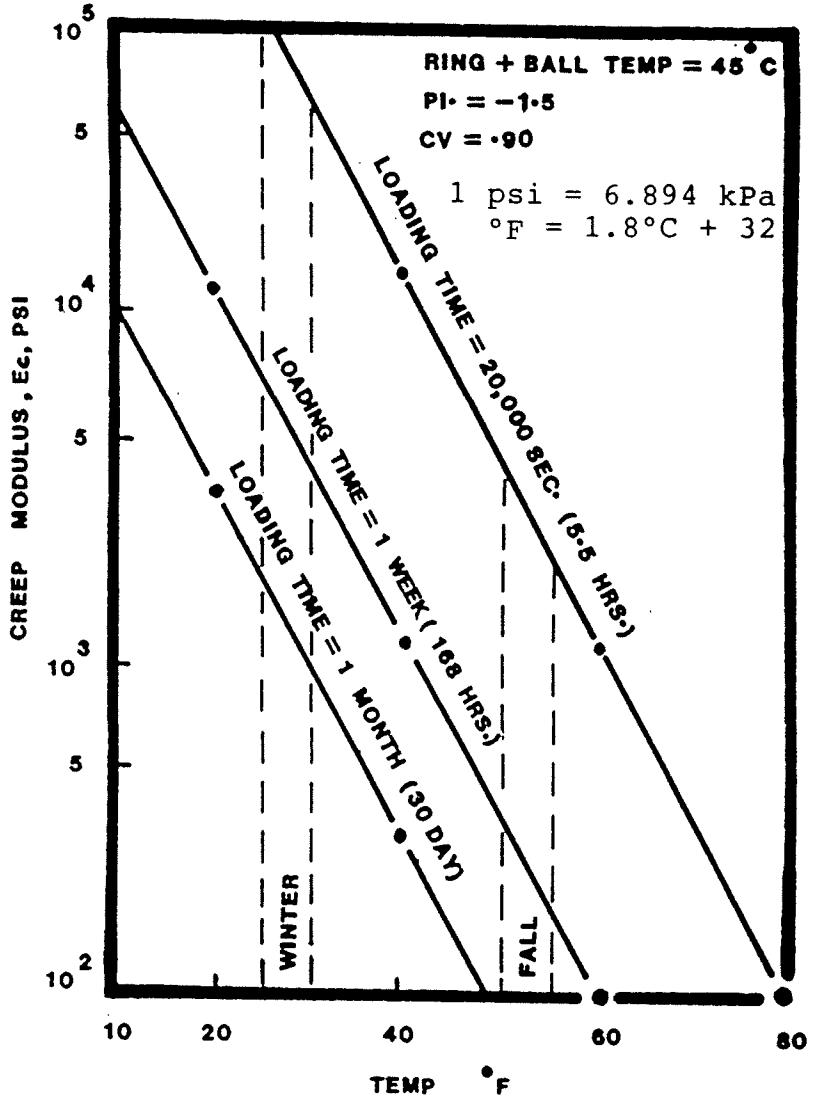

Figure 27. Creep moduli with temperature.

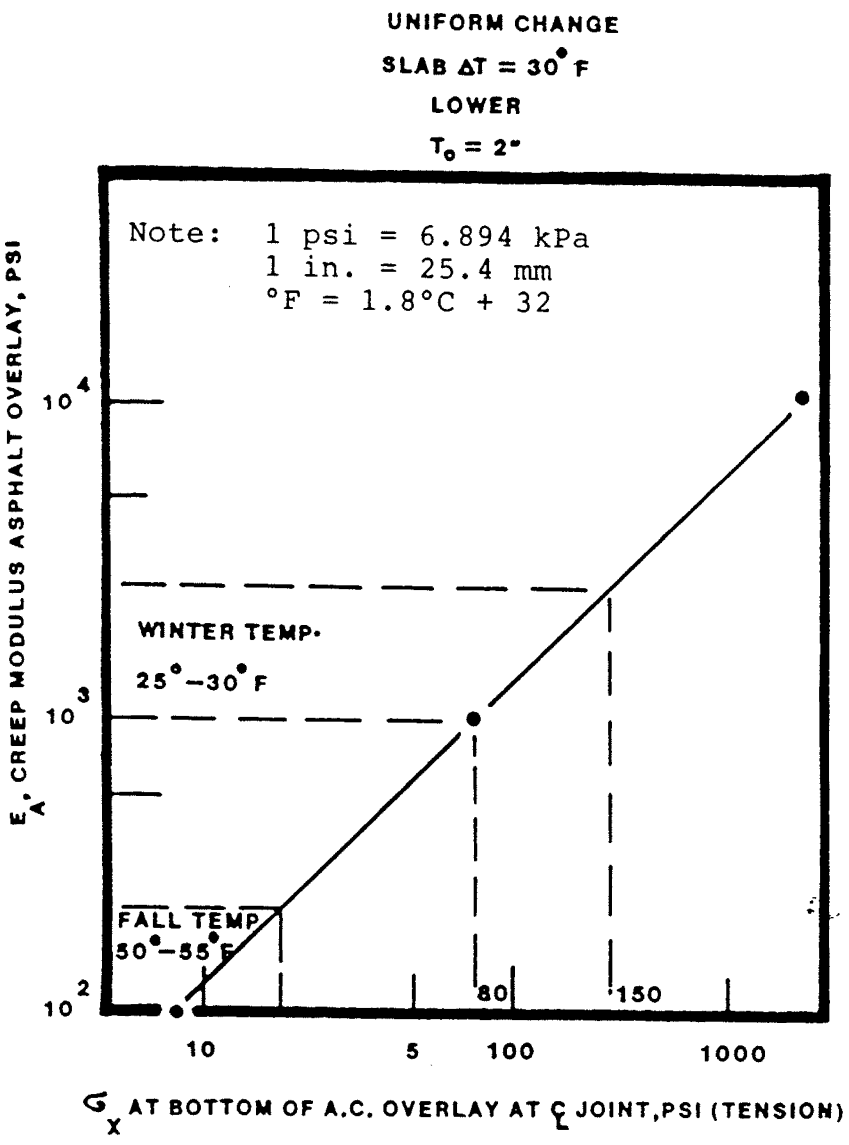

Figure 28. Stress due to uniform temperature change.

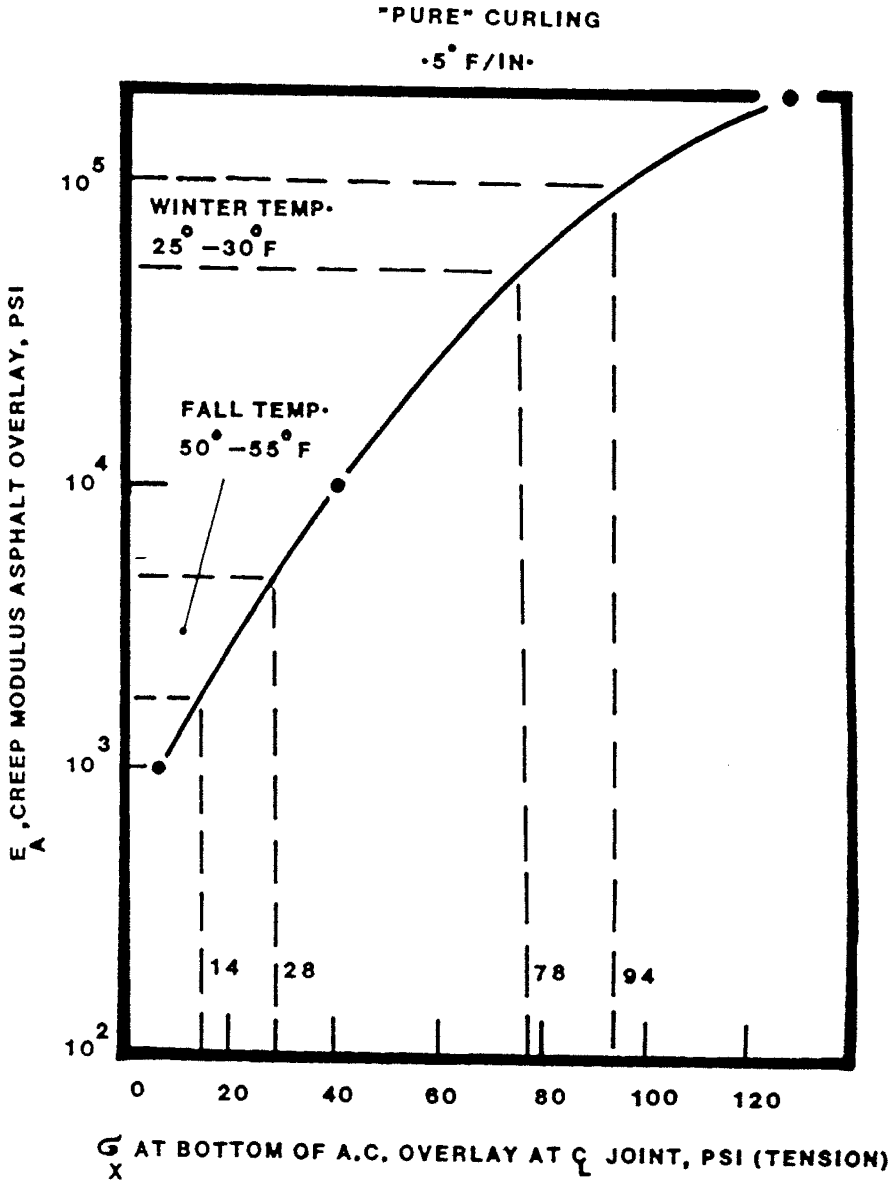

Figure 29. Stress due to curling.

shorter loading times than seasonal uniform temperature change means that a higher Ea should be used for curling load than for uniform temperature change stress calculations. The higher Ea will result in higher overlay stresses which should be considered when comparing seasonal and curling-induced loading conditions.

Figures 27 and 28 can be used to compare the two thermal loading conditions. In the fall (temperature 50 to 55 °F (10 to 13 °C)) Ea of 100-200 psi (689 to 1379 kPa) for uniform slab temperature change (1-month loading time) and Ec of 2000 to 5000 psi (13.8 to 34.5 MPa) (5.5-hour loading time) for curling loading is obtained from figure 29. From figures 27 and 28 the curling load would produce a stress of about 21 psi (145 kPa), while the uniform temperature change (ΔT=30 °F (16.7 °C)) produces a stress of about 12 psi (83 kPa). On the basis of equal maximum overlay stress, the two loading conditions can be equated by CG =(σ x curl/ σ x seasonal) (ΔT)

$$0.5\ ^\circ F/in = (21/12)(30) = 52/5\ ^\circ F$$

or: (37)

$$0.01\ ^\circ C/mm = 26.7\ ^\circ C \text{ seasonal change}$$

Therefore a seasonal change of 52.5 °F (29.2 °C) would be required to produce the same overlay stress as curling with CG = .5 °F/in (.01 °C/mm). Similar analysis for winter temperature ranges, (20 to 25 °F (-6.7 to -3.9 °C)), yields the following equation:

$$0.5\ ^\circ F/in \text{ curl} = 22.4\ ^\circ F \text{ seasonal change}$$

or: (38)

$$0.01\ ^\circ C/mm \text{ curl} = 11.4\ ^\circ C \text{ seasonal change}$$

Since both curling and seasonal change produce joint opening, which induce similar overlay stress distributions, it is believed that it is reasonable to equate the two loading conditions, in this manner. The ability to equate curling loads to seasonal changes is important since laboratory tests need not try to induce curling in the PCC slab. Uniform temperature changes can be simulated by applying horizontal tensile forces on the PCC slab which produce joint opening. The amount of joint opening is a function of the T and slab length L being simulated. Seasonal temperature change, T, could be converted to equivalent curling gradient, CG, using equations similar to equations 37 and 38. Therefore, simulated temperature conditions at the time of failure, or cracking of the laboratory model could be expressed as either ΔT or CG at the test temperature for a full-scale slab of length L.

Figure 30 shows the relationship between overlay modulus and predicted joint displacement for the finite element model. For Ea below 1500 psi, (10.3 MPa), movement nearly equals that for free unrestrained thermal movement (α . ΔT .L/2). From figure 27, the expected modulus is below 1500 psi (10.3 MPa) for long loading times (greater than 1 month) and temperatures greater than 25 ^{o}F (-3.9 ^{o}C). Laboratory test temperature and loading times should be chosen, such that the tension creep modulus of the overlay will be less than 1500 psi (10.3 MPa). The joint opening can then be calculated using the $\alpha.\Delta T.L/2$ expression. This will simulate joint openings which occur in real pavements at temperatures above about 25 ^{o}F (-3.9 ^{o}C).

Figure 31 shows that overlay stress is linearly related to displacement at the top of the joint. The slope of the stress-joint displacement line is a function of overlay modulus. The overlay stresses are independent of the type of thermal load. At constant overlay modulus, a horizontal displacement of x will produce the same overlay stress x regardless of whether this displacement was produced by slab curling or uniform temperature change. This is further evidence that curling can be equated to seasonal temperature change.

3.1.2 Traffic Loading

Both theoretical considerations, as well as various field installations of treatments to retard reflection cracking, indicate that traffic loading can cause or accelerate crack formation, particularly if the load transfer of a crack/joint is relatively low. Both the ARE and the Arkansas methods assume that differential shear forces are responsible.[22,30] However, preliminary investigations with the SAPIV finite element program indicate that in the absence of voids or partial support under one slab, the critical stress occurs when the traffic loading is directly over the joint; the joint at this point acts as a stress concentrator.[38]

These considerations led up to the development of a general elastic analysis program that could compute the stresses in the overlay due to all the types of loading, namely traffic loading and thermal loading due both to daily variations in the vertical temperature gradient and to variations in seasonal concrete average temperature. The resulting EFRON program is described in section 3.3.

3.2 The Elastic Model

Field and laboratory data have indicated that fabrics imbedded in pavement structures enhance the fatigue life and retard reflection cracking. To support these significant experimental data, various mechanistic models have been

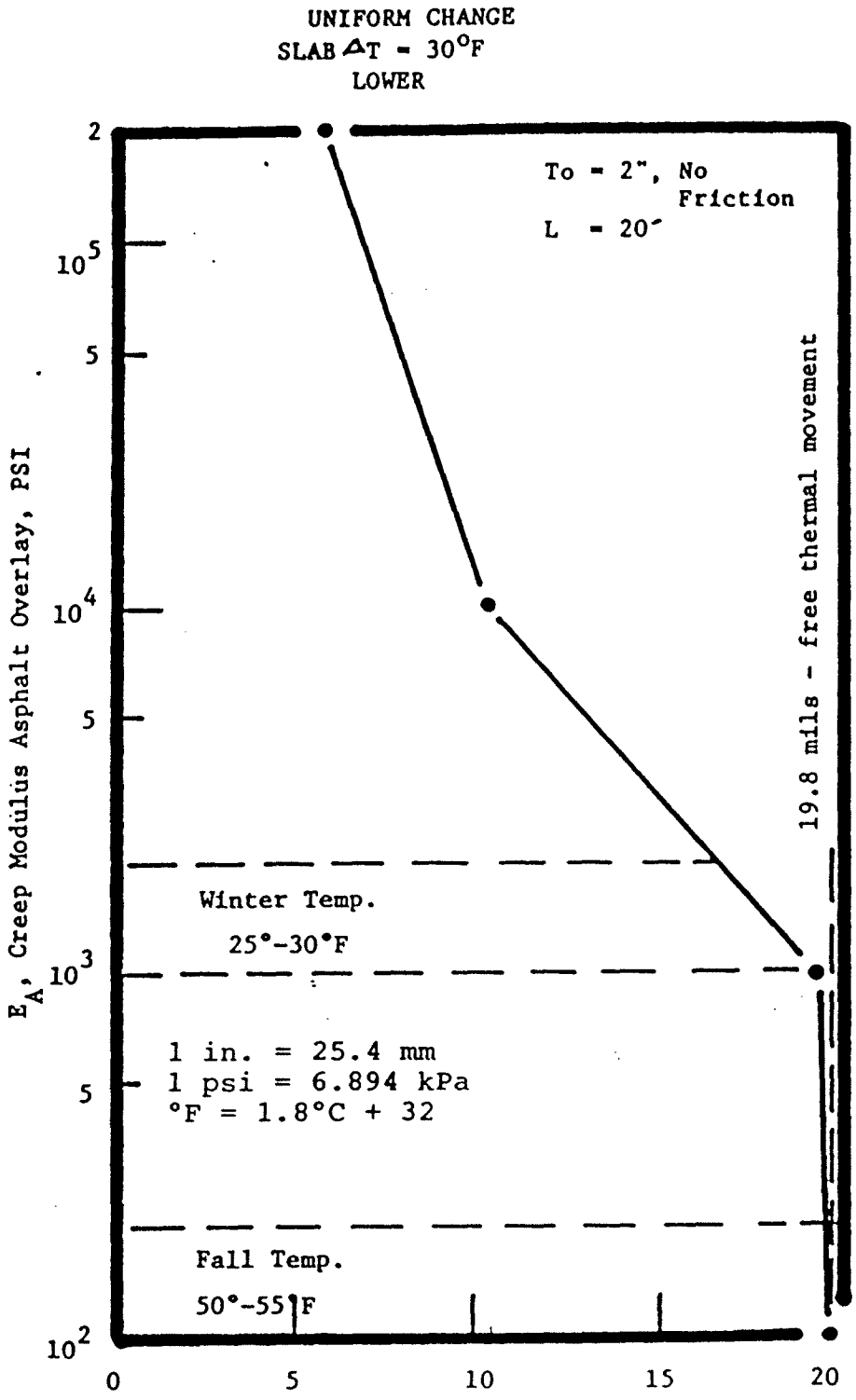

Figure 30. Joint opening as a function of overlay modulus.

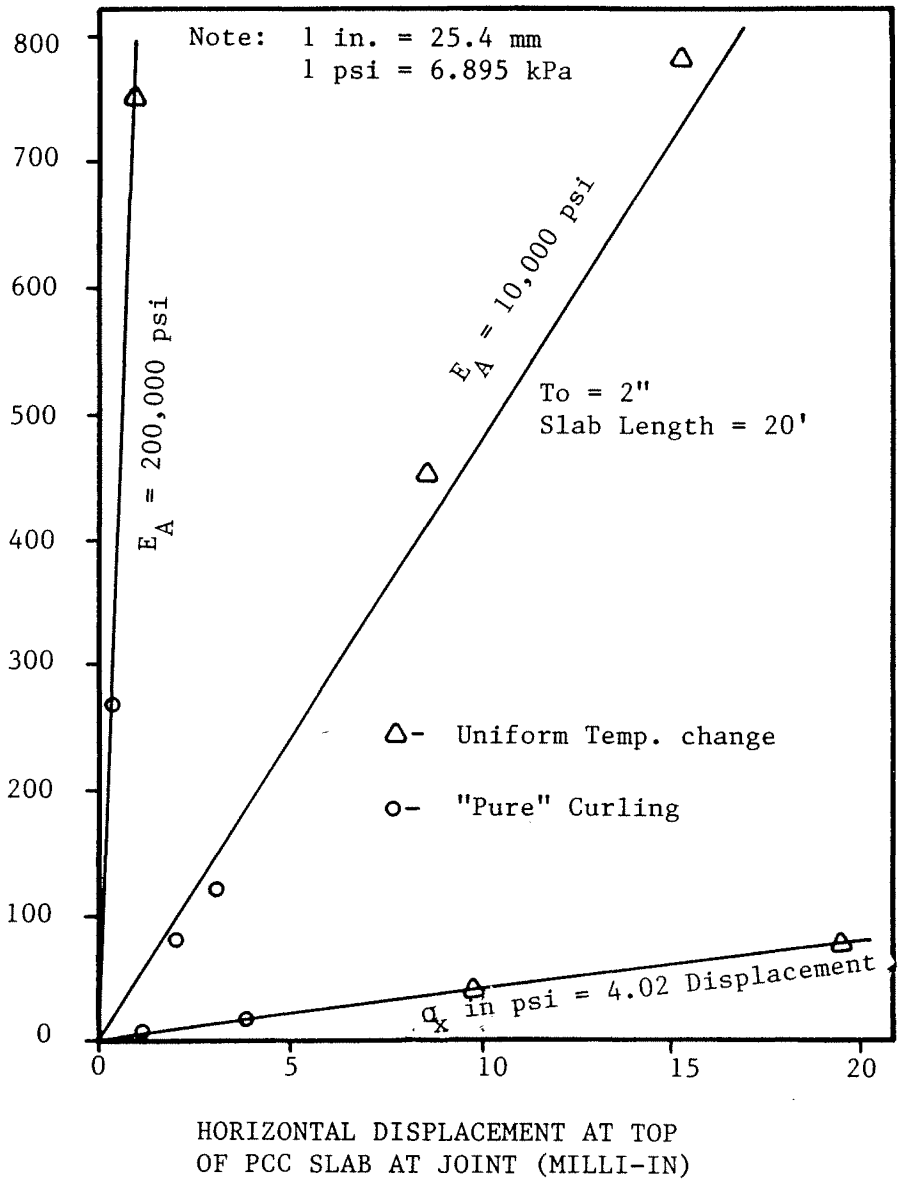

Figure 31. Overlay stress as a function of joint movement.

postulated which present a theoretical basis for the observed phenomena. The so-called "fabric effectiveness" is attributed to three mechanisms which might act singly or simultaneously to effectively retard crack growth in pavements.

To explain the blunting mechanism of geotextiles, one should consider the current state of practice in which bitumen-saturated geotextile is laid on the top of an existing pavement surface or is imbedded within an asphaltic-layered system.

In the case of rehabilitation of an existing pavement, the tips of all existing cracks and discontinuities in the old pavement lie directly beneath the bitumen-saturated fabric. In the case of a new pavement, where the geotextile is imbedded in the lower third of the structure, a propagating fatigue crack tip encounters the bitumen-saturated layer. From the fracture mechanics viewpoint, it is postulated that the crack growth is a consequence of the changing of the crack tip profile. During a cyclic deformation of a pavement under many loads, a crack tip undergoes the phenomenon of blunting and resharpening. The formation of a plastic zone, and its spread ahead of a crack tip during tensile loading cycles, (elastic contraction of the material surrounding the crack), imposes a residual stress which resharpens the crack tip, aiding its growth. The rate at which a crack may propagate, and the path it follows, depend entirely on the energy balance at the crack tip. The presence of a viscous layer of finite thickness ("bitumen-saturated geotextile") produces a large amount of plastic deformation which could blunt the tip and thus retard crack propagation. It is postulated that bitumen-impregnated geotextiles, of finite thickness, could alter the energy balance at the crack tip:

$$\dot{U} = \dot{V} + \dot{T} + \dot{D} \qquad (39)$$

where

U = the work done by the external loads

V = the elastic stored energy

T = the kinetic energy

D = irreversible energy, viscous dissipation, plastic work and surface energy

The dot in the above equation indicates the rate of change or differentiation with time. Obviously, the viscous dissipation rate of fabric-reinforced systems is dependent on

the thickness of the tack coat as well as the viscoelastic nature of the fabric itself. A soft nonwoven fabric, with intermediate modulus, when saturated with sufficient quantity of viscoelastic tack coat, could enhance the blunting mechanism as discussed previously. A double layer system could be formed to sandwich the viscous material to form a viscoelastic constraint.

It has also been hypothesized that the addition of geotextiles reinforces the pavement structure by increasing the relative horizontal stiffness, and subsequently reducing the local strains and stresses responsible for fatigue crack propagation. It could be argued from the fracture mechanics point of view, that a low stress intensity factor is achieved by lowering stresses and strains at localized crack tip regions, which subsequently reduce the crack growth rate. Both theoretical and experimental data suggest that in soft ground reinforcement application, the fabric stiffness may play a significant role. However, unpublished proprietary work, recently done by the authors, has shown that for moduli values in excess of 50,000 psi (345 MPa), the stress intensity factor is not sensitive to the stiffness or modulus of the bitumen-impregnated geotextile. Therefore, the significance of geotextile stiffness, when imbedded in a flexible pavement and saturated with asphalt cement, is questionable. In a soft ground reinforcement application, however, the geotextile responds as a tensile membrane with substantial elastic-plastic yielding, and shear distortion occurring in the soils beneath it. Theoretical elastic-plastic analysis of the soft ground support condition was utilized to formulate figure 32. This figure shows that the deflection under load is significantly reduced, as the fabric modulus increases.

According to the Buffer Zone concept, as a propagating crack, in a rather stiff medium, reaches a relatively softer zone, the crack tip blunts and may turn its direction by 90 degrees, growing horizontally along the soft zone. A crack running along the interface would result in the debonding of the asphalt-impregnated geotextile from the existing pavement surface. Recent field data from South Africa, using sand as a bondbreaker, as well as theoretical analysis of reflection cracking, confirms that the debonding mechanism retards crack growth in overlay pavements, thus indicating a reduction in the stress-intensity factor. Factors affecting debonding mechanisms are fabric thickness, saturated geotextile modulus, and required modulus ratio between the asphalt mixture and the saturated geotextile.

As was discussed in the previous sections, thermal stresses result from both seasonal and daily changes in slab temperature. The thermal loading can be represented by the superposition of two different thermal conditions: Uniform change (ΔT) in slab temperature and "Pure" curling.

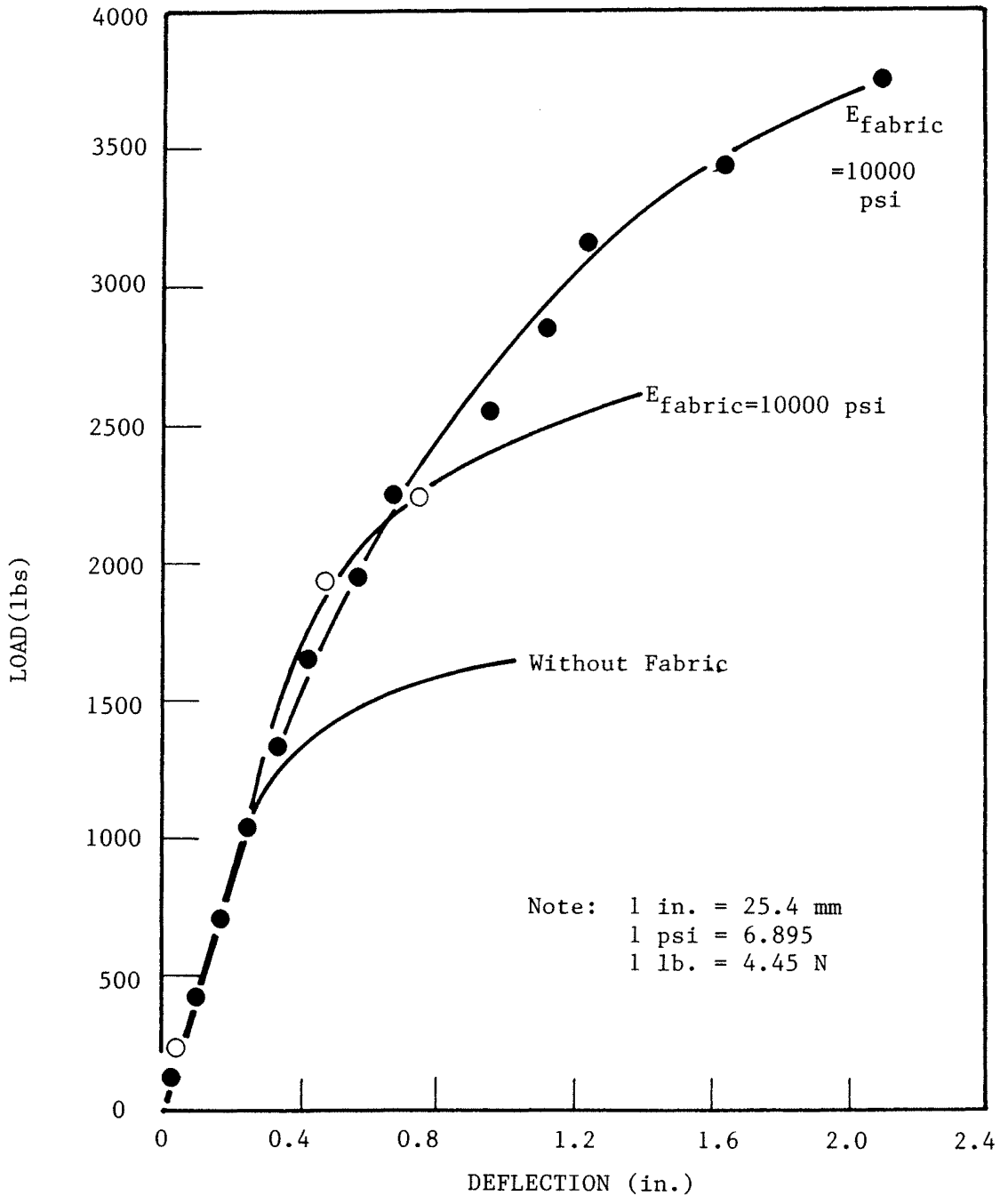

Figure 32. Load vs deflection for system with/without fabric.

Since both curling and seasonal change produce joint openings, which induce similar overlay stress distribution, it is believed that it is possible to equate the two loading conditions as was shown in section 3.1.1. It was shown that the slope of the stress-joint displacement line is a function of overlay modulus. The overlay stresses are independent of the type of thermal load. At constant overlay modulus, a horizontal displacement of x will produce the same overlay stress, regardless of whether this displacement was produced by slab curling or uniform temperature change. This is further evidence that curling can be equated to seasonal temperature change.

3.3 The EFRON Program

The previous sections of this chapter described the requirements of an elastic model required for the analysis of reflection cracking. These requirements have been coded into a computer program EFRON, which is a two-dimensional finite element program. A three-dimensional finite element approximation would probably be the most accurate representation of the pavement-overlay-foundation (OPF) system; however, the number of linear equations involved in the solution of any nonacademic problem is so large that it makes this approximation economically unreasonable and very sensitive to numerical errors. Therefore, a two-dimensional analysis is used.

A brief description of the program capabilities appears in the following section, and appendix A contains the user instruction for this program. The reader is referred to reference 39 for a detailed mathematical description.

3.3.1 Model Description

The finite element modeling of the overlay-pavement-foundation (OPF) structure, for both flexible and rigid pavement, is divided into the following components, as shown in figure 33:

- Overlay
- Fabric
- Existing slabs
- Slab foundation contact zone
- Elastic solid foundation
- Joint structure if present
- Crack

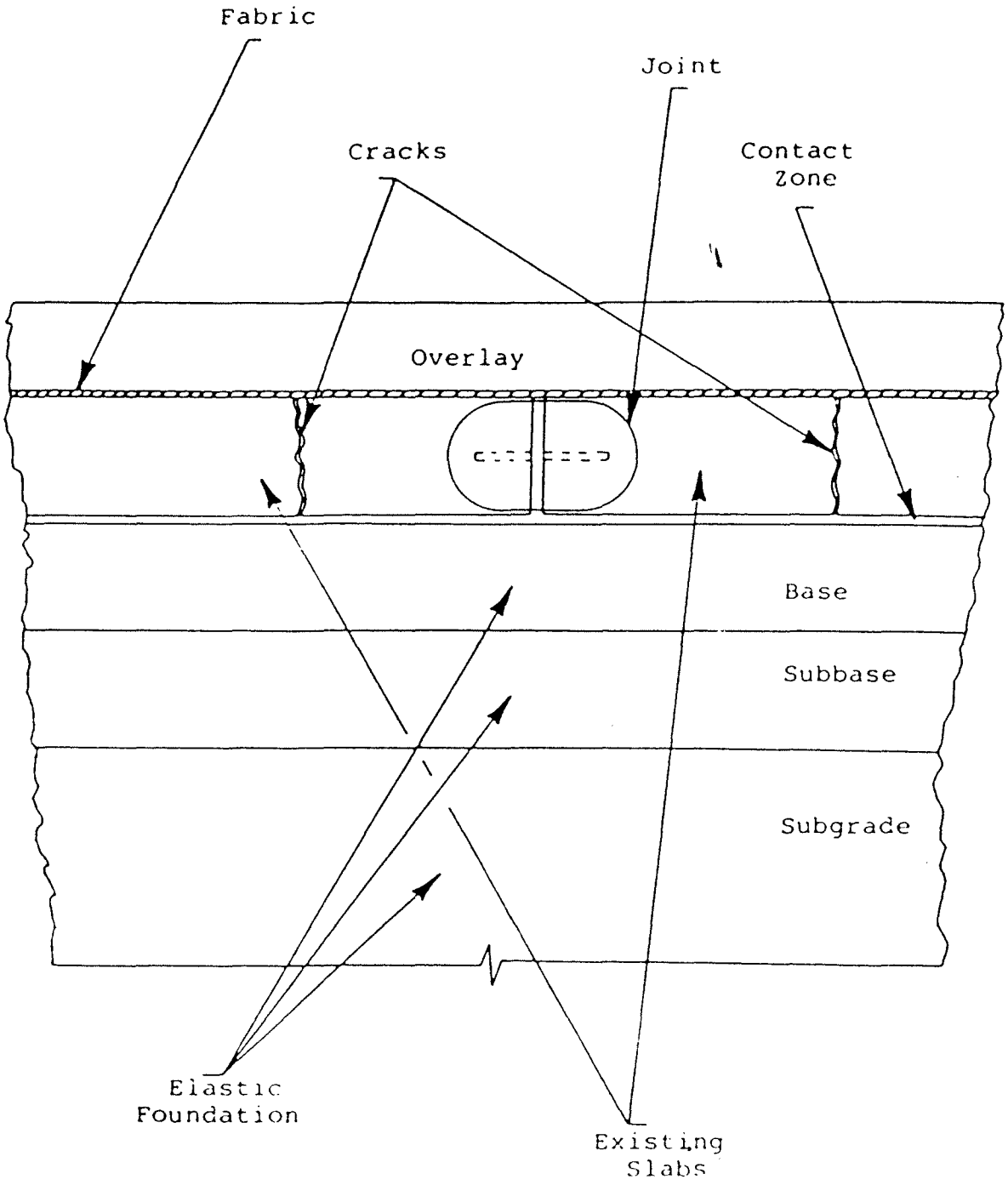

Figure 33. Structural elements of the pavement.

Each of these structural elements has its own finite element type, mesh, and material properties. A 2-dimensional isoparametric Wilson element with imcompatible modes are used. [38] The materials may be either isotropic or orthotropic; i.e., the modulus may differ depending on direction.

In addition to external mechanical load (due to traffic) and thermal loads (which are assumed to be related to the temperature at the nodes of the element), body forces due to gravity are also included. The latter play an important role when considering slab curling or voids and partial contact. It should be emphasized here that, unlike models utilizing Winkler foundation, the model described here is based on the assumption that tensile reactions between slab and foundation cannot exist, i.e., the subgrade does not pull a slab down in the event of partial contact; rather, gravity forces act to try to force the slab into contact with the foundation.

The overlay structure, as well as the existing slab are assumed to be homogeneous and isotropic whereas the fabric, which could be composed of up to four layers, is assumed to be orthotropic since the fabric tack coat system acts considerably stiffer in the vertical direction than it does under tension in the horizontal direction. The fabric layers may be of any width, but must be symmetric about the joint.

The joint and cracks (which are identical to plain joints) are modeled as elements with a very low modulus; i.e., they represent material with no shear resistance. The dowel bar, if it exists, is approximated by one of three types of elements, shown in figure 34. The type 1 element corresponds to the body of the dowel bar with effective elastic modulus **Ee computed from:**

$$E_e(be \cdot he^3)/12 = E_d(\pi d^4/64) \qquad (40)$$

where:

Ee = modulus of dowel bar

d = bar diameter

be,he = as defined in figure 34

The type 2 and 3 elements are used to model the horizontal degrees of freedom of the dowel bar. These elements have a very low elastic modulus; in addition, type 3 element also has a very low shear modulus.

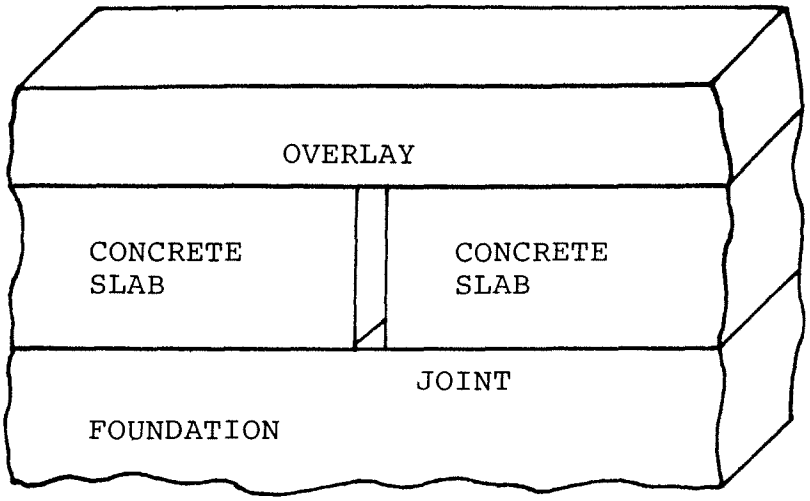

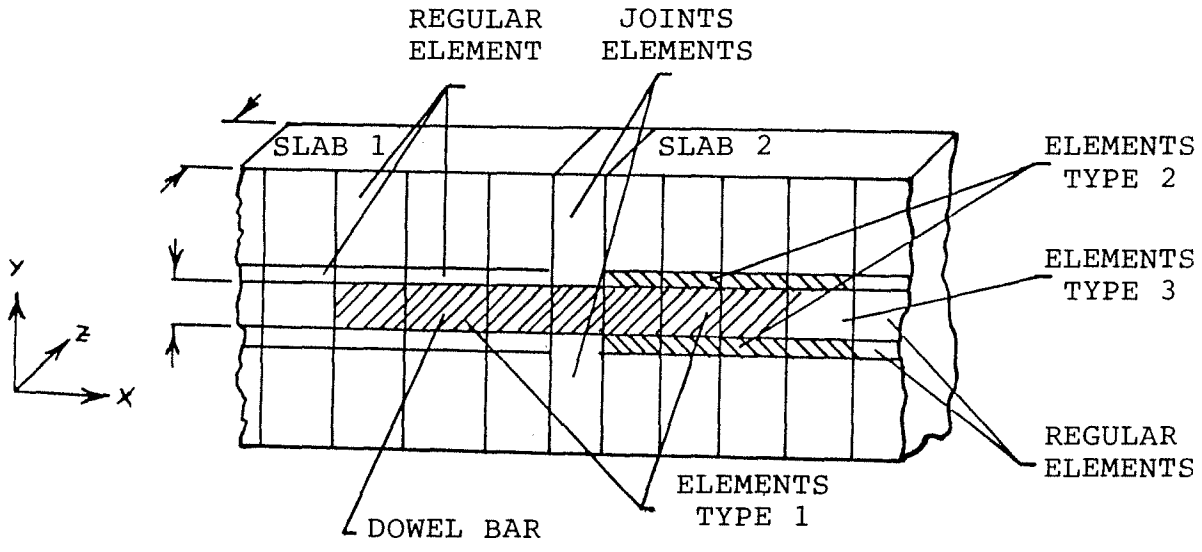

Figure 34. Finite element representation of plain and doweled joints.

The major reason for such a complicated model of the dowel bar is to transfer bending moment from slab to slab. This would not be possible in any other finite element model using bar or beam types of elements because of the existence of only two degrees of freedom in each nodal point of the two-dimensional element.

To incorporate dowel bar looseness, an effective (reduced) dowel bar diameter is used, which can be calculated from:

$$d' = d\ [1 - 10.5L - 12.58L^{.7} \log(E_s/1000)] \qquad (41)$$

where:

d' = Effective dowel bar diameter

d = Actual dowel bar diameter

L = Amount of looseness (inches)

Es = Subgrade modulus (PSI)

This equation is a result of the parametric study described in chapter III of reference 40.

The finite element model of the crack(s) is identical to the plain joint model described above. Up to ten different cracks could be included in a single problem. The crack pattern is not necessary, nor does it have to be identical for both slabs, if vertical load is present. However, for a horizontal temperature load, an identical crack pattern must be used if cracks are present.

As was discussed above, this model uses an elastic solid foundation to represent the subgrade, instead of the usual Winkler type of foundation. It was also stated that an elastic solid foundation is necessary, so that voids and partial contact conditions can be modeled realistically. Further, the elastic solid subgrade acts more reasonably under normal loading, in that a force applied at one location on the foundation is felt everywhere, instead of just compressing one spring only, as in the Winkler foundation. An unfortunate consequence of the elastic solid foundation is the fact that the subgrade stiffness matrix is fully populated instead of being diagonal, as for the Winkler foundation; this makes the solution of the problem somewhat more complicated.

A detailed discussion of the elastic solid foundation is given in reference 40. The discussion presented in reference 40 is for a three-dimensional foundation; however, the two-dimensional foundation required here is based on precisely the same concepts, with the exception that integration is carried out along a line instead of along the area of the element.

In addition to the elastic foundation, the EFRON program provides, as an option, Winkler and rigid-type supports. This option is provided so that the user can compare the results from the two different representations. It should be emphasized, however, that the Winkler foundation is not a reasonable representation of a real foundation and should not be used in general.

An initial void could be assumed under the existing slab(s), as shown in figure 35. In the finite element model, a void is reflected by replacing with zeros all diagonal and off diagonal elements of the stiffness matrix associated with the node where the void exists, i.e.,

$$kji = 0 \qquad j = 1, N \tag{42}$$

where k represents the elements of the stiffness matrix and i is the nodal number where the void exists.

The correct finite element model of the slab-foundation contact zone is extremely important in the case of a temperature load, or a vertical mechanical load which can produce either a partial contact of the slab or a large horizontal displacement. (Partial contact due to a void formation was discussed previously). Special "joint" elements are used in this model to achieve a more realistic finite element approximation of the contact zone.

The joint element was first introduced by Goodman as a finite element model representing joints and seams in the analysis of rock mass structures.[41] The configuration of the joint element is as shown in figure 36. It consists of a pair of straight lines with four nodal points. The element has zero width, a unit length, and a thickness b in the direction normal to the plane of the element (x-y plane). The nodal point pairs (1,4) and (2,3) initially have identical coordinates.

The joint element is assumed to have essentially no resistance to a net tension in the direction normal to the sides 1-2 and 3-4, i.e., in the y′ direction. It offers high resistance to compression in the y′ direction, and may deform somewhat under normal pressures, particularly if there are crushable irregularities or compressible filling materials.

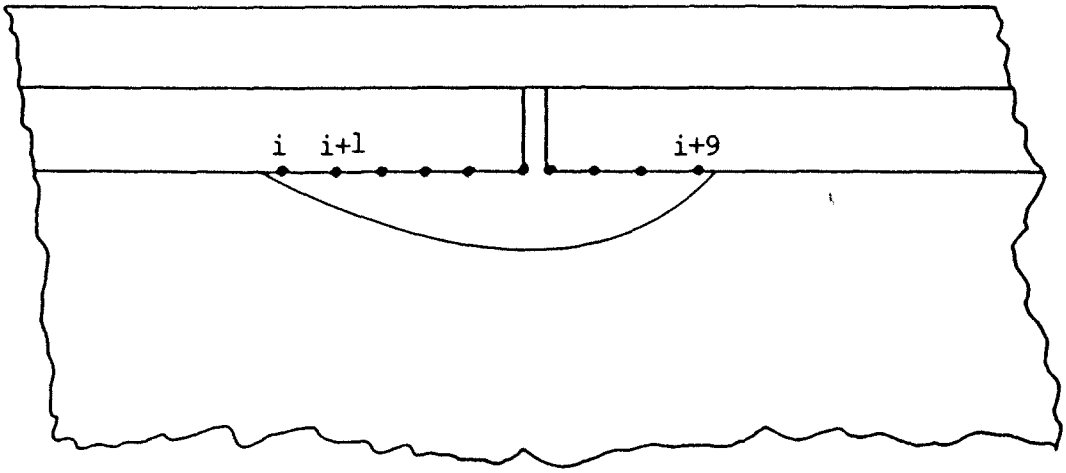

Figure 35. Void under existing slab.

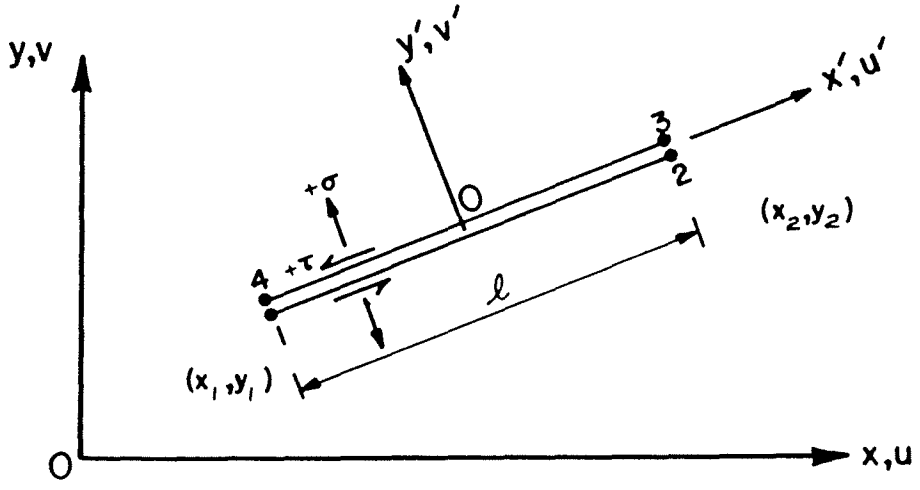

Figure 36. A joint element in local and global coordinates.

It also offers shear resistance in the x' direction under normal pressures. However, at no point within the element can the shear stresses exceed shear strength of the joint.

The resulting shear stresses must be compared with the shear strength of the element. The shear strength at any point within the element is assumed to be of the form:

$$\tau_s = c + \sigma \tan \phi \qquad (43)$$

where τ_s is the shear strength, c is the cohesion, and ϕ is the angle of friction of the material, and is the normal compressive stress at that particular point. The shear stresses at the nodal points are checked with the corresponding shear strength. If at any node the stress exceeds the shear strength, it is reduced to the shear strength value. The excess shear stress is used to compute the corresponding equivalent nodal loads, and are applied back as a new load vector in the iteration procedure.

The element normal stresses are also checked for tension. If any nodal normal stress is tensile, the normal and shear stresses at the particular node are reduced to zero, and the corresponding nodal loads are applied back as a new set of load vectors in the iteration procedure. The iteration process is repeated until all of the nodal normal stresses are essentially compressive, and the nodal shear stresses do not exceed the nodal shear strength. The iteration scheme used, is based upon the initial stress concept proposed by Zienkiewicz.[42]

The EFRON model can be used to analyze the response to both thermal and dynamic load-associated stresses. However, this model utilizes elastic material properties in the problem solution. Traffic loading occurs over a short time span, and can be analyzed within an elastic model, especially if dynamic moduli are used for layer characterization. However, thermal loads are applied over long time periods (12 hours for thermal gradients and up to 6 months for seasonal effects) so that viscoelastic asphaltic concrete properties have to be considered. This problem is considered in the next section.

3.4 Development of a Mechanistic Model

In search for a mechanistic approach to the problem of reflective cracking, the theoretical work by Schapery and others, to analyze fracture of a viscoelastic material, seemed promising for adoption in this research.[34] Schapery et al. have successfully applied this approach to the fracture characterization of metals. In this analysis, however, there is a need to employ caution in the

mathematical treatment of the developed model along three lines: first, that the simplifying assumptions must not violate the theory while at the same time realistically model the mechanics of beams fracture; second, the developed model should require easy-to-find input parameters that could be obtained from the large scale testing data to be obtained in this study; and third, some modification to the model is required, since this study is dealing with different materials (asphaltic mixtures and fabrics) than were used by the above cited researchers.

3.4.1 Crack Initiation and Propagation in Viscoelastic Media

To date, most of the fracture mechanics approaches assume that material behavior is either linear elastic or viscoelastic. The stress field in a plane viscoelastic body, subjected only to prescribed traction forces, is the same as that in an elastic body of the same geometry and loading provided that the resultant force on any closed boundary vanishes. It follows as a corollary, that the stress intensity factors, K, for similarly loaded linear elastic and viscoelastic bodies satisfying this condition, are equal. For an elastic material, the stress intensity factor K is independent of the crack growth rate a; however, for linear viscoelastic material, two cases arise: 1) for a very slowly growing crack (quasi-elastic case), the material will respond with long decade line creep compliance $J(\infty)$, being the material characterizing parameter, and 2) for a very rapidly propagating crack growth (dynamic case), $a \rightarrow \infty$, the material will respond with the short decade time creep compliance, J(0) being the material characterizing parameter. Therefore, the viscoelastic stress analysis solution will not only depend upon the appropriate use of the correspondence principle, but will also depend on what crack speed will develop (or can reasonably be assumed) under the specified loading conditions; i.e., quasi-elastic or dynamic analysis is used.[43]

Consider figure 37 for a viscoelastic medium, subjected to stresses acting along the crack plane (Mode I) in the neighborhood of a crack tip (indicated by O, and located at $x = a(t)$), where the crack plane is defined by $y = 0$. It is convenient to define a reference system attached to the moving crack tip as $r = x - a(t)$. The region $o < r < \alpha$ is termed the cohesive zone, where the material exhibits nonlinear material behavior (more precisely nonproportional stress/strain/time behavior). This zone was first recognized by Dugdale in his cohesive fracture model.[35] The material behavior outside this zone is assumed to be linear viscoelastic. The basic problem is to find the following:

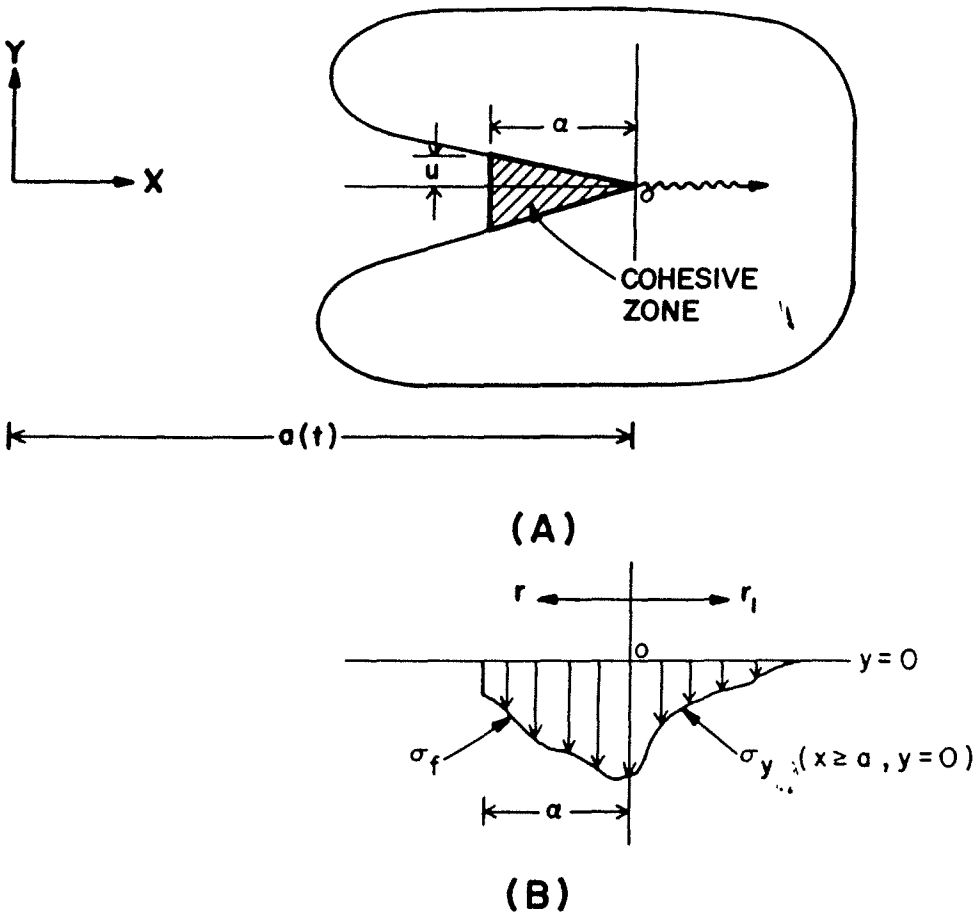

Figure 37. Crack in a viscoelastic medium.

- The size of the cohesive zone,
- The crack opening displacement, U
- The crack growth rate, a

3.4.2 Boundary Value Problem Elastic Solution

When a solution for the equivalent elastic problem is known, the solution to the viscoelastic problem could be found using the correspondence principle method.[43] This principle emerged from observing that the only difference between formulating a boundary value problem for a linear elastic or viscoelastic medium, is in the assignment of the Young's modulus of elasticity, E and Poisson's ratio, μ. In other words, if the elastic solution exists for a boundary value problem, then the corresponding viscoelastic solutions could be found by simply replacing the material constants (E, ν, G, K) of the elastic solutions, by their viscoelastic equivalents. This principle applies in the case of stationary crack; however, two conditions have to be met in order to use the correspondence principle for growing cracks. The first condition is that the cohesive stresses σ_f are independent of the material constants. Such a requirement could be met by prescribing σ_f a priori, as is the case in the Dugdale model.[35] The second condition is that the displacement in the plane of the crack could be expressed in separable form of two multiplicable functions; one for the material constants, and the other for the geometry. Such a requirement could be met if the resultant force on any closed loop is identically zero.

It follows from the above discussion that if Ue is the elastic displacement field for a unit value of creep compliance, then the corresponding viscoelastic displacement Uve could be written as:

$$U_{ve} = \int_0^t J(t-\tau) \frac{2U_e}{2\tau} d\tau \qquad (44)$$

Using the condition of small scale yielding, (α << a (t)), and considering figure 37, the elastic solution, following Dugdale approach [35], could be written as:

$$\sigma_y = \frac{H(r_1)}{\sqrt{2\pi r_1}} \left[K - \int_0^{\alpha} \frac{\sigma_f(\xi)}{\sqrt{\xi}} d\xi \right] \; ; \; r_1 \to 0 \qquad (45)$$

$$U_y = 4KH(r)\sqrt{r/2\pi} - \frac{2}{\pi} H(r_1) \int_0^{\alpha} \sigma_f(\xi) \ln \left[\frac{\sqrt{\xi} + \sqrt{\pi}}{\sqrt{\xi} - \sqrt{\pi}} \right] d\xi \quad (46)$$

The requirement that the stress σ_y be nonsingular at the crack tip ($r = 0$) will yield:

$$K = \sqrt{\frac{2}{\pi}} \int_0^{\alpha} \frac{\sigma_f(\xi)}{\sqrt{\xi}} d\xi \quad (47)$$

Substituting equation 47 in equation 46 will yield

$$U_y = \frac{H(r)}{\pi} \int_0^{\alpha} \sigma_f(\Psi) \left[2\sqrt{\frac{r}{\Psi}} - \ln \frac{\sqrt{\Psi} + \sqrt{r}}{\sqrt{\Psi} - \sqrt{r}} \right] d\Psi \quad (48)$$

where

σ_y = The crack plane stress

$H(r)$ = unit step function

σ_f = stress in the cohesive zone

ξ, ψ = dummy variables

U_y = crack opening displacement

K = stress intensity factor

α = size of the cohesive zone

3.4.3 Determination of the Cohesive Zone Size,

To meet the first condition of the correspondence principle, the cohesive stress σf has to be predetermined. Assuming that $\sigma f = \sigma fmax(r)$, where $\sigma fmax$ is the maximum value of σf, (i.e., the indirect tensile strength), and $\phi(r)$ is a multiplication function evaluated at any point at a distance r from the crack tip, the size of the cohesive zone, α, could be found by substituting $\sigma fmax$ (r) into equation 47.

$$K = \sqrt{\frac{2}{\pi}} \int_0^{\alpha} \frac{\sigma_{f\,max}\,\phi(r)}{\sqrt{\xi}}\, d\xi \qquad (49)$$

Making the change of variable $\eta^2 = \xi/\alpha$; $2\eta d\eta = d\,\xi/\alpha$

Then $\xi \rightarrow 0$ implies that $\rightarrow \eta \quad 0$

and $\xi \rightarrow \alpha$ implies that $\eta \rightarrow 1$

Substituting these in equation 49 yields:

$$K = \sqrt{\frac{2}{\pi}} \int_0^{1} \frac{\sigma_{f\,max}\,\phi(r)}{\eta\sqrt{\alpha}} * 2^{\eta}\alpha d^{\eta} \qquad (50)$$

Squaring both sides and rearranging terms:

$$\alpha = \frac{\pi}{8} \frac{K^2}{\sigma^2_{f\,max}\, I^2} \qquad (51)$$

where:

$$I = \int_0^{1} \phi(r) d^{\eta};\ 0 \leq I \leq 1$$

3.4.4 Determining of the Viscoelastic Displacement, Uve

Using the correspondence principle (typified by equation 44) as applied to the elastic crack opening displacement Uy in equation 48 yields:

$$U_{ve} = \frac{8}{\pi}\sigma_{f\,max} \int_{t_1}^{t} J(t-\tau)\, \frac{2}{2\tau}\, \sqrt{\alpha a(t)-X)} -$$

$$\frac{\alpha+x-a(\tau)}{2} \ell\eta\, \frac{\sqrt{\alpha} + \sqrt{a(\tau)-x}}{\sqrt{\alpha} - \sqrt{a(\tau)-x}}\, d\tau \qquad (52)$$

where $t \geq t_1$; and t_1 is the time at which the crack tip reaches the generic point x; vis., $\xi(x,t) = a(t) - x = 0$. Although not explicity shown in the above equation, x and α may also be time dependent.

It follows from equation 52 that the viscoelastic displacement could be obtained if the quantities (σfmax), J(t), and α are determined. Be reminded that for a constant cohesive stess, α depends only on the stress intensity factor K. Therefore, if information on the creep compliance J(t), fracture strength σfmax, and the stress-intensity factor K could be determined experimentally or from field measurements, then equation 52 establishes a relationship between the crack opening displacement in a viscoelastic material, crack length as function of time a(t), and the time at any specified crack length.

3.4.5 Determination of the Failure Time

Equation 52 is valid within two time bounds, t_1 and t. The lower bound, t_1, defines the time required to initiate a crack, and advance its tip to a point $x = a(t_1)$. It is worth mentioning that Schapery indicated that the time, t_1, required to propagate crack the distance, α, is approximately three times the initiation time. The upper bound, t, defines the time required to advance the crack, or equivalently increase the crack opening displacement any specified length. At the time of rupture, the crack opening displacement reaches a critical value, Uc, and the time elapsed is defined as the failure time, tf. The work of fracture, γ, of an element in the cohesive zone till rupture occurs, could be expressed by:

$$\gamma = \frac{1}{2} \int_{t_1}^{t_2} \sigma_f \frac{\partial U_Y}{\partial t} dt \qquad (53)$$

or equivalently, using change of variables, as:

$$\gamma = \frac{1}{2} \int_{\alpha}^{C} \sigma_f \frac{\partial U}{\partial r} dr \quad ; \quad \dot{a} > 0 \qquad (54)$$

where: C is the crack length at failure

If $\sigma_f = \sigma$ is constant, then equation 54 reduces to:

$$\gamma = \frac{1}{2}\sigma U_c = \frac{1}{2}\sigma \Delta t_f \qquad (55)$$

where: Uc is the initial joint opening displacement at failure

If the creep compliance of the asphaltic overlay could be written in the form:

$$J(t) = J_o + J_2 t^m \qquad (56)$$

then using equations 52, 55, and 56, and making the change of variables $S = a(t-t)/\alpha$ will lead to the following equation for the crack growth rate, a:

$$\dot{a} = \frac{\pi}{8}\left[\frac{J_2 I}{2\gamma(1-K^2/K_\infty^2)}\right]^{1/m} \frac{K^{2+2/m}}{\sigma_y^2} \qquad (57)$$

where:

$$I = \frac{1}{2}\int_1^0 S^m \ln\frac{1-\sqrt{1-2}}{1+\sqrt{1-2}}\, ds \qquad (58)$$

and:

J_0, J_2, m = creep compliance constants

K, K_∞ = initial and unbound stress intensity factors

Equation 57 is the general equation for the crack opening rate (the derivation of this equation is given in appendix B); however, the parameter measured in the laboratory tests is the time of failure at a specific joint

opening rate. It is therefore convenient to rewrite this equation to yield the failure time, tf.

The work of fracture 2γ, required to produce a unit of surface area is given by:

$$2\gamma = J_o K_\infty^2 \tag{59}$$

Introducing equation 59 into equation 57 and rearranging terms yields:

$$\frac{da}{dt} = \frac{\pi}{8\sigma_f^2}\left(\frac{J_2 I}{C_o}\right)^{1/m}\left(\frac{K^2}{K_\infty^2 - K^2}\right)^{1/m} K^2 \quad \text{or}$$

$$dt = \frac{8\sigma_f^2}{\pi}\left(\frac{J_o}{J_2}\right)^{1/m}\left(\frac{K_\infty^2}{K^2} - 1\right)^{1/m}\frac{1}{K^2}\,da \tag{60}$$

Integrating both sides yields:

$$\int_{t_o}^{t_f} dt = \frac{8\sigma_f^2}{\pi}\left(\frac{C_o}{C_2 I}\right)^{1/m}\int_{a_o}^{a_\infty}\left(\frac{K_\infty^2}{K^2} - 1\right)^{1/m}\frac{1}{K^2}\,da \tag{61}$$

$$t_f = t_o + \frac{8\sigma_f^2}{\pi}\left(\frac{Co}{C_2 I}\right)^{\frac{1}{m}}\int_{ao}^{a_\infty}\left(\frac{K_\infty^2}{K^2} - 1\right)^{\frac{1}{m}}\frac{1}{K^2}\,da \tag{62}$$

where:

t_f is the failure time

t_o is crack initiation time, assumed to be zero

a_o is the initial crack length

a_∞ is the crack length for which the crack propagation rate becomes unbounded

K is the stress intensity factor corresponding to crack length a

K_∞ is the stress intensity factor corresponding to the crack length a_∞

I is a constant defined in equation 58

The developed model requires easy to find input parameters that could be obtained from laboratory tests. These parameters are the properties of the overlay material such as the creep compliance, J(t), the fracture strength, f, the joint opening rate as a function of time, and the fracture toughness, KIC. The determination of KIC also requires the applied load on the stress developed as a result of thermal load. Other input data, required only for model verification, are measured values of the applied load, P(t), and the corresponding values of the crack length, a(t), at different time intervals.

Using these input parameters, the model predicts the time at which failure occurs, tf, and the crack opening displacement, u(t), at different time intervals.

In conclusion, crack propagation in viscoelastic medium is governed by two equations: 52 and 57. Equation 52 defines a relation between the crack opening displacement, (Uve), crack length, (a(t)), and time t , provided that three material parameters are known. These parameters are: the creep compliance, J(t), fracture strength, (σ_y), and the Mode I stresses intensity factor, K. Once the crack opening displacement-time relationship is determined, then the crack length-time relationship could be found; or vise versa.

Equation 57 defines a relationship between the crack growth rate, (a) and critical crack opening displacement, (Uc), provided that the same material parameters of equation 52 are known. It should be noted that the critical crack opening displacement is related to fracture work by equation 55. Integrating the crack growth rate with respect to time, will yield the history of crack growth and hence determining the failure time, tf. The above models have been computerized in a program called RECK, and the listing is found in appendix D. The use of the above computer program will enable prediction of the critical crack opening displacement Ucr, and the time required until failure occurs, tf, as a result of thermal loads. It should be noted that, as was shown in Section 3.1.1, the analysis due to vertical temperature gradients is identical to that described above; except that the creep compliance values corresponding to 12 hour loading cycles is used. The model is applicable to both laboratory specimens and field pavements; the laboratory tests use the mechanically induced joint opening as a function time as an input parameter, whereas for the analysis of field pavements, the thermally induced joint opening as a function of time is needed. The development of this value is discussed in the section 3.4.7.

3.4.6 Effect of Fabric on the Crack Opening Displacement and Failure Time Prediction

The inclusion of a fabric layer within the overlay pavement structure is expected to prevent of delay reflection cracking. The purpose of this fabric, as a reinforcing layer, is to physically restrain the opening movement of the crack as the joint underneath opens. As has been discussed, there are several other approaches to the reflection cracking problem, including stress-relieving interlayers (such as SAMI), crack arresting interlayer (such as the Arkansas open-graded layer), and pre-overlay rehabilitation.

A mechanistic approach to determining the effect of fabrics or interlayers on crack growth rate is to include these layers in stress analysis; and the EFRON program is capable of handling up to 5 such interlayers (which may be of any width). The difficulty with this approach is that the in-situ properties (creep modulus, Poisson's ratio, tensile strength, fracture toughness) are very difficult to determine. It had been hoped that these properties could be deduced from the results of fatigue tests; however, the analysis of small-scale beams in reference 39 showed that this is not possible within an elastic system - it was shown in that study that the interlayer properties would have to be a function of the applied stress as well. Therefore an empirical approach is used here to include the effect of the interlayers ; namely, the analysis is conducted assuming that the interlayers (fabric or SAMI) is not present, and comparing the predicted failure time with the actual failure time to obtain a fabric effectiveness factor.

3.4.7 Analysis of Field Pavements

As was discussed in Section 3.1.1, daily variation of temperature gradients and the seasonal variation of average pavement temperature result in changes in the joint opening, i.e., in Uve, the crack opening displacement. This displacement can be calculated using the EFRON program, provided that the rate of change of temperature (average or curling gradient) is known. Thus, the field case is identical to the laboratory beam case, with the exception that the load developed as a result of the temperature drop will have to be computed using EFRON for the field case, instead of using the measured values for the laboratory case. The load is required to evaluate the Mode I (opening mode) stress intensity factor KI.

The following procedure is used to evaluate field pavements:

1. The joint opening and the resulting stress in the asphalt above the joint are determined using the EFRON program for monthly increments of temperature drop.

2. EFRON is rerun (using a load applied horizontally to the ends of the slab), in order to find the horizontal pull required to reach the same critical stress (in the asphalt above the joint) as in step 1.

3. The results of step 1 and 2 computation are input into the RECK program, and the incremental crack growth is determined.

CHAPTER IV. LABORATORY TESTING

4.1 Types of Testing

This study is concerned with the evaluation of the cracking resistance of asphalt-concrete overlays of both flexible and rigid pavements. Both fabric-reinforced overlays, as well as SAMI layers are considered. In order to evaluate the cracking resistance of these systems, the following tests were conducted under the conditions described below:

1. Fatigue resistance under vertical load of asphalt overlays over asphalt bases for both control and fabric reinforced conditions, using three types of treatment and two types of induced crack severity in the base beam. All tests performed at 72 $\pm$ 2 ^{o}F (22 $\pm$ 1.3 ^{o}C). Control conditions are conventional overlays without fabric reinforcement.

2. Fatigue resistance under vertical load of asphalt overlays over portland cement concrete bases for both control and fabric reinforced conditions, using two types of fabric membrane. All tests performed at 40 $\pm$ 2 ^{o}F (4.$\pm$ 1.3 ^{o}C).

3. Fatigue resistance under vertical load of asphalt overlays consisting 2 inches (51mm) of conventional asphalt concrete mix over 2 inches (51mm) of open-graded "Arkansas" mix. All tests performed at 40 $\pm$ 2 ^{o}F (4.4 $\pm$ 1.3 ^{o}C).

4. Testing of overlay beams under simulated thermal stresses. The beams were asphalt overlays over concrete bases for both control and fabric reinforced conditions, using two types of fabric and the fiber SAMI membrane. All tests performed at 40 $\pm$ 2 ^{o}F (4.4 $\pm$ 1.3 ^{o}C).

5. Fatigue resistance under vertical load and simulated thermal stresses of asphalt concrete overlays over concrete bases for both control and fabric reinforced conditions, using two types of fabric and the fiber SAMI membrane. All tests performed at 40 $\pm$ 2 ^{o}F (4.4 $\pm$ 1.3 ^{o}C).

The beam testing simulates the behavior of full scale pavement with flexible overlays under traffic and thermal loading as experienced in highways. Figure 38 illustrates the concept for an overlay condition. Fabric reinforcement involves placement of an engineering fabric or geotextile underneath the asphalt overlay. The purpose of fabric reinforcement is to enhance the crack resistance of the bound overlay layer.

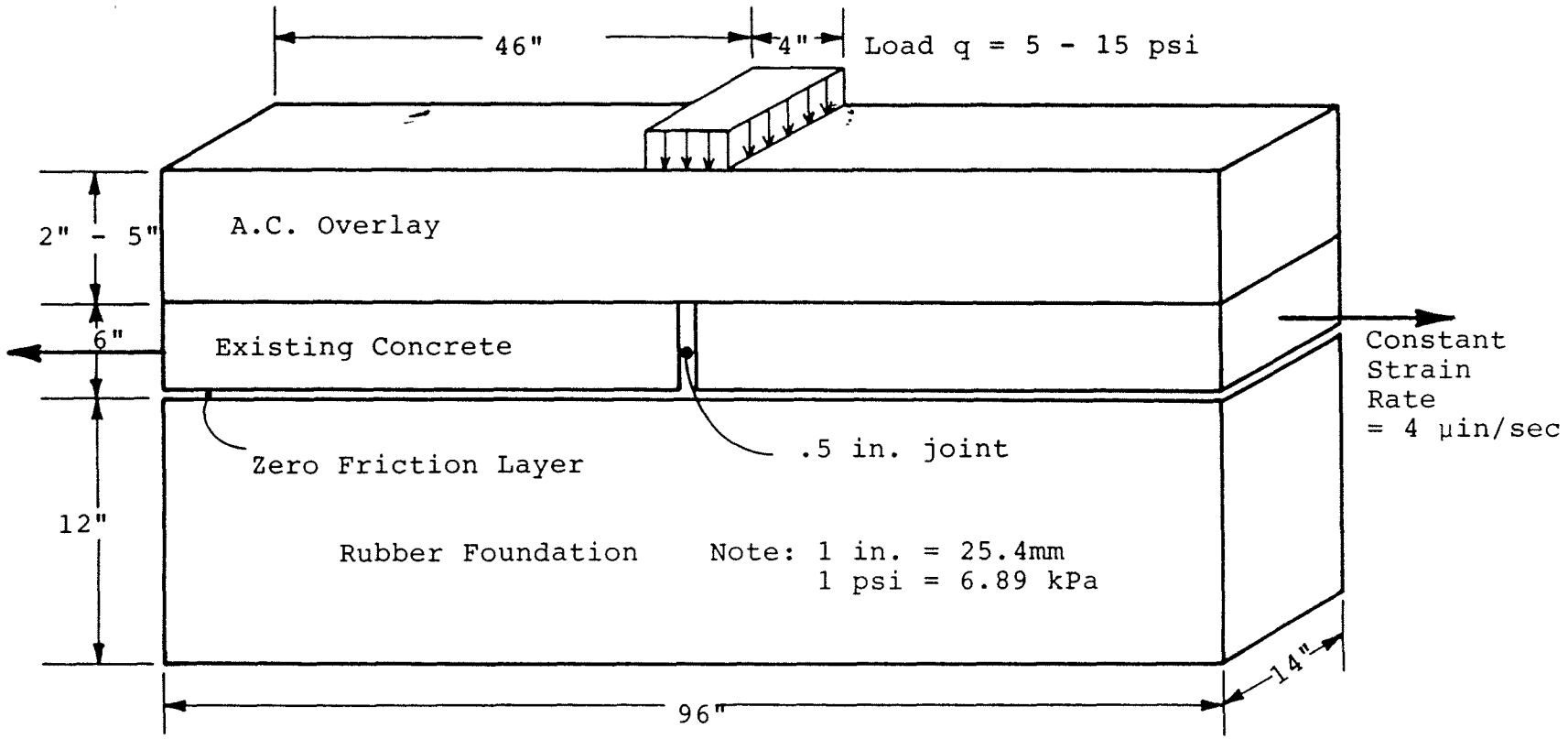

Figure 38. Laboratory simulation of overlaid concrete pavement.

Simulation of reflective cracking of rigid pavement overlays requires modeling of both thermal and traffic loading conditions. Thermal stresses result from both seasonal and daily changes in slab temperature. The thermal loading can be represented by the superposition of two different thermal conditions, as was discussed earlier:

- Uniform change in slab temperature: this condition represents the seasonal change in average slab temperature which occurs over long periods of time.

- Pure curling condition: daily, or short time period, temperature variation within the slab. For pure curling, the average slab temperature remains unchanged, but the upper surface of the slab is at a different temperature from the lower surface, with the temperature assumed to be linearly related to the slab depth.

The flexible overlays over rigid base were subjected to simulated thermal loads experienced in the field. The pavements were modeled using beams with externally applied displacements that produced joint movements similar to those experienced in the field due to thermal loading. Uniform seasonal reduction in slab temperature was simulated, by applying horizontal tensile forces to the PCC slab pavements. Traffic forces were simulated by applying dynamic vertical loads to the experimental model, which was a beam supported on an elastic foundation.

4.2 Treatment Selection

1. For fatigue resistance of asphalt overlays over asphalt bases three types of treatment were chosen to represent low, medium and high tensile moduli. Two out of the three treatments were fabric membranes of low and high moduli and the third treatment was with a "SAMI" interface membrane made from a mix of asphalt cement (AC-20) and Polypropylene fibers (medium modulus type). The pertinent fabric properties, as furnished by the manufacturers, are in table 2 (Fabrics B and P).

2. For beams with asphalt overlays over concrete bases, three types of treatment were chosen. One high-modulus fabric, a fiber SAMI interlayer, and a 2 in. (51mm) thick open graded "Arkansas" asphalt concrete interlayer were used. The pertinent fabric properties as furnished by the manufacturers are in table 2 (Fabrics O).

4.3 Mix Design

A brief discussion on the mix design of concrete used for rigid base, and mix design used for asphalt base and overlays is given in the following sections.

Table 2
Fabric properties.

PROPERTY	FABRIC P LOW MODULUS	FABRIC O HIGH MODULUS	FABRIC B HIGH MODULUS	TEST METHOD
Weight (oz).	4	4.9	8.9	
Modulus (psi)	NA	NA	NA	ASTM D 1682
Tensile Strength (lbs)	90	112	90	ASTM D 1682
Elongation (percent)	55	62	55	ASTM D 1682
Burst Strength (psi)	NA	246	280	Mullen Burst
Asphalt Retention (gsy)	0.20	0.20	0.20	Texas DOT - 3099
Shrinkage	NA	NA	<2	Texas DOT - 3099

* Furnished by manufacturer
NA = Not available from manufacturer
1 oz. = 28g
1 lb = 454g
1 psi = 6.894 kPa
1 gsy = 4.527 lit./m2

4.3.1 Cement Concrete Base Beams

Two different sizes of aggregates from a local aggregate supplier were utilized for the manufacture of cement concrete beam specimens. The aggregates used were #57 crushed gravel as coarse aggregate, and natural sand as fine aggregate. The aggregate gradation limits were in accordance with ODOT specifications; actual gradation chosen for preparing the mix design is shown in table 3. The quantities of the constituents of concrete; namely, coarse and fine aggregate, cement and water, were chosen as per ODOT specifications for class C concrete after making the necessary adjustments for water absorbed by the dry aggregate, and for the net water requirement of concrete due to presence of water in the polymer additive. The calculated mixture proportions were checked by means of trial batches. The quantities by weight of the several constituents of regular concrete are indicated in table 4. The slump selected was three inches (76 mm), entrained air 4.0 percent, and water cement ratio of 0.40. To prepare test specimens for the rigid base, a full scale test pavement was constructed with special provisions for specimen handling, as well as treatment installation. The construction of the test pavement was according to Ohio Department of Transportation specifications,

Table 3
Aggregate gradation limits.

#57 Limestone Sieve Size	% Passing	Natural Sand Sieve Size	% Passing
1-1/2"	100	3/8"	100
1"	95-100	#4	95-100
1/2"	25-60	#8	70-100
#4	0-10	#16	45-80
#8	0-5	#30	25-60
		#50	5-30
		#100	1-10
		#200	0-4

Note: 1 in = 25.4 mm

Table 4
Portland cement concrete mix data.

Cement Content	= 658 lb/C.Y. (390 kg/cu.m)
Coarse Aggregate	= 1737 lb/C.Y. (1030 kg/cu.m)
Absorption	= 1.2%
Specific Gravity	= 2.64
Fine Aggregate	= 1107 lb/C.Y. (657 kg/cu.m)
Absorption	= 2.7%
Specific Gravity	= 2.50
Water/Cement Ratio	= .40
Percent Additive Air	= 4.0
Slump	= 3"(76 mm)
Compressive Strength (28 days)	= 4800 psi (33.1 MPa)

(ODOT 450). The test pavement was of size 14 ft 3 in by 26 ft 10 in (4.3 x 8.2 m) to obtain 46 samples of rigid base beam for tests, with expansion joints at the center of the individual samples. The expansion joint was formed with steel castings according to ODOT 711.07 specifications, and with preformed fillers meeting AASHTO M153 specifications. A plan of the test pavement showing location of joints is attached (figure 39). The test pavement was 6 inches (152 mm) thick. Ready mixed concrete was obtained for construction of the test pavement. All items of work related to test pavement construction (concrete base) were completed in 1 day. Cylinders & beams were made from the concrete used for test pavement construction for laboratory tests. The concrete pavement was constructed in September, 1982. Based on laboratory test data of concrete used for the test pavement, the treatment installation work was started on the 16th day after the date of casting of the pavement. As already indicated, two treatments (O Fabric and fiber SAMI) were selected for installation over the concrete base before overlay, and the third treatment consisted of a 2 in (51 mm) thick layer of open-graded Arkansas mix, overlaid with 2 in (51 mm) of asphaltic concrete surface course mix. The treatment installations were carried out by specialized crews representing the manufacturers.

4.3.2 Asphalt Concrete Base Beams and Overlays

Two different sizes of aggregates obtained from the local aggregate supplier were utilized for the manufacture of asphalt concrete specimens. The aggregates used were #8 crushed limestone as coarse aggregate, and natural sand as fine aggregate. The #8 crushed aggregate generally showed sharp, angular, and gritty particles, and for the most part, contained at least one fractured face in the particles, and were reasonably free from excessive dust or other deleterious coatings, weathered pieces, or excessive flaky and/or elongated pieces. Measured water absorption of particle size ranged from between 2.9 percent and 3.2 percent. Aggregate gradation conformed to ODOT specifications for asphalt concrete surface course. Asphalt cement (AC-20) used in this investigation was obtained from Chevron Asphalt Company. Table 5 gives details about the aggregate gradation of #8 limestone aggregate and natural sand, used in development of ODOT 404 mix. Design of aggregate blends for this investigations is based on:

- Raw material aggregates and their individual gradings

- General conformance with ODOT specifications for 404 mix.

For mix design investigation, five levels of binder were used, namely: 5.5, 6, 6.5, 7, and 7.5 percent by weight of total mix. The optimum asphalt content for the selected aggregate gradation (table 6) was determined using Marshall design procedures, and 75 blows/face compaction efforts. Optimum asphalt content was determined as the average of asphalt content

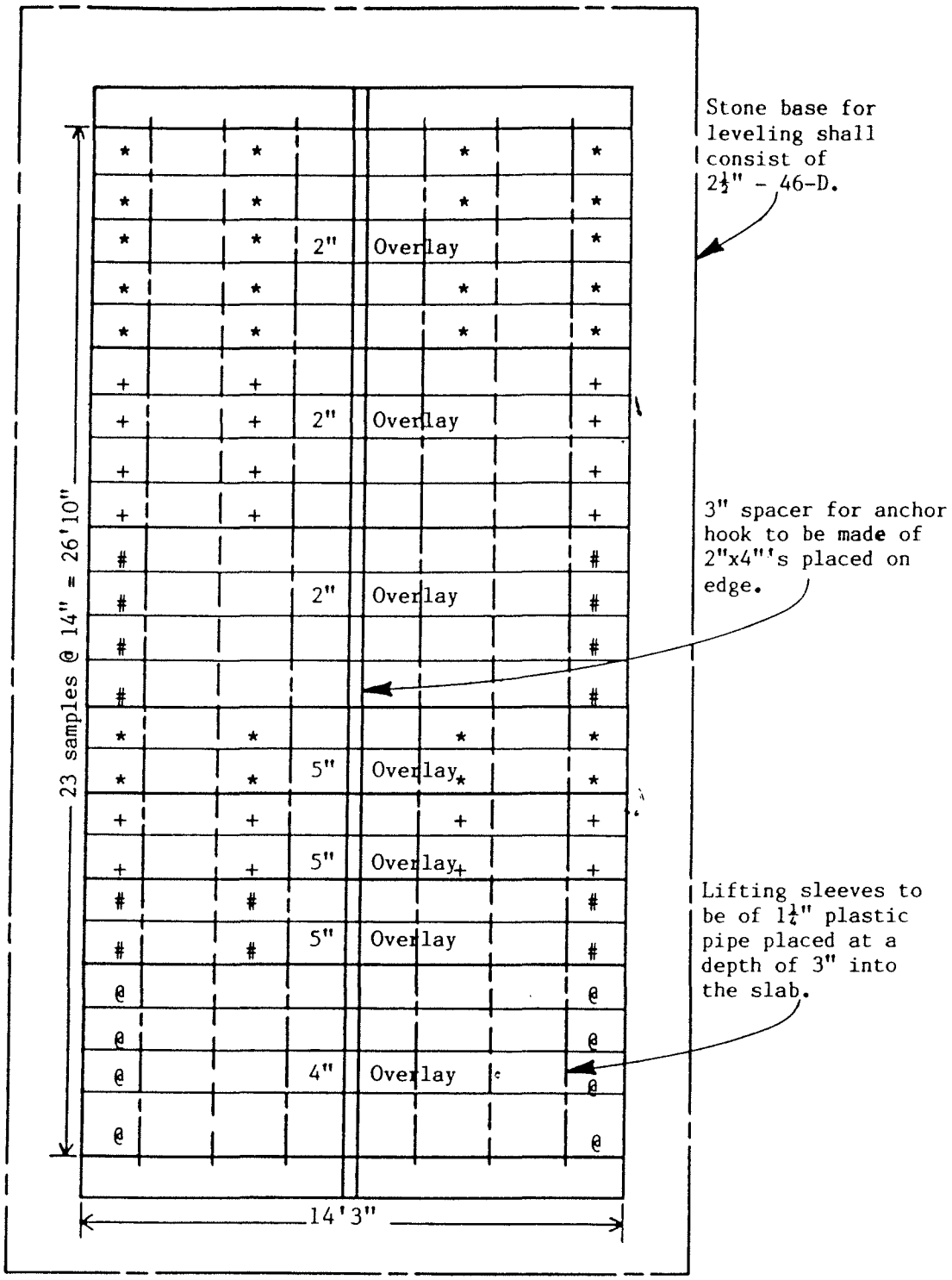

RIGID PAVEMENT BEAMS

- Overlay with AC-20 tack coat
- Overlay with Owens Corning Fabric
- Overlay with SAMI tack coat
- Arkansas open graded mix

Figure 39. Plan of test pavement for flexible overlay over rigid pavement.

for optimum stability, density, and 4% air voids. Table 7 shows the Marshall mix design properties for this mix.

4.4 Final Sample Preparation

4.4.1 Flexible Overlays Over Rigid Base

The rigid base was initially built as a test pavement of size 26 ft 10 in by 14 ft 3 in x 6 inches thick (8.2 m x 4.3 m x 154 mm), as described in section 4.3.1. The test pavement was treated with high modulus woven fabric membrane, SAMI, and open-graded asphalt aggregate system (Arkansas). The first two treatments were installed by manufacturers' representatives. Various phases of construction and installation of SAMI and high modulus fabric are presented in the attached photographs (figures 40A, 40B, and 40C). The test pavement was divided into different sections, as shown in figure 39, for obtaining sufficient number of beam specimens required for laboratory tests. The treatments are briefly described below:

- SAMI - This treatment is comprised of a mixture of asphalt cement (AC-20) and polypropylene fibers according to manufacturers recommendations. AC-20 was heated to 240 ^{o}F (115 ^{o}C) and the fibers (pre-determined quantity) were mixed with the heated AC-20. Mixing was continued for 60 to 90 seconds, to obtain a thick mix of the material and then placed over the prepared concrete base beam. Two and five inches thick (51 and 127 mm) asphalt concrete overlays were placed over the SAMI-treated base beam and the overlay compacted with a vibratory roller according to ODOT specifications.

- High modulus fabric membrane - The prepared concrete base beam was treated with a tack coat using Roadbond heated to 300 ^{o}F (149 ^{o}C), and then the woven fabric membrane was placed over the tack coat. The fabric surface was brushed to bring it into complete contact with the tack coat. Thereafter, the top of the fabric was treated with another layer of tack coat using Roadbond. The rate of application of Roadbond before and after placement of the fabric membrane was 0.25 and 0.15 gallon per square yard of the area covered, respectively (1.13 and 0.68 litres per square meter). Two- and five-inch (51 and 127 mm) thick asphalt concrete overlays were placed over the treated base beam and the overlay compacted with a vibratory roller.

- Arkansas treatment: The prepared concrete base beam was overlaid initially with a 2-inch (51 mm) thick

Table 5
Asphalt concrete aggregate gradation.

#8 Limestone		Natural Sand	
Sieve Size	% Passing	Sieve Size	% Passing
1/2"	100	3/8"	100
3/8"	85-100	#4	90-100
#4	10-30	#8	65-100
#8	0-10	#16	40-85
#16	0-5	#30	20-60
		#50	7-40
		#100	0-20
		#200	0-10

1 inch = 25.4 mm

Table 6
Aggregate gradation for asphaltic concrete.

Sieve Size	% Passing	ODOT 404 Gradation
1/2"	100	100
3/8"	97.5	90-100
#4	58.8	45-75
#16	28.4	15-45
#50	8.5	3-22
#200	4.5	0 -8

1 inch = 25.4mm

Table 7
Asphalt concrete mix design properties.

A.C. Content	- 6.2%
Stability	- 1810 lbs. (833 kg)
Flow	- 11
Air Voids	- 4.5
Unit Wt.	- 141 pct.
VMA	- 15

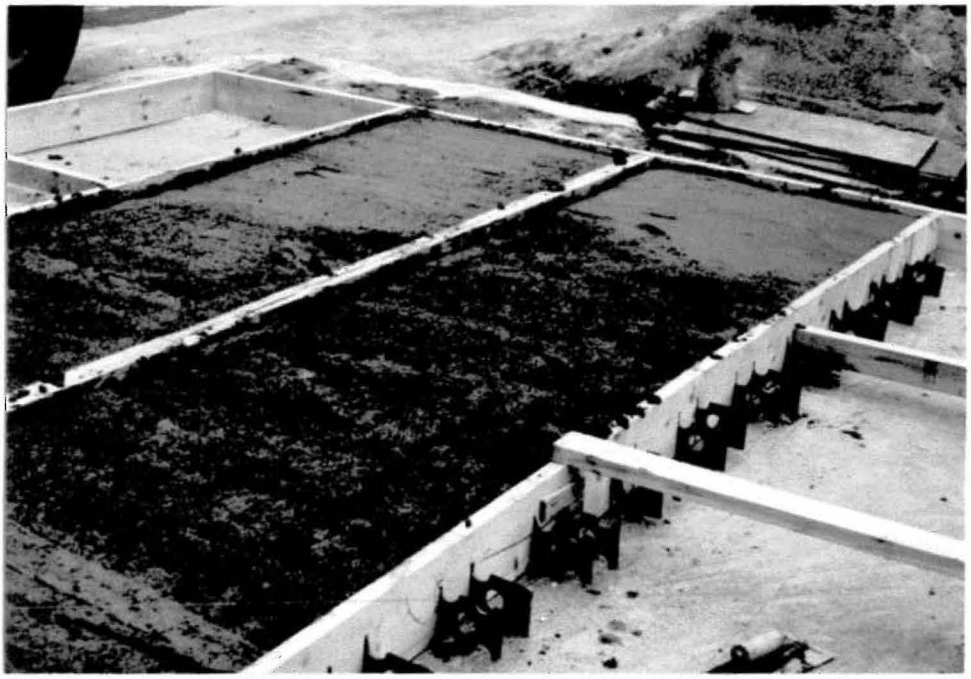

1. Concrete poured into forms.

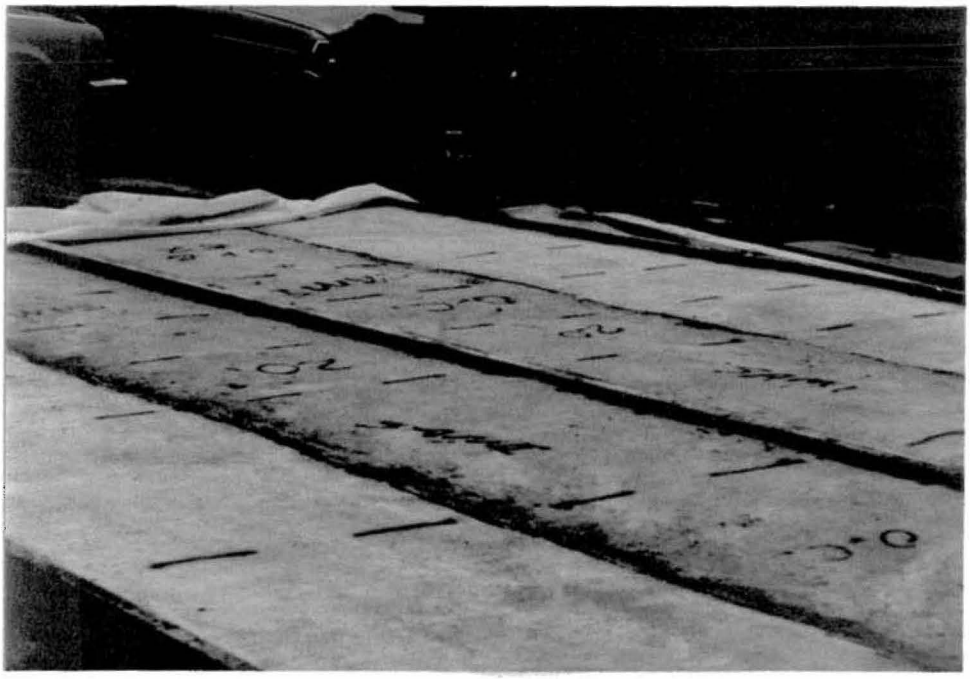

2. Finished concrete.

Figure 40A. Construction of test beams.

3. Installation of high-modulus fabric.

4. Installation of fiber-asphalt Sami.

Figure 40B. Construction of test beams.

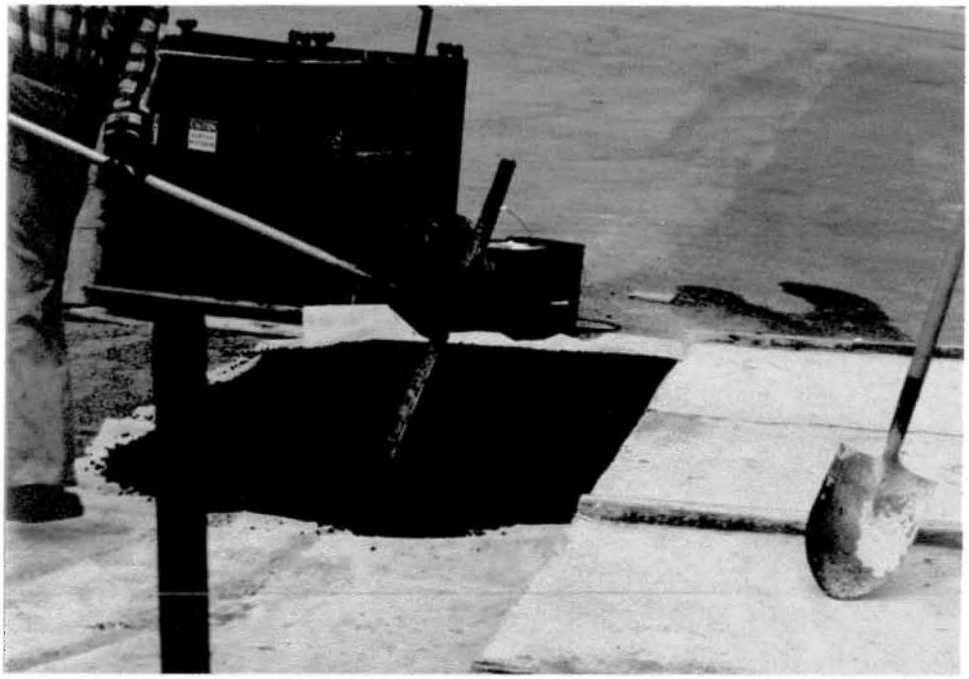

5. Paving for additional samples of overlay over flexible sections.

6. Compaction of flexible sections.

Figure 40C. Construction of test beams.

asphalt concrete open-graded mix, followed by 2 inches (51 mm) of ODOT 404 asphalt concrete mix. Tack coat was not used. The overlays were compacted with a vibratory roller.

- Control beams: The prepared concrete base beam was treated with a tack coat of asphalt cement (AC-20) at the application rate of 0.25 gallon per square yard (1.13 litres per square meter). An asphalt concrete overlay conforming to ODOT specifications was placed over the tack-coated concrete base beam, (2 and 5 inches in thickness (51 and 127 mm)) and compacted with a vibratory roller.

A 2-inch (51 mm) thick overlay placement was performed in one lift, and a 5-inch (127 mm) thick overlay was placed in two equal lifts. Thereafter, to obtain test speciments, the test pad was saw cut with a portable concrete saw. Table 8 shows the list of test specimens.

4.4.2 Flexible Overlays Over Flexible Base

Asphalt concrete (ODOT 404) mix, as described in section 4.3.2, was used for the fabrication of the base and overlay beams. A warehouse concrete floor was used for the fabrication of the beam specimens. The various stages of sample preparation are described below:

- Stage I: Test pavement of size 10 ft by 70 ft (3.1 by 21.3 m) was built with asphalt concrete according to ODOT specifications. The pavement was 4 inches (102 mm) thick and was built in two layers of equal thickness. Saw cuts were made in the base beam for crack severity "A" and "B", as shown in the attached sketch (figure 41). Crack severity "A" consisted of beams with 5 cracks, at the center and on either side of center at 6-in (152 mm) intervals, and crack severity "B" beams had 3 cracks, at the center and at each side of center at 12-in (305 mm) intervals. After the saw cut was made, the beams were provided with three types of treatment as described in the next stage.

- Stage II: The treatment to the asphalt base was similar to the procedure adopted for treatment to the rigid base beams, except that the membranes used were different. The base beam was treated with a low modulus and a high modulus fabric membrane. The third type of treatment was with "SAMI." The control treatment was carried out in the same way as for the rigid base.

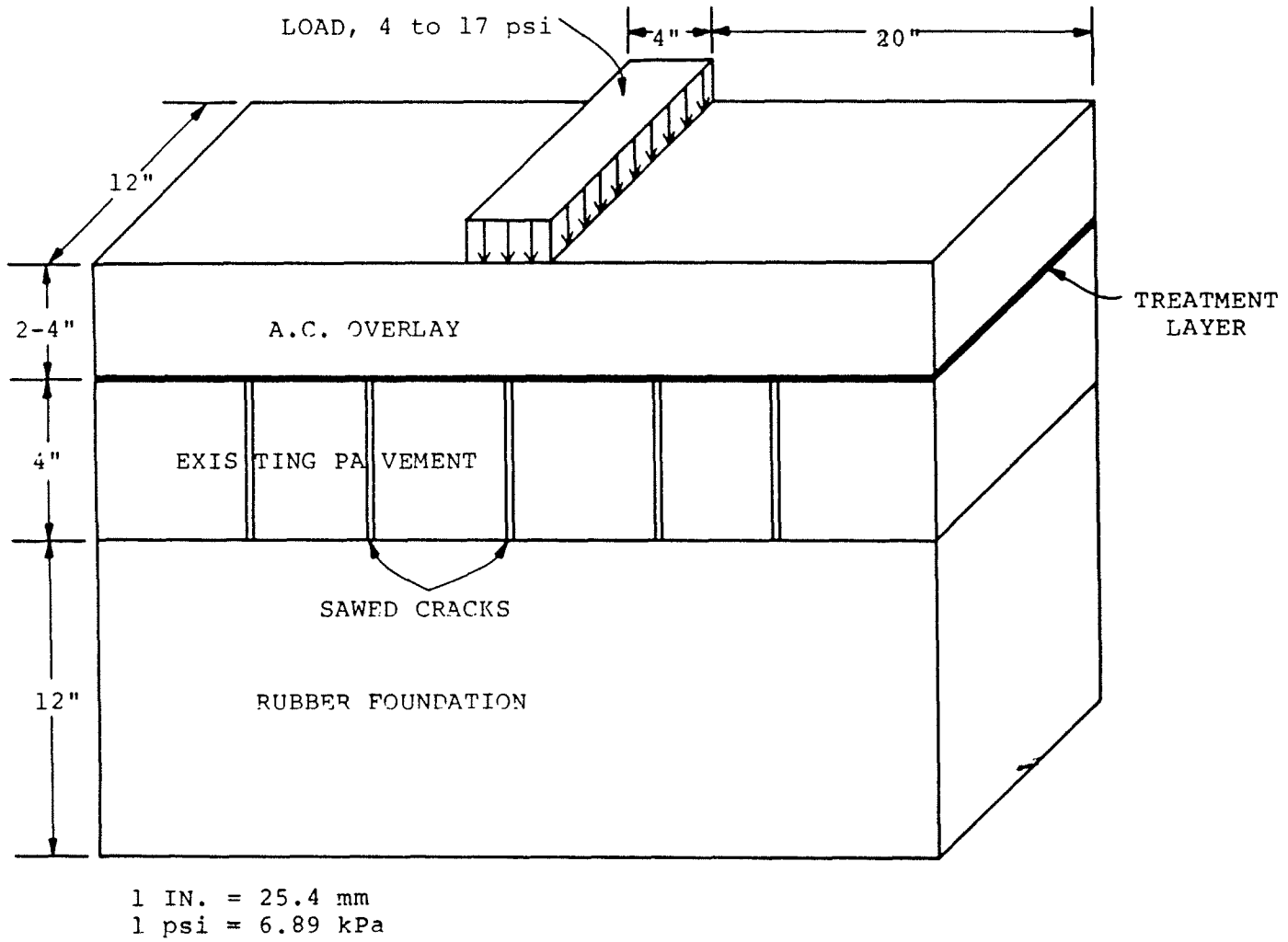

Figure 41. Laboratory simulation of overlaid flexible pavement.

Table 8
Rigid pavement overlay beams.

	Sample Type	Total # of Beams
A.	2" (5cms) thick overlay with ODOT 404 asphalt concrete over 6" (152 mm) thick cement concrete beams, with AC-20 tack coat.	10
B.	Same as "A" above but with High Modulus Woven Fabric at 2" (51 mm) depth. (Tack coat on both faces of fabric).	8
C.	Same as "A" above but with SAMI treatment at 2" (5cms) depth.	8
D.	5" (12.5cms) thick overlay with ODOT 404 asphalt concrete over 6" (152 mm) thick cement concrete beams, with AC-20 tack coat.	4
E.	Same as "D" above but with High Modulus Woven Fabric at 5" (127 mm) depth (Tack coat on both faces of fabric).	4
F.	Same as "D" above but with SAMI tack coat at 5" (127 mm) depth.	4
G.	4" (10cms) thick overlay with 2" (51 mm) of asphalt concrete open-graded and 2" (51 mm) of ODOT 404, over 6" (152 mm) thick cement concrete beams (Arkansas treatment).	8

- Stage III: The beams treated with membrane and the control beams were overlaid with 2 and 4 inches (51 and 102 mm) of asphalt concrete according to ODOT specifications. After the overlay, the overlay portion was sawcut to test sample size. Each fabricated beam was 48 inches long, 12 inches wide and 6 to 8 inches in depth (1200 x 300 x 150 to 200 mm). The depth varied depending on the overlay thickness (2 or 4 inches (51 mm or 102 mm).

Details of the beam samples fabricated for crack severity "A" and crack severity "B" are listed in tables 9 and 10. Photographs of various stages of sample preparation are shown in figures 42A through 42C.

Even though 80 beam samples were required for the tests, 16 additional samples, (two in each type of treatment), were fabricated for use. These beams consisted of one crack at the center of the beam, or crack severity "C."

The fabricated fatigue sawcut specimens, already placed on a stiff support, were carefully transported to the laboratory, to await testing. All precautions were taken to prevent bending and any possible damage to the beam sample.

Table 9
Four inch (102 mm) asphalt concrete overlay.

Beam Type	Crack Severity "A"	Crack Severity "B"	Total No. of Specimens
Control	5	5	10
Fiber "SAMI"	4	4	8
Low Modulus Fabric (Non-woven)	4	4	8
High Modulus Fabric (Non-woven)	4	4	8

Table 10
Two inch (51 mm) asphalt concrete overlay.

Beam Type	Crack Severity "A"	Crack Severity "B"	Total No. of Specimens
Control	5	5	10
Fiber "SAMI"	6	6	12
Low Modulus Fabric (Non-woven)	6	6	12
High Modulus Fabric (Woven)	6	6	12

Photo 1. Finished pavement section before sawing for test specimens.

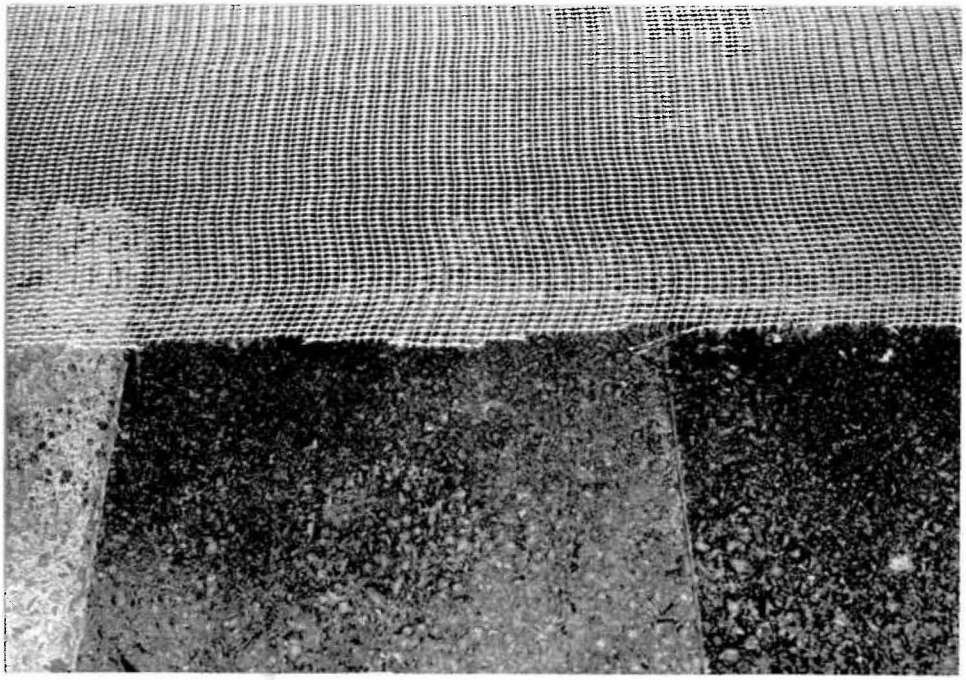

Photo 2. High modulus fabric placed over cracked pavement.

Figure 42A. Construction of flexible test beams.

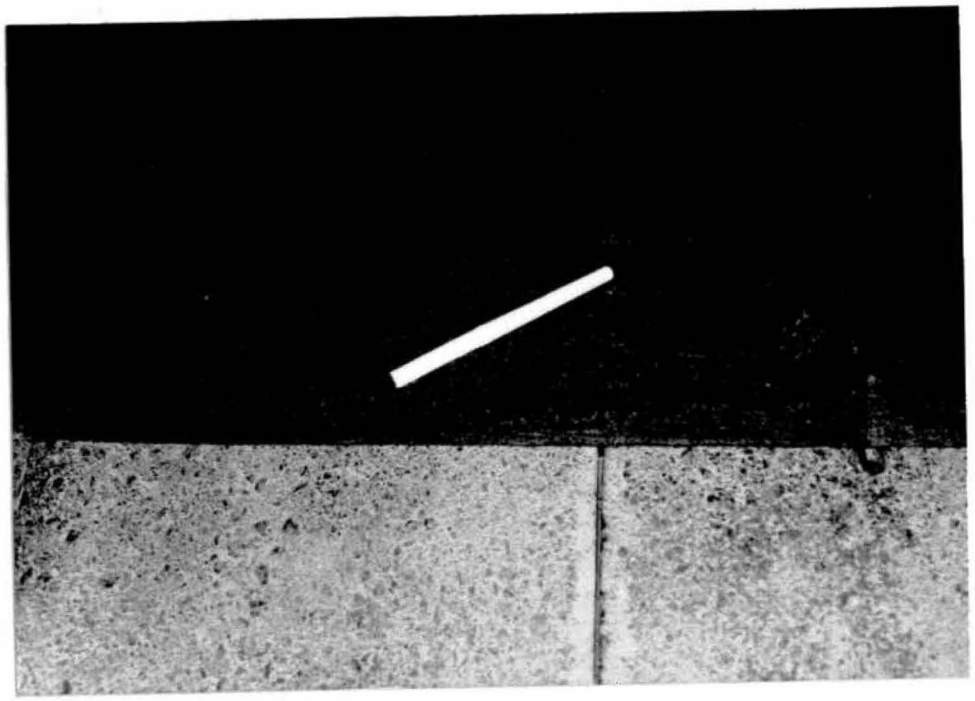

Photo 3. Low modulus fabric placed over cracked pavement.

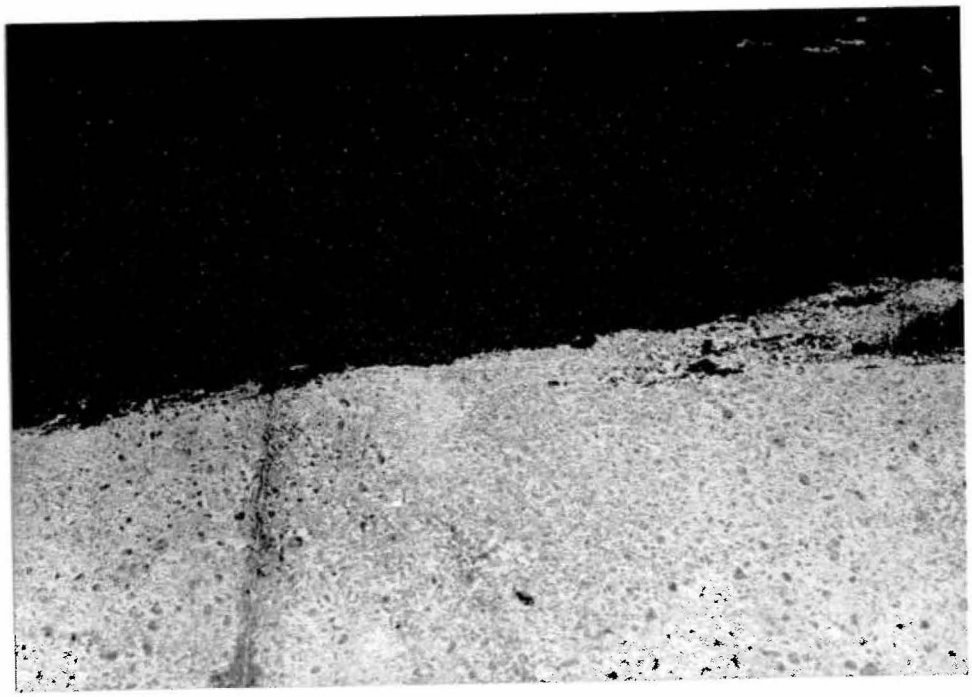

Photo 4. Fiber-asphalt Sami layer placed over cracked pavement.

Figure 42B. Construction of flexible test beams.

Photo 5. Paver being loaded for placement of overlay.

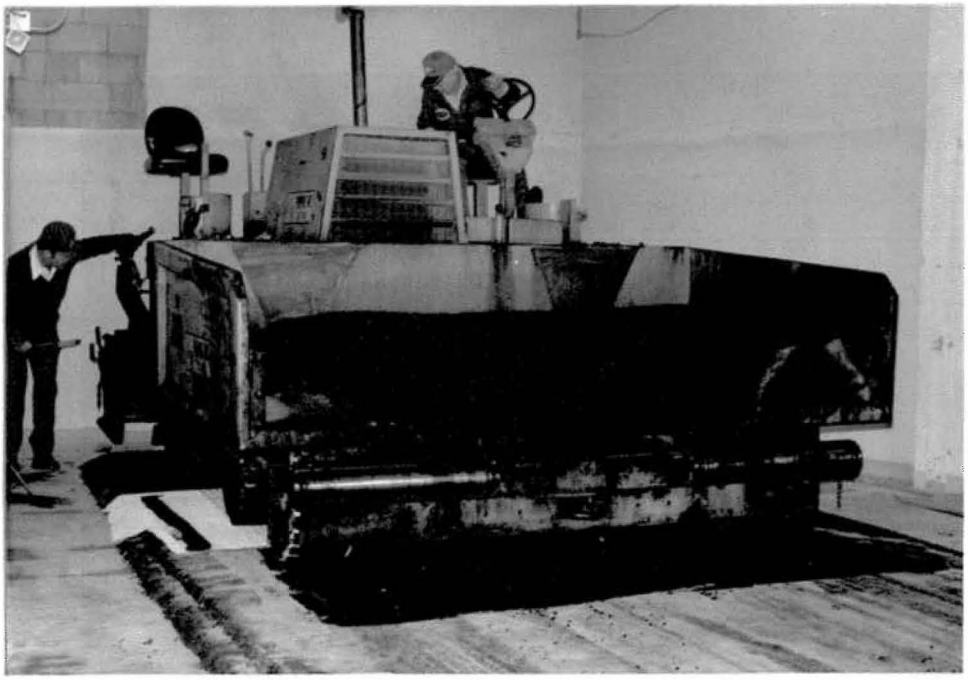

Photo 6. Paver placing overlay.

Figure 42C. Construction of flexible test beams.

4.5 Laboratory Testing

4.5.1 Flexible Overlay Over Flexible Base

The fatigue experiments were conducted using a beam on elastic foundation with geometry as shown in figure 41. The selection of this experimental setup was based on the two-dimensional modeling of a pavement structure, in which a beam representing the pavement is supported on an elastic foundation. The dimensions of the beam and foundation, as well as the stiffness characteristics of foundation, are selected with consideration to stress and strain at the bottom of the pavement, structure subjected to traffic loading. The test setup is the same as that used previously by Resource International and researchers at Ohio State University to study the fatigue properties of asphaltic mixtures.

An MTS electro-hydraulic testing system was used to apply the dynamic load for the fatigue tests. The dynamic loading consisted of 10 Hz haversine pulses repeated at the rate of 2 pulses per second, resulting in a recovery period of 0.4 seconds between loads.

The fatigue progress was monitored during the test program and the crack propagation recorded as a function of the number of cycles of loading. Tests were conducted at different vertical loads as indicated in table 11. The fatigue testing system used, is shown in the attached photographs, (figure 43).

4.5.2 Flexible Overlay Over Rigid Base

The beam samples used for the three types of tests were 84 inches long, 14 inches wide, and 8 to 11 inches in thickness (2130 by 360 by 200 to 280 mm), depending on whether the overlay was 2 or 5 inches (51 or 127 mm) thick. The base beam in all cases was 6 inches (152 mm) thick. For the testing of the beams, a special environmental chamber was fabricated to maintain the test temperature at 40 $\pm$ 2 $^{\circ}$F(4.4 $\pm$ 1.3 $^{\circ}$C) during the entire period of test. The following three types of tests were performed.

- Fatigue resistance under vertical load of asphalt overlay over concrete base. Seven beams were to be tested under this category.

- Tests under horizontal and vertical stresses, of asphalt overlay over concrete base under a constant horizontal strain rate of 0.4 micro inch (.001 microns) per second. Thirteen beams were to be tested under this category.

Figure 43. Test setup for flexible overlay samples.

Table 11
Loads used for testing flexible/flexible beams.

Beam Type*	2" (51mm) Overlay	4" (102mm) Overlay
Control	589: 392: 294	785: 589
Fiber SAMI	589: 392: 294	785: 589
Low Modulus Fabric (Non-Woven)	589: 392: 294	785: 589
High Modulus Fabric (Woven)	589: 392: 294	785: 589

*For 2 inches (51 mm) overlay two samples were tested at each stress level. For 4 inches (102 mm) overlay two samples were tested at each stress level. All tests were performed at 72 $\pm$ 2 ^{O}F (22 $\pm$ 1.3 ^{O}C)

- Fatigue resistance under vertical load and simulated thermal loading (average strain rate of 0.4 micro inch (.001 microns) per second) of asphalt overlays over concrete base. Nineteen beams were to be tested under this category.

Simulation of reflective cracking of rigid pavement overlays requires modeling of both thermal and traffic load condition. Thermal stresses result from both seasonal and daily changes in slab temperature. Model pavements designed for this research study involved application of external forces to produce joint movements equal to those of full scale pavements under field thermal loading. Traffic forces were simulated by applying dynamic vertical loads to the model which was a beam supported on an elastic foundation.

Thermal contraction was simulated by applying a horizontal displacement to the ends of the beam. The horizontal pull was applied by a hydraulic piston in displacement (stroke) control mode through a 2.5 to 1 wedge in order to reduce the applied strain rate below the limits of the MTS apparatus. A ramp function was used - it was intended that this loading mode would result in a constant joint opening rate. However, the loads developed during these tests were substantially greater than had been anticipated; consequently, since the reaction frame was not sufficiently stiff, the resulting joint opening rate was also a function of the specimen stiffness. Another problem with the equipment was that the maximum joint opening (plus frame

deflection) that could be obtained through the wedge - piston system was 0.2 in (5.1 mm); this meant that the system had to be reset several times during the course of some tests.

The developed horizontal load and the joint opening displacement (on both sides of the beam) were monitored during the temperature simulation tests, and the crack growth rate and applied vertical load were monitored when vertical load was present.

4.6 Other Laboratory Tests

Other tests required for materials characterization of asphalt and concrete are modulus of resilience, creep compliance, indirect tensile strength, and fracture toughness tests. Specimens for these tests were obtained by coring unused portions of the test beams.

The test procedure recommended by Kenis was used in creep compliance tests, but the method described in appendix E was used to develop a creep compliance function of the form of equation 56.[44] The procedure developed at Ohio State University was used for fracture toughness tests.[28]

CHAPTER V. ANALYSIS OF TEST DATA

5.1 Laboratory Results of Flexible Overlays Over Flexible Pavements

As discussed in chapter IV, a total of 96 specimens were tested, representing four different treatments. Each specimen was tested under constant load, but the load was varied from specimen to specimen in order to achieve a range in Nf, the number of load applications to failure. Failure in this case was defined as the number of applications required for the crack to go all the way through the overlay.

The existing pavement was "cracked" artificially by sawing through the pavement layer prior to overlay placement, as was discussed in chapter IV. Each specimen had either five cracks at the center and at 6-inch (152-mm) intervals, severity A, three cracks at the center and at 12-inch (305-mm) intervals, severity B, or one crack at the center, severity C. A double layer of teflon was placed between the specimen and the gum rubber foundation; therefore, the analysis was done assuming a frictionless interface.

The 2-D finite element program, EFRON, was used to compute the critical strains in the overlay for each test specimen, taking into consideration both specimen dimensions as well as crack severity. Since the properties of the asphalt-saturated fabrics were not known, it was assumed initially that the fabric properties were the same as that of the overlay as was discussed in section 3.4.6. It was hoped that this procedure would result in parallel curves of strain vs. Nf, with fabric reinforced systems having longer fatigue lives. The fabric properties could then be deduced from the amount of shift required in the Nf curves. The number of applications to failure as a function of critical strain are plotted for each treatment in figures 44 through 47, and figure 48 shows a plot of all data. As may be seen from these figures, a reasonably coherent relationship exists between strain and Nf, although some scatter exists in this data. It is suspected that the variation in bond strength (between original pavement and overlay/ treatment) is the primary cause of this variation. In fact, one test point, in each of figures 44, 46, and 47, was omitted from further analysis because these specimens developed severe debonding after only a few hundred load applications.

The test points corresponding to each crack severity level are identified in figures 44 through 47. Since the different crack severities do not form any consistent pattern, it can be concluded that the effect of crack severity on critical strains has been satisfactorily included in the analyses models.

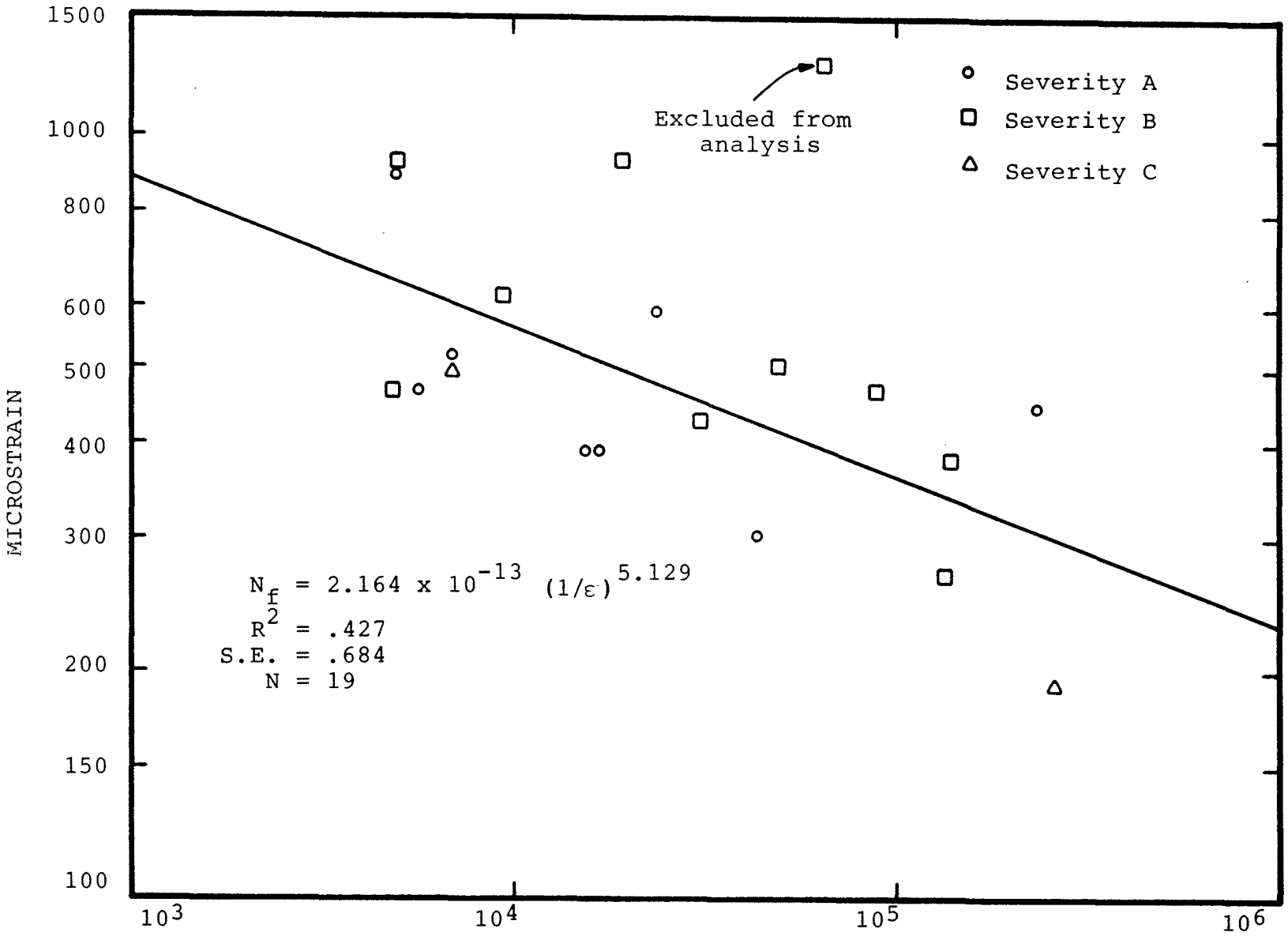

Figure 44. Strain vs N_f for control beams.

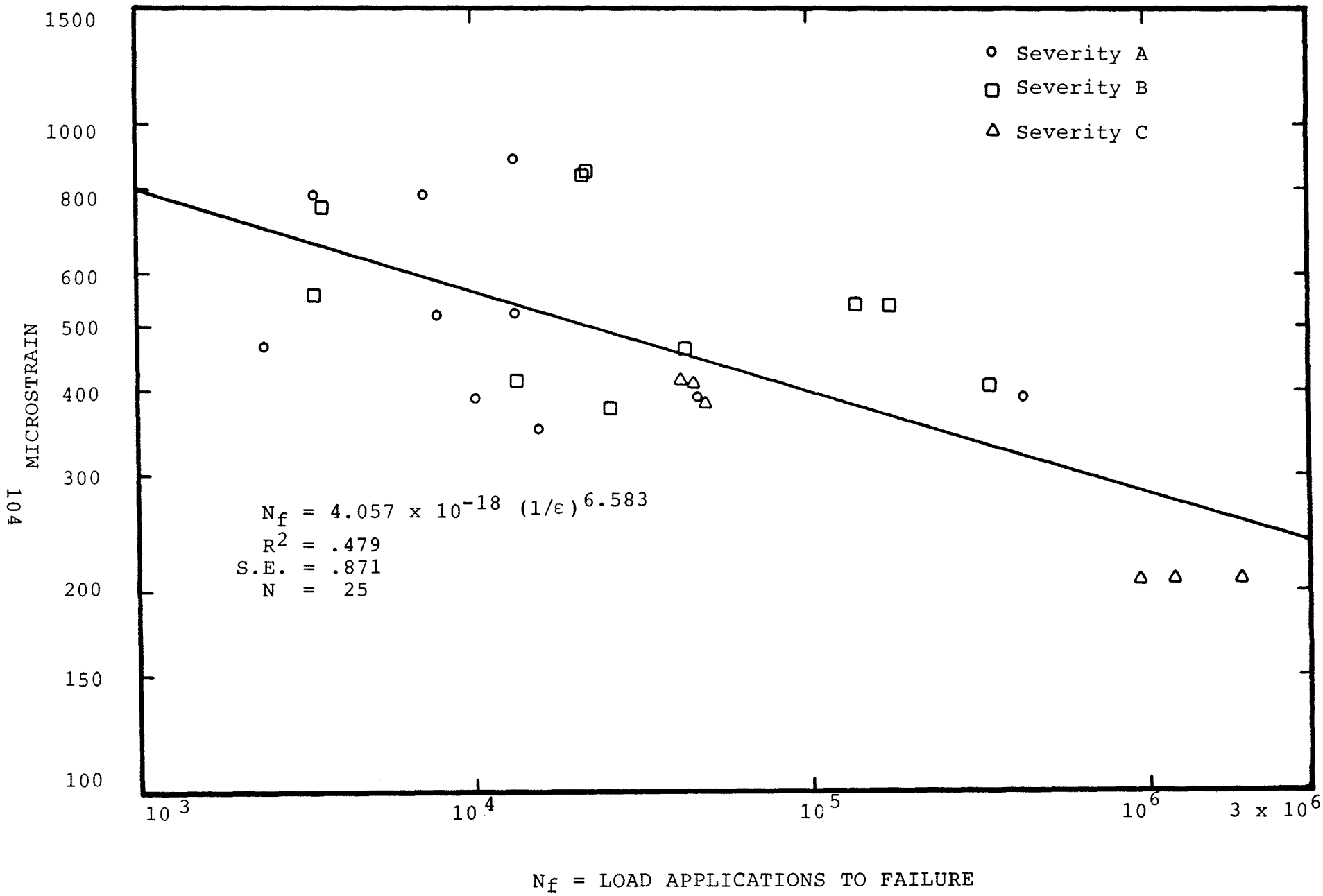

Figure 45. Strain vs N_f for low modulus fabric.

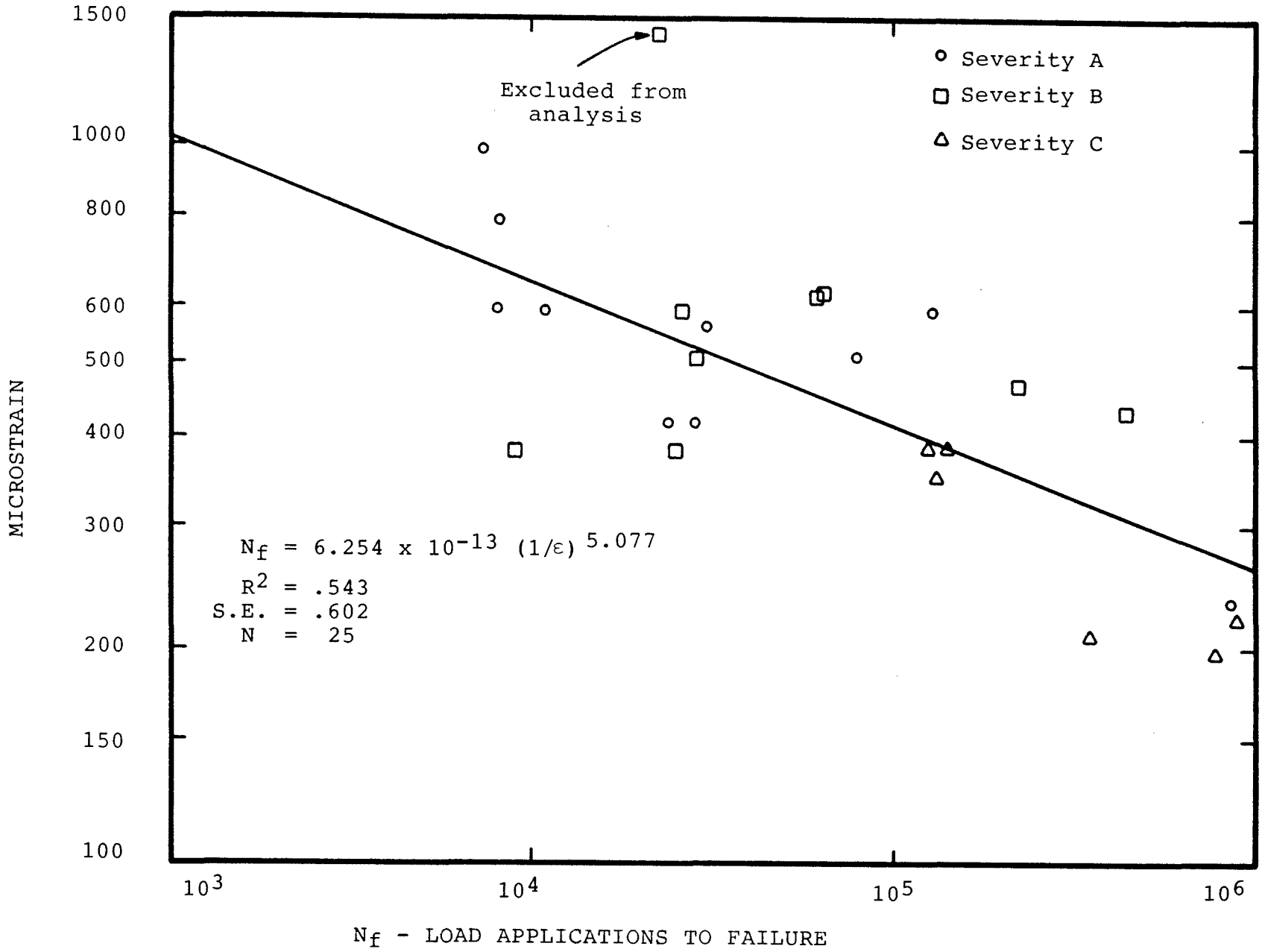

Figure 46. Strain vs N_f for high modulus fabric.

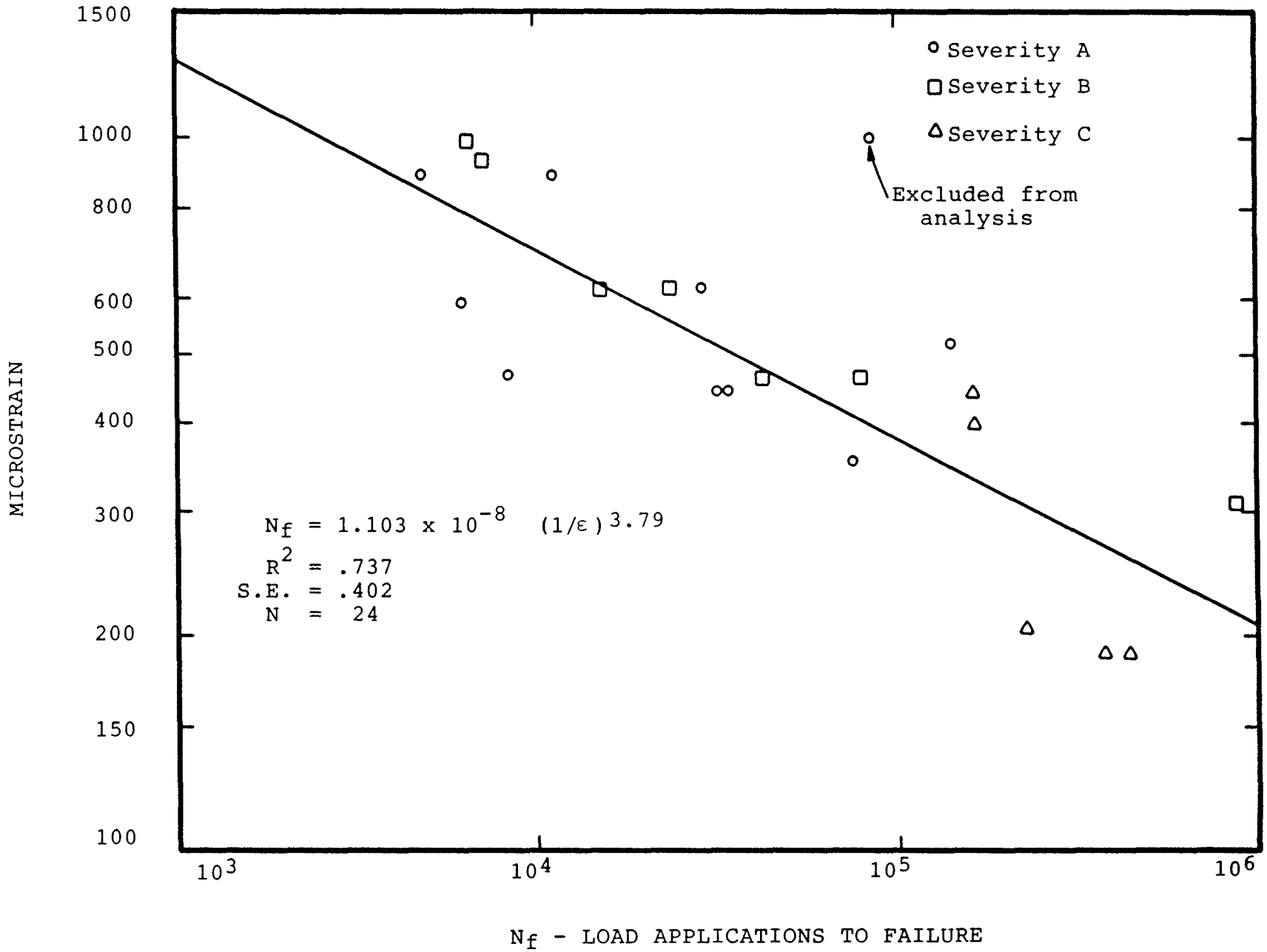

Figure 47. Strain vs N_f for fiber Sami.

Regression equations of the form:

$$Nf = k1\ (1/\varepsilon)^{k2} \qquad (63)$$

were developed for each treatment, as well as for all data combined. These equations and the pertinent statistical information (R Square and Standard Error) are shown in figures 44 through 48, and summarized in table 12, and figure 49. It can be seen from table 12 that the correlation coefficients (R Square) for all but the fiber SAMI model are rather low, and the Standard Errors of estimate (in terms of log Nf) are quite high - only the fiber SAMI model has statistics comparable to the field performance distress functions developed from the AASHO Road Test data using layer theory.

Although regression equations are quite different in form, the predicted fatigue lives are not all that different, especially when considering the standard error of estimate associated with each model. As may be seen from figure 49, the equations for no fabric and low and high modulus fabric predict comparable fatigue lives, but curve 4 for fiber SAMI interface appears to be somewhat different; however, this difference is very difficult to determine from figure 48.

The statistical parameters (correlation coefficient and standard error) presented in table 12 indicate that the combined equation (based on all data) represents the data about as well as do the individual models, except possibly the fiber SAMI data. If there is no significant difference in the behavior with no fabric and low and high modulus fabric, but there is a difference with fiber SAMI, as is suggested by the plots in figure 49, then it might be expected that a regression equation developed from all but the fiber SAMI data should show an improvement of the statistical parameters (R Square and Standard Error) even though the population decreases by 24 members. This, however, is not the case, as is shown in table 12. In fact, the correlation coefficient for this model is lower than for all but the no fabric model, and the Standard Error is higher than for all but the low modulus fabric, even though these models have populations approximately 3 times smaller. Thus, the conclusion, that the performance of the fiber SAMI treatment is significantly different from that of the other treatment, does not seem to be justified.

The "Student-T-test" is generally used to determine if a statistically significant difference exists in a series of measurements. However, since the specimens were tested at widely varying strain levels, the test cannot be applied to Nf values. The T-test can, however, be applied to the error between predicted (from the regression equation) and measured Nf values. The results of this analysis are shown in tables 13 through 15, corresponding to 90, 95, and 99 percentile confidence levels.

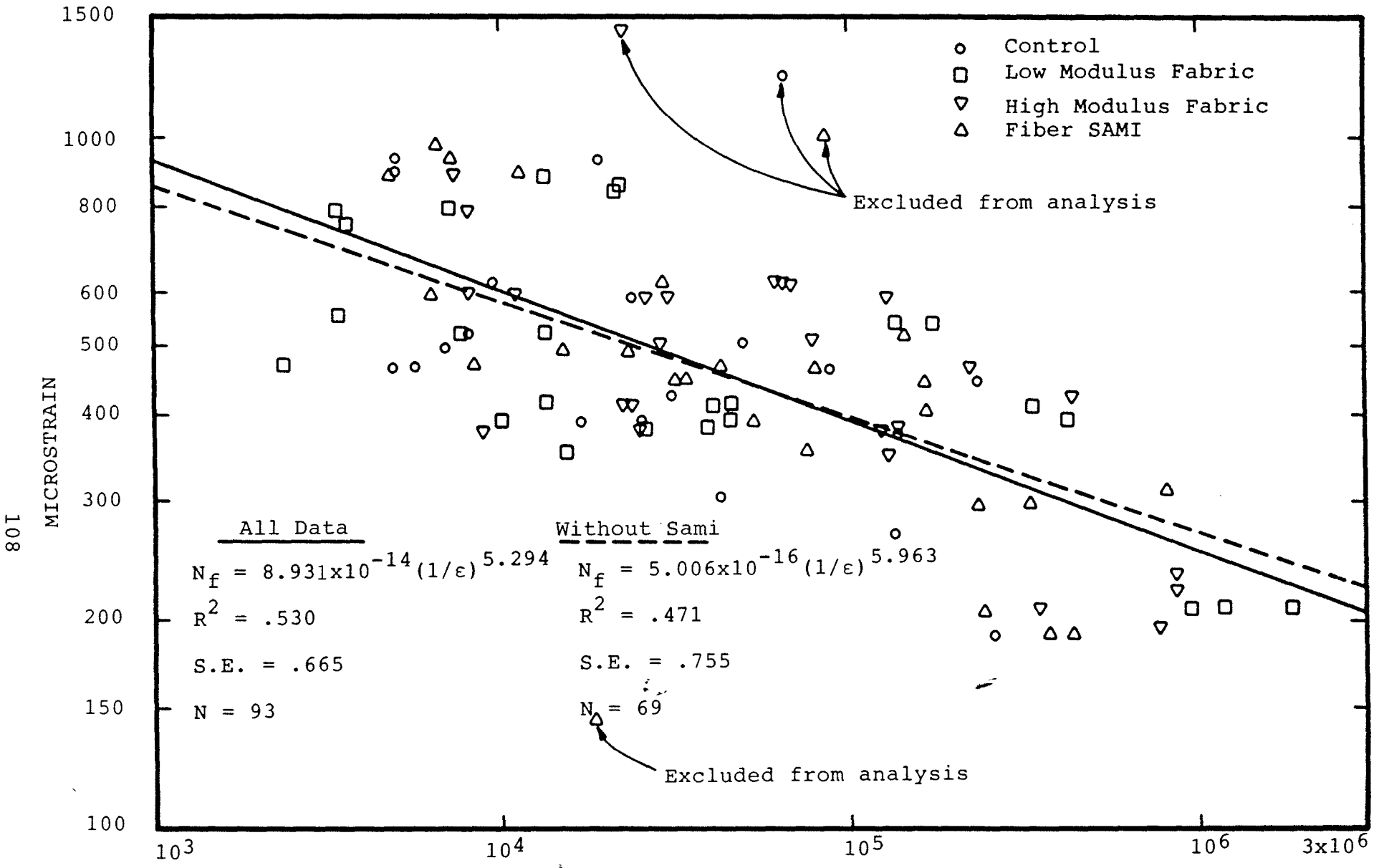

Figure 48. Strain vs. N_f - all tests.

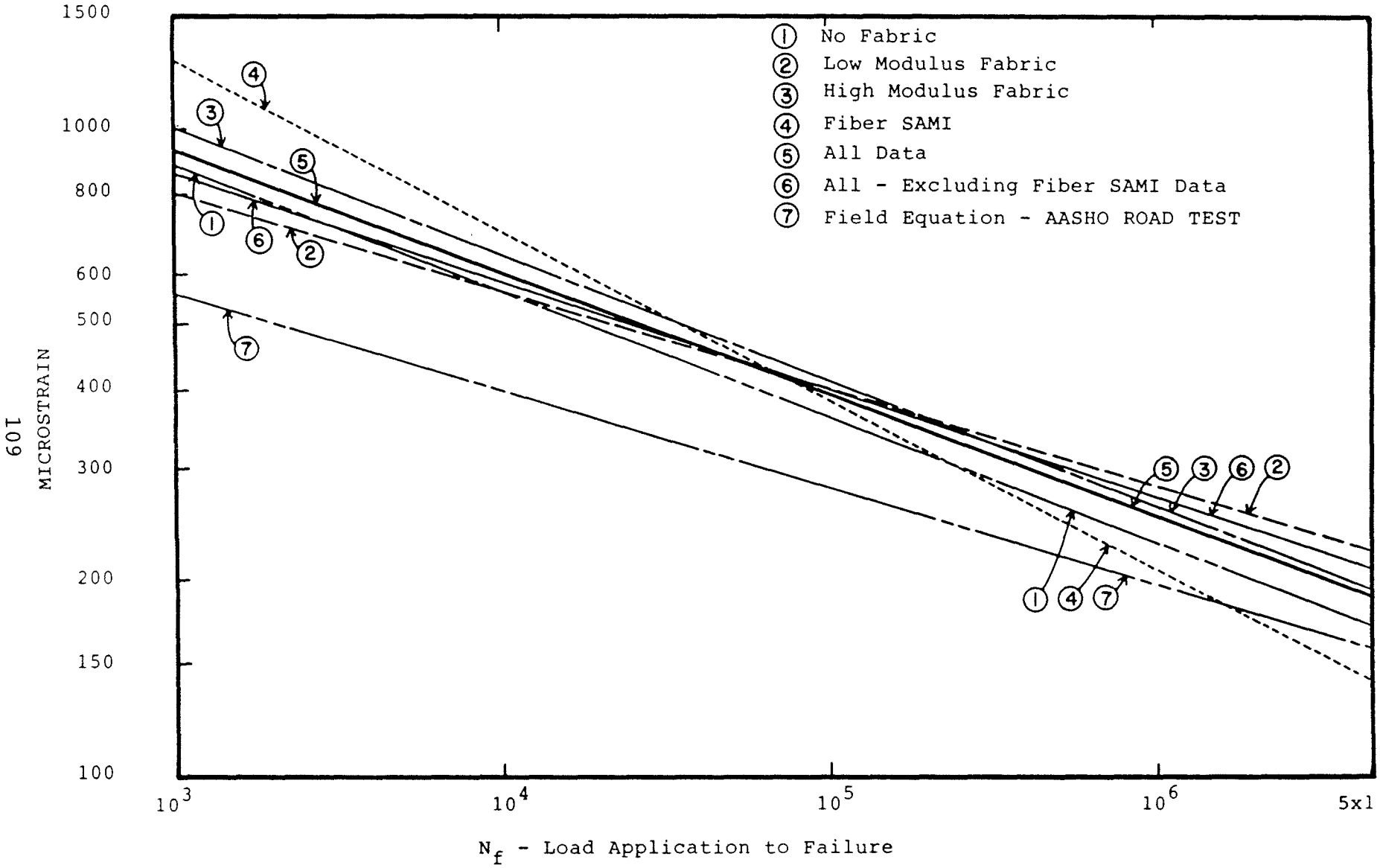

Figure 49. Regression equations for flexible overlay over flexible pavement.

Table 12
Regression equations relating strain to Nf, flexible overlay over flexible pavement laboratory tests.

Fabric	No. of Tests	K1	K2	R	Std. Error*
None	19	2.164×10^{-13}	5.129	.427	.684
Low Modulus	25	4.057×10^{-18}	6.583	.479	.871
High Modulus	25	6.254×10^{-13}	5.077	.543	.602
Fiber SAMI	24	1.103×10^{-8}	3.790	.737	.402
All Combined	93	8.931×10^{-14}	5.294	.530	.665
All Excl. SAMI	69	5.006×10^{-16}	5.963	.471	.755
AASHO ROAD TEST+	23	2.940×10^{-19}	6.619	.817	.382

* Standard error expressed terms of log Nf
\+ Developed using layer theory analysis of AASHO flexible pavements for maximum strain under dual tire.

The Student T-test tests the hypothesis that the models are statistically the same, i.e., PASS means that there is statistically no significant difference in the models, and FAIL indicates that the difference is significant at the specified confidence level. Thus, the results in table 15 indicate that at 99 percent confidence level, the SAMI model is different from all other models. These results apparently disagree with the decrease in correlation coefficient and the increase in standard error discussed above. Therefore, more detailed analysis was carried out in order to determine the extent of differences in these models.

An analysis of variance was therefore carried out according to the procedure described in reference 45. This procedure is a standard analysis technique and will not be repeated here.

Table 13
Student T test for 90 percentile confidence level.

MODEL	VS. MODEL	DF	CALCULATED T	90 P/C CONF. LEVEL TABLE T	PASS/FAIL
None	Low	42	1.457	1.683	PASS
None	SAMI	41	3.358	1.683	FAIL
None	High	42	0.982	1.683	PASS
None	All	110	0.343	1.660	PASS
None	All-S	110	0.518	1.660	PASS
Low	SAMI	47	4.605	1.679	FAIL
Low	High	48	2.488	1.679	FAIL
Low	All	116	2.372	1.659	FAIL
Low	All-S	116	1.277	1.659	PASS
SAMI	High	47	2.253	1.679	FAIL
SAMI	All	115	3.210	1.659	FAIL
SAMI	All-S	115	3.818	1.659	FAIL
High	All	116	0.832	1.659	PASS
High	All-S	116	1.679	1.659	FAIL
All	All-S	184	1.453	1.645	PASS

-S: Fiber SAMI samples excluded

Table 14
Student T test for 95 percentile confidence level.

MODEL	VS. MODEL	DF	CALCULATED T	95 P/C CONF. LEVEL TABLE T	PASS/FAIL
None	Low	42	1.457	2.019	PASS
None	SAMI	41	3.358	2.020	FAIL
None	High	42	0.982	2.019	PASS
None	All	110	0.343	1.983	PASS
None	All-S	110	0.518	1.983	PASS
Low	SAMI	47	4.605	2.014	FAIL
Low	High	48	2.488	2.013	FAIL
Low	All	116	2.372	1.981	FAIL
Low	All-S	116	1.277	1.981	PASS
SAMI	High	47	2.253	2.014	FAIL
SAMI	All	115	3.210	1.982	FAIL
SAMI	All-S	116	3.818	1.982	FAIL
High	All	116	0.832	1.981	PASS
High	All-S	116	1.679	1.981	PASS
All	All-S	184	1.453	1.960	PASS

-S: Fiber SAMI samples excluded

For the purpose of analysis, the regression equations were developed to fit the Nf - strain data in the form of:

$$\log (\text{strain}) = A + B \log (Nf) \tag{64}$$

for each of the four treatments used. Equation 64 rather than

$$\log (Nf) = A + B \log (\text{strain}) \tag{65}$$

was used because equation 64 results in a better fit to the test data.

The results of the analysis of variance are presented in table 16. The conclusions of the analysis of variance are that at the 95 percentile confidence level, all treatments are the same, whereas at the 90 percentile confidence level, the low modulus fabric is different from the fiber SAMI, and all other treatments are the same. Even here, the F* value (for low modulus - fiber SAMI) is only slightly greater than the corresponding F value for 90 percentile; at 92 percentile level, the difference in these treatments would not be statistically significant. Consequently, the conclusion is inescapable that fabric reinforcement is of little value in overlays of flexible pavements. This conclusion is at variance with many laboratory studies and some field studies; however, most laboratory studies do not include an analysis of variance to determine if the apparent differences are significant statistically. It is suspected that careful analysis of the statistical significance may make these differences smaller.

It was stated earlier that since the fabric properties were not known, the fabric layer was treated as being part of the overlay, i.e., with the same properties as the overlay. It can be argued that this is an unrealistic representation of the fabric layer and therefore, the conclusions are questionable. However, that argument is not valid since the data did not show any difference between the treatments. Had the Nf-strain relationship for the fabric-treated specimens and the control specimens been different, it would have been possible to deduce the fabric properties from this difference. Since the analysis did not show any difference among the various treatments, it can be concluded that the treatments did not significantly alter the overlay properties.

One further argument exists in favor of the method used; namely, that the Nf of the various treatments were approximately the same under the same loading conditions. Since the specimen dimensions (thickness and width) varied from specimen to specimen, the effect of these variations on load is somewhat more difficult to determine than for strains; nevertheless, significant differences were not found.

Table 15
Student T test for 99 percentile confidence level.

MODEL	VS. MODEL	DF	CALCULATED T	99 P/C CONF. LEVEL TABLE T	PASS/FAIL
None	Low	42	1.457	2.700	PASS
None	SAMI	41	3.358	2.702	FAIL
None	High	42	0.982	2.700	PASS
None	All	110	0.343	2.624	PASS
None	All-S	110	0.518	2.624	PASS
Low	SAMI	47	4.605	2.689	FAIL
Low	High	48	2.488	2.686	PASS
Low	All	116	2.372	2.620	PASS
Low	All-S	116	1.277	2.620	PASS
SAMI	High	47	2.253	2.689	PASS
SAMI	All	115	3.210	2.621	FAIL
SAMI	All-S	115	3.818	2.621	FAIL
High	All	116	0.832	2.620	PASS
High	All-S	116	1.679	2.620	PASS
High	All-S	116	1.675	2.620	PASS
All	All-S	184	1.453	2.576	PASS

-S: Fiber SAMI samples excluded

Table 16
Comparison of treatments.

Treatment	F*	F(90)	F(95)
N - P	.33	2.46	3.26
N - H	1.75	2.46	3.26
N - B	.95	2.46	3.26
P - H	2.83	2.46	3.26
P - B	.64	2.46	3.26
H - B	.98	2.46	3.26

N - no fabric
P - Low modulus fabric
H - Hercules fiber SAMI
B - High modulus fabric

5.2 Laboratory Results of Flexible Overlays Over Rigid Pavements

Three types of tests were run on the rigid overlay samples:

- Vertical load alone.
- Horizontal pull alone.
- Combination of the above.

Each of these types of tests are described in the following sections.

5.2.1 Vertical Load

These series of tests were intended to simulate traffic loading and its contribution to crack formation. Only a few tests were run to establish a trend since the fatigue equation developed in the flexible series could be used to characterize asphalt fatigue; this equation would only need to be shifted to reflect the change in test temperature. Figure 50 shows the individual tests as well as the regression line (dot-dash line) derived from the flexible fatigue data described in section 5.1. As is seen from this figure, there is significant scatter in this data, but the solid line, derived based on a shift of the 72 ^{O}F (22 ^{O}C) data to the 40 ^{O}F (4 ^{O}C), is a reasonable fit to this data. The big outliers are the C (control) and the H (fiber SAMI) beams.

The critical strains used in the Nf calculation were derived using the EFRON computer program, with the pertinent properties listed in table 17.

5.2.2 Horizontal Pull Tests

These series of tests were intended to simulate the effect of seasonal temperature drop on joint opening and crack formation. As was discussed in section 4.5.2, the test setup consisted of the beam being pulled apart at more-or-less constant strain rate and observing the joint opening, developed load and crack propagation as a function of time. In all, 13 specimens were tested, which included 2 specimens with the Arkansas open-graded cushion course which could not be used for analysis. These specimens (Arkansas treatment) debonded from the concrete very quickly into the test; consequently, the strain resulting from the joint opening was not transmitted to the overlay.

The test results (time to failure) are plotted as a function of the asphaltic concrete cross section (beam width times overlay thickness) in figure 51. The lines represent the best fit lines through the data points, with the constraint that the lines must go through zero. The equations of the regression lines, along

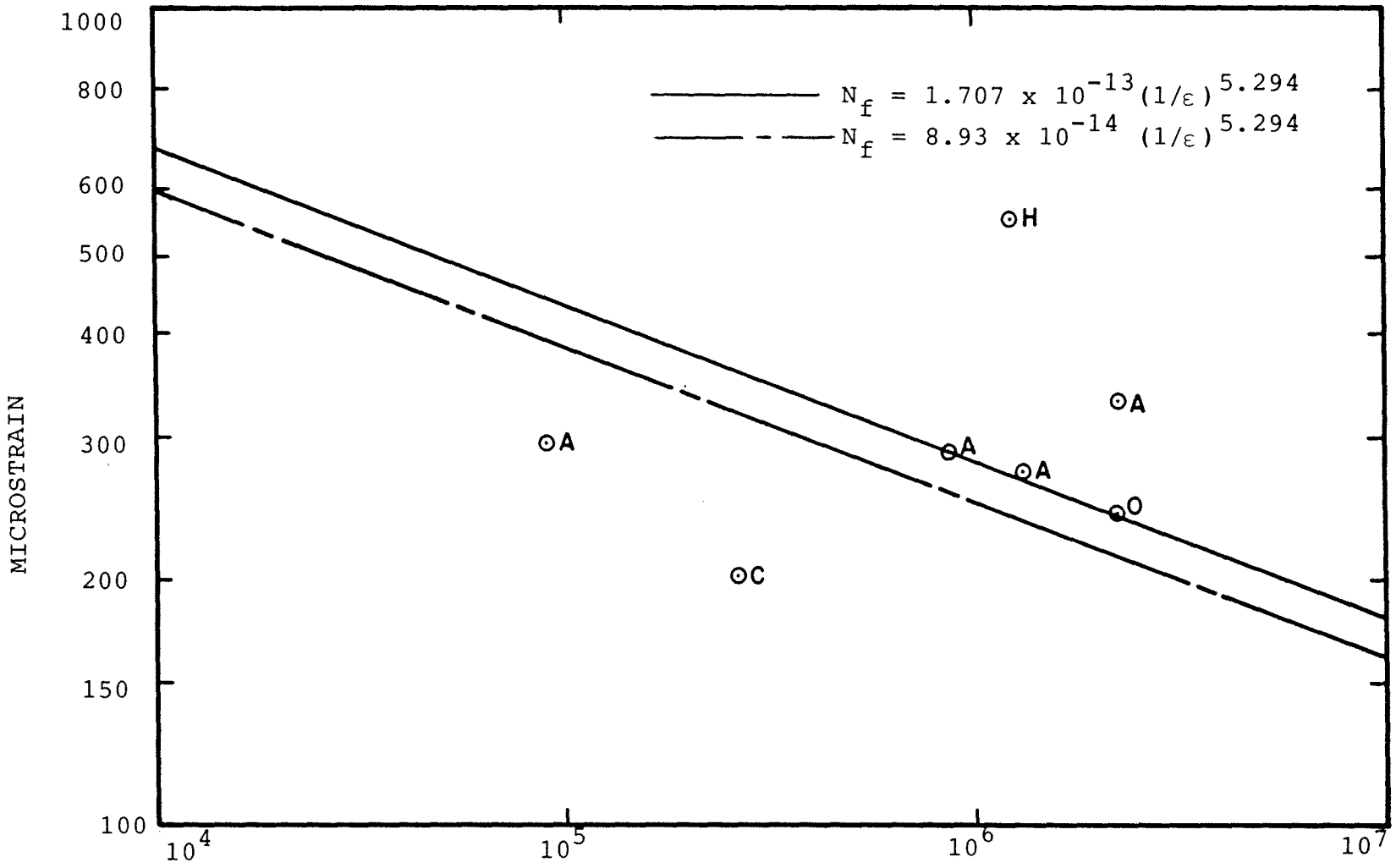

N_f = Load Applications to Failure

Figure 50. Fatigue tests of A.C. overlay over PCC.

Table 17
Data for fatigue tests.

Sample No.	Width In. (mm)	Hov In. (mm)	Load lbs. (N)	Strain Micro	Nf Thousands
150	13.8 (351.)	2.5 (63.5)	300 (1332)	241	2225
36H	14.2 (362.)	2.0 (50.8)	550 (2442)	553	1242
2A	14.0 (356.)	4.5 (114.)	450 (1998)	292*	880
4A	14.0 (356.)	4.5 (114.)	450 (1998)	292*	91
24A	15.0 (381.)	4.5 (114.)	450 (1998)	273*	1324
27A	14.5 (368.)	4.0 (102.)	550 (2442)	331*	2283
20C	14.0 (356.)	2.0 (50.8)	200 (888)	205	268

Modulus of AC = 1,250,000 psi (8.62 GPa)
*Modulus of cushion layer = 700,000 psi (4.83 GPa)
Modulus of concrete = 4,500,000 psi (31.0 GPa)
Modulus of foundation = 150 psi (1.03 MPa)

with the root mean square error, are also shown in this figure. Although there is scatter in the data, it is apparent that the high modulus fabric (points 0) increases the time to failure significantly (1.95 times), whereas the fiber SAMI material (points H) appear to have a very small effect - the effectiveness from this analysis is about 1.08. However, when considering the scatter in the data, the effectiveness of 1.08 is not significant. It is, however, encouraging that this effect is positive (greater than one) rather than negative.

The model developed in chapter III was also applied to this data. Equation 62 (Program RECK) was used to predict the time to failure from the following input information:

- joint opening vs time
- developed load vs time
- test temperature
- creep compliance
- modulus of resilience
- indirect tensile strength
- fracture toughness

(the first three items were measured for each test; the remaining variables were determined from laboratory tests discussed in section 4.6). It should be pointed out that the analysis of failure time assumes that the creep compliance can be expressed in the form given in equation 56. Appendix E gives details of one method that can be used in fitting test data with this form.

As was discussed in section 3.4.6, the in-situ fabric properties are not known; therefore the analysis was conducted assuming that the fabric had the same properties as the overlay. Thus, if the prediction model (RECK) is successful and if the fabrics have a beneficial effect, the predicted failure time should agree with the actual failure time for the control samples, and should be lower by the fabric effectiveness factor for the treated specimens.

The results of this analysis are shown in table 18. The significant values in this table are under the column heading T/T', i.e., the ratio of actual failure time to the predicted failure time. It can be seen that this data is remarkably consistent (the results for the control beam have somewhat greater scatter but the average of the two outliers is close to that of the other two results) and the fabric effectiveness, as measured by the time ratio, is close to that obtained from figure 51. Although the RECK model seems to under-predict the time to failure by about 10 percent (this is partly due to the fact that the program considers failure to occur when the crack length reaches 90 percent of the overlay thickness (the stress indensity factor becomes unbounded at the surface)), the agreement with the measurements is very good.

Table 18
Results of horizontal pull tests.

Sample No.	Width in (mm)	Hov in (mm)	Lab T Hrs	Pred T' Hrs	T/T'
9C	14.2 (361)	5.89 (149)	265.0	241.3	1.098
10C	14.0 (356)	5.00 (127)	295.0	212.3	1.390
21C	14.0 (356)	2.00 (51)	171.0	152.9	1.118
45C	14.5 (368)	2.50 (64)	31.0	44.8	0.692
6H	13.8 (349)	5.00 (127)	250.0	225.4	1.109
13H	14.0 (356)	2.75 (70)	143.5	127.8	1.115
14H	13.8 (349)	2.68 (68)	150.0	131.2	1.144
7O	14.5 (368)	5.00 (127)	440.0	238.7	1.843
8O	14.3 (363)	5.30 (135)	424.0	235.2	1.803
17O	14.0 (356)	2.30 (58)	217.0	119.0	1.824
18O	14.0 (356)	2.43 (62)	379.0	206.9	1.832

C Control
H SAMI
O High Modulus Fabric

As further verification of the model, the test data from reference [39] was also analyzed. The test conditions for these tests were somewhat different; the test used 2 and 3 inch (51 and 76 mm) thick conventional (unreinforced) overlays of 3 x 3 x 24 inches (76 x 76 x 610 mm) concrete beam. Also, instead of

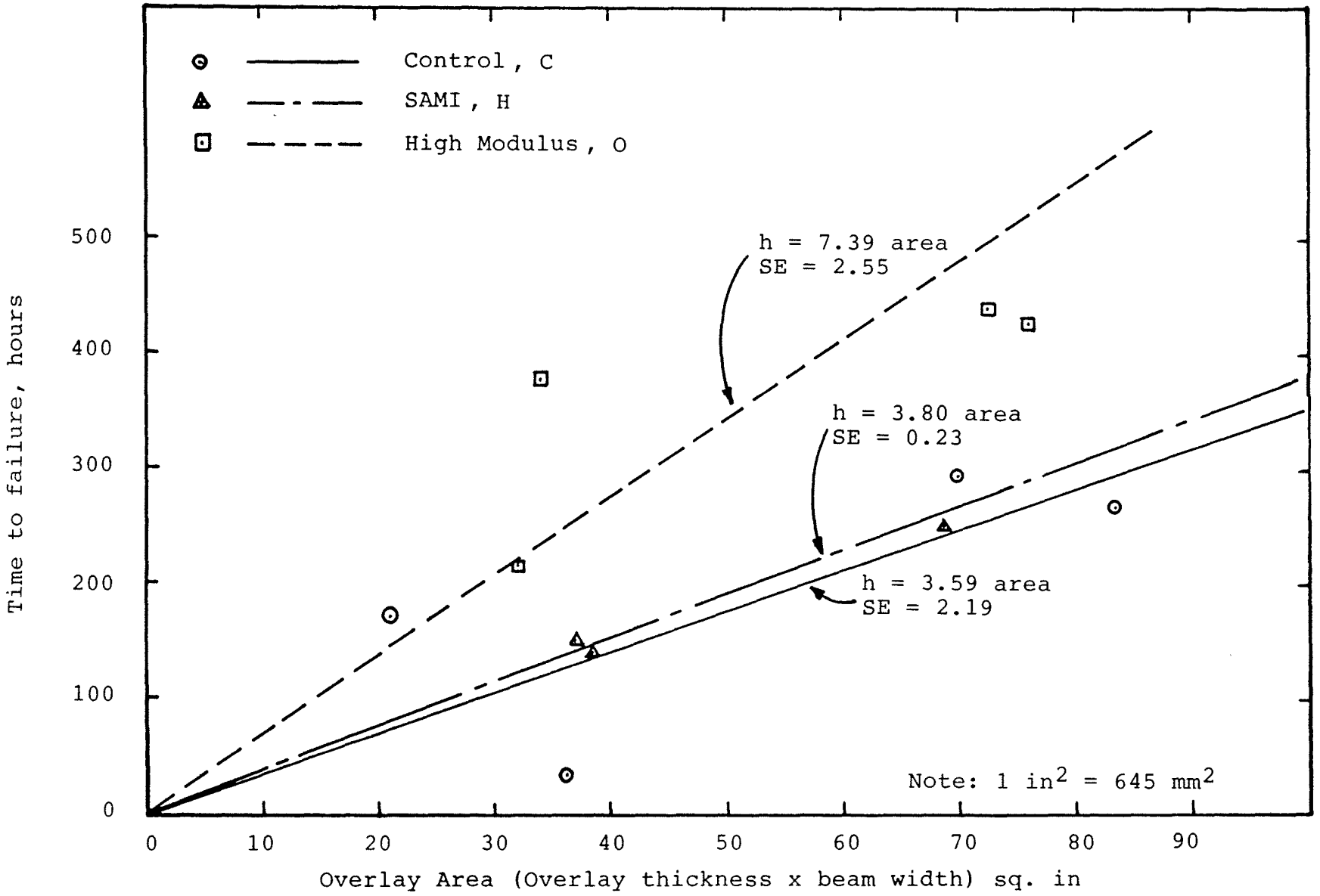

Figure 51. Results of horizontal pull tests.

applying a constant strain rate to the beams, a constant load was applied, and the crack length and joint opening were monitored.

The RECK program was again used, but the input data for these cases were the applied load and the crack length as function of time. Other pertinent information for these tests are: fracture toughness KIC = 800 psi (5.5 MPa); indirect tensile strength, y = 150 psi (1.03 MPa), and the creep compliance is:

$$J(t) = .000001\ (.25 + 5t^{.33}) \qquad (66)$$

where t is the transformed time. The output from these analyses are the predicted joint opening as a function of time, and the time to failure. Figure 52 shows a typical result, and the other data are presented in the figures in appendix F - again the agreement is excellent. It is also encouraging that although the small-scale and large-scale tests are quite different, the model is able to handle both cases equally well.

5.2.3 Combined Loading Tests

These tests were used to simulate the combined effect of traffic loading and seasonal temperature changes. As was discussed in section 4.5.2., these tests consisted of an applied vertical load to simulate traffic loading, and a more-or-less constant applied joint opening rate to simulate the effect of temperature. The joint opening rate used here was the same as was applied to the beams discussed in the previous section. In all, 19 specimens were prepared for testing; but, 4 specimens debonded (overlay from the concrete foundation) during handling and were excluded from consideration.

The test data (time to failure) are plotted as a function of the overlay cross sectional area in figure 53. The same regression technique discussed in section 5.2.2 was again used to fit the data; the regression lines for the combined loading case are represented by the dot-dash lines in figure 53. Although some scatter exists in this data, the trend of increasing time to failure with increasing overlay thickness (or cross sectional area) is quite clear. The scatter in this data, as measured by the root mean square error, is somewhat less than for the horizontal pull alone tests, but this may be the result of more data points.

Also shown in figure 53 are the regression lines for the horizontal pull tests. As can be seen from the comparison of lines, the times to failure are shorter for the combined loading case, although fatigue (traffic loading) does not play a very important role in these tests.

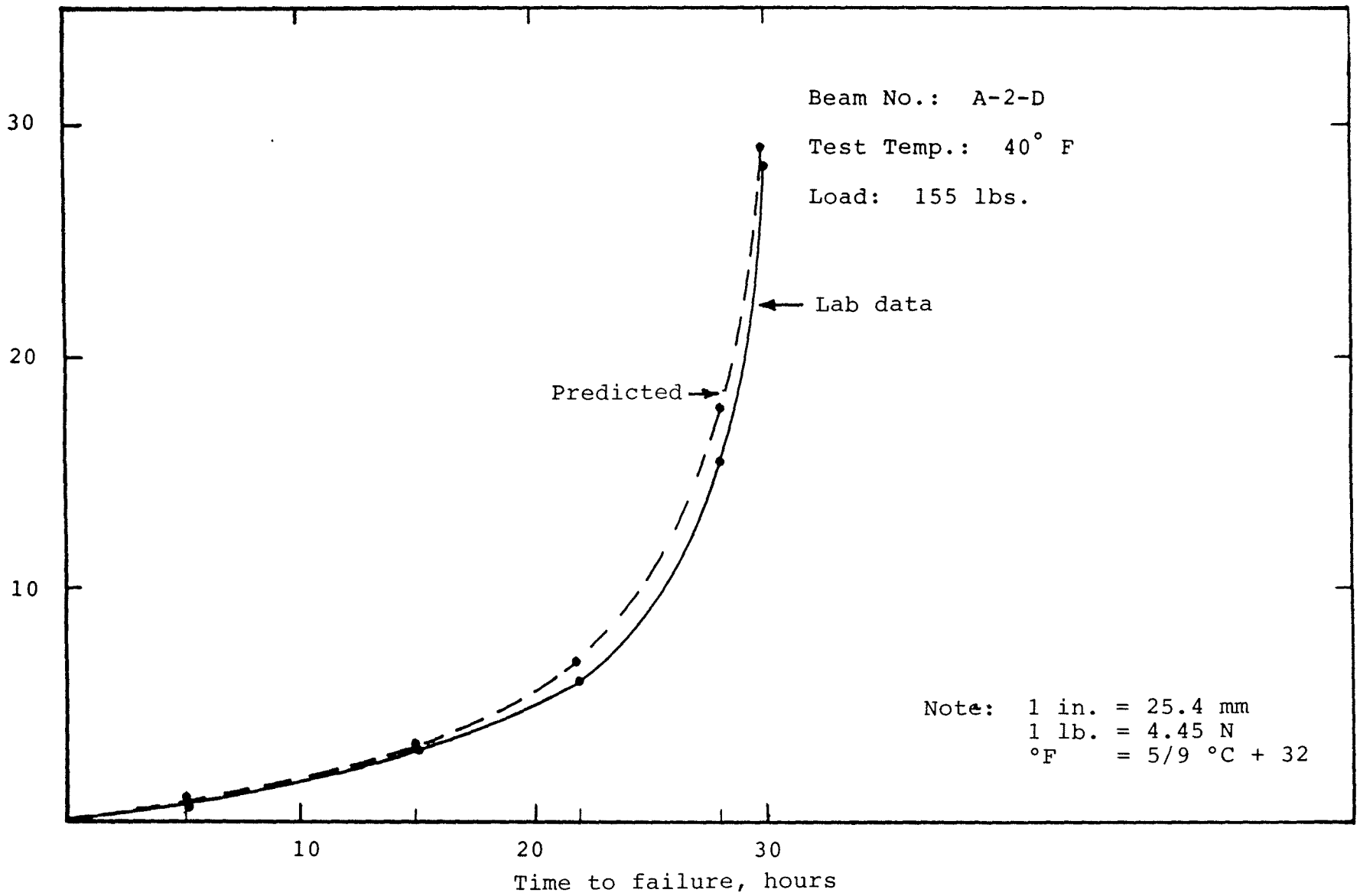

Figure 52. Comparison of actual and predicted joint opening for small-scale beams.

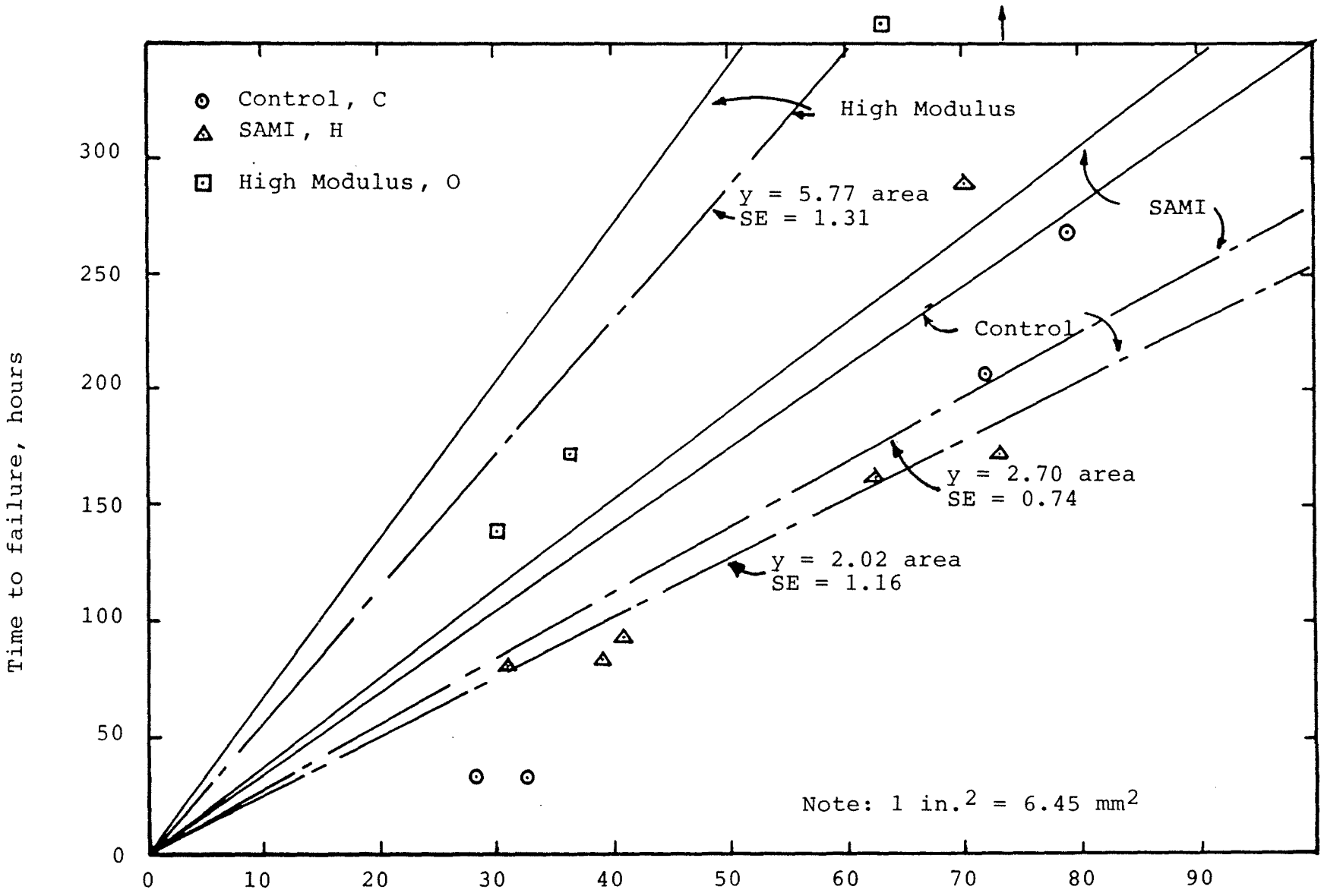

Figure 53. Results of combined loading tests.

The tests data was also analyzed using RECK, and the strain analysis was done using EFRON. The results of these analyses are presented in table 19. It should be reiterated here that the critical strain was computed assuming that dynamic loading alone was present, and the time to failure analyses was done assuming that thermal load only existed. These assumptions are needed because the rates of loading for these cases are vastly different, resulting in different values of creep modulus. Also, as in the previous cases, all analysis was done assuming that the reinforcing layer has the same properties as the control (overlay) material. These assumptions make it somewhat more difficult to draw conclusions; however, comparison of the failure times and time ratios (table 19) for the control beams shows that fatigue does not contribute significantly to failure. The same conclusion is indicated by the time ratios for the SAMI and fabric reinforced beams, since the effectiveness factor is about the same as was obtained from horizontal pull alone tests. The effectiveness factors for both the SAMI and the high modulus fabric appear to be slightly higher (1.25 and 1.92 respectively) in the combined loading tests - - this might be explained by the fact that although a constant strain rate was applied to the beam-frame system, the frame shared less of the strain as time (and crack length) increased, thus resulting in an accelerated joint opening rate over that expected for the horizontal pull alone tests. In this case the predicted time to failure would be shorter, resulting in greater apparent effectiveness factors.

Table 19 also contains the number of load applications to failure for the laboratory tests and those predicted from critical strain using the distress function:

$$N = 1.707 \times 10^{-13} \left(1/\varepsilon\right)^{5.294} \qquad (67)$$

derived in section 5.2.1. It is shown in table 19 that the actual number of load application to failure is significantly lower than that predicted from equation 68, again indicating that the simulated thermal movement is the prime factor in failure. The ratio of applications to failure, Nf'/Nf, shows that there is little difference between the SAMI and control specimen, particularly when considering the scatter in the data. However, this ratio is significantly smaller for the high modulus fabric, which would be expected if the fabric effectiveness is greater than one.

Although there is some scatter in the data, and the number of tests is limited (the testing program took almost two years to complete), the test results show that the high modulus fabric is effective in reducing reflection cracking but that the fiber SAMI is of questionable value.

Table 19
Combined loading tests.

Sample No.	Width in	Hov in	Lab T Hrs	Pred T' Hrs	T/T'	Micro Strain	Nf Lab millions	Nf' millions	Nf'/Nf
22C	13.8	2.06	32.0	48.8	0.656	252	0.232	1.91	8.30
32C	15.0	5.25	269.0	208.0	1.293	122	1.037	90.90	46.93
33C	14.1	5.10	207.0	210.5	0.983	135	1.490	52.47	35.21
46C	13.8	2.38	30.3	49.8	0.608	214	0.218	4.59	21.08
5H	14.0	5.00	291.0	201.7	1.443	140	2.095	43.28	20.66
11H	14.2	2.75	84.0	60.0	1.400	173	0.605	14.19	23.45
12H	14.9	2.75	94.5	64.7	1.461	165	0.680	17.84	26.24
28H	14.2	5.20	173.0	160.2	1.080	130	1.246	63.31	50.81
29H	14.0	4.45	162.0	203.5	0.796	177	1.166	12.61	10.81
37H	13.5	2.25	80.8	61.0	1.325	232	0.582	2.94	5.05
16O	14.5	2.50	172.5	83.8	2.058	191	1.242	8.33	6.71
30O	14.0	4.50	368.0	176.9	2.080	163	2.650	19.33	7.29
31O	14.4	5.12	430.0	235.5	1.826	132	3.096	59.58	19.24
39O	13.5	2.25	239.0	131.9	1.812	232	1.721	2.94	1.71
40O	13.5	2.24	138.8	75.3	1.843	234	0.999	2.86	2.86

C Control
H SAMI
O High Modulus Fabric
* Predicted from $Nf = 1.707 \times 10^{-13} (1/\varepsilon')^{5.294}$
Note: 1 in. = 25.4 mm.

The scatter in the data is most probably caused by variation in tack coat and bond strength between the overlay and concrete. This conclusion is indicated by the fact that the SAMI specimens were more consistent (had lower RMSE) than any other specimens, regardless of the type of analysis.

CHAPTER VI. ANALYSIS OF FIELD DATA

6.1 Analysis Model

As was discussed in chapter II, two of the mechanisms contributing to reflection crack formation are thermal stresses resulting from daily variation in the vertical temperature gradient of the concrete slab, and the seasonal change in the average concrete temperature. It was shown in section 3.1.1 that both mechanisms result in changing the joint opening, which can be calculated using the EFRON program, described in section 3.3.

The change in joint opening is the result of variation in temperature over a period of time; i.e., the rate at which the joint opening changes can be calculated if the time rate of change of temperature (either seasonal or daily temperature gradient) is known. This change in joint opening is precisely the parameter required for the failure analysis described in section 3.4 and its subsections. Thus, the same theory and models used to analyze the laboratory test response to thermal loading are directly applicable to the analysis of full-scale pavements. Of course, this analysis requires certain input data such as the elastic material properties (moduli and Poisson's ratio) the asphaltic concrete creep compliance, the master creep compliance, indirect tensile strength, fracture toughness, the equivalent horizontal load that produces the same stress in the asphalt over the joint as thermal contraction, the pavement geometry (thickness, overlay thickness joint/crack spacing) as well as the coefficient of friction between the concrete slab and the subbase/subgrade. One method of obtaining the friction value is to make the joint movement measurements as a function of slab temperature recommended by the ARE method; however, since the coefficient of friction is most likely variable from location to location, the values presented in table 20 may be used without appreciable loss of accuracy.[22]

6.2 Field Application

The literature is full of references to reflection cracking studies; however, very few of these studies also contain the data required for a rational analysis of performance, and fewer still have the data described in the previous section. A thorough search using the TRIS system yielded the New York study by McCullagh which contained three overlay projects that could be used with the developed model; and even this report did not contain the pertinent A.C. properties (modulus, creep compliance, fracture toughness, indirect tensile strength) required by the model.[46] The following assumptions were made in this analysis:

Table 20
Coefficient of friction for various materials.

Subbase Type	Coef. of Friction
Surface treatment	2.2
Lime stabilization	1.8
Asphalt stabilization	1.8
Cement stabilization	1.8
River gravel	1.5
Crushed stone	1.5
Sandstone	1.2
Clay subgrade	1.0
Sandy soil	0.9
Tar paper	1.6
Polyethylene sheet	0.5

1. The master creep compliance is given by

$$J(t') = .000001[\ .25 + 5(\ t\ 10^{-7.91 + 113T}\ )^{1/3}\ ] \quad (68)$$

where:

t' = transformed time
t = time in seconds
T = temperature, F

which is a modification of Schapery's equation from reference 34 to include the average time-temperature shift factor from reference 44.

2. The indirect tensile strength as a function of temperature, T, is given (in psi) by reference 47:

$$y = 1205\ e^{-.0316T} \quad (69)$$

3. The fracture toughness is 1200 psi (8.3 MPa). This value represents an average over the temperature range considered.

4. The friction coefficient between the slab and subbase is 0.9 (the results are rather insensitive to variations of this value).

5. The 1983 temperature history from reference 48 is applicable.

6. The temperature dropped at a uniform rate from the maximum to the minimum average daily temperature in 6 months.

7. It is assumed that the crack grows only during the time when temperature is decreasing.

Table 21 shows rest of the data for the three New York projects. Since much of the data had to be assumed, these projects are included here to illustrate the new method rather than for model verification.

Table 21
Project data.

PROPERTY	5S	9L	29
Overlay Thickness, in (mm)	2.5 (63.5)	2.5 (63.5)	2.5 (63.5)
Concrete Thickness, in (mm)	8.0(203.2)	8.0(203.2)	8.0(203.2)
Joint/Crack Spacing, ft (m)	45. (13.7)	45. (13.7)	94. (28.7)
Max. Daily Temp. * ^{o}F (^{o}C)	76.0(24.4)	81.5(27.5)	80. (26.7)
Min. Daily Temp. * ^{o}F (^{o}C)	3.5(-15.8)	-1.5(-18.6)	-6.0(-21.1)

* Average of Daily High and Low Temperatures

The first step in this analysis is to divide the design period (6 months for seasonal temperature change) into some number of intervals and determine the average temperature during the interval - - one month in the following examples. If the temperature is assumed to drop uniformly (assumption 6 above, then the loading time t in equation 69 per analysis interval is proportional to the average temperature at that interval; i.e.,

$$t = to\ (Th - T)/(Th - Tl) \qquad (70)$$

where:

Th = maximum average daily temperature
Tl = minimum average daily temperature
T = current temperature
to = time (in seconds) for temperature to drop from Th to Tl (6 months)

The next step is to determine the creep compliance and the creep modulus (inverse of compliance) and use these values with the EFRON program to compute the joint opening and critical stress (in the asphalt layer above the joint).

The EFRON program is also used to determine the equivalent horizontal load (pull) required to generate the same critical stress above the joint as was found in the previous step. This can be done by assuming a load, calculating the resultant stress and taking the ratio of stresses (from this step and previous step). Rigorously this should be an iterative process since iteration is required whenever the shear stress exceeds the maximum shear (at the slab-subbase interface); however, this effect is negligible for all practical purposes.

The results of EFRON analysis are shown in tables 22 through 25. The projects 5S, 9L and 29 are actual projects from reference 45, and project 29' is the same as 29 except that the joint spacing has been reduced to 45 feet (13.7 m) to illustrate the effect of joint spacing. Also shown in tables 22 through 24 is the history of reflection cracking development (under the column heading % of joints cracked).

The results of the EFRON analysis (joint opening and load) are input into RECK along with temperatures, indirect tensile strength, fracture toughness, and the geometry of the pavement. The output of the RECK program is the predicted time (in hours) for the reflection crack to grow to 90 percent of the way through the overlay. The 90 percent value, rather than 100 percent is used because the stress intensity factor becomes unbounded at the surface and, in any case, the crack growth rate beyond 90 percent is very rapid.

It should be noted that because of assumption 7 above, if the time to failure is less than 4320 hours, the failure time in months is obtained simply by dividing the time by 720; however, if the failure time is between 4320 and 8640 hours, the time in months is 6 + time/720, and if the time is between 8640 and 12960 hours, the time in months is 12 + time/720, etc.

Table 26 shows the predicted time, in months, for failure, and the corresponding percentage of reflection cracking that actually occurred. While the agreement between predicted and actual failure times is not perfect, the predicted times are reasonably consistent with observed cracking. Also, the comparison of results for projects 29 and 29' indicates that shortening joint spacing decreases the amount of joint opening and increases the time to failure, as is expected.

A comparison of projects 5S, 9L and 29' shows the effect of temperature, although since both maximum and minimum temperatures change for these projects, the temperature effect is somewhat more difficult to isolate. However, comparison of 9L and 29' (where the temperature drop is nearly the same) shows that lower

Table 22
Analysis for project 5S.

Time Mo.	Avg. Temp. °F	°C	Avg. Modulus psi	(MPa)	Joint Opng in	(mm)	Load lb	(N)	% Joints Cracked
0	76.0	(24.4)	2.15	(14.8)	0	0	0	(0)	0
1	70.0	(21.1)	2.20	(15.2)	.0371	(0.942)	198	(880)	--
2	57.9	(14.4)	3.60	(24.8)	.0734	(1.864)	255	(1134)	64.0
3	45.8	(7.7)	9.00	(62.1)	.1066	(2.708)	454	(2019)	72.0
4	33.8	(1.0)	23.0	(159.)	.1339	(3.401)	841	(3741)	96.0
5	21.7	(-5.7)	58.0	(400.)	.1526	(3.876)	1396	(6209)	96.0
6	9.5	(-12.5)	153.	(1055)	.1628	(4.135)	1975	(8788)	96.0

Table 23
Analysis for project 9L.

Time Mo.	Avg. Temp °F	°C	Avg. Modulus psi	(MPa)	Joint Opng in	(mm)	Load lb	(N)	% Joints Cracked
0	81.5	(27.5)	0.94	(6.48)	0	0	0	(0)	0
1	74.6	(23.7)	1.26	(8.69)	.0432	(1.097)	182	(810)	-
2	60.7	(15.9)	2.85	(19.6)	.0858	(2.179)	257	(1143)	23.1
3	46.9	(8.3)	7.85	(54.1)	.1240	(3.150)	474	(2108)	61.5
4	33.1	(0.6)	23.5	(162.)	.1550	(3.937)	976	(4341)	42.3
5	19.2	(-7.1)	70.0	(483.)	.1774	(4.506)	1736	(7722)	80.3
6	5.4	(-14.8)	200	(1379)	.1838	(4.669)	2414	(10737)	88.5

Table 24
EFRON analysis for project 29.

Time Mo.	Avg. Temp °F	°C	Avg. Modulus psi	(MPa)	Joint Opng in	(mm)	Load lb	(N)	% Joints Cracked
0	80.0(	26.7)	1.15(7.92)		0	0	0	0	0
1	72.8(	22.7)	1.50(10.3)		.0878(2.230)		693(	3082)	-
2	58.5(	14.7)	3.40(23.4)		.1700(4.318)		863(	3839)	-
3	44.2(	6.8)	10.1(69.6)		.2374(6.030)		1326(	5898)	72.5
4	29.9(	-1.2)	30.9(213.)		.2805(7.125)		2082(	9261)	74.5
5	15.5(	-9.2)	100.(689.)		.3000(7.620)		2829(	12583)	98.0
6	1.2(	-17.1)	290.(1999)		.3077(7.816)		3240(	14412)	98.0

Table 25
EFRON analysis for project 29'.

Time Mo.	Avg. Temp °F	°C	Avg. Modulus psi	(Mpa)	Joint Opng in.	(mm)	Load lb	(kg)	% Joints Cracks
0	180.0(	26.7)	1.15(7.92)		0	0	0	0	NA
1	72.8(	22.7)	1.50(10.3)		.0446(1.133)		195(	885)	NA
2	58.5(	14.7)	3.40(23.4)		.0878(2.230)		293(	1303)	NA
3	44.2(	6.8)	10.1(69.6)		.1265(3.213)		573(	2549)	NA
4	29.9(	-1.2)	30.9(213.)		.1559(3.960)		1192(	5302)	NA
5	15.5(	-9.2)	100.(689.)		.1720(4.369)		2060(	9163)	NA
6	1.2(	-17.1)	290.(1999)		.1792(4.552)		2660(	11832)	NA

Table 26
Predicted failure times.

	5S	9L	29	29'
Jnt. Opening in (mm)	.163(4.14)	.285(4.67)	.308(7.82)	.179(4.5)
Predicted Times Hrs.	8986	4830	1622	4120
Predicted Time Mo.	24.5	12.7	2.3	5.7
% Cracking at Time	100	100	<72.5	NA
Time at 100% Crack	15	7	8	NA

minimum temperature result in a reduction of the time to failure, i.e., reflection cracking is more severe in colder climates.

CHAPTER VII
SUMMARY AND CONCLUSION

7.1 Summary

This study has been concerned with the development of a mechanistic model to analyze the reflection cracking phenomenon, both in the field and in laboratory simulation. A thorough review of literature resulted in the development of a laboratory testing model, that can be used to evaluate the effectiveness of fabrics or other treatments to control or delay reflection crack formation. The model uses 12 x 96 in (305 x 2438 mm) beams subjected to vertical and/or horizontal loads, which simulate the effect of traffic and/or seasonal temperature changes. In all, 96 beams representing a flexible overlay over cracked flexible pavement and 39 beams representing flexible overlay over rigid pavement were tested. The tests were run on control beams (conventional overlay), as well as beams with different treatments. The treatments for overlays over flexible pavements were low and high modulus fabric and fiber SAMI; and high modulus fabric, fiber SAMI and open graded "Arkansas" interlayers for overlays over rigid pavements.

Based on a thorough review of existing reflection cracking analysis methods, a new model was developed that incorporates the viscoelastic properties of asphaltic concrete. This model has been implemented in two computer programs, EFRON and RECK. EFRON is a 2-dimensional finite element program using elastic layer properties; however, these are developed from the creep compliance data for the appropriate temperature and loading time. RECK performs a viscoelastic crack propagation and failure time analysis based on modification of the viscoelastic model developed by Schapery.[34]

The EFRON program can be used to compute stresses and strains as a result of temperature changes ; both seasonal temperature drop and daily variation in the vertical temperature gradient can be considered. Additionally, the response can be determined to vertical loading (traffic), as well as to horizontal pull (simulated thermal change), or a combination of all types of loading may be considered. The EFRON program is used for fatigue (vertical load) analysis, is used to determine the joint opening rate as a function of temperature drop rate for field pavements, and is also used to determine the equivalent horizontal load (pull) required to develop the same critical stress in the overlay above the joint as is produced by temperature changes. The latter is required to evaluate the stress intensity factor KI.

The RECK program is a general viscoelastic crack propagation model that computes crack length and time to failure if the joint

opening as a function of time is input, or the joint opening if the crack growth rate is input. It can therefore be used to analyze laboratory tests of beams subjected to horizontal pull (constant horizontal load) or the beams subjected to constant joint opening rate (variable horizontal load), as well as to in-service pavements subjected to thermal loads.

It should be noted that the EFRON analyses in this report have been done based on initial conditions (no crack), rather than on progressive cracking, in order to minimize the amount of computer time required; however, a progressive crack analysis is possible manually (the mesh needs to be changes based on predicted crack length from RECK). It is doubtful if the benefits are worth the greatly increased computer time.

7.2 Conclusions

The developed model has been applied to two types of laboratory beams (horizontal load and horizontal strain rate) with equal success. The model has also been applied to several in-service pavements to predict failure time. Since much of the input data for the field pavements had to be assumed, these projects cannot be considered as model verification; nevertheless, the agreement with actual cracking history is very good.

The analysis model is based on mechanistic fracture mechanics principles, except that the inclusion of fabric is done based on laboratory-determined fabric effectiveness factors, since the analysis showed that non-linear (stress-dependent) analysis is required in order to include fabric (treatment) effects based on their properties. However, the laboratory tests are simple (though somewhat time consuming to conduct) so this is not a serious drawback.

As was mentioned, the laboratory testing was conducted on large-scale beams (12 x 96 in (305 x 2438 mm)); however, the analysis of small-scale beams (3 x 24 in (76 x 610 mm)) shows that this size is adequate to evaluate the effectiveness of fabrics when used with rigid pavements.

The fatigue test results of overlay of flexible pavements show that the various treatments used in this study were relatively ineffective in reducing reflection cracking, at least at the 95 percentile confidence level. This conclusion may, in part, be the result of scatter in the data; had more tests been conducted (96 beams were included in this study), the outcome may have been somewhat different.

The test results of overlays of rigid pavements show that high-modulus fabrics are beneficial in delaying reflection crack formation - - the use of one high-modulus fabric increased the time to failure by a factor of 1.9 - - but the fiber SAMI appeared to be ineffective.

7.3 Recommendations

Based on the work described in this report, the developed reflection cracking analysis model shows promise as a performance prediction model, and appears to fit the field data quite well. However, as was stated above, much of the required input data had to be assumed since this data (creep compliance and modulus, indirect tensile strength, fracture toughness) is not available for field pavements. It is therefore recommended that follow-up studies of reflection cracking treatments also include some laboratory investigations to characterize the overlay material properties. Only then can the model be completely verified.

APPENDIX A

EFRON USERS MANUAL

1. PROGRAM CAPACITY

EFRON is a computer program designed to analyze stress-strain distribution for existing pavements covered with rigid or flexible overlays. It is based on the theory described in chapter 3 of this report and in more detail in reference 32.

An existing pavement structure can be supported by an N-layered elastic foundation (N<3) which is represented in this program by a stiffness matrix computed based upon Burmeister's solution of three dimensional semi-infinite space. The overlay structure can contain an engineering fabric which can act as a bond breaker and/or as a reinforcement. EFRON utilizes a two-dimensional finite element approach and has the following capabilities:

- Slabs can have a variable length and can be divided for regular or irregular finite element mesh, which is automatically created by the program.

- Boundary conditions are assumed by the program depending on assumed load type, support structure, and boundary condition option.

- Three types of the foundations can be specified as an option:

    - Solid elastic
    - Winkler
    - Rigid

- Three load types, or any combination of these, are available:

    - Vertical Load (mechanical)
    - Vertical temperature gradient (daily temperature change)
    - Uniform temperature load (seasonal temperature change)

- Number of support layers can be varied from one to three.

- Iteration of procedure can be specified as an option due to partial contact and/or elasto-plastic shear resistance between slab and foundation. A special bond type element has been applied for this feature.

- Engineering fabric is simulated by N-layered strips which can be placed at any position in the overlay. The number of fabric layers (N) can vary from zero (no fabric) to

four. Each layer of this strip can have separate material and geometric properties.

- All material properties of the structure may be orthotropic and/or temperature dependent. This feature is extremely important for a fabric whose modulus in vertical direction is different in the vertical and horizontal direction.

- Transverse joint may be plain or doweled.

- Dowel bar looseness can be specified between 0 and 8 mils (0 and .2mm) by a stiffness reduction function developed by Resource International, Inc.

- Variable size void under the slabs can be specified.

- Plane stress or plane strain analysis can be specified.

- New pavement or overlay design can be performed.

- Up to 10 different cracks can be specified in different locations of the slabs.

A simplified flow chart of the EFRON computer program is shown in figure 54.

2. FINITE ELEMENTS MESH AND BOUNDARY CONDITIONS

A finite element mesh, as well as boundary conditions, will be generated automatically by the program depending on input parameters (see below for input instructions and mesh examples). However, the following recommendations for the use of boundary conditions option and mesh type options should be considered:

- Use regular mesh in the case when thermal loads are applied to the structure (IR=0).

- Restrict horizontal movement on each edge in the above case (IBC=0). This boundary condition means that this is a double symmetry case.

- Using a partial restriction in x,y directions is recommended in case of a simulation of the support of the infinite or very long slab. This is a Winkler type of spring and its axial stiffness calculation is not very precise.

- Do not use a very small or very large element size in case of regular mesh. A very small size significantly increases computation time. A very large size decreases result credibility. Recommended size is 1/12 - 1/15 of a single slab length.

Program Logic for EFRON

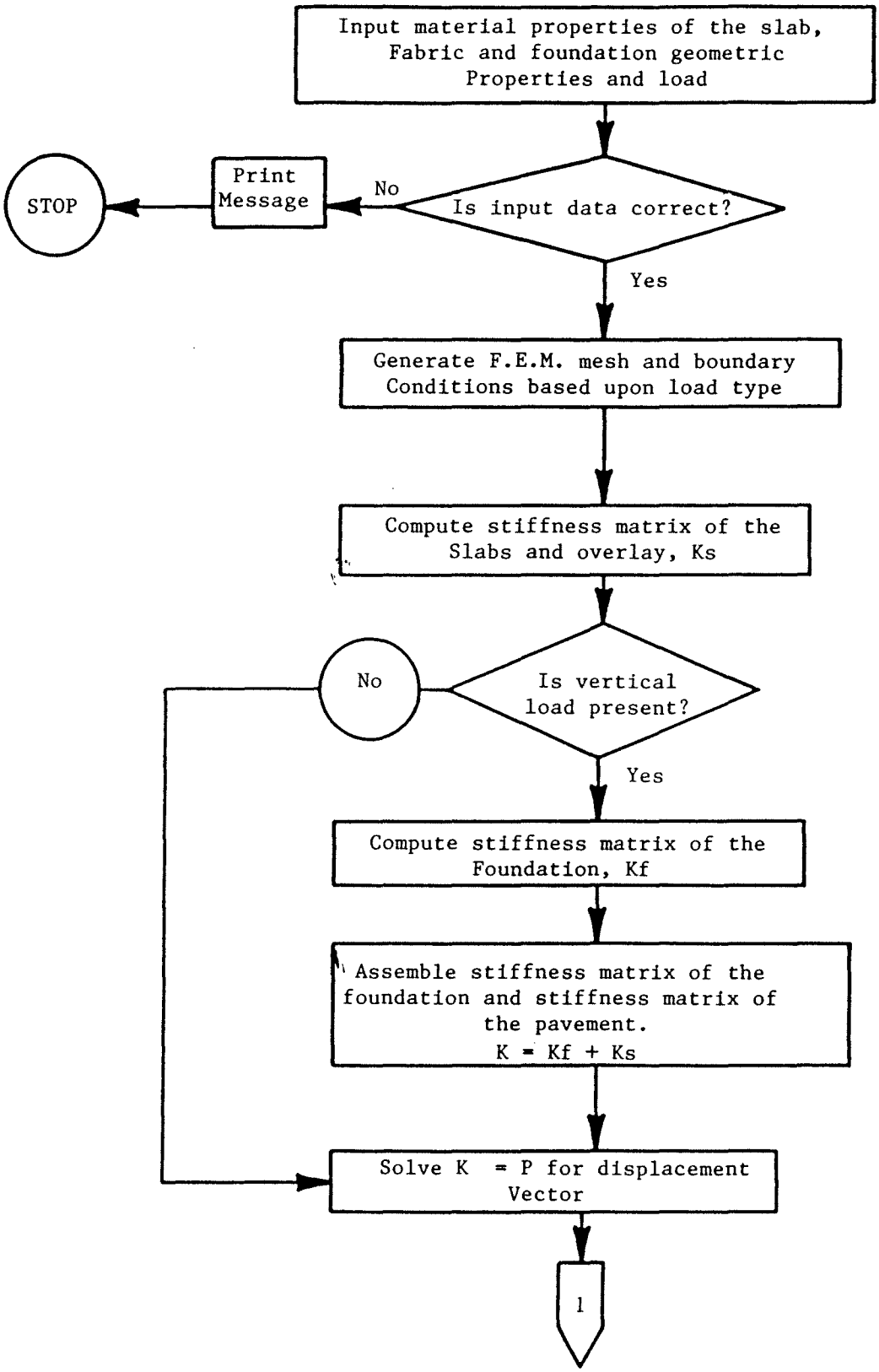

Figure 54. Flow chart of EFRON.

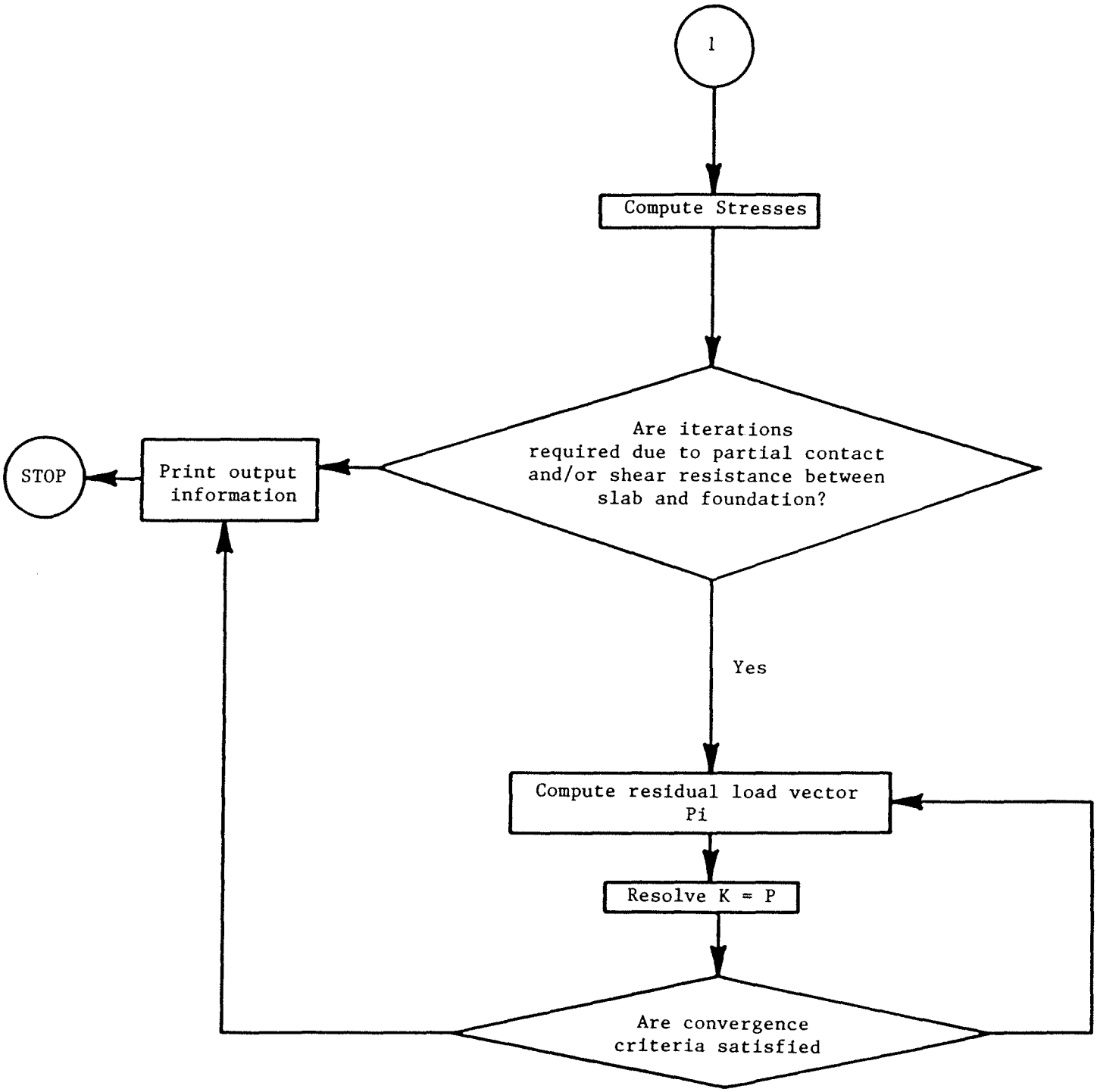

Figure 54. Flow chart of EFRON (continued).

- Assume a minimum vertical element size (DLSIZE) equal

DLSIZE = .2*TH(1)

where:

TH(1) is the Overlay thickness

This assumption will result in a more correct stress above the joint.

Figure 55 shows a two-dimensional representation of the overlayed pavement structure used in the finite element (EFRON) program. This figure shows also the definition of several of the input variables. Figure 56 shows a possible FEM mesh for this pavement which is an irregular mesh in this case. As was stated above, the irregular mesh is recommended in the case of wheel load (mechanical load), but a regular mesh should be used with thermal loads.

The information required as input is described in table 27 in conjunction with figures 55 through 57. The makeup of the data deck is shown in figure 58. It may seem from these figures as if a great deal of data is required; however, the input data is in general not difficult to generate once the user has decided on the appropriate options.

3. RECOMMENDATIONS FOR INPUT MATERIAL PROPERTIES

As was stated previously, the slab support layers are characterized by using elastic layer theory; therefore, elastic material properties are required (Young's modulus, Poisson's ratio, and layer thickness) for each foundation layer as well as for the concrete slab. Additionally, flexural strength (28-day, 3-point loading) is required for concrete.

a. The flexural strength (modulus of rupture) of most airport concretes is around 600 to 800 psi (4.1 to 5.5 MPa). This value is generally available from test data but may be estimated from unconfined compressive strength tests using the following ACI relationship.

$$fc = a\ f'c \qquad (68)$$

where:

fc is the flexural strength

f'c is the compressive strength of standard y in by 12 in (152 x 305 mm) cylinders

a is a constant ranging from 7 to 10 for British units and 0.58 to 0.83 for International units.

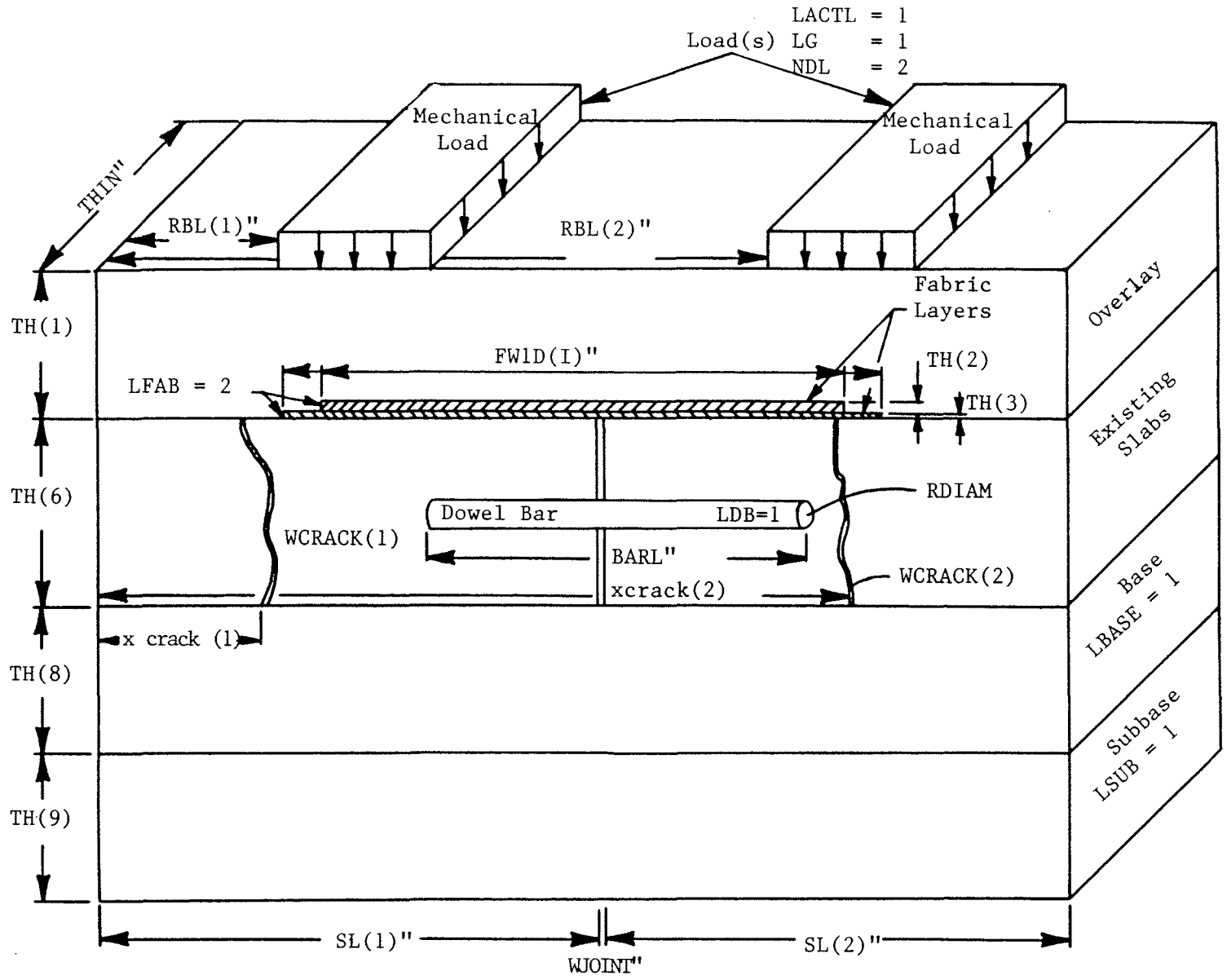

Figure 55. 2-dimensional representation of pavement system.

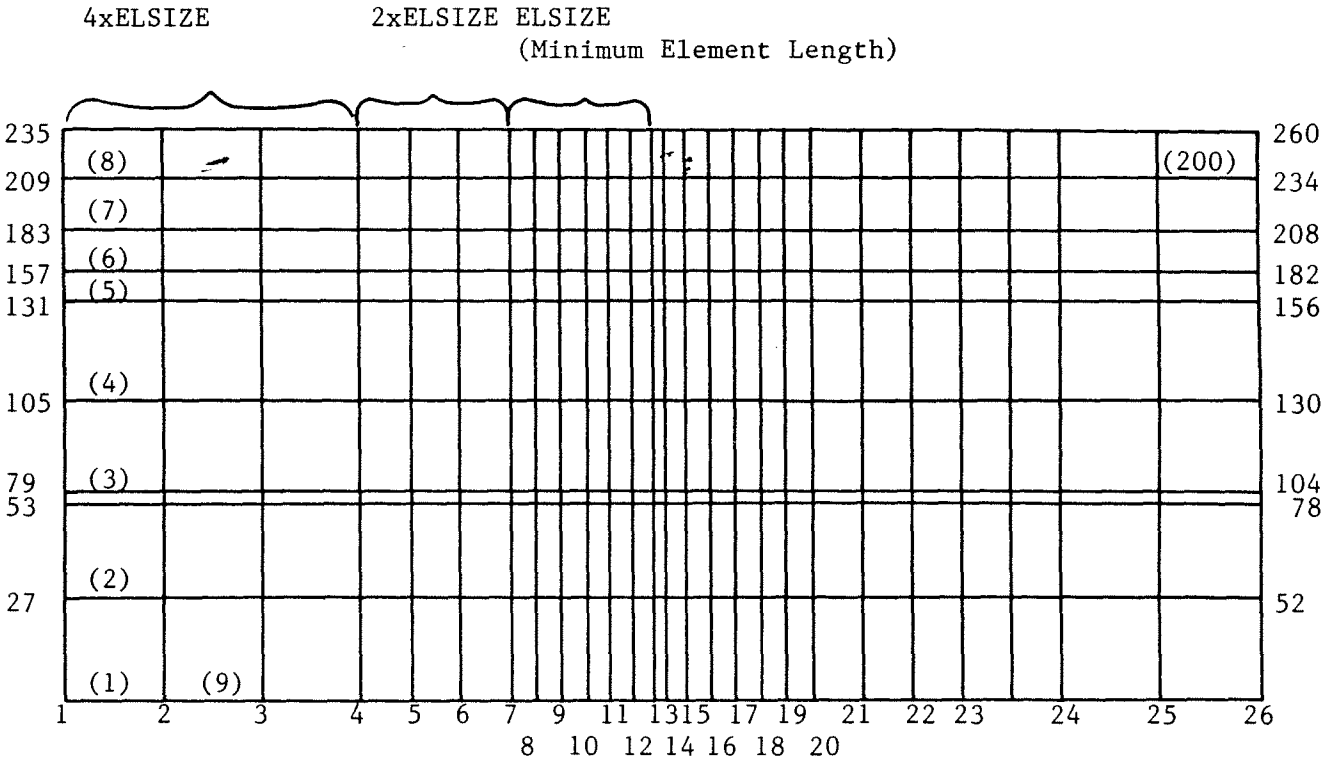

Note: The minimum element size (ELSIZE) is not uniform within an irregular mesh.

Figure 56. Example of an irregular mesh, IR = 1.

If output is desired for one or N groups of elements only:

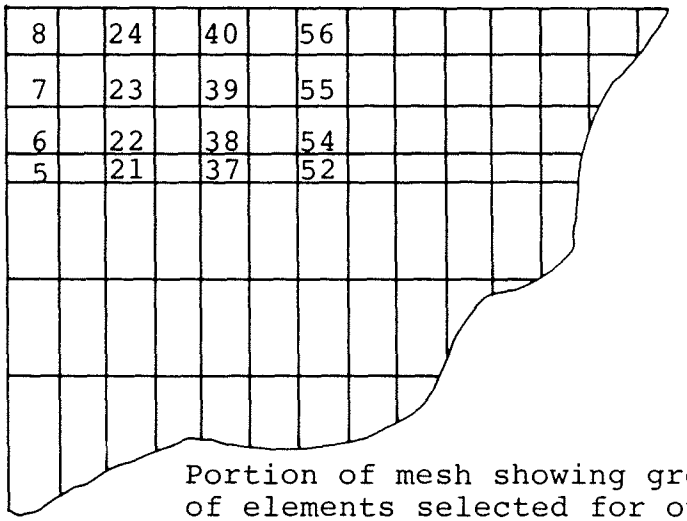

Portion of mesh showing groups of elements selected for output.

Input cards, starting from card XXIII to N cards would be:

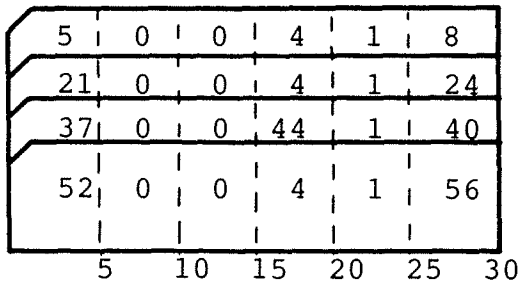

To output selectively information on N groups of elements, N cards must be used. LASTEL on all but the very last card must be blank; this indicates to the program that there are more cards to follow, on the last card LASTEL must be 777 to indicate there are no more cards or groups of elements to output.

Figure 57. Example of selective output, IO = Ø.

Column # / Card #	5	10	15	20	25	30	35	40	45	50	55	60	65	70	75	80	Comments
I																	
II	1																
III	1	2	3	4	5	6	7	8	9	10	11	12	13	14			
IV	1	2	3	4	5	6											
V	1		2		3		4		5								
VI	1		2		3		4		5								
VIA	1		2		3												
VII	1		2		3		4		5		6						
VIII	1		2		3												
IX	1		2		3		4		5								
X	1																
XI	1		2		3		4		5								
XII	1		2														

Note: Numbers refer to variables, refer to table #1.

Figure 58. Makeup of data deck.

Table 27

Description of input data.

CARD	FORMAT	VARIABLE	COL.	DESCRIPTION & VALUE RANGE	COMMENTS
I	20A4	1 Title	1-80	Any alphanumeric data.	
II	A1	1 LDTYPE	1	Design Type Option. '1' - New Pavement Design. LDTYPE = '0' - Overlay Design.	
III	14I5	1 LACTL	1-5	Mechanical Load Indicator. '0' - No Mechanical Load. LACTL = 1 - 'Mechanical & Gravity.' Horizontal Temperature Load Indicator. 0 - No Uniform Temp. Change. LTEMP = 1 - 'Uniform Temp. Change.' Temperature Gradient Indicator 0 - No Vertical Temp. gradient. LTG = 1 - 'Vertical Temp. Gradient.' Number of Iterations. 0 - No Iterations. ITER = N	$N \leq 25$

Table 27 (continued)

CARD	FORMAT	VARIABLE	COL.	DESCRIPTION & VALUE RANGE	COMMENTS
III cont'd		5 LDB	21-25	Dowel Bar Option. 0 - No Dowel Bars. LDB = 1 - Dowel Joint.	
		6 LFAB	26-30	Number of Fabric Layers. 0 - No Fabric. LFAB = 1 2 3 4	Only 3 in case of "NEW" pavement design.
		7 LBASE 7 LBASE	31-35	Base Option. 0 - No Base. LBASE = 1 - Base.	Further explanation of LBASE in Fig. 2
		8 LSUB	36-40	Subbase Option. 0 - No Subbase. LSUB = 1 - Subbase.	Further explanation of LSUB in Fig. 2
		9 LVOID	41-45	Void Option. 0 - No Void. LVOID = 1 - Void.	
		10 LSHOUL	46-50	Shoulder Boundary Condition Option. 0 - No Shoulder. LSHOUL = 1 - Shoulder.	Further explanation of LSHOUL in Fig. 2 If L should = 1 IBC must be 1

Table 27 (continued)

CARD	FORMAT	VARIABLE	COL.	DESCRIPTION & VALUE RANGE	COMMENTS
III cont'd		11 IBC	51-55	Side Boundary Condition Option. -1 - Free. IBC = 0 - Restricted in X Direction 1 - Partially restricted in X & Y Direction.	Further explanation of IBC in Fig. 2
		12 IRIG	56-60	Support Condition Option. 0 - Elastic Subgrade. IRIG = 1 - Rigid Subgrade. -1 - Winkler Type Subgrade	For IRIG = 1 IBC must be $\leq$ 0
		13 NANAL	61-65	Design Type. 2 - Plane Stress Analysis. NANAL = 1 - Plane Stress Analysis.	
		14 NCRACK	66-70	Number of Intermediate Crack. 0 - No Cracks. NCRACK = N $\leq$ 10	Further explanation of NCRACK in Fig. 2 Only for rigid or Winkler support.
IV	6I5	1 NMG	1-5	Mesh Generator Option. 0 - Mesh will be created manually NMG = 1 - Mesh will be created by program.	Extra information is necessary for NMG = 0
		2 NGRAF	6-10	Graphical Output Option. 0 - No Graphical Output.	Required hardware-Tektronix 4025.

Table 27 (continued)

CARD	FORMAT	VARIABLE	COL.	DESCRIPTION & VALUE RANGE	COMMENTS
IV cont'd		2 NGRAF (cont'd)		NGRAF = 1 - Graphical Output.	
		3 LG	11-15	Load Generator Option. 0 - Every Nudal Point Load Must be entered. LG = 1 - Load Vector will be calculated by given distributed load.	
		4 IR	16-20	Mesh Type Option 0 - Regular Mesh. IR = I - Irregular Mesh.	Further explanation of IR in Fig. 3 & 4
		5 INFROST	21-25	Stiffness Information Option. -1 - Complete Matrix Information. NFOST= 0 - No Matrix Information. 1 - Stiffness Matrix Information.	Matrix information of Logical Unit 7.
		6 IO	26-30	Input/Output Option. -1 - Complete F.E.M. Information. IO = 0 - Selective Output. (Refer to Card XXIV). 1 - Full Output.	All information on Logical Unit 6.
V	8F10.0	1 XCRACK(1)	1-10	X Coordinate for Crack Location.	Omit this card if NCRACK = 0 Use another card if necessary.
		2 WCRACK(1)	11-20	Crack Width.	

Table 27 (continued)

CARD	FORMAT	VARIABLE	COL.	DESCRIPTION & VALUE RANGE	COMMENTS
V cont'd	8F10.0	2 WCRACK(1) . . . . XCRACK(10) XCRACK(10)	11-20		
VI	4F10.0	1 SL(1)	1-10	Length of Slab #1.	(For Entire Card).
		2 SL(2)	11-20	Length of Slab #2.	Use Card #VIA
		3 WJOINT	21-30	Joint Width. (in.)	LDTYPE = '1'
		4 ELSIZE	31-40	Minimum Element Length. (in.)	Further explanation in Fig. 2
		5 DLSIZE	41-50	Minimum Element Vertical Size. (in.)	Used only for bottom of Overlay.
VIA	2F10.0	1 SL(1)	1-10	Length of Slab.	Use this Card Only if LDTYPE = '1'.
		2 ELSIZE	11-20	Minimum Element Size. (in.)	

Table 27 (continued)

CARD	FORMAT	VARIABLE	COL.	DESCRIPTION & VALUE RANGE	COMMENTS
VIA cont'd.		3 DLSIZE	21-30	Minimum Element Vertical Size (in.).	
VII	6F10.0	1 TH(1)	1-10	Thickness of the Top Layer.	
		2 E(1,1)	11-20	Elastic Modulus of the Top Layer.	
		3 V(1,1)	21-30	Poisson's Ratio of Top Layer.	
		4 ALFA(1)	31-40	Coefficient of Thermal Expansion.	
		5 E(1, 4)	41-50	Shear Modulus of the Top Layer.	
		6 THIN	51-60	Width of the Slab.	Omit this Variable if NANAL = 1.
VIII	F10.0	FWID	1-10	Fabric Width for Fabric Layer #I. Minus Joint Width.	1) Omit Cards VIII & IX if LFAB = 0.
IX	5F10.0	1 TH(1)	1-10	Thickness of Fabric Layer (I).	
		2 E(I, 1)	11-20	Elastic Modulus of Fabric Layer (I)	2) Repeat Cards VIII & IX for LFAB times.
		3 V(I, 1)	21-30	Poisson's Ratio of Fabric Layer (I).	
		4 ALFA(I)	31-40	Coefficient of Thermal Expansion.	I = 1, 2, 3, 4
		5 E(I, 4)	41-50	Shear Modulus of Fabric Layer (I).	

Table 27 (continued)

CARD	FORMAT	VARIABLE	COL.	DESCRIPTION & VALUE RANGE	COMMENTS
X	F10.0	FPOS	1-10	Position of the Fabric from the Bottom of the Top Layer.	Omit this card if LDTYPE = 0
XI	5F10.0	1 TH(6)	1-10	Same as Card VII (for Layer #2)	
		2 E(6.1)	11-20	Same as Card VII (for Layer #2)	
		3 V(6,1)	21-30	"	
		4 ALFA(6)	31-40	"	
		5 E(6,4)	41-50	"	
XII	2F10.0	1 ESUB	1-10	Subgrade Modulus.	Omit this card if IRIG = 1.
		2 VSUB	11-20	Subgrade Poisson's Ratio.	
XIII	3F10.0	1 TH(8)	1-10	Base Thickness.	Omit this Card if LBASE = 0.
		2 E(8,1)	11-20	Base Modulus.	Omit Cards XII, XIII, XIV
		3 V(8,1)	21-30	Base Poisson's Ratio	if LACTL = 0.
XIV	3F10.0	1 TH(9)	1-10	Subbase Thickness.	Omit this Card if LSUB = 0.
		2 E(9,1)	11-20	Subbase Modulus.	
		3 V(9,1)	21-30	Subbase Poisson's Ratio.	

Table 27 (continued)

CARD	FORMAT	VARIABLE	COL.	DESCRIPTION & VALUE RANGE	COMMENTS
XV	2F10.0	1 VWID(1)	1-10	Void Size for Slab #1, measured from the joint.	Omit Card if LVOID = 0.
		2 VWID(2)	11-20	Void Size for Slab #2, measured from the joint.	
XVI	5F10.0	1 RDIAM	1-10	Diameter of the Dowel Bar (in.)	Omit Card if LDB = 0.
		2 ALOOS	11-20	Looseness of the Dowel Bar (in.)	
		3 E(10,1)	21-30	Modulus of the Dowel Bar.	
		4 V(10,1)	31-40	Poisson's Ratio of the Dowel Bar.	
		5 BARL	41-50	Dowel Bar Length (in.)	
XVII	2F10.0	1 ARATIO	1-10	Convergence Criteria. Must be between 0 & 1.	If ARATIO = 0, Default Value of ARATIO = .1
		2 TFORCE	11-20	(Presently not used in Program).	
XVIII	F10.0	UTEMP	1-10	Uniform Temperature Change (°F).	Omit Card if LTEMP = 0.
XIX	F10.0	TG	1-10	Vertical Temperature Gradient	Omit Card if LTG = 0.
XX	5F10.0	1 SNORM	1-10	Normal Stiffness for Joint Element (psi).	
		2 SSHR	11-20	Shear Stiffness for Joint Element (psi).	

Table 27 (continued)

CARD	FORMAT	VARIABLE	COL.	DESCRIPTION & VALUE RANGE	COMMENTS
XX cont'd.		3 THE	21-30	Coefficient of Thermal Expansion.	
		4 FRIC	31-40	Coefficient of Friction.	
		5 COH	41-50	Cohesion.	
XXI	15,F10.0	1 NLO	1-5	Nodal Point Number.	Omit Card if LG = 1.
		2 AFORCE	6-15	Load Magnitude.	Repeat Card XXI as many times as necessary.
		3 NDIR	16-20	Load Direction NDIR = 0 y direction NDIR = 1 x direction	Last Card of this set must be blank.
XXII	15	NDL	1-5	Number of Distributed Loads.	Omit Card if LG = 0.
XXIII	3F10.0	1 RBL	1-10	X Coordinate of Beginning of Dist. Load.	Omit this Card if LG = 0.
		2 RLOAD	11-20	Magnitude of Load.	Repeat this Card NDL times.
		3 PRES	21-30	Load Pressure.	
XXIV	6I5	1 NELM	1-5	Beginning Element Number (see mesh).	Use this Card only if IO = 1.

Table 27.(continued)

CARD	FORMAT	VARIABLE	COL.	DESCRIPTION & VALUE RANGE	COMMENTS
XXIV		2 IOOP	6-10	Output options must always remain 1, 0, 8, 16, 20 or blank.	
		3 IOSTEP	11-15	Output options must always remain 1, 0, 8, 16, 20 or blank.	
		4 NMN	16-20	Number of repetitions (elements in the group).	
		5 NELST	21-25	Element Step Number.	Explained in Fig. 3
		6 LASTEL	26-30	For more groups use or blank. For no more groups use 777.	Repeat this Card until LASTEL = 777 for as many groups of elements you would like to output.

The lower value should be used with high-strength concrete and the higher value for low strength concrete.

b. The dynamic (tangent) modulus of highway concrete is around 5 million psi (34.5 GPa) within a range of 3.5 to 6 million psi (24.1 to 41.4 GPa). In the absence of specific test data, it may be estimated from the following ACI relationship:

$$Ec = 43\ P^{1.5} * f'c \text{ (in psi)}$$

$$Ec = 0.056\ p^{1.5} f'c \text{ (in kPa)} \qquad (69)$$

where:

Ec is the tangent modulus
p is the concrete unit weight
f'c is the compressive strength

Equation 69 is generally given for the secant modulus. Since the tangent modulus is usually 20 to 30 percent higher than the secant modulus, the coefficients in equation 69 have been increased by 30 percent over the values recommended by ACI for secant modulus (for a more conservative design) because critical stresses in concrete increased with increasing concrete modulus.

c. The Poisson's ratio values in table 20 are recommended. The analysis is rather insensitive to Poisson's ratio so that precise values are not required.

d. Subgrade modulus may be obtained from laboratory tests in triaxial compression, or may be estimated from AASHTO soil classification, soil support values, or modulus of subgrade reaction, using figure 59 to estimate the CBR value, and equation 3 to compute the modulus.

$$Es = 1500\ CBR \text{ (in psi)}$$

$$Es = 10.3\ CBR \text{ (in MPa)} \qquad (70)$$

e. Granular base/subbase moduli may be obtained from laboratory tests in triaxial compression, or may be estimated from equation 71:

The lower value should be used with high-strength concrete and the higher value for low strength concrete.

b. The dynamic (tangent) modulus of highway concrete is around 5 million psi (34.5 GPa) within a range of 3.5 to 6 million psi (24.1 to 41.4 GPa). In the absence of specific test data, it may be estimated from the following ACI relationship:

$$Ec = 43\ P^{1.5} * f'c \text{ (in psi)}$$

$$Ec = 0.056\ p^{1.5} f'c \text{ (in kPa)} \qquad (69)$$

where:

Ec is the tangent modulus
p is the concrete unit weight
f'c is the compressive strength

Equation 69 is generally given for the secant modulus. Since the tangent modulus is usually 20 to 30 percent higher than the secant modulus, the coefficients in equation 69 have been increased by 30 percent over the values recommended by ACI for secant modulus (for a more conservative design) because critical stresses in concrete increased with increasing concrete modulus.

c. The Poisson's ratio values in table 20 are recommended. The analysis is rather insensitive to Poisson's ratio so that precise values are not required.

d. Subgrade modulus may be obtained from laboratory tests in triaxial compression, or may be estimated from AASHTO soil classification, soil support values, or modulus of subgrade reaction, using figure 59 to estimate the CBR value, and equation 3 to compute the modulus.

$$Es = 1500\ CBR \text{ (in psi)}$$

$$Es = 10.3\ CBR \text{ (in MPa)} \qquad (70)$$

e. Granular base/subbase moduli may be obtained from laboratory tests in triaxial compression, or may be estimated from equation 71:

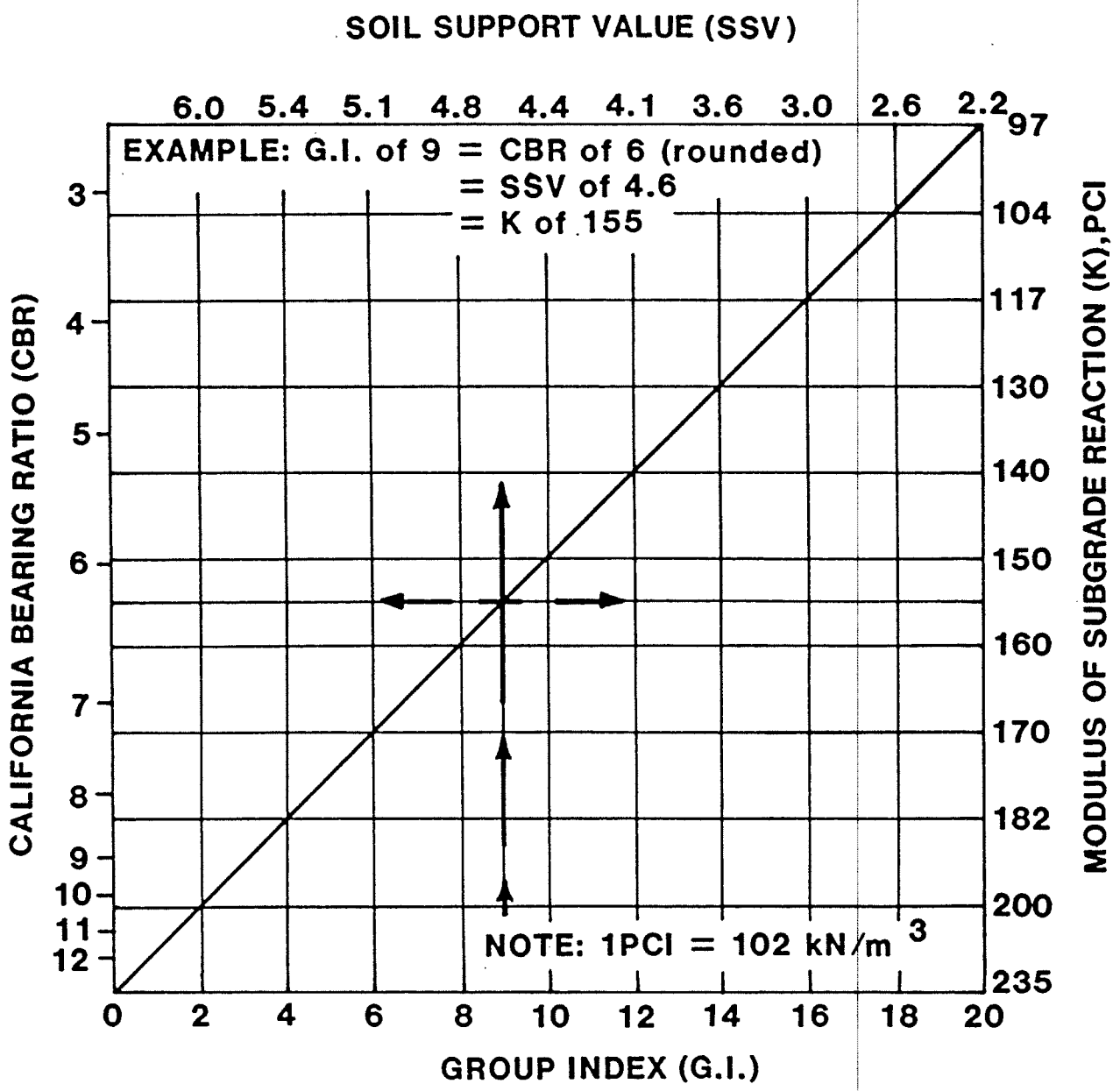

Figure 59. Relationship between soil parameters.

$$E_{n-1} = 11.06\, E_n^{0.837} \quad \text{(in psi)} \qquad (71)$$

where:

E_n = modulus of the nth layer above it

E_{n-1} = modulus of the layer

This equation is a compromise between the Shell COE, and Kentucky models and recognizes the fact that the degree of compaction of granular materials depends on the modulus of the underlying layer. If both a subbase and a base layer is used, equation 71 should be applied twice, first to determine the subbase modulus from subgrade, then the base modulus from subbase modulus. Sinsitivity analyses using both elastic layer theory as well as the RISC program show that the critical stress in concrete is only slightly dependent of the value of the base/subbase modulus; therefore, exact values for these layers are not required.

f. The modulus of asphalt bases is temperature dependent and should be estimated at mean annual temperature. This mean temperature depends on the slab thickness and the base thickness as well as on the mean annual air temperature, but using mean annual air temperature will be adequate in most cases. Figure 60 may be used in absence of test data.

g. The moduli of cement-treated bases are quite variable, depending on aggregate type and the cement contents therefore, the use of laboratory test data is recommended.

The above discussion should provide the user some guidelines in the selection of input parameters required for this design program. However, since the program has the capability of analyzing a wide variety of programs, some planning and forethought is recommended.

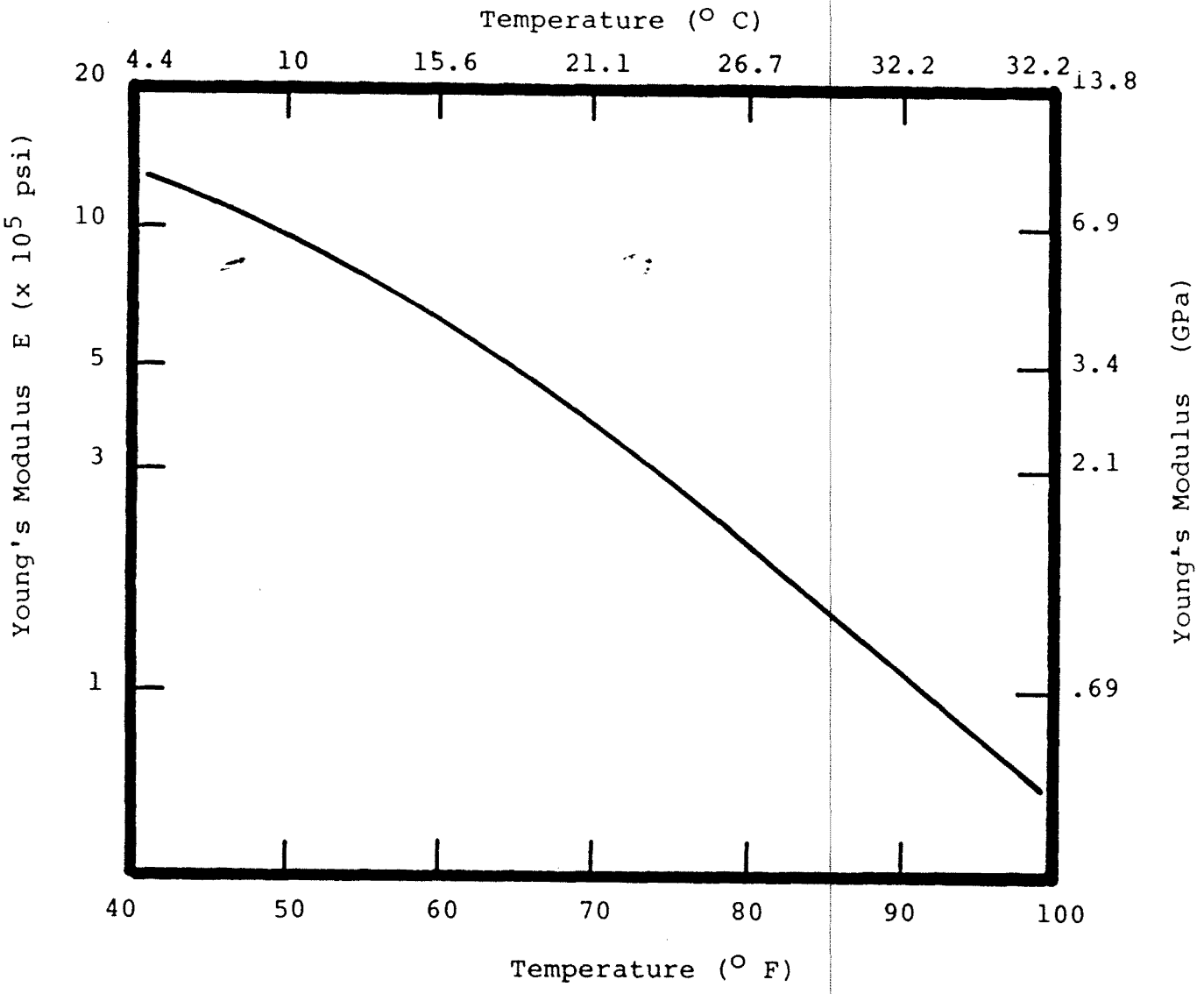

Figure 60. Assumed temperature dependence of Young's modulus of AC pavements and AC base materials.

APPENDIX B

DERIVATION OF EQUATION 57

$$U_{ve} = \frac{8}{\pi} \sigma_f \int_{t_1}^{t} J(t-\varepsilon) \frac{df}{d\varepsilon} d\varepsilon$$

Where:

$$f = \sqrt{\alpha(a-x)} - \frac{\alpha+x-a}{2} \ell\eta \frac{\sqrt{\alpha} + \sqrt{a-x}}{\sqrt{\alpha} - \sqrt{a-x}}$$

Let $a-x = r$

$$f = \sqrt{\alpha r} - \frac{\alpha-r}{2} \ell\eta \frac{\sqrt{\alpha} + \sqrt{r}}{\sqrt{\alpha} - \sqrt{r}}$$

$$\frac{df}{d\varepsilon} = \frac{df}{da} \frac{da}{d\varepsilon} = \frac{df}{da} \dot{a}$$

$$\frac{df}{da} = \frac{\alpha}{2\sqrt{\alpha r}} - \frac{-1}{2} \ell\eta \frac{\sqrt{\alpha} + \sqrt{r}}{\sqrt{\alpha} - \sqrt{r}} - \frac{\alpha-r}{2}$$

$$\frac{(\sqrt{\alpha} - \sqrt{r})}{(\sqrt{\alpha} - \sqrt{r})} \frac{(\sqrt{\alpha} - \sqrt{r}) \frac{1}{2}\sqrt{r} + (\sqrt{\alpha} + \sqrt{r}) \frac{1}{2}\sqrt{r}}{(\sqrt{\alpha} - \sqrt{r})^2}$$

$$= \frac{1}{2} \frac{\alpha}{r} + \frac{1}{2} \ell\eta \frac{\sqrt{\alpha} + \sqrt{r}}{\sqrt{\alpha} - \sqrt{r}} - \frac{\alpha-r}{2} \frac{2\sqrt{\alpha}}{2\sqrt{r}(\sqrt{\alpha} + \sqrt{r})(\sqrt{\alpha} - \sqrt{r})}$$

$$= \frac{1}{2} \frac{\alpha}{r} + \frac{1}{2} \ell\eta \frac{\sqrt{\alpha} + \sqrt{r}}{\sqrt{\alpha} - \sqrt{r}} - \frac{\alpha-r}{2} \frac{\sqrt{\alpha}}{\sqrt{r}(\alpha-r)}$$

$$= \frac{1}{2} \frac{\alpha}{r} + \frac{1}{2} \ell\eta \frac{\sqrt{\alpha} + \sqrt{r}}{\sqrt{\alpha} - \sqrt{r}} - \frac{1}{2} \frac{\alpha}{r}$$

$$= \frac{1}{2} \ell\eta \frac{\sqrt{\alpha} + \sqrt{r}}{\sqrt{\alpha} - \sqrt{r}}$$

Therefore:

$$\frac{df}{d\varepsilon} = \frac{1}{2} \ell\eta \frac{\sqrt{\alpha} + \sqrt{r}}{\sqrt{\alpha} - \sqrt{r}} \cdot \dot{a}$$

$$U_{ve} = \frac{8}{\pi}\sigma_y \int_{t_1}^{t} J(t-\xi) \cdot \frac{1}{2}\left[\ell n \frac{\sqrt{\alpha} + \sqrt{r}}{\sqrt{\alpha} - \sqrt{r}}\right] \cdot \dot{a}\,d\xi \qquad \text{(B-1)}$$

$$U_{ve} = \frac{8}{\pi}\sigma_y \int_{t_1}^{t_2} J(t_2-\xi) \cdot \frac{1}{2}\left[\ell n \frac{\sqrt{\alpha} + \sqrt{r}}{\sqrt{\alpha} - \sqrt{r}}\right] \cdot \dot{a}\,d\xi \qquad \text{(B-2)}$$

Let:

$$S = \frac{\dot{a}(t_2-\xi)}{\alpha} \implies \alpha\,ds = -\dot{a}\,d\xi$$

$$\xi \to t_1 \qquad S = \frac{\dot{a}(t_2-t_1)}{\alpha} = 1$$

$$\xi \to t_1 \qquad S = \frac{\dot{a}(t_2-t_2)}{\alpha} = 0$$

$$U_c = \frac{8}{\pi}\sigma_y \int_1^0 C\left(\frac{\alpha S}{\dot{a}}\right) \frac{1}{2} \ell n \frac{1 - \sqrt{\frac{r}{\alpha}}}{1 + \sqrt{\frac{r}{\alpha}}} (-\alpha\,ds)$$

$$= \frac{8}{\pi}\sigma_y \int_1^0 C\left(\frac{\alpha S}{\dot{a}}\right) \frac{1}{2} \ell n \frac{1 - \sqrt{\frac{r}{\alpha}}}{1 + \sqrt{\frac{r}{\alpha}}} (\alpha\,ds)$$

$$= \frac{8}{\pi}\sigma_y \cdot \frac{\alpha}{2} \int_1^0 C\left(\frac{\alpha S}{\dot{a}}\right) \ell n \frac{1 - \sqrt{\frac{r}{\alpha}}}{1 + \sqrt{\frac{r}{\alpha}}}\,ds$$

$$2\delta = \delta_c\sigma_y = \frac{8}{\pi}\sigma_y^2 \cdot \frac{\alpha}{2} \int_1^0 J\left(\frac{\alpha S}{\dot{a}}\right) \ell n \frac{1 - \sqrt{\frac{r}{\alpha}}}{1 + \sqrt{\frac{r}{\alpha}}}\,ds$$

But: $\alpha = \frac{\pi}{8}\left(\frac{K^2}{\sigma_y^2}\right)$

$$2\delta = \frac{K^2}{2} \int_1^0 J\left(\frac{\alpha S}{\dot{a}}\right) \ell n \frac{1 - \sqrt{\frac{r}{\alpha}}}{1 + \sqrt{\frac{r}{\alpha}}}\,ds \qquad \text{(B-3)}$$

But $\frac{r}{\alpha} = 1-S$ can be proven as follows:

$$S = \frac{\dot{a}(t_1-\xi)}{\alpha} \; ; \quad r = a-x_1 \quad \rightarrow \quad \dot{r} = \dot{a}-\dot{x}_1 \quad \rightarrow \quad \dot{r} = \dot{a}$$

$\therefore$

$$S = \frac{\dot{r}(t_2-\xi)}{\alpha}$$

$$= \frac{\dot{r}(t_2-t_1-\xi+t_1)}{\alpha}$$

$$= \frac{\dot{r}[(t_2-t_1) + (t_1-\xi)]}{\alpha}$$

$$= \frac{\dot{a}(t_2-t_1)}{\alpha} + \frac{\dot{r}(\xi-t_1)}{\alpha}$$

$$S = 1 - \frac{r}{\alpha}$$

$$\frac{r}{\alpha} = 1 - S$$

Hence:

$$\sigma = \frac{1}{2}\sigma_y U_c = \frac{K^2}{4}\int_1^0 J\left(\frac{\alpha S}{\dot{a}}\right) \ell n \frac{1 - \sqrt{1-S}}{1 + \sqrt{1-S}} \qquad \text{(B-4)}$$

Let $J(t-\xi) = J_o + J_2 t^m$

$$J\left(\frac{\alpha S}{\dot{a}}\right) = J_o + J_2\left(\frac{\alpha S}{\dot{a}}\right)^m \qquad \text{(B-5)}$$

Substitute B-5 into B-4

$$2\sigma = \frac{K^2}{2}\int_1^0 \left\{J_o + J_2\left(\frac{\alpha S}{\dot{a}}\right)^m\right\} \ell\eta\frac{1 - \sqrt{1-S}}{1 + \sqrt{1-S}}\, ds$$

(B-6)

$$2\sigma = \frac{K^2}{2} J_o\int_1^0 \ell\eta\frac{1 - \sqrt{1-S}}{1 + \sqrt{1-S}}\, ds + \frac{K^2}{2} J_2\left(\frac{\alpha}{\dot{a}}\right)^m\int_1^0 S^m\ell\eta\frac{1 - \sqrt{1-S}}{1 + \sqrt{1-S}}\, ds$$

Let $I = \frac{1}{2}\int_1^0 S^m \ell\eta\frac{1 - \sqrt{1-S}}{1 + \sqrt{1-S}}\, ds$ (B-7)

And $I = \int_1^0 \ell\eta\frac{1 - \sqrt{1-S}}{1 + \sqrt{1-S}}\, ds = 2$ (B-8)

Substitute B-7 and B-8 into B-6:

$$2\sigma = \frac{K^2}{2}J_o * 2 + K^2 J_2\left(\frac{\alpha}{\dot{a}}\right)^m I$$

$$2\sigma = K^2 J_o = K^2 J_2 I\left(\frac{\alpha}{\dot{a}}\right)^m$$

$$\frac{\dot{a}}{\alpha}^m = \left[\frac{K\ J_2 I}{2\sigma\left|1 - \frac{K\ J_o}{2\sigma}\right|}\right]$$

Since $K = \frac{2\sigma}{J_o}$ then,

$$\dot{a} = \alpha\left[\frac{K^2 J_2 I}{2\sigma\left(1 - \frac{K^2}{K^2_\infty}\right)}\right]^{1/m}$$

But $\alpha = \frac{\pi}{8} \frac{K^2}{\sigma_y^2}$

$$\dot{a} = \frac{\pi}{8} \frac{K^2}{\sigma_y^2} \left[\frac{K^2 J_2 I}{2\sigma(1 - K^2/K^{2\infty})} \right]^{1/m}$$

$$\dot{a} = \frac{\pi}{8} \left[\frac{J_2 I}{2\sigma(1 - K^2/K^{2\infty})} \right]^{1/m} \frac{K^{2+2/m}}{\sigma_y^2} \qquad \text{(B-9)}$$

APPENDIX C

FORMULA FOR STRESS INTENSITY FACTOR FOR TESTED BEAM

The opening mode stress intensity factor, K_I, for beam tested under horizontal load, P, is given by:

$$K_I = [F_p(a/t_1)*P*(t_1-2_a)+F_M(a/t_1)*3P*(t_1+t_2)]*R$$

where:

$$R = \frac{\sqrt{a}}{(t_1-a)\sqrt{t_1(t_1-a)}}$$

t_1 is the overlay thickness

t_2 is the concrete thickness

a is the crack length

F_P and F_M are function of (a/t_1) and are given by:

$$F_P = 1.12 - 3.68\,(a/t_1) + 11.95\,(a/t_1)^2 - 25.85\,(a/t_1)^3 + 33.10(a/t_1)^4 - 22.44(a/t_1)^5 + 6.18(a/t_1)^6$$

$$F_M = 1.12 - 2.95(a/t_1) + 7.68(a/t_1)^2 - 14.64(a/t_1)^3 + 17.59(a/t_1)^4 - 11.55(a/t_1)^5 + 3.13(a/t_1)^6$$

APPENDIX D

THE BERM PROGRAM

D.1 USERS MANUAL

D.1.1 Introduction

This computer program is designed to analyze reflective cracking of overlays of flexible or rigid pavements above underlying cracks or joints due to thermal loading only (loads induced by the horizontal temperature movement and vertical curling and warping of the slabs) after the construction of the overlays.

This program is based on the analysis of the fracture mechanics of a viscoelastic material by Schapery and others.[34,35]

Schapery's work has been adapted, with some modification, to develop the mathematical formulations of the present model described in chapter 3. The reason behind using such an approach emerges from the fact that engineering materials, especially the asphaltic mixtures and fabrics, exhibit time dependent behavior and hence the crack initiation and propagation are time dependent events.

D.1.2 Input and Output for the Developed Model

The developed model requires easy to find input parameters that could be obtained from laboratory tests. Part of these parameters are the properties of the overlay material such as the creep compliance, J(t), the fracture strength, f, and the fracture toughness, K . The other part of the input data are the load-crack opening displacement values. For a laboratory test, the induced thermal loadings are simulated by applying a variable horizontal pull and measuring the joint opening. For a field case, the joint opening can be calculated over a specific period of time knowing the temperature variation within that time. Also, an equivalent horizontal pull can be calculated to simulate the induced thermal stresses. The joint opening and load calculations can be performed using the computer program EFRON.

Using the previous input data, the program predicts the time at which failure occurs. Also a part of the output is the crack lengths at different time intervals.

D.1.3 Description of Input Data

Table 28 shows a description of the input data.

Table 28
Description of input data.

CARD	FORMAT	VARIABLE	COL.	DESCRIPTION AND VALUE RANGE	COMMENTS
1	3I5	ICASE	1-5	Case Option: = 1 - 'Laboratory Test' = 2 - 'Field Case'	
		IOPN	6-10	Beam Option: = 1 - 'Small Scale Laboratory Beam' = 2 - 'Large Scale Laboratory Beam' = Ø - 'Field Case'	
		NB	11-15	Beam or Field Case Number	
2	I15	NUMNP	1-5	Number of Time Stations at which Joint Openings are Measured.	
3	3D15.6	TH1	1-15	Overlay Thickness	For a Field Case take WID = 1.00
		TH2	16-30	Concrete Base Thickness	
		WID	31-45	Beam Width (for Laboratory Case)	
4	3D15.6	CONI	1-15	Value of C_1 in the Creep Compliance Equation. (Default value = 0.080×10^{-6}) Value of C_2 in the Creep Compliance Equation (Default Value = 0.7920×10^{-5}) Value of m in the Creep Compliance Equation (Default value = 0.345).	For Default values, Leave Card No. 4 Blank

Table 28 (continued).

CARD	FORMAT	VARIABLE	COL.	DESCRIPTION & VALUE RANGE	COMMENTS
5	1D15.6	RKC	1-15	The Fracture Toughness of the Overlay Material	
6 N	5D15.6	PT(I)	1-15	Time at which Joint Opening and load are measured.	N = 5+NUMNP I = 1,2,3,..., NUMNP
		PL(I)	16-30	Load induced at Time PT(I).	For Default values for SIGY, Leave Columns 61-75 Blank.
		DELTA(I)	31-45	Joint Opening at Time PT(I).	
		TEMP(I)	46-60	Temp. at Time PT(I).	
		SIGY(I)	61-75	Fracture Strength of the Overlay Material at Time PT(I).	

The equation used for creep compliance J(t) is:

$$J(t,T) = C_1 + C_2 (t \times 10^{C3})^m$$

where:

C_1, C_2 and m are constants; the program uses the following default values if non-zero values for these constants are not input.

$C_1 = 0.3935 \times 10^{-6}$ $C_2 = 0.787 \times 10^{-5}$ $m = 0.345$

C_3 is a function of temperature and is given by:

$C_3 = -5.019 + 0.07171\ T.$

The fracture strength of the overlay material is given by:

$$y = 1205\ e^{-0.0316\ T}$$

```
C
C                    *  M A I N  P R O G R A M  *
C                    ****************************
C
C...THIS PROGRAM IS USED TO PREDICT THE CRACK OPENING 'DELTA' FOR
C...THE TESTED BEAMS
C
C...INPUT DATA:
C...***********
C...   NUMNP...= NUMBER OF MEASUREMENTS
C...   PT(I)...= TIME OF MEASUREMENT NUMBER I
C...   PL(I)...= LOAD AT MEASUREMENT NUMBER I
C...   TH1.....= OVERLAY THICKNESS
C...   TH2.....= CONCRETE THICKNESS
C...   WID.....= BEAM WIDTH
C...   TEMP....= TEST TEMPERATURE
C...   SIGY....= FRACTURE STRENGTH OF THE OVERLAY MATERIAL
C
C...THE CREEP COMPLIANCE USED IN THIS PROGRAM TAKES THE FORM:
C...   J(PT,TEMP) = C1 + C2*(PT*10**(C3))**RM   WHERE;
C...   C1,C2,RM ARE CONSTANTS AND ARE GIVEN BY:
C...   C1   = 0.393500E-06
C...   C2   = 0.787000E-05
C...   RM   = 0.345000E 00
C...   C3 IS A FUNCTION OF TEMPRATURE AND IS GIVEN BY:
C...   C3 = -5.019 + 0.07171*TEMP
C
      IMPLICIT REAL*8(A-H,O-Z)
      COMMON/CDATA/NUMNP,NUMEL,NEN
      COMMON/GGDRT/GPT(60),WT(60),SHP(2,2),LE(2),NGP
      COMMON/MATPR/CON1,CON2,RM,TEMP(40),SIGY(40)
      COMMON/CSECD/TH1,TH2,WID
C
      DIMENSION PT(40),PL(40),UA(40),US(40),FN(40),DELTA(40)
      DIMENSION S(40,40),FF(40),FB(40),FC(40),DA(40),DF(40)
C
  110 CONTINUE
C
C...CLEAR THE ARRAYS
C
      DO 35 I=1,40
      PT(I)     = 0.00
      PL(I)     = 0.00
      UA(I)     = 0.00
      FN(I)     = 0.00
      DELTA(I)  = 0.00
      FF(I)     = 0.00
      FB(I)     = 0.00
      FC(I)     = 0.00
      DA(I)     = 0.00
      DF(I)     = 0.00
      SIGY(I)   = 0.00
      TEMP(I)   = 0.00
      US(I)     = 0.00
   35 CONTINUE
C
C...   READ INPUT DATA
C
      READ(5,100) ICASE,ICRN,NB
```

```
      READ(5,100) NUMNP
      READ(5,201) TH1,TH2,WID
      READ(5,201) CON1,CON2,RM
      READ(5,201) RKC
      DO 10 I=1,NUMNP
      READ(5,201) PT(I),PL(I),DELTA(I),TEMP(I),SIGY(I)
   10 CONTINUE
C
C...  DEFAULT VALUES
      IF(CON1 .EQ. 0.00) CON1 = 0.8000D-07
      IF(CON2 .EQ. 0.00) CON2 = 0.7920D-05
      IF(RM   .EQ. 0.00) RM   = 0.3450D 00
      IF(WID  .EQ. 0.00) WID  = 0.1000D 01
      DO 11 I=1,NUMNP
      IF(SIGY(I) .EQ. 0.00) GO TO 12
      GO TO 11
   12 SIGY(I) = 1205.00*DEXP(-0.03160*TEMP(I))
   11 CONTINUE
      SIGY(1) = 0.00
C
      WRITE(6,101)
C
      IF(ICASE .EQ. 1) WRITE(6,102) NB
      IF(ICASE .EQ. 2) WRITE(6,103) NB
  102 FORMAT(17X,'L A E D R A I D R Y  C A S E  S T U D Y',//,
     .       17X,'* * * * * * * * * *  * * * *  * * * * * *',//,
     .       23X,'BEAM NUMBER:',I5,//)
  103 FORMAT(17X,'F I E L D  C A S E  S T U D Y',//,
     .       17X,'* * * * *  * * * *  * * * * * *',//,
     .       23X,'CASE NUMBER:',I5,//)
      WRITE(6,104) RKC
      DO 13 I=1,NUMNP
      WRITE(6,105) PT(I),SIGY(I),TEMP(I)
   13 CONTINUE
      WRITE(6,106) CON1,CON2,RM
      WRITE(6,107) TH1,TH2,WID
      NUMEL = NUMNP-1
      NP1   = NUMNP + 1
      NEN   = 2
      DO 15 I=1,NUMNP
      IF(ICASE .EQ. 1) PT(I) = PT(I)*0.3600D 04
      IF(ICASE .EQ. 2) PT(I) = PT(I)*0.2592D 07
      PL(I) = PL(I)/WID
   15 CONTINUE
      TT = PT(NUMNP) - PT(1)
      PI = 3.1415926
C
      NGP = 10
      A1 = 0.00
      B1 = 0.00
      CALL SDATA(A1,B1)
C
      CALL FUNI(RM,BI)
C
      A1 = 0.00
      B1 = 0.00
      CALL SDATA(A1,B1)
C
      IF(ICPN .EQ. 2 .OR. ICPN .EQ. 0) GO TO 50
      IF(TEMP(1).GE.70.0) GO TO 60
```

```
      DO  25  I=1,NUMNP
      T       = PT(I)/TT
      T1      = - 0.2128*T**1
      T2      =   6.4300*T**2
      T3      = -33.6456*T**3
      T4      =  79.1126*T**4
      T5      = -85.9677*T**5
      T6      =  35.2312*T**6
      SUM     = (T1 + T2 + T3 + T4 + T5 + T6)*TH1
      UA(I) = DABS(SUM)
   25 CONTINUE
      GO TO 70
   60 CONTINUE
      DO  55  I=1,NUMNP
      T       = PT(I)/TT
      T1      = - 0.5330*T**1
      T2      =  11.2869*T**2
      T3      = -58.7745*T**3
      T4      =  136.580*T**4
      T5      = -145.314*T**5
      T6      =  57.6577*T**6
      SUM     = (T1 + T2 + T3 + T4 + T5 + T6)*TH1
      UA(I) = DABS(SUM)
   55 CONTINUE
      GO TO 70
   50 CONTINUE
      IF(ICPN .EQ. 0) GO TO 41
      IF(ICPN .EQ. 2) GO TO 42
   41 CONTINUE
      ALFA   = 1.60 + (.500D-03*RKC/3.00
      BETA   = 0.95
      GO TO 43
   42 CONTINUE
      ALFA   = 1.09 + 0.500D-04*RKC/4.00
      BETA   = 0.80
   43 CONTINUE
      CF     = BETA*TH1/(PT(NUMNP)**ALFA)
      DO  65  I=1,NUMNP
      UA(I) = CF*PT(I)**ALFA
   65 CONTINUE
      DO  38  I=1,NUMNP
      US(I) = UA(I)
   38 CONTINUE
   70 CONTINUE
C
      TOL = 0.001
      MXIT = 4
      DO  30  I=2,NUMNP
      ICOUNT = 0
   40 CONTINUE
      CALL SINFC2(I,UA,PL,FN)
      CALL FUNCB(I,PT,FN,DELTA,FUN)
      FB(I) = FUN
      FC(I) = -FB(I) + DELTA(I)
      UA(I) = UA(I) + 0.100 00
      CALL SINFC2(I,UA,PL,FN)
      CALL FUNCB(I,PT,FN,DELTA,FUN)
      FF(I) = FUN
      UA(I) = UA(I) - 0.100 00
      DF(I) = (FF(I)-FB(I))/0.10
```

```
      DA(I) = - FB(I)/DF(I)
      UA(I) = UA(I) + DA(I)
      IF(UA(I).LT.0.CC.OR.UA(I).GT.TH1) GO TO 27
      ICOUNT = ICOUNT + 1
      IF(DABS(DA(I)).LE.TOL.OR.ICOUNT.GT.MXIT) GO TO 30
      GO TO 40
   30 CONTINUE
   27 CONTINUE
      DO 36 I=1,NUMNP
      UA(I) = US(I)
   36 CONTINUE
      IF(ICPN .EQ. 2) UA(NUMNP) = UA(NUMNP)*WID/14.00
      WRITE(6,108) UA(NUMNP)
      WRITE(6,500)
      DO 45 I=1,NUMNP
      PL(I) = PL(I)*WID
      IF(ICASE .EQ. 2) PT(I) = PT(I)/0.2592D 07
      IF(ICASE .EQ. 1) PT(I) = PT(I)/0.3600D 04
      WRITE(6,105) PT(I),PL(I),DELTA(I)
   45 CONTINUE
      IF(ICASE .EQ. 2) TMI = PT(I    )*0.2592D 07
      IF(ICASE .EQ. 1) TMI = PT(I    )*0.3600D 04
      RL = 0.00
      DO 21 I=1,NUMNP
      RL = RL + PL(I)
   21 CONTINUE
      RL = RL/NUMNP
      PF = RL
      ACI = UA(1     )
      ACF = UA(NUMNP)
      RKM = RKC
      IF(ICASE .EQ. 2) CALL SINFC3(ACF,PF,RKM)
      PI = 3.1415926
      C1 = (CON1/(CON2*PI))**(1.0/RM)
      C2 = 8.00/PI
      TT = 0.00
      DO 20 I=1,NUMEL
      C3 = SIGY(I+1)**2
      CC = C1*C2*C3
      A1 = UA(I)
      A2 = UA(I+1)
      IF(ICASE .EQ. 1) RL = (PL(I) + PL(I+1))/(2.0*WID)
      CALL FUNRK(A1,A2 ,RL,RKM,XINTG,ICASE)
      TT = TT + CC*XINTG
   20 CONTINUE
      TMF = TMI + TT
      TMFH = TMF/3600.00
      TMFM = TMFH/720.0
      IF(ICASE .EQ. 1) WRITE(6,600)  TMFH
      IF(ICASE .EQ. 2) WRITE(6,601)  TMFM
      READ(5,100) IEXIT
      IF(IEXIT.EQ.0) GO TO 85
      GO TO 110
  100 FORMAT(5I5)
  101 FORMAT(1H1)
  105 FORMAT(5D15.5)
  201 FORMAT(5D12.6)
  250 FORMAT(5D12.4)
  104 FORMAT(17X,'OVERLAY MATERIAL PROPERTIES',/,
     .       17X,'******* ******** **********',//,
```

```
     .          5X,'FRACTURE TOUGHNESS (KIC).............=',1D15.6,///,
     .          5X,'TIME',11X,'SIGY',10X,'TEMP',/,
     .          5X,'****',11X,'****',10X,'****',/)
 106 FORMAT(//,5X,'CREEP COMPLIANCE EQUATION IS :',/,
     .     5X,'J(PT,TEMP) = ',D12.4,' + ',D12.4,'*(PT*10**(-5.019 ',
     .     '+ 0.07171*TEMP))**',D12.4,//)
 107 FORMAT(20X,' MATERIAL DIMENSIONS',/,
     .      20X,' ********* **********',//,
     .          5X,'OVERLAY THICKNESS (TH1)..............=',1D15.6,/,
     .          5X,'CONCRETE THICKNESS (TH2).............=',1D15.6,/,
     .          5X,'BEAM(OR SLAB) WIDTH (WID)............=',1D15.6)
 108 FORMAT(5X,'MAX. CRACK LENGTH ..................=',1D15.6,//)
 500 FORMAT(8X,'TIME',11X,'LOAD',10X,'DELTA',/,
     .          8X,'****',11X,'****',10X,'*****',/)
 600 FORMAT(//,5X,'FAILURE TIME ..(HOURS).............=',1D15.6)
 601 FORMAT(//,5X,'FAILURE TIME ..(MONTHS)............=',1D15.6)
  85 CONTINUE
     WRITE(6,101)
     STOP
     END
C    ****************************************************
     SUBROUTINE FUNCP(I,PT,FN,DELTA,FUN)
C    ****************************************************
     IMPLICIT REAL*8(A-H,O-Z)
     COMMON/CDATA/NUMNP,NUMEL,NEN
     COMMON/GQDRT/GPT(60),WT(60),SHP(2,2),LE(2),NGP
     COMMON/MATPR/CON1,CON2,RM,TEMP(40),SIGY(40)
     DIMENSION PT(40),FN(40),DELTA(40)
     PI = 3.1415926
     II = I-1
     T2 = 0.0D 00
     DO 20 IE = 1,II
     DO 30 M=1,NGP
     T1 = 0.0D 00
     CALL SHAP(IE,M,PT,XSJ)
     CALL FUNK(IE,M,PT,I,FK)
     DO 40 K=1,NEN
     KK = IE+K-1
  40 T1 = T1 + FN(KK)*SHP(2,K)
     T3 = DABS(T1)
  30 T2 = T2 + FK*T3*XSJ
  20 CONTINUE
     FUN = DELTA(I) - 8.0D0*SIGY(I)*T2/PI
     RETURN
     END
C    ****************************************
     SUBROUTINE FUNK(IE,M,PT,K,FK)
C    ****************************************
     IMPLICIT REAL*8(A-H,O-Z)
     COMMON/GQDRT/GPT(60),WT(60),SHP(2,2),LE(2),NGP
     COMMON/MATPR/CON1,CON2,RM,TEMP(40),SIGY(40)
     DIMENSION PT(40)
     A   = PT(IE+1) - PT(IE)
     S   = GPT(M)
     E   = (S + 1.0D 00)/2.0D 00
     Z   = A*E  + PT(IE)
     C1  = -5.019 + 0.07171*TEMP(IE+1)
     C2  = 10.0**C1
     C3  = C2**RM
     FK  = CON1 + CON2*C3*(PT(K)-Z)**RM
```

```
      RETURN
      END
C     ********************
      SUBROUTINE SDATA(A,B)
C     ********************
      IMPLICIT REAL*8(A-H,O-Z)
      COMMON/GQDRT/GPT(60),WT(60),SHP(2,2),LE(2),NGP
      DIMENSION D(60),E(60)
      LE(1) = -1
      LE(2) =  1
      N = NGP
      EPS = 1.0D-09
C...CALCULATE THE COEFFICIENTS B(N),C(N)
      A1 = A + B
      B1 = B - A
      D(1) = 0.0D 00
      E(1) = 0.0D 00
      DO 5 I=2,NGP
      RC = I - 1
      RF = 2*I
      R1 = 2*I - 1
      R2 = 2*I - 2
      R3 = 2*I - 3
      D(I) = A1*B1/((A1+RF)*(A1+R2))
      IF(A1.EQ.-1.0D 00.AND.I.EQ.2) GO TO 6
      T1 = 4.0D 00*RC*(A+RC)*(B+RC)*(A1+RC)
      T2 = (A1+R1)*(A1+R3)*(A1+R2)**2
      E(I) = T1/T2
      GO TO 5
    6 T1 = 4.0D 00*(A+1.0D 00)*(B+1.0D 00)
      T2 = (A1+3.0D 00)*(A1+2.0D 00)**2
      E(I) = T1/T2
    5 CONTINUE
C...FOR N=1 :
      GPT(1) = 0.0D 00
      WT (1) = 2.0D 00
      FN = N
      FF = FGM(A + 1.0D 00) + FGM(B + 1.0D 00) - FGM(A1 + 2.0D 00)
      BETA = DEXP(FF)
      CC = 2.0D 00**(A1 + 1.0D 00)*BETA
      DO 10 J=2,N
   10 CC = CC*E(J)
      DO 120 I=1,N
      IF(I-1) 120,20,30
   20 AN = A/FN
      BN = B/FN
      R1 = (1.0D 00+A)*(2.78D 00/(4.0D 00*FN*FN)+0.768D 00*AN/FN)
      R2 = 1.0D 00+1.48D 00*AN+0.96D 00*BN+0.452D 00*AN*AN
     .     +0.83D 00*AN*BN
      XT = 1.0D 00-R1/R2
      GO TO 110
   30 IF(I-2) 120,40,50
   40 R1 = (4.1D 00+A)/((1.0D 00+A)*(1.0D 00+0.156D 00*A))
      R2 = 1.0D 00+0.06D 00*(FN-8.0D 00)*(1.0D 00+0.12D 00*A)/FN
      R3 = 1.0D 00+0.012D 00*B*(1.0D 00+0.25D 00*DABS(A))/FN
      RT = R1*R2*R3
      XT = XT-ET*(1.0D 00-XT)
      GO TO 110
   50 IF(I-3) 120,60,70
   60 R1 = (1.67D 00+0.28D 00*A)/(1.0D 00+0.37D 00*A)
```

```
            R2  = 1.0D 00+(.22D 00*(FN-8.0D 00)/FN
            R3  = 1.0D 00+8.0D 00*B/((6.28D 00+B)*FN*FN)
            RT  = R1*R2*R3
            XT  = XT - RT*(GPT(I) - XT)
            GO TO 110
         70 IF(N-I-1) 100,90,80
         80 XT  = 3.0D 00*GPT(I-1) - 3.0D 00*GPT(I-2) + GPT(I-3)
            GO TO 110
         90 R1  = (1.0D 00+(.235D 00*B)/(0.766+0.119*B)
            R2  = 1.0D 00/(1.0D 00+0.639D 00*(FN-4.0D 00)/
           .     (1.0D 00+0.71D 00*(FN-4.0D 00)))
            R3  = 1.0D 00/(1.0D 00+20.0D 00*A/((7.5D 00+A)*FN*FN))
            RT  = R1*R2*R3
            XT  = XT + RT*(XT - GPT(I-2))
            GO TO 110
        100 R1  = (1.0D 00+(.37D 00*B)/(1.67D 00+0.28D 00*B)
            R2  = 1.0D 00/(1.0D 00+0.22D 00*(FN-8.0D 00)/FN)
            R3  = 1.0D 00/(1.0D 00+8.0D 00*A/((6.28D 00+A)*FN*FN))
            RT  = R1*R2*R3
            XT  = XT + RT*(XT - GPT(I-2))
        110 CALL ROOT(XT,N,A,B,DFN,FN1,D,E,EPS)
            GPT(I) = XT
            WT (I) = CC/(DFN*FN1)
        120 CONTINUE
            RETURN
            END
C           ***************
            FUNCTION FGM(W)
C           ***************
            IMPLICIT REAL*8(A-H,O-Z)
C...CALCULATE LN(GAMMA(W)) FOR W REAL AND GAMMA(W) POSITIVE.
C...USES STIRLING'S FORMULA
            PI = 3.14159265358980 00
            X  = W
            M  = 0
            FK = -1.0D 00
            IF(X-0.50D 00) 1,2,2
          1 M  = 1
            XPI = X*PI
            X  = 1.0D 00 - X
          2 FK = FK + 1.0D 00
            IF(X+FK-8.0D 00) 2,2,3
          3 Z  = X+FK
            ZZ = Z*Z
            Y  = (Z-0.50D 00)*DLOG(Z)-Z+0.91893853320470 00
           .    +((((( 4146.0D 00/ZZ+1820.0D 00)/ZZ-1287.0D 00)/ZZ
           .    +1716.0D 00)/ZZ-6006.0D 00)/ZZ+180180.0D 00)/Z/2162160.0D 00
            IF(FK) 6,6,4
          4 IK = FK
            DO 5 I=1,IK
            FK = FK-1.0D 00
          5 Y  = Y-DLOG(X+FK)
          6 IF(M) 7,11,7
          7 P  = PI/DSIN(XPI)
            IF(P) 8,8,10
          8 WRITE(6,100)
            Y  = 0.0D 00
            GO TO 11
         10 Y  = DLOG(P)-Y
         11 FGM= Y
```

```
  100 FORMAT(10X,'N=',1D15.5,/,
     .       10X,'GAMMA IS NEGATIVE')
      RETURN
      END
C     ****************************************
      SUBROUTINE ROOT(X,N,A,B,DPN,PN1,D,E,EPS)
C     ****************************************
C...IMPROVES THE APPROX. ROOT X. AND;
C...OBTAIN DPN&PN1 WHERE:
C...DPN = DERIVATIVE OF P(N) AT X
C...PN1 = VALUE OF P(N-1) AT X
      IMPLICIT REAL*8(A-H,O-Z)
      DIMENSION D(1),E(1)
      ITER = 0
    1 ITER = ITER + 1
      CALL RECUR(P,DP,PN1,X,N,A,B,D,E)
      G  = P/DP
      X  = X-G
      IF(DABS(G)-EPS) 3,3,2
    2 IF(ITER-10) 1,3,3
    3 DPN = DP
      RETURN
      END
C     ****************************************
      SUBROUTINE RECUR(PN,DPN,PN1,X,N,A,B,D,E)
C     ****************************************
      IMPLICIT REAL*8(A-H,O-Z)
      DIMENSION D(1),E(1)
      P1 = 1.0D 00
      P  = X+(A-B)/(A+B+2.0D 00)
      DP1 = 0.0D 00
      DP  = 1.0D 00
      DO 10 J=2,N
      Q  = (X-D(J))*P  - E(J)*P1
      DQ = (X-D(J))*DP - E(J)*DP1 + P
      P1 = P
      P  = Q
      DP1 = DP
   10 DP  = DQ
      PN  = P
      DPN = DP
      PN1 = P1
      RETURN
      END
C     ************************************
      SUBROUTINE SHAP(IE,M,PT,XSJ)
C     ************************************
C...SHAPE FUNCTIONS ROUTINE FOR 1-D ISOP. ELEM.
C...CALLED BY MAIN ROUTINE
      IMPLICIT REAL*8(A-H,O-Z)
      COMMON/CDATA/NLMAP,NUMEL,NEN
      COMMON/GQDRT/GPT(60),WT(60),SHP(2,2),LE(2),NGP
      DIMENSION PT(40)
      E  = GPT(M)
C...FORM 2-NODE QUADRATURE SHAPE FUNCTIONS
      DO 10 I=1,2
      SHP(1,I) = (1.0D+LE(I)*E)/2.0D0
   10 SHP(2,I) = LE(I)/2.0D0
C...CONSTRUCT DETERMINANT OF JACOBIAN
      XS = 0.0D 00
```

```
      DO 50 K=1,NEN
      L = K+IE-1
   50 XS = XS + PT(L)*SHP(2,K)
      DO 70 I=1,NEN
   70 SHP(2,I) = SHP(2,I)/XS
      XSJ = XS*WT(K)
      RETURN
      END
C     ************************
      SUBROUTINE SOLV2(A,DX,N)
C     ************************
      IMPLICIT REAL*8(A-H,O-Z)
      DIMENSION A(40,40),DX(40)
      M = N+1
      DO 21 I=2,N
      DO 21 J=I,N
      RA = A(J,I-1)/A(I-1,I-1)
      DO 31 K=1,M
      A(J,K) = A(J,K)-RA*A(I-1,K)
   31 CONTINUE
   21 CONTINUE
      DO 41 I=2,N
      K=N-I+2
      DO 51 J=I,N
      L = N-J+1
   51 A(L,M) = A(L,M)-RA*A(L,K)
   41 CONTINUE
      DO 61 I=1,N
   61 DX(I) = A(I,M)/A(I,I)
      RETURN
      END
      SUBROUTINE STIF(I,UA,PL,FN)
C     **************************
      IMPLICIT REAL*8(A-H,O-Z)
      COMMON/CSECD/TH1,TH2,WIC
      DIMENSION UA(40),PL(40),PM(40),SG(40),WD(40),RK(40),FN(40)
      COMMON/MATPR/CON1,CON2,FM,TEMP(40),SIGY(40)
      PI = 3.1415926
      II = I-1
      DO 10 K=II,I
      PM(K) = PL(K)*TH2/2.00
      SG(K) = 6.00*PM(K)/TH1**2
      R     = UA(K)/TH1
      R1    = 1.0 - R
      A1    = R1**1.50
      A2    = R1**0.50
      A3    = R1
      F1    = 3.52/A1 - 4.35/A2 + 2.13*A3
      R2    = PI*R/2.0
      B1    = DSIN(R2)
      B2    = DCOS(R2)
      B3    = DTAN(R2)
      B4    = 0.199*(1.0 - B1)**4
      B5    = DSQRT(B3/R2)
      F2    = B5*(0.923 + B4)/B2
      RK(K) = 2.0*PL(K)*F1/DSQRT(PI*UA(K)) + SG(K)*F2*DSQRT(PI*UA(K))
      WD(K) = PI*(RK(K)/SIGY(K))**2/8.00
      DK    = DSQRT(WD(K))
      DE    = DSQRT(UA(K))
      DS = DABS((DK+DE)/(DK-DE))
```

```
      DL      = DLOG(DS)
      FN(K)   = DSQRT(WC(K)*UA(K)) - 0.50*(WO(K)-UA(K))*DL
   10 CONTINUE
      RETURN
      END
      SUBROUTINE SINFC2(I,UA,PL,FN)
C     ****************************
      IMPLICIT REAL*8(A-H,O-Z)
      COMMON/CSECD/TH1,TH2,WID
      COMMON/MATPR/CON1,CON2,FM,TEMP(40),SIGY(40)
      DIMENSION UA(40),PL(40),WO(40),RK(40),FN(40)
      PI = 3.1415926
      II = I-1
      DO 10 K=1,I
      IF(K.EQ.1) GO TO 10
      PP   = PL(K)*(TH1+TH2)/2.00
      R1   = UA(K)/TH1
      R2   = R1*R1
      R3   = R1*R2
      R4   = R1*R3
      R5   = R1*R4
      R6   = R1*R5
      FF   = 1.12078 -  3.6822*R1 + 11.9543*R2 - 25.8521*R3
     .               + 33.0976*R4 - 22.4422*R5 +  6.1784*R6
      FM   = 1.12135 -  2.9500*R1 + 7.6812*R2 - 14.6437*R3
     .               + 17.5883*R4 - 11.5497*R5 +  3.12800*R6
      C    = TH1 - UA(K)
      C1   = 3.0*TH1 - 2.0*C
      C2   = DSQRT(UA(K)/(C*TH1))/C
      RK(K)   = 1.000*(FF*PL(K)*C1 + 6.0*FM*BM)*C2
      WC(K)   = PI*(RK(K)/SIGY(K))**2/8.00
      DW      = DSQRT(WC(K))
      DC      = DSQRT(UA(K))
      DS   = DABS((DW+DC)/(DW-DC))
      DL      = DLOG(DS)
      FN(K)   = DSQRT(WC(K)*UA(K)) - 0.50*(WO(K)-UA(K))*DL
   10 CONTINUE
      RETURN
      END
      SUBROUTINE FUNRK(A1,A2,FL,FKM,RR,ICASE)
C     ***************************************
      IMPLICIT REAL*8(A-H,O-Z)
      COMMON/GQDRT/GPT(60),WT(60),SHP(2,2),LE(2),NGP
      COMMON/MATPR/CON1,CON2,FM,TEMP(40),SIGY(40)
      RR   = 0.00
      DJ   = (A2-A1)/2.0
      DO 10 M=1,NGP
      E    = GPT(M)
      S    = WT(M)
      X    = (1.0 + E)*DJ + A1
      CALL SINFC3(X,FL,RK)
      TT = RKM
      IF(ICASE .EQ. 1) TT = FKM*DABS(((RKM-800.0)/(1.10*RKM) - 1.0))
      T1   = (TT/RK)**2 - 1.00
      IF(T1.LT.0.0)  GO TO 20
      T2   = T1**(1.0/FM)
      T3   = T2/RK**2
      GO TO 30
   20 CONTINUE
      T3 = 0.00
```

```
      30 RR   = RR + T3*S*DJ
      10 CONTINUE
         RETURN
         END
         SUBROUTINE FUNJ(FM,RJ)
         IMPLICIT REAL*8(A-H,O-Z)
         COMMON/GQDRT/GPT(60),WT(60),SHP(2,2),LE(2),NGP
         DJ = 0.50
         RJ = 0.00
         DO 10 M=1,NGP
         E  = GPT(M)
         S  =  WT(M)
         X  = (1.00+E)*DJ
         D  = DSQRT(1.00-X)
         F  = 0.50*(X**FM)*DLOG((1.0+D)/(1.0-D))
      10 RJ = RJ + F*S*DJ
         NGP = 2
         RETURN
         END
         SUBROUTINE SINFC3(A,P,SI)
C        ************************
         IMPLICIT REAL*8(A-H,O-Z)
         COMMON/CSECD/TH1,TH2,WID
         COMMON/MATPR/CON1,CON2,FM,TEMP(40),SIGY(40)
         PI = 3.1415926
         PM = P*(TH1+TH2)/2.00
         R1 = A/TH1
         R2 = R1*R1
         R3 = R1*R2
         R4 = R1*R3
         R5 = R1*R4
         R6 = R1*R5
         FF = 1.12078 -  3.6822*R1 + 11.9543*R2 - 25.8521*R3
     .                + 33.0976*R4 - 22.4422*R5 +  6.1784*R6
         FM = 1.12135 - 2.95005*R1 + 7.68012*R2 - 14.64370*R3
     .                + 17.5883*R4 - 11.5497*R5 +  3.12800*R6
         C  = TH1 - A
         C1 = 3.0*TH1 - 2.0*C
         C2 = DSQRT(A/(C*TH1))/C
         SI = (FF*P*C1 + 6.C*FM*PM)*C2
C        SI = SI/2.0
         RETURN
         END
```

APPENDIX E

A METHOD FOR DETERMINING THE MASTER CREEP COMPLIANCE FUNCTION

1. Assume that the time-temperature shift function, A, can be determined from:

$$\log A = a + b\,T$$

and that A = 1 at T = 70 F (21 C) then:

$$A = 10^{-70b + bT}$$

2. Assume that the master creep compliance can be represented by:

$$J(t,T) = Jo + J1(tA)^{1/m}$$

or

$$\begin{aligned} \text{Log } (J-Jo) &= \text{Log } J1 + 1/m \log t + 1/m \log A \\ &= \log J1 + 1/m\,(\log t - 70B + bT) \\ &= \log J1 + 1/m\,X \end{aligned}$$

3. Assume a value for Jo and use linear regression to find log J1 and 1/m for various values of b.

4. Select the value of b that minimizes the standard error of estimate (SEE).

5. Assume a new value for Jo and repeat steps 3 and 4 until SEE is minimized. Note that Jo must be lower than the lowest value of J in the test data. Note also that Jo affects J at short times and low temperatures; at higher values of t and T, the effect of Jo is negligible. Jo can, therefore, be estimated by first running the analysis with Jo = o, plotting the data, and noting where the test data deviates from a straight line.

APPENDIX F
SMALL SCALE BEAM TESTS

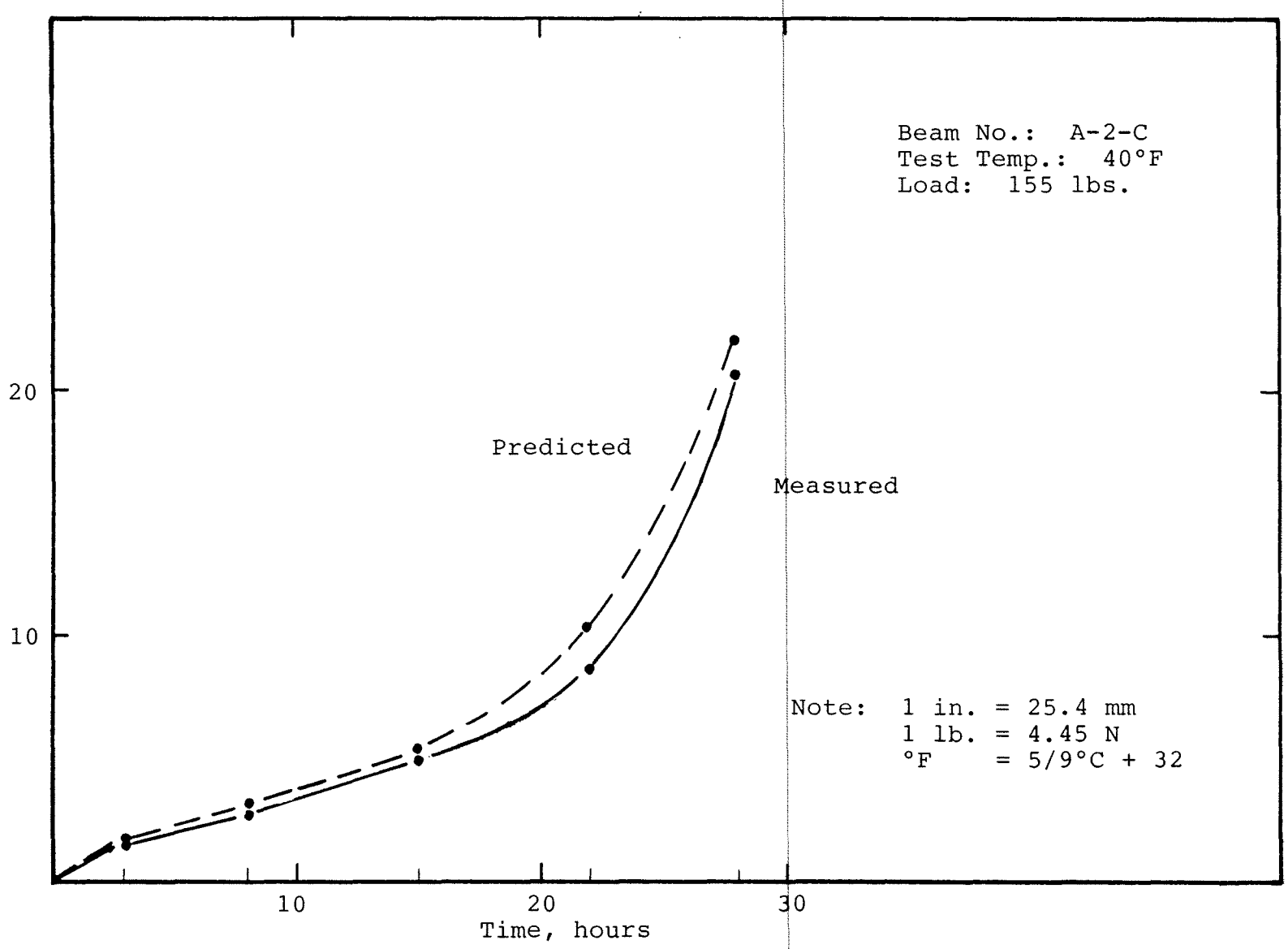

Figure 61. Joint opening vs time for small-scale beams.

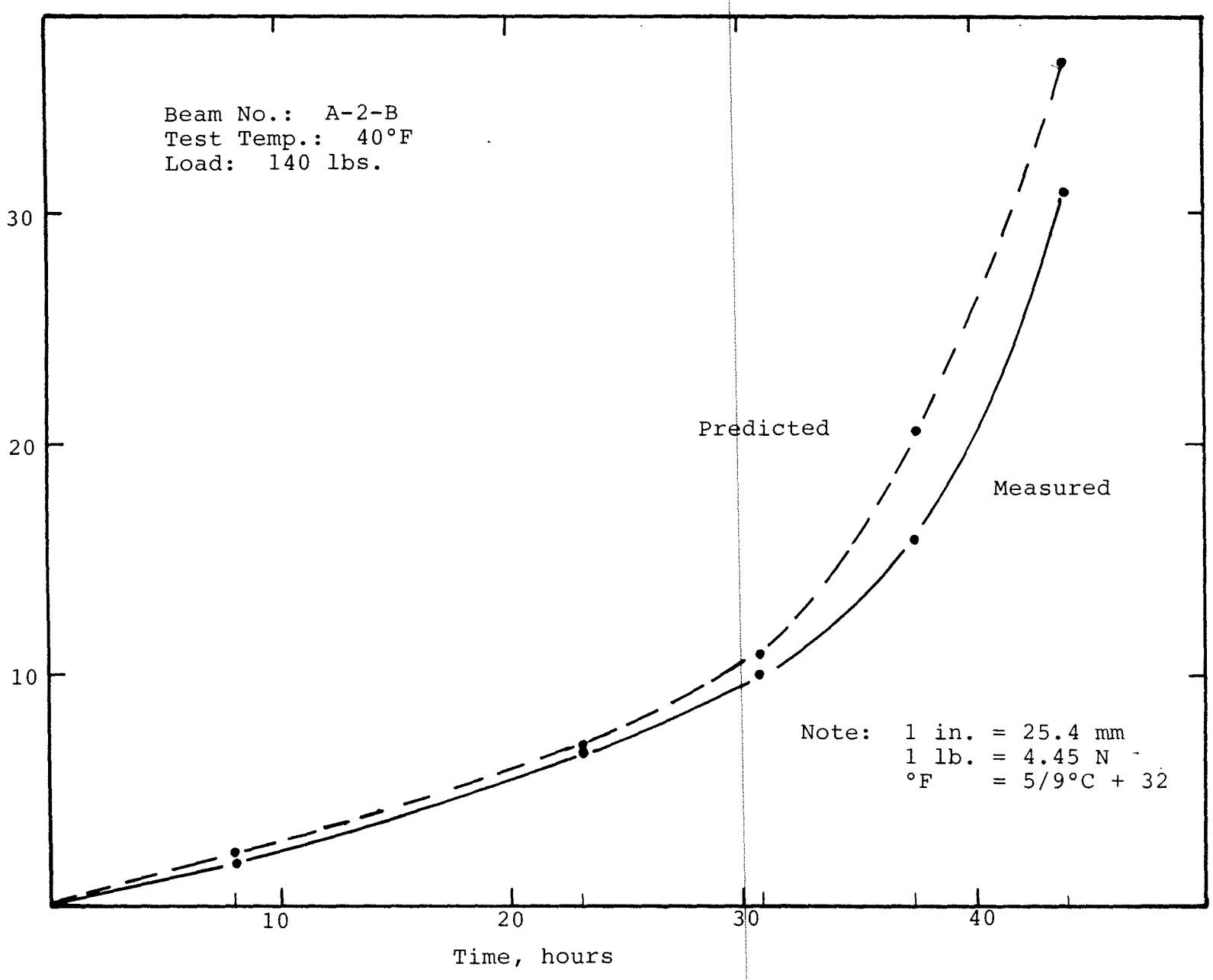

Figure 62. Joint opening vs time for small-scale beams.

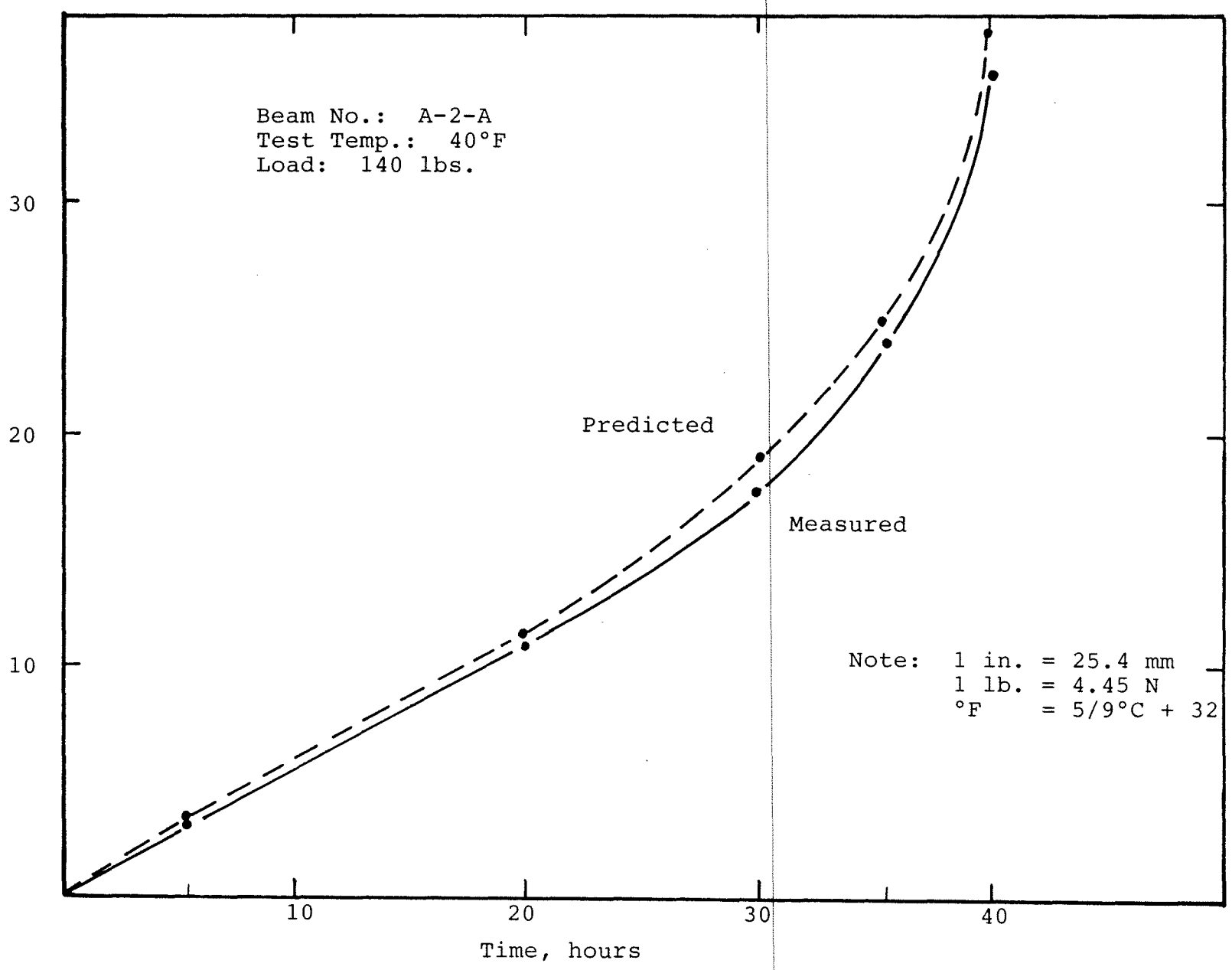

Figure 63. Joint opening vs time for small-scale beams.

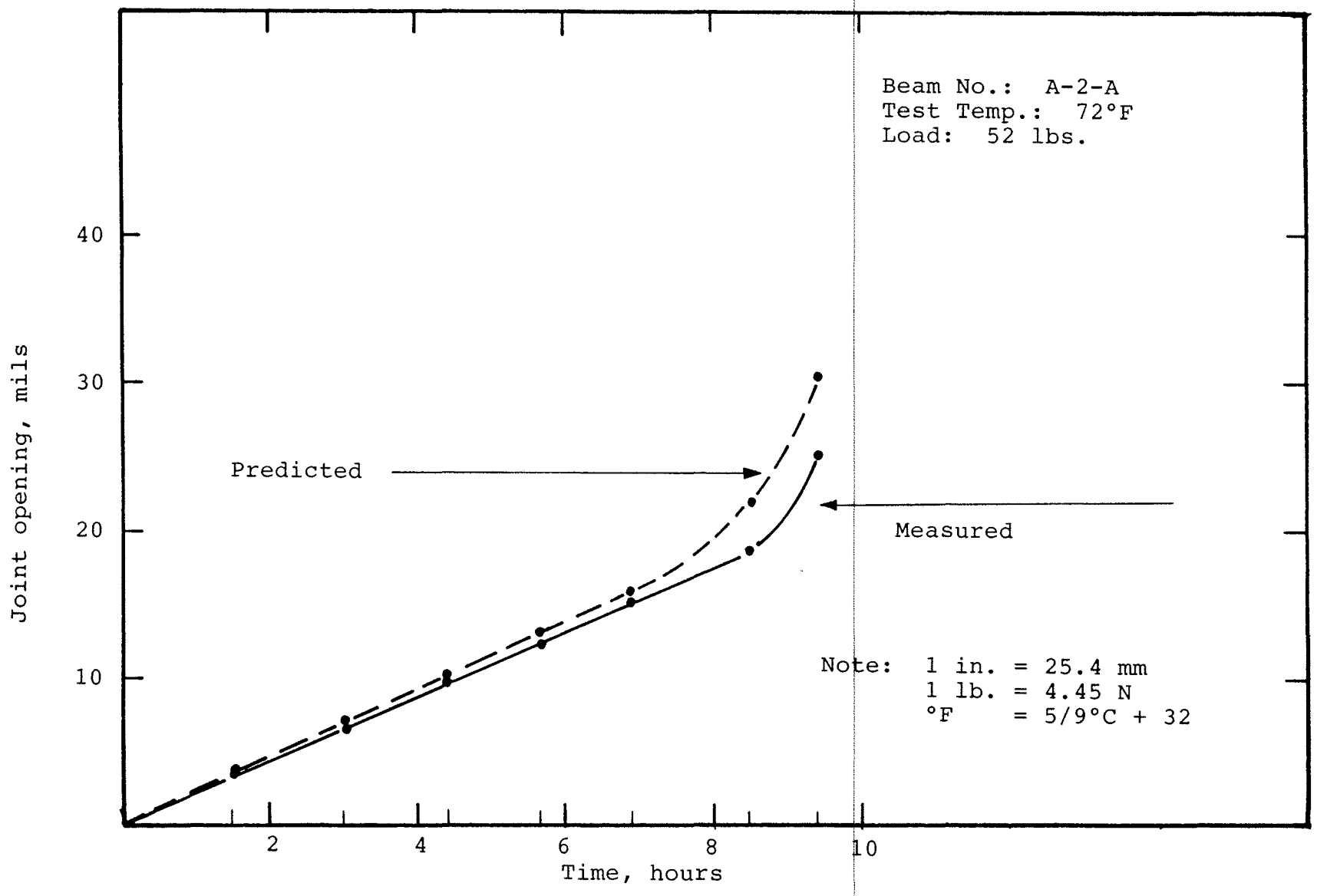

Figure 64. Joint opening vs time for small-scale beams.

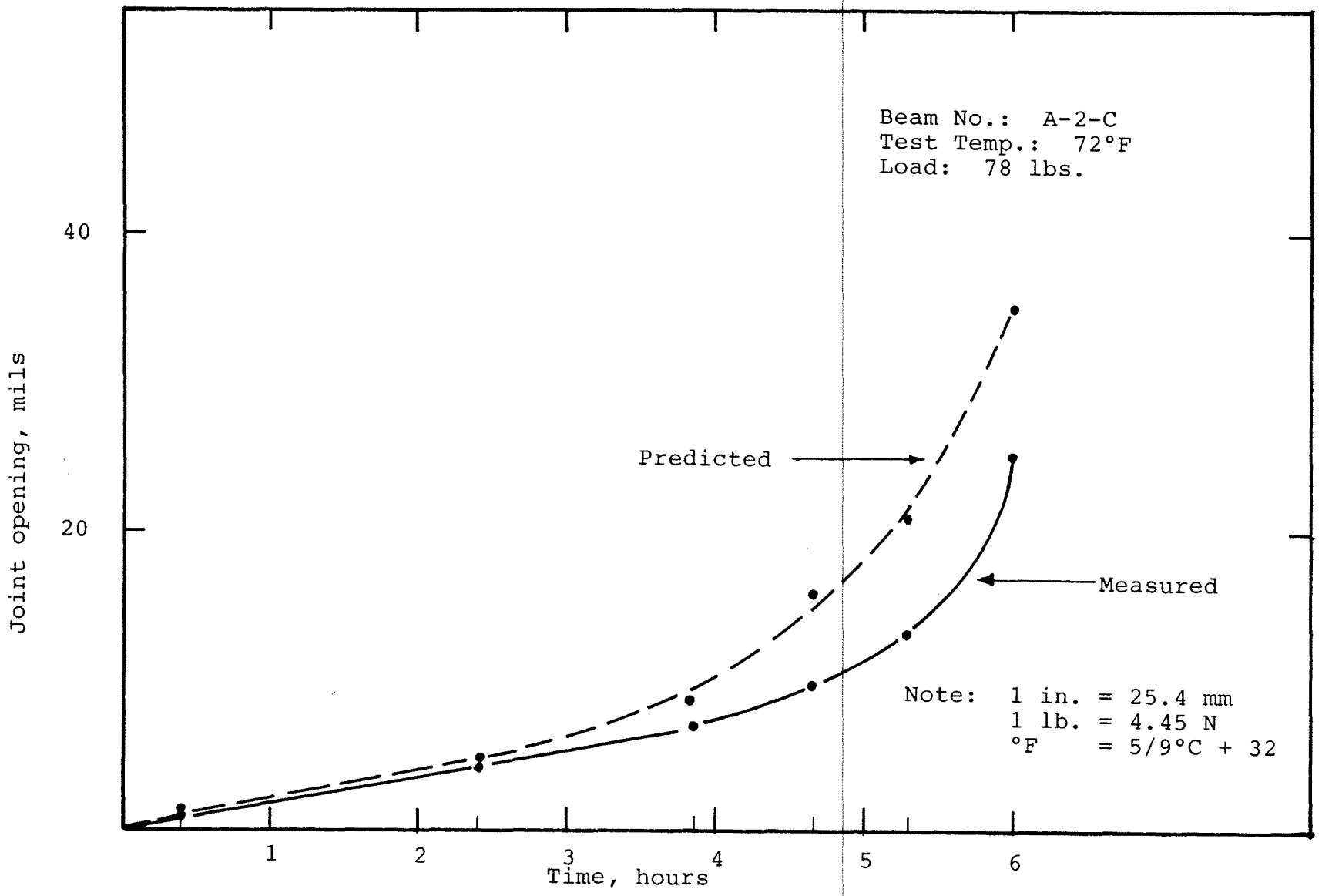

Figure 65. Joint opening vs time for small-scale beams.

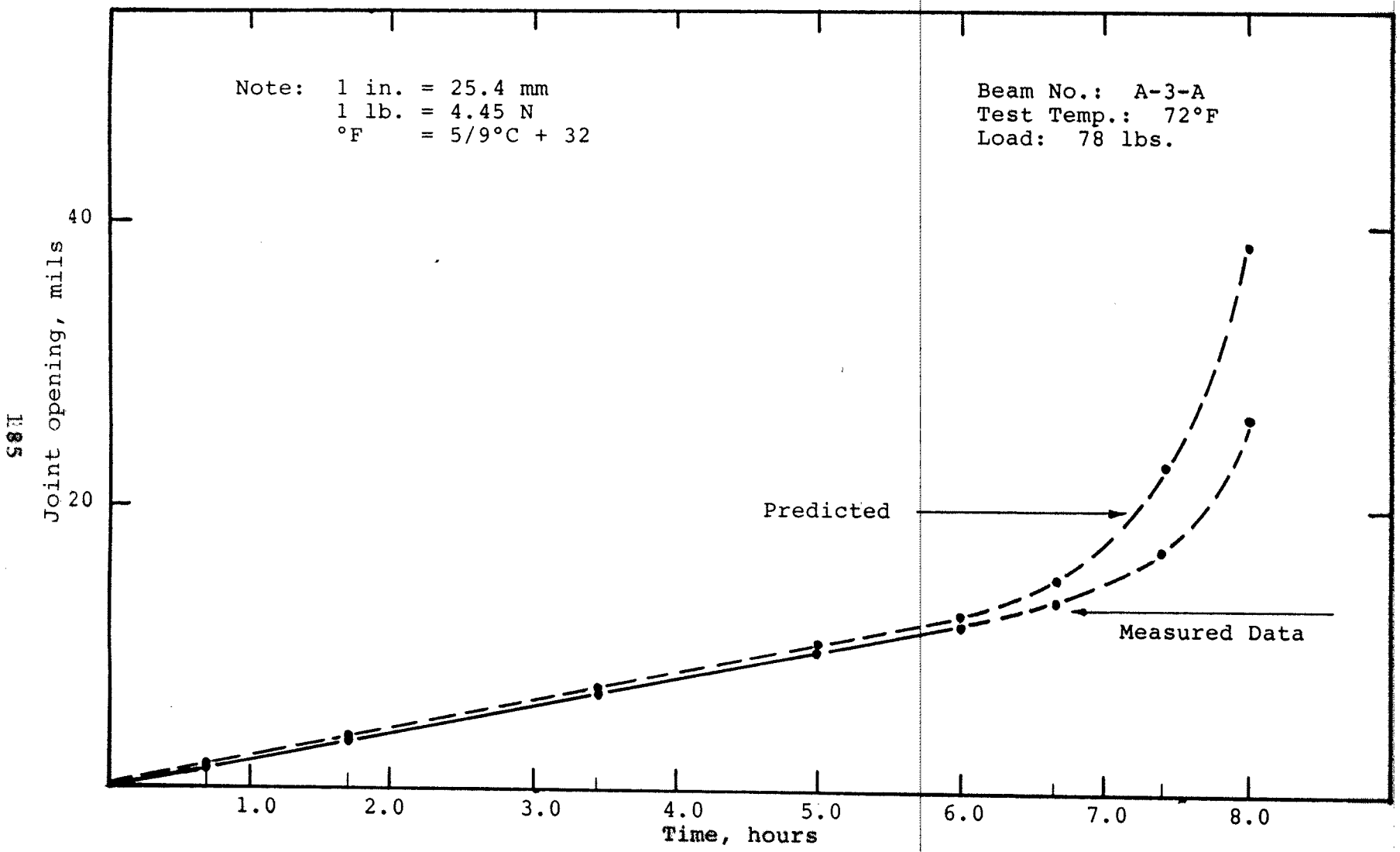

Figure 66. Joint opening vs time for small-scale beams.

REFERENCES

1. McGhee, K.H., "Attempts to Reduce Reflection Cracking of Bituminous Concrete Overlays on Portland Cement Concrete Pavements," Transportation Research Record 700, Transportation Research Board, 1979.

2. Way, George, B., "Prevention of Reflection Cracking in Arizona," Transportation Research Record 756, Transportation Research Board, 1980.

3. McCullagh, F.R., "Reflection Cracking of Bituminous Overlays on Rigid Pavements," Special Report 16, Engineering Research and Development Bureau, New York Department of Transportation, 1973.

4. Vicelja, J.L., "Methods to Eliminate Reflection Cracking in Asphalt Concrete Resurfacing Over Portland Cement Concrete Pavements," Proceedings of the Association of Asphalt Paving Technologists, Vol. 32., 1963.

5. Coople F., and L.T. Oehler, "Michigan Investigation of Soil-Aggregate Cushions and Reinforced Asphaltic Concrete for Preventing or Reducing Reflection Cracking of Resurfaced Pavements," Highway Research Record 239, Highway Research Board, 1968.

6. McLaughlin, Aston, "Reflection Cracking of Bituminous Overlays for Airport Pavements, A State of Art," FAA-RD-79-57, Federal Aviation Administration, Washington, D.C., May, 1979.

7. Asphalt Institute, Construction Leaflet No. 16, December, 1975.

8. Piggott, W. et al., "Improved Hot Mix Asphalts Containing Reclaimed Rubber," Proceedings of the Association of Asphalt Paving Technologists, 1977.

9. Steward, J. et al., "Guidelines for Use of Fabrics in Construction and Maintenance of Low-Volume Roads," Reprint FHWA-TS-78-211, Federal Highway Administration, Washington, D.C., 1978.

10. _____ "Sample Specification for Engineering Fabrics," U.S. DOT Publication, FHWA-TS-78-211, Federal Highway Administration, Washington, D.C., 1978.

REFERENCES (continued).

11. Luther, M.S., Majidzadeh, K., and Chang, C.W., "Mechanistic Investigation of Reflection Cracking of Asphalt Overlays," Transportation Research Record 572, Transportation Research Board, 1976.

12. Jackson, Ralph D., "Preventive Measures for Reflective Cracking of Asphalt Concrete State of the Art," Preliminary Report, U.S. Army Corps of Engineers, Vicksburg, MI., March 1979.

13. Velz, P.G., "Effect of Pavement Breaker Rolling on Crack Reflectance in Bituminous Overlay," Highway Research Record No. 11, Highway Research Board, 1963.

14. Lyon, J.W., "Heavy Pneumatic Rolling Prior to Overlaying: A 10-Year Project Report," Highway Research Record 327, Highway Research Board, 1970.

15. Sherman, G.B., "Reflection Cracking, Pavement Rehabilitation: Proceedings of a Workshop," FHWA RD-74-60, Federal Highway Administration, Washington, D.C., June 1974.

16. Smith, L.L., and W. Gardner, Jr., "Welded Wire Fabric Reinforcement for Asphaltic Concrete," Highway Research Board Bulletin 322.

17. "Sulphur-Asphalt Technologies Near Commercialization," Sulphur Institute Sulphur Research & Development, Volume 1, 1978.

18. Meyer, R.P. et al., "Temperature Susceptibility Evaluation of Sulphur-Asphalt Mixtures," Proceedings of the Association of Asphalt Paving Technologists, Volume 46, 1977.

19. Kimble, F.W., "Conditioning An Existing Concrete Pavement For Bituminous Resurfacing," Highway Research Board Bulletin 123, 1956.

20. Wood, W.A., "Methods of Minimizing Reflection Cracking in Bituminous Overlays," FHWA Notice N5140.9, Federal Highway Administration, Washington, D.C., January 1976.

21. Majidzadeh, K., and Sucharieh, G. "The Study of Pavement Overlay Design: Final Report," Ohio State University, Columbus, Ohio, 1977.

22. Treybig, H.J., et al., "Overlay Design and Reflection Cracking Analysis for Rigid Pavements - Volume 1," FHWA-RD-77-66, Washington, D.C., August, 1977.

23. Huekelom, W., and Klomp, A.J.G., "Road Design Dynamic Loading," Proceedings of the Asphalt Paving Technologists, Volume 33, 1964.

24. Luther, M.S., "The Fracture Mechanics Approach to Reflection Cracking," M.S. Thesis, The Ohio State University, Columbus, Ohio, 1974.

25. Sih, G.C., "Strain-Energy-Density Factor Applied to Mixed Mode Crack Extension Problems," Institute of Fracture and Solid Mechanics Technical Report, Lehigh University, Lehigh, Pennsylvania, 1972.

26. Irvin, G.R., "Fracture Mechanics," Structural Mechanics, Proceedings of First Naval Symposium, Pergammon Press, New York, 1960.

27. McClintock, F.A., and Walsh, J.B., Proceedings of the 4th U.S. National Congress of Applied Mechanics, pp. 1015, 1962.

28. Majidzadeh, K., et al., "Application of Fracture Mechanics for Improved Design of Bituminous Concrete," Final Report, FHWA-RD-76-91, Federal Highway Administration, Wasington, D.C., June 1976.

29. German F.P., and Lytton R.L., "Methodology for Predicting the Reflection Cracking Life of Asphalt Concrete Overlays," Research Report 207-5 Texas Transportation Institute, March, 1979.

30. Schapery, R.A., "A Theory of Crack Growth in Viscoelastic Media," Mechanics and Materials Research Center, Texas A & M University, College Station, Texas, 1973.

31. Ahlborn, G., "Elastic Layered Systems with Normal Loads," Institute of Transportation and Traffic Engineering, University of California, Berkeley, California, 1972.

32. Seeds, S.B., McCullough, F.B., and Carmichael, R.F., "Arkansas Reflection Cracking Analysis and Overlay Design Procedure," Report No. VA--3/1, University of Arkansas, Fayetteville, Arkansas, April, 1983.

33. Majidzadeh, K., and Ilves, G.J., "Evaluation of Rigid Pavement Overlay Design Procedures," FHWA/RD-83/090, Federal Highway Administration, Washington, D.C., December, 1983.

34. Schapery, R.A., "A Theory of Crack Initiation and Growth in Viscoelastic Media, I. Theoretical Development," International Journal of Fracture, Volume II, No. 1, February, 1975.

35. Dugdale, D.S., "Yielding of Steel Sheets Containing Slits," Journal of the Mechanics and Physics of Corresp. Principle.

36. California Simulation of Temperature Grade.

37. PCA Simulation of Temperature Grade.

38. Wilson, Edward L., "Solid Sap: A Static Analysis Program for Three Dimensional Solid Structures," Report UC SESM 71-19, University of California, Berkeley, California, September, 1971.

39. Majidzadeh, K., Ilves, G.J., Sklyut, H., and Kumar, V.R., "Mechanistic Methodology for Airport Pavement Designs with Engineering Fabrics," DOT/FAA/PM-84/9, I, Federal Aviation Administration, Washington, D.C., August, 1984.

40. Majidzadeh, K., Ilves, G.J., and Sklyut, H., "Mechanistic Design of Rigid Pavements - Volume I," Final Report, DTFH11-9568, Federal Highway Administration, Washington, D.C., November, 1983.

41. Goodman, Richard E., Taylor, Rober L., and Brekke, Tor L., "A Model for the Mechanics of Jointed Rock," Proc. ASCE J. of the Soil Mechanics and Foundations Division, 94, No. SM3, May, 1968, pp. 637-59.

42. Zienkiewicz, O.C., "The Finite Element Method in Engineering Science," London, McGraw-Hill, 1971.

43. Graham, G.A.C., "The Correspondence Principle of Linear Viscoelastic Theory for Mixed Boundary Value Problem Involving Time-Dependent Boundary Regions," Quarterly of Applied Mathematics, Vol 26, 1968, pp. 167-174.

44. Kenis, W.J., "Predictive Design Procedures, VESYS User's Manual," FHWA-RD-77-154, Federal Highway Administration, Washington, D.C., January, 1978.

45. Nater, J., and Wasserman, W., "Applied Linear Statistical Model," Irvin-Dorsey Limited, Georgetown, Ontario, 1974, pp. 161-166.

46. McCullagh, F.R., "Reflection Cracking of Bituminous Overlays on Rigid Pavements," Special Report 16, Engineering Research and Development Bureau, New York State Department of Transportation, State Campus, Albany, New York, February, 1973.

47. Karaki, A., "The Engineering Characteristics of Hot-Recycled Asphalt Materials," MS Thesis, The Ohio State University, Columbus, Ohio, 1984.

48. _____, "Climatological Data Annual Summary, New York 1983, Volume 88 Number 13, NOAA ISSN 0364-6041.